

**TARGETING DRUG-RESISTANT CANCER-DRIVER KINASES WITH
ALKYNYLNICOTINAMIDE COMPOUNDS**

by

Elizabeth Larocque

A Dissertation

Submitted to the Faculty of Purdue University

In Partial Fulfillment of the Requirements for the degree of

Doctor of Philosophy



Department of Chemistry

West Lafayette, Indiana

May 2020

THE PURDUE UNIVERSITY GRADUATE SCHOOL
STATEMENT OF COMMITTEE APPROVAL

Dr. Herman Sintim, Chair

Department of Chemistry

Dr. Mingji Dai

Department of Chemistry

Dr. Gaurav Chopra

Department of Chemistry

Dr. Danzhou Yang

Department of Medicinal Chemistry and Molecular Pharmacology

Approved by:

Dr. Christine Hrycyna

*To my friends and family whom I could not have gotten through this process without your love
and support.*

*To my Nana, Judith Larocque
July 19, 1932- November 22,2017*

ACKNOWLEDGMENTS

I would like to thank Dr. Sintim, who has given me countless advice and guidance during my time at Purdue University. I would also like to thank my committee members Professor Mingji Dai, Professor Gaurav Chopra, and Professor Danzhou Yang.

I would also like to thank former Sintim Lab members Dr. Jie Zhou and Dr. Clement Opoku-Temeng who taught me cell culture and docking and Dr. Xiaochu Ma and Dr. Naga Nemishetti who both taught me synthesis and help expand our alkynyl based compound library.

To Delmis Hernandez and Elizabeth Chu who I could always turn to for advice and have become some of my closest friends here I will never be able to thank you enough. Also thank you to all Sintim lab members both at Purdue University and the University of Maryland who I have spent countless hours within lab for all the hard work that we've put in I look forward to looking at the progress we continue to make.

TABLE OF CONTENTS

LIST OF TABLES	8
LIST OF FIGURES	9
LIST OF ABBREVIATIONS.....	12
ABSTRACT	14
CHAPTER 1. INTRODUCTION	15
1.1 Protein Kinase	15
1.2 Structure.....	17
1.2.1 The SH1 domain (Kinase Domain).....	17
1.2.2 SH2/3 Domain.....	19
1.3 Function	19
1.3.1 Receptor Kinases	19
1.3.2 Non-Receptor Kinases	21
1.3.3 Pseudokinases.....	22
1.3.4 Atypical Kinases.....	23
1.4 Kinase Mutations.....	23
1.4.1 Gain-of-Function/ Activating Mutation.....	24
1.4.2 Loss- of-Function/ Inactivating Mutation.....	24
1.4.3 Over-Expression or Amplification	24
1.4.4 Fusion.....	25
1.5 Treatment of Cancer with Kinase inhibitors.....	26
1.6 Relapse in Cancer Treatment	30
1.6.1 Epithelial Growth Factor Receptor (EGFR)	30
1.6.2 Bruton’s Tyrosine Kinase (BTK)	31
1.6.3 BCR-ABL1	32
1.6.4 FMS-like Tyrosine Kinase 3 (FLT3).....	34
1.7 Summary	37
1.8 References.....	37

CHAPTER 2. ALKYNYLNICOTINAMIDE-BASED COMPOUNDS AS ABL1 INHIBITORS WITH POTENT ACTIVITIES AGAINST DRUG-RESISTANT CML HARBORING ABL1(T315I) MUTANT KINASE	47
2.1 Abstract	47
2.2 Introduction.....	47
2.3 Results and Discussion	49
2.3.1 Structural analysis of alkynyl aminoisoquinolines and alkynylaminonaphthyridine:	49
2.3.2 IC ₅₀ determination of select analogues against ABL1 and ABL1(T315I):.....	56
2.3.3 Aminoisoquinolines and aminonaphthyridines potently inhibit the proliferation of ABL1-driven CML cell lines:.....	57
2.4 Conclusion	62
2.5 Experimental Section:.....	63
2.5.1 Molecular docking with GOLD software:	63
2.5.2 General aromatic amide coupling procedure:	63
2.5.3 General aliphatic amide coupling procedure:	63
2.5.4 General Sonogashira Coupling:.....	64
2.5.5 Cell Culture	64
2.5.6 Cellular proliferation assays:.....	64
2.5.7 Evaluation of compounds activity against ABL1 and ABL1(T315I) in CML cell lines KCL22 and KCL22-IR (by KinaSense, West Lafayette, IN, USA)	65
2.6 Acknowledgements:	66
2.7 Conflict of Interest:.....	66
2.8 References:.....	66
CHAPTER 3. NICOTINAMIDE-PONATINIB ANALOGS AS POTENT ANTI-CML AND ANIT-AML COMPOUNDS	69
3.1 Abstract	69
3.2 Introduction.....	69
3.3 Results and Discussion	70
3.3.1 The necessary nitrogen, a high-level medicinal chemistry design strategy:.....	70
3.3.2 Synthesis of Ponatinib Analogs:.....	72
3.3.3 Anticancer activities of nicotinamide analogs and ponatinib:	74

3.3.4	Compounds exhibited potent inhibition against key kinases	75
3.3.5	Ponatinib is a more promiscuous kinase inhibitor than HSN748.....	76
3.4	Conclusion:	80
3.5	Experimental Section:.....	81
3.5.1	General Cell Culture Procedure:	81
3.5.2	General Kinase Assay Procedure (provided by Reaction Biology):	81
3.5.3	General Sonogashira Coupling:.....	81
3.6	Supporting Information:	84
3.7	Author Information:.....	84
3.8	Acknowledgement:.....	85
3.9	Funding Sources:.....	85
3.10	Contributions:	85
3.11	References.....	85
CHAPTER 4. PYRIDO[3,4- <i>b</i>]PYRAZINE BASED COMPOUNDS AS POTENTIAL ANTICANCER AGENTS.....		89
4.1	Abstract.....	89
4.2	Introduction.....	89
4.3	Results and Discussion	92
4.3.1	Synthesis of pyrido[3,4- <i>b</i>]pyrazine based analogs.....	92
4.3.2	Compounds potently inhibit AML and CML cell lines.....	94
4.4	Conclusion	96
4.5	References.....	96
APPENDIX A. CHAPTER 2 SUPPORTIVE INFORMATION		98
APPENDIX B. CHAPTER 3 SUPPORTIVE INFORMATION		142
APPENDIX C. CHAPTER 4 SUPPLEMENTAL INFORMATION.....		156
PUBLICATIONS.....		189

LIST OF TABLES

Table 1.1 Class, subfamilies, and kinases of tyrosine receptor kinases.....	20
Table 1.2 Types and receptors serine/threonine receptor kinases	21
Table 1.3 Examples of non-receptor tyrosine kinases	22
Table 1.4. Select kinase IC ₅₀ and cell line IC ₅₀ data for approved CML inhibitors.....	34
Table 1.5. Examples of potency and binding affinity of select FLT3 inhibitors.....	36
Table 2.1 Calculated logP and antiproliferative activities of alkynyl analogs	59
Table 2.2: Inhibition of cellular ABL1 activity by imatinib, ponatinib, and HSN compounds	62
Table 3.1 Calculated LogP values and HPLC retention times	73
Table 3.2: IC ₅₀ of library against CML cell lines	74
Table 3.3: IC ₅₀ of ponatinib and HSN748 against several kinases.....	77
Table 3.4: Activities of HSN748 and ponatinib against FLT3, ABL1, FGFR and RET-driven cancers.....	80
Table 4.1. Antiproliferation activity of compound library against AML and CML cell lines	95

LIST OF FIGURES

Figure 1.1. Basic representation of kinase function.....	15
Figure 1.2 ⁵ Kinase tree of the human protein kinase families.....	16
Figure 1.3 Crystal structure of FLT3 (PDBID: 4RT7) to high light several key motifs within the kinase domain such as ATP Pocket, Hinge Region, α C-Helix, DFG motif, Activation Loop and Catalytic Loop.....	18
Figure 1.4 Over laying crystal structures (Blue: PDBID: 2GQG, and Green: PDBID: 3K5V) to show conformational changes in the DFG-motif.....	19
Figure 1.5. Schematic representation of how ligand binding triggers kinase activation	20
Figure 1.6. Regular expression verses over-expression of a receptor kinase leads to the over activation of downstream pathways.....	25
Figure 1.7. Translocation between Chromosome 9 and Chromosome 22 create the Philadelphia Chromosome.....	25
Figure 1.8 Approved kinase inhibitors from 2001-2020.....	28
Figure 1.9 A) Structures of all approved kinase inhibitors with similar features colored B) Examples of binding modes of select kinase inhibitors.....	29
Figure 1.10. Current Approved EGFR inhibitors	30
Figure 1.11. Approved BTK inhibitors	32
Figure 1.12. Approved BCR-ABL1 inhibitors	33
Figure 1.13. When FLT3 is unmutated the kinase requires ligand binding be be turned “on”. However, when the FLT3-ITD is present in either one or both kinases in the dimer, ligand is no longer needed and the receptor is constantly in its active state	34
Figure 1.14. FLT3 receptor with main domains shown as well as common mutations. Image from Taylor and Francis https://doi.org/10.1080/10428194.2017.1399312	35
Figure 1.15. Inhibitors that target FLT3 for AML. Midostaurin and gilteritinib are both approved by the FDA. Other have either gone through clinical trail and failed or are currently in clinical trial	36
Figure 2.1 Current first- and second-generation CML drugs	48
Figure 2.2 Initial Alkynyl compounds, which inspired the synthesis of new ABL1 inhibitors (see Figure 2.6)	50
Figure 2.3 Optimization stragety to improve drug-like properties and potency of first-generation compounds HSN356 and HSN286	51

Figure 2.4 Ponatinib and compound 9 bound to the ABL kinase domain. A) docked ponatinib bound to the ABL kinase domain. B) Docked compound 9 bound to the ABL kinase domain. All compounds were docked against PDBID: 3OXZ using GOLD software [23]. The hinge region is shown in green, the key T315 is colored red.....	52
Figure 2.5 ABL residues within 6 Å of the bound ponatinib (blue). Key hydrophobic residues are labeled. T315 is colored red, while residues that are part of the hinge region are green.....	53
Figure 2.6 Alkynyl aminoisoquinolines and aminonaphthyridines tested in study	54
Figure 2.7 Enzymatic inhibition against ABL1 wild-type and common mutations T315I and E255K. Screening of compounds was done as a service at Reaction Biology Corporation	55
Figure 2.8 Compounds 16 (HSN608), 15 (HSN459), 28 (HSN431), and 29 (HSN576) inhibit A)ABL1 and B) ABL1(t315I) at nanomolar IC ₅₀ values	56
Figure 2.9 Dose-response curves for inhibition of ABL1 and ABL1(T315I) in KCL22 and KCL22-IR, respectively, by imatinib, ponatinib, HSN431, HSN459, HSN576, and HSN608. IC ₅₀ values were determined by KinaSense (West Lafayette, IN, USA)	61
Figure 3.1 Examples of the necessary nitrogen concept. Introduction of nitrogen into initial hits led to remarkable activity enhancement as seen in A) cell division cycle 7 (Cdc7) kinase inhibitors; B) 5-HT3AR inhibitors; C) PLK1 inhibitors.....	70
Figure 3.2 A) nitrogen and methyl scan of ponatinib B) other ponatinib analogs.	72
Figure 3.3 Representative synthesis of analogs (HSN748). Conditions: i: HATU, DIPEA, DMF, 45°C, overnight. Yield = 85%; ii: Pd(PPh ₃) ₂ Cl ₂ , PPh ₃ , CuI, DMF, TEA, 45 °C, overnight. Yield = 53%. See SI for details about other analogs.....	73
Figure 3.4 Kinase inhibition against key kinases. Compounds were screened at the following concentrations; FLT3(ITD) – 4 nM, FLT3(D835Y) and c-Src - 111 nM, ABL1(T315I), MNK1&2 at 123 nM. Percent inhibition is with respect to DMSO control, which is 0% inhibition. Data provided by Reaction Biology Corp.	76
Figure 3.5: Dose response curves of ponatinib and HSN748 against Src and FLT3 (D835Y).....	78
Figure 3.6: Active sites of various kinases with bound ponatinib (orange). Gatekeeper residues of each kinase are shown in red, DGF- motifs are shown in purple, amino acid residues within 4 Å of ponatinib are shown in green. A) KIT, PDBID: 4V0I; B) ABL1 with the T315I mutation PDBID: 3IK3; C) FGFR1, PDBID: 4V01; D) FGFR4, PDBID: 4UXQ.....	79
Figure 4.1. Approved kinase inhibitors that contained isoquinolines, quinolines, indazoles, quinazolines, quinazolinones, quinoxalines, and oxindole	90
Figure 4.2.Examples of increased potency with the addition of a strategic methyl group (additional methyl groups shown in red). Increase in potency can be seen in inhibition of A) p38α B) OX ₁ R and C)S1P ₁	91
Figure 4.3. Previous analogs synthesized by the Sintim Lab that feature fused six-membered ring systems. HSN608 was reported as a potent inhibitor of ABL1 ⁷	91
Figure 4.4. Synthetic pathways for pyrido[3,4- <i>b</i>]pyrazine analogs.....	93

Figure 4.5. pyrido[3,4-*b*]pyrazine compound library93

Figure 4.6 Docking of HSL211 (left) and HSL476 (right) with FLT3 (PDBID: 4RT7). Both compounds have nitrogen that binds to the cystine at the 694 position in the hinge region (red). The free amine allows for an extra polar contact with the glutamic acid in the hinge region.96

LIST OF ABBREVIATIONS

ABL1	Abelson murine leukemia viral oncogene homolog 1
AKT	Protein kinase B
ALA	Alanine
AML	Acute Myeloid Leukemia
ATP	Adenosine triphosphate
BCR	Breakpoint Cluster Region protein
BRAF	v-Raf murine sarcoma viral oncogene homolog B
BTK	Bruton's tyrosine kinase
CLL	Chronic Lymphocytic Leukemia
CML	Chronic Myeloid Leukemia
DFG	aspartic acid (Asp), phenylalanine (Phe), Glycine (Gly)
EGFR	Epidermal Growth Factor Receptor
ERBB3 (HER3)	Human Epidermal Growth Factor Receptor
ERK	Extracellular signal-Regulated Kinase
FES	Feline Sarcoma Oncogene
FGFR	Fibroblast Growth Factor Receptor
FLT3	FMS-like tyrosine kinase 3
GLU	Glutamic acid
HCK	Hematopoietic Cell Kinase
ITD	Internal tandem duplication
JAK	Janus Kinase
JH	Janus Homology
KIF5B	Kinesin family member 5B
KIT	KIT proto-oncogene receptor tyrosine kinase
LEU	Leucine
LYN	LCK/Yes novel tyrosine kinase
MAPK	mitogen-activated protein kinase
MCL	Mantle Cell Lymphoma

MET	Mesenchymal to Epithelial Transition
NSCLC	Non-small cell lung cancer
PDGFR	Platelet-derived growth factor receptor
PHE	Phenylalanine
PI3K	Phosphoinositide 3-kinase
PRO	Proline
pTyr	Phosphotyrosine
RAF	Rapidly accelerated fibrosarcoma
RAS	Rat sarcoma
RET	Rearranged during transfection
RTK	Receptor tyrosine kinase
SH	SRC homology
SRC	Proto-oncogene tyrosine-protein kinase src
STAT	Signal transducer and activator of transcription
SYK	Spleen tyrosine kinase
TFG	Transforming growth factor
THR	Threonine
TYK2	Tyrosine kinase 2
TYR	Tyrosine

ABSTRACT

Cancer treatment was revolutionized when imatinib, a protein kinase inhibitor, was approved for the treatment of chronic myeloid leukemia (CML) in 2001. Imatinib increased the five-year survival rate of CML to over 90%. Imatinib is successful because it can selectively target BCR-ABL1, the mutant kinase driver to CML. Since then, there have been over 50 small molecules approved by the FDA to treat various cancers, which are driven by aberrantly expressed or mutated protein kinases. These kinase inhibitors (KIs) target kinases such as KIT (to treat gastrointestinal stromal tumors), EGFR (to treat lung cancer), and MEK (to treat melanoma) and often inhibit the kinases by binding to the ATP binding site or an allosteric site. Despite the successes seen with these approved KIs, responses are often transient. Most patients relapse after only a few months of responding to first and second generation KIs due to mutations to the kinases and/or upregulation of compensatory pathways. For cancer-driver kinases such as BCR-ABL1 or FLT3-ITD, which are oncogenic due to a fusion protein (BCR fused to ABL1) or internal tandem duplication within the juxtamembrane domain (FLT3), relapse can also occur due to the emergence of additional mutations in the kinase domain (a phenomenon termed secondary mutation). For example, secondary mutation (T315I or E255K) in BCR-ABL1 leads to imatinib resistance whereas secondary mutation (F691L or D835Y/V/H) in FLT3-ITD leads to resistance to many first- and second-generation FLT3 inhibitors. Gilteritinib, a recently approved FLT3 inhibitor drug for acute myeloid leukemia (AML) is not effective against AML harboring FLT3-ITD (F691L). Thus, there is a clinical need for novel chemotypes that inhibit drug-resistant kinases, especially those containing secondary mutations.

Many of the FDA-approved kinase inhibitors contain common heterocycles such as quinolines, indazoles, quinazolines, quinazolinones, quinoxalines, and oxindole. The majority of KIs also contain groups that enhance aqueous solubility, such as morpholine and piperazine rings. Additionally, many KIs contain halogen substituents (mainly Cl and F). This thesis introduces novel kinase inhibitors, which contain the less explored isoquinolines, naphthyridines, and pyrido[3,4-b]pyrazine cores. These newly introduced kinase inhibitors potently inhibit drug-resistant ABL1 and FLT3 kinases, harboring secondary mutations, and have the potential for clinical translation against relapsed leukemia.

CHAPTER 1. INTRODUCTION

1.1 Protein Kinase

Enzymes that regulate the biological activity of proteins via the phosphorylation of an amino acid residue from ATP are known as protein kinase¹. Kinases can exist in different states (active or inactive) depending on environmental or cellular conditions. When the kinase switches from an inactive form to an active form it allows for the binding of ATP, which then allows for the signaling pathway to be activated².

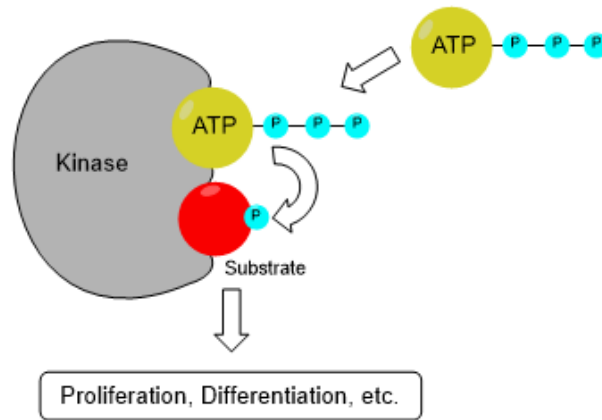


Figure 1.1. Basic representation of kinase function

There are currently over 500 known kinases in the human genome³. They are broken down into several families based on structure and function similarities (Figure 1.2)^{4,5}. One main distinction among kinases is which amino acid within the active site takes part in phosphorylation. Kinases can either receive the γ -phosphate at either a tyrosine or at a serine/threonine⁴. Each kinase plays a role in several different cellular processes such as differentiation and proliferation. Disruption of these pathways has been linked to various diseases such as cancer⁶.

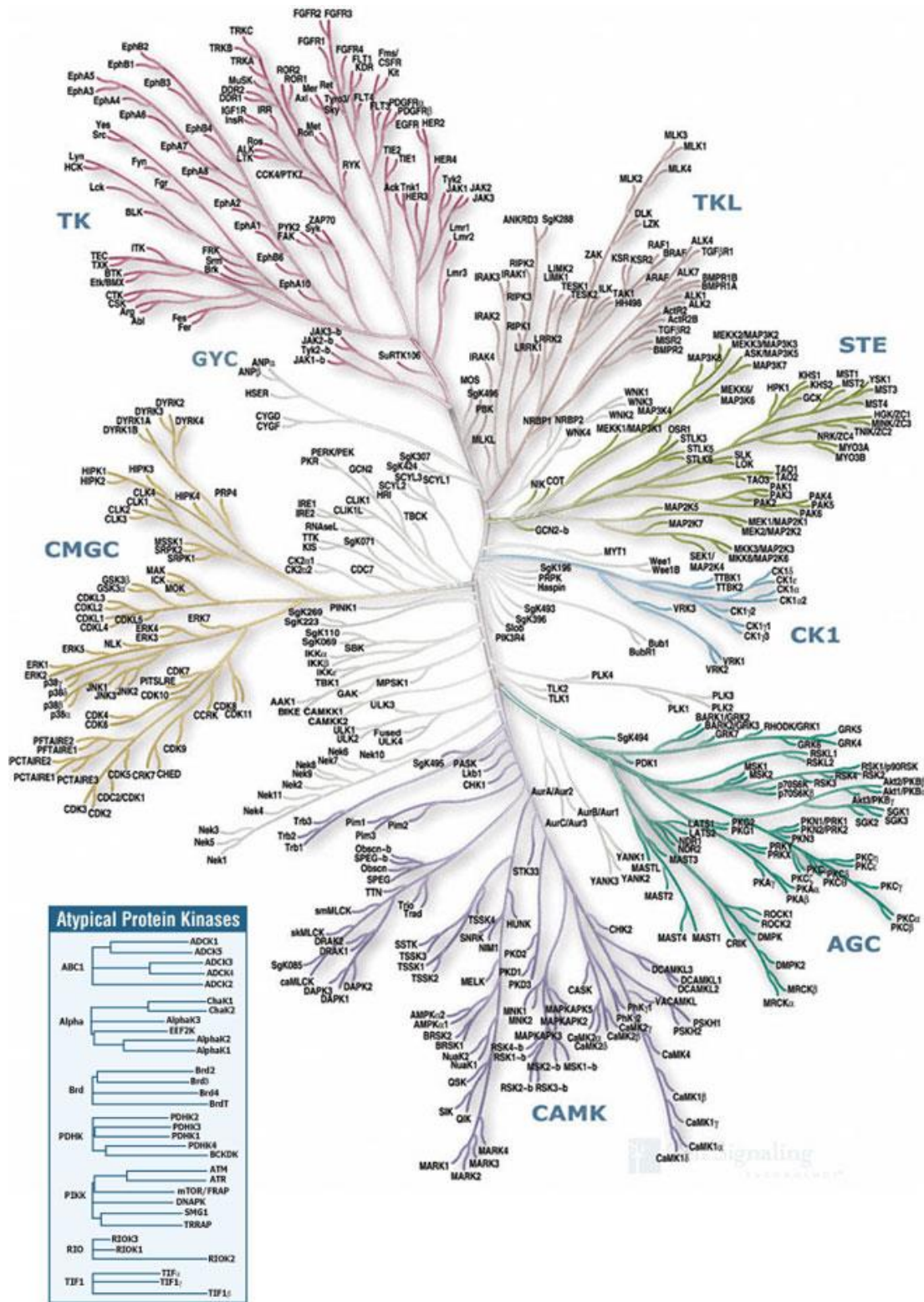


Figure 1.2⁵ Kinase tree of the human protein kinase families Illustration reproduced courtesy of Cell Signaling Technology, Inc. (www.cellsignal.com)

1.2 Structure

Kinases are known to have very similar structures that is highly conserved between kinases. All kinases contain a SH1 or kinase domain, which is where ATP binding occurs. Some kinases, such as non-receptor kinases, also contain SH2 and SH3 domains as well as a unique kinase domain^{7,8}.

1.2.1 The SH1 domain (Kinase Domain)

While different types of kinases may vary in the overall structure, such as a RTKs and cytoplasmic kinases, the kinase domains have a conserved structure among them regardless of their family. Key kinase domain features include the ATP Pocket, Hinge Region, α C-Helix, DFG motif, Activation Loop and Catalytic Loop (Figure 1.3). The kinase domain contains an N-lobe, consisting of five β -sheets and an α C-helix, and the C-lobe which primarily consists of α -helices⁹. The α C-helix in the N-lobe plays a role in the catalysis and the transition between the active and inactive states of the kinase¹⁰. The DFG-motif consists of aspartic acid (D), phenylalanine (F), and glycine (G) residues, also plays a role in the active and inactive states of the kinase¹¹.

The activation loop participates in substrate binding and proper positioning of the substrate for phosphorylation¹². It also contains one or more phosphorylation sites, which are important for the kinase activation process. The catalytic loop coordinates one of the necessary Mg^{2+} ions that are needed for ATP binding¹³.

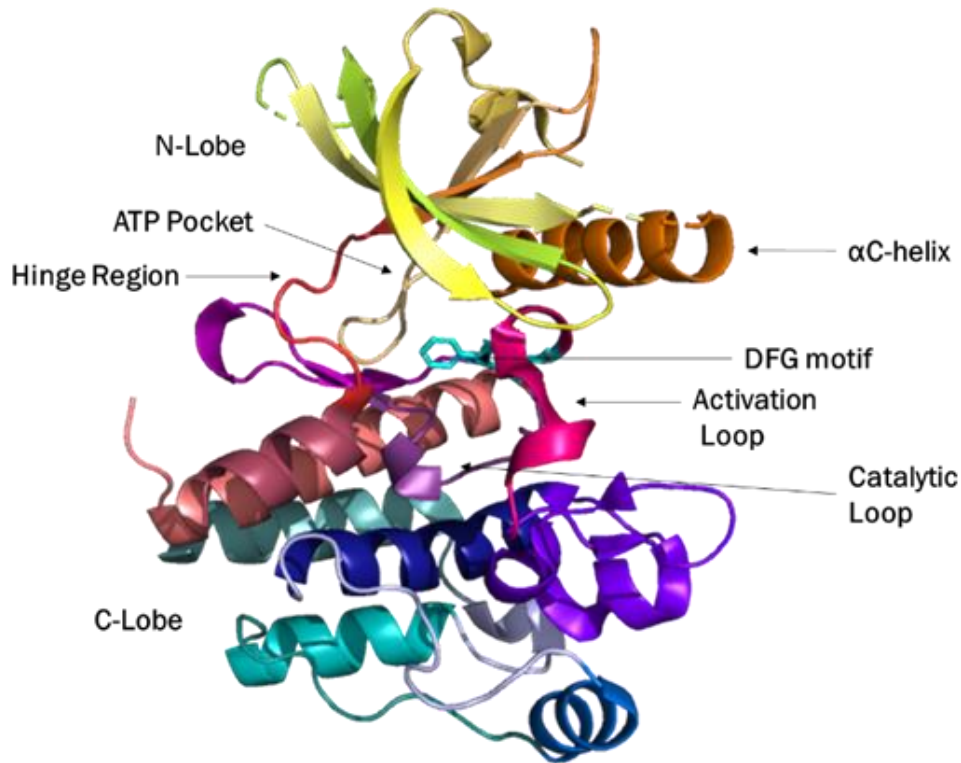


Figure 1.3 Crystal structure of FLT3 (PDBID: 4RT7) to highlight several key motifs within the kinase domain such as ATP Pocket, Hinge Region, α C-Helix, DFG motif, Activation Loop and Catalytic Loop

The DFG-motif, located in the activation loop, can either be in an “in” or “out” conformation. When this motif is in the “in” conformation, the kinase is in its active form and when it is in the “out” conformation the kinase is in the inactive form¹⁴. When the kinase shifts to its active conformation, with the DFG- motif “in”, the aspartic acid coordinates to a magnesium ion¹⁵. This prepares the terminal phosphate group on ATP for transfer to the kinase. The phenylalanine shifts to under the C-helix which allows for proper positioning for it and the activation loop¹⁵. Once the phosphate group is transferred, the kinase can then move back to its inactive, DFG “out” form¹⁵.

BCR-ABL1 kinase, is a fusion kinase consisting of ABL1 kinase fused to BCR to create the Philadelphia chromosome oncogene¹⁶. The crystal structure for both types of ABL1 kinase (DFG-in or DFG-out) have been solved, in complex with inhibitors^{17,18}. Figure 1.4 shows the overlay of two BCR-ABL1 crystal structures (Blue: PDBID: 2GQG, and Green: PDBID: 3K5V).

The magenta residues show the DFG-motif “in” conformation while the yellow residues show a DFG “out” conformation.

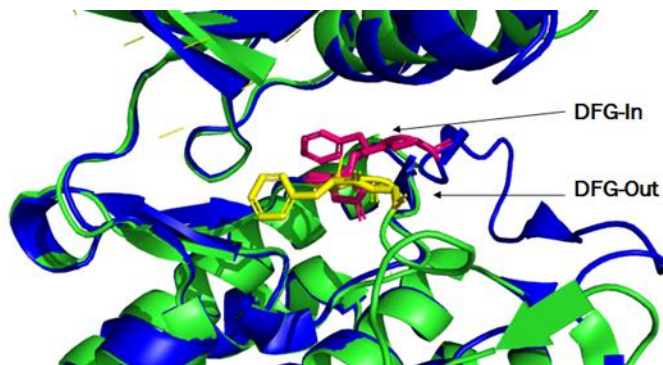


Figure 1.4 Over laying crystal structures (Blue: PDBID: 2GQG, and Green: PDBID: 3K5V) to show conformational changes in the DFG-motif

1.2.2 SH2/3 Domain

The SH2 domain binds to phosphorylated residues on other proteins, while the SH3 domain dictates protein-protein interactions¹⁹. The SH2 domain consists of about 100 amino acids that have the ability to bind pTyr residues¹⁹. This domain can selectively bind to specific kinases depending on the amino acid sequences around the corresponding pTyr^{20,21}. The SH3 domain contains about 60 amino acids that form 5-8 β -strands²². The SH3 domain recognizes proline rich sequences in other kinases which allows for substrate binding²².

Not all kinases have both a SH2 and a SH3 domain. For example, the FES family of kinases only contain a SH2 domain and do not contain a SH3 domain²³. The FAK family of kinases do not have a SH2 domain or a SH3 domain²⁴.

1.3 Function

1.3.1 Receptor Kinases

Receptor kinases are regulators in cellular processes and are located on the surface of the cell²⁵. They regulate processes such as cell proliferation, differentiation, and survival as well as metabolism, cell migration and cell cycle control²⁶.

Receptor kinases also have a similar overall architecture. This includes an extracellular ligand binding region(s) that connects through a single transmembrane α -helix to the cytoplasmic

region. The cytoplasmic region can contain one or more protein tyrosine kinase domain or a pseudo kinase domain²⁷. RTKs also contain additional C-terminal and juxtamembrane regulatory regions²⁷.

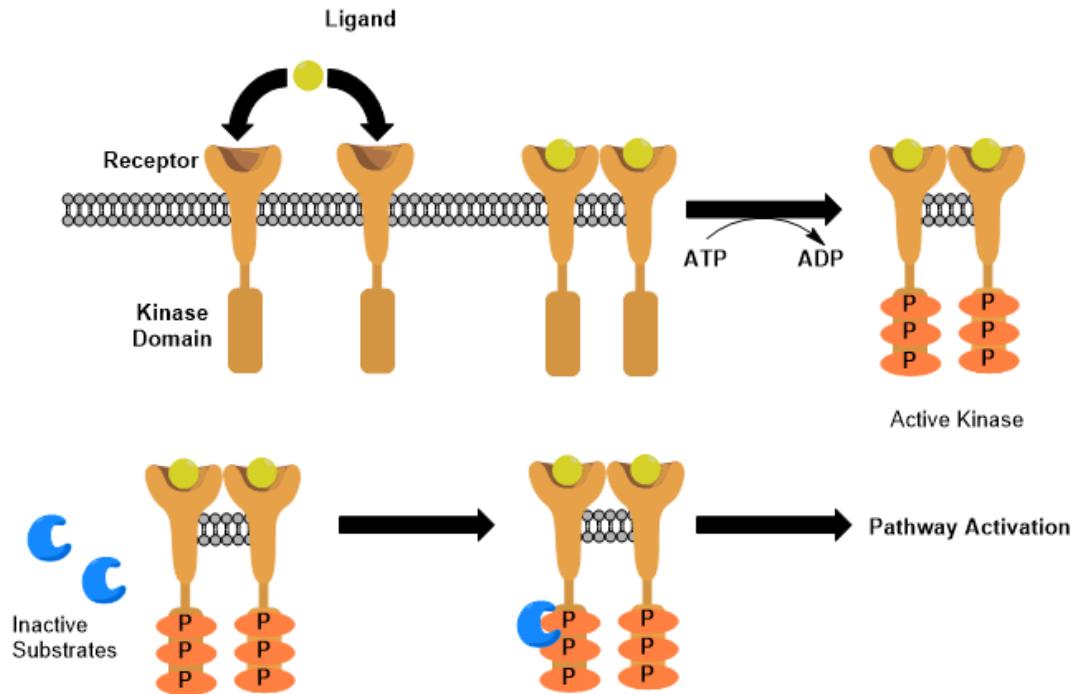


Figure 1.5. Schematic representation of how ligand binding triggers kinase activation

Receptor kinases are activated upon extracellular ligand binding. Upon ligand binding, receptors dimerize and initiate the activation pathway²⁵. This dimerization allows ATP to enter the binding site of the kinase and phosphorylates an amino acid residue within the active site (tyrosine, serine, or threonine, depending on the kinase type)²⁸. Substrates can then bind to the activated protein and allow for downstream signaling and cellular processes to occur (Figure 1.5)²⁹.

Table 1.1. Class, subfamilies, and kinases of tyrosine receptor kinases

Class	Subfamily	Kinases
I	EGFR	EGFR, ERBB2-4
II	Insulin R	INSR, IGF1R
III	PDGFR	PDGFR α , PDGFR β , M-CSFR, KIT, FLT3
IV	VEGFR	VEGFR1-3
V	FGFR	FGFR1-4
VI	CCK	CCK4

Table 1.1. continued

VII	NGFR	TRKA, TRKB, TRKC
VIII	HGFR	MET, RON
IX	EFHR	EPHA1-6, EPHB1-6
X	AXL	AXL, MER, TYRO3
XI	TIE	TIE, TEK
XII	RYK	RYK
XIII	DDR	DDR1, DDR2
XIV	RET	RET
XV	ROS	ROS
XVI	LTK	LTK, ALK
XVII	ROR	ROR1, ROR2
XVII	MUSK	MUSK
XIX	LMR	AATYK1-3
XX	Undetermined	RTK106

There are 58 known tyrosine receptor kinases which are separated into 20 subfamilies, which phosphorylate a tyrosine in the active site (Table 1.1)²⁵. Examples of receptor tyrosine kinases include FLT3, FGFR1-4, and PDGFR α/β . Serine/threonine receptor kinases are less common than receptor tyrosine kinases. There are only 13 receptor serine/threonine kinases which are divided into 3 types (Table 1.2)³⁰. One example includes TGF- β which is produced by T-cells and plays a role in regulating replication, differentiation, bone formation and haematopoiesis³¹.

Table 1.2. Types and receptors serine/threonine receptor kinases

Type	Receptors
I	ALK1, ALK2, BMPR1A (ALK3), ALK4, TGFBR1 (ALK5), BMPR1B (ALK6), ALK7
II	ActR2, ActR2B, MISR2, BMPR2, TGFBR2
III	TGFBR3

1.3.2 Non-Receptor Kinases

Non-receptor protein kinases are located in the cytoplasm and rely on the signaling cascade for activation⁷. Non-receptor tyrosine protein kinases can be divided into 9 subfamilies based on their overall structure (Table 1.3)³². These structural distinctions are based on their catalytic domain, pTyr binding domain (SH2 domain), and protein – protein interaction domain (SH3)⁷. They contain a similar structure to the receptor kinases however, they lack a ligand binding domain

and a transmembrane spanning region³³. They can include both tyrosine kinases as well as serine/threonine protein kinases.

Table 1.3. Examples of non-receptor tyrosine kinases

Family	Kinase(s)
ABL	ABL1, ARG
ACK	ACK1, TNK1
CSK	CSK, MATK
FAK	FAK, PYK2
FES	FES, FER
JAK	JAK1, JAK2, JAK3, TEK
SRC	SRC, FGR, FYN, YES1, BLK, HCK, LCK, LYN
SYK	SYK, ZAP70
TEC	TEC, BMX, BTK, ITK, TXK

Unlike receptor kinases, which are activated upon ligand binding, non-receptor protein kinase activation varies more depending on the kinase. Src is a kinase that has been heavily studied for its implication in cancer³⁴. Like other non-receptor kinases, Src kinase consists of a SH1 catalytic domain, a SH2 domain, a SH3 domain, a unique domain, and a myristoyl group³⁵. The three components that control the activity of Src are often referred to as the latch, clamp, and switch³⁶. The latch is formed when the SH2 domain binds to the pTyr530 at the C-terminus tail thus stabilizing the SH2 domain³⁶. However, when the pTyr530 is displaced from the binding pocket the kinase can unlatch and will no longer lock the catalytic domain into the inactive position³⁷. The SH3 domain binds to the N-lobe of the kinase domain with the help of a proline at the 249 position from the SH2 domain²². The clamp comes as a result of the SH2 and SH3 domains binding to the kinase domain that allows for an autoinhibition of the enzyme³⁷. The switch is the activation loop in the kinase domain, which allows for the change between the active and inactive states of the following the autophosphorylation via partner SRC molecules³⁸. Once the unlatching occurs from the SH2 domain, the tyrosine419 can go through autophosphorylation. This phosphorylation stabilizes the kinase into its active state³⁶.

1.3.3 Pseudokinases

Pseudokinase domains lack amino acids that are usually needed to correctly align the ATP and metal ions needed to phosphorylate the protein substrate³⁹. About 10 % of kinases in the

proteome contain intracellular pseudokinase domains that lack one or more of the conserved catalytically important residues⁴⁰. Despite low catalytic activity, these kinases could still carry out their signaling roles⁴¹. Pseudokinases are believed to fall into four roles; modulator, competitor, anchor, and signal integrator⁴². Although pseudokinases lack the typical catalytic activity, they are still able to form homo- and hetero-dimers which could still allow these kinases to regulate cellular activity³².

The JAK family consists for JAK1, JAK2, JAK3 and TYK⁴³. The JH1 domain contains a traditional kinase domain (similar to a SH1), that is activated by cytokine receptors⁴⁴. The JH2 domain is a pseudokinase domain that lacks the catalytically active Asp⁴⁴. This Asp is needed for the transfer the γ - phosphate to the alcohol on the tyrosine residue⁴⁴. JH1 is negatively regulated by JH2. Despite the lack of Asp residue, it is still believed that JAK2 signaling is regulated via ATP-binding⁴⁴.

1.3.4 Atypical Kinases

Typically, kinases have a very conserved structure. However, there is a small cluster of about 58 kinases that have a very low sequence similarity, known as atypical kinases⁴⁵. Unlike typical kinases, which have a glycine rich p-loop needed for catalytic activity, atypical kinases lack this loop⁴⁵. Typical kinases also contain an Ala-Pro-Glu motif which atypical kinases lack this motif. Instead they contain a Pro-Phe-X-Leu-Thr motif with the Thr being phosphorylated⁴⁵.

Lipid kinases phosphorylate lipids that are found both on the plasma membrane and on the membranes of the organelles⁴⁶. Lipid kinases are considered atypical kinases. These kinases play a role in cell signaling and endocytosis and exocytosis as well as other trafficking events⁴⁷. They also play an important role in insulin signaling and could be seen as a target for chronic pain^{48,49}. Examples of lipid kinases include PI3K and SYK1/2¹⁵.

1.4 Kinase Mutations

Kinases allow for very regulated cellular processes. Any disruption or mutation within these kinases can result in either attenuation of catalytic activity or enhanced and/or uncontrolled activity, leading to various diseases. This includes cancer, degenerative diseases and immune system diseases⁵⁰.

1.4.1 Gain-of-Function/ Activating Mutation

Gain-of-function mutations can be seen across multiple types of cancers. These mutations cause an enhanced activity of the kinase⁵¹. In a gain of function mutation, receptor tyrosine kinases are no longer subject to the typically regulated process of ligand binding in a receptor kinase that leads to activation⁵². These mutations can be in the extracellular domain, transmembrane domain, or the juxtamembrane domain⁵². Point mutations, reduplication of DNA sequences which contain a proto-oncogene and chromosomal translocation can all lead to a gain-of-function mutation⁵³.

EGFR somatic mutations are an example of gain-of-function mutations. This mutation within the kinase domain allows for hyperactivity, which then causes an unregulated downstream cascade which leads to oncogenic properties⁵⁴. Other gain-of-function point mutations include D835 in FLT3, D816 in KIT, and V600 in BRAF⁵⁵⁻⁵⁷.

1.4.2 Loss- of-Function/ Inactivating Mutation

Loss of function or inactivating mutations causes kinases to have little to no function. When the loss of function occurs in a tumor-suppressor protein such as p53, cancer can form. Tumor suppressor, p53, aids in regulation of cellular processes such as DNA repair and apoptosis⁵⁸. When DNA is damaged this protein determines if the DNA will repair itself or if it will undergo apoptosis⁵⁹. Mutations in this protein has been linked to urinary, breast, and ovarian cancer^{60,61}. There is currently no treatment that allows for the reactivation of the function of the tumor suppressor⁶².

1.4.3 Over-Expression or Amplification

Over-expression of a receptor tyrosine kinase leads to an increase in kinase activity due the presence of more receptors (Figure 1.6). While this is often due to gene amplification, overexpression can also occur due to transcriptional/translational enhancement⁶³.

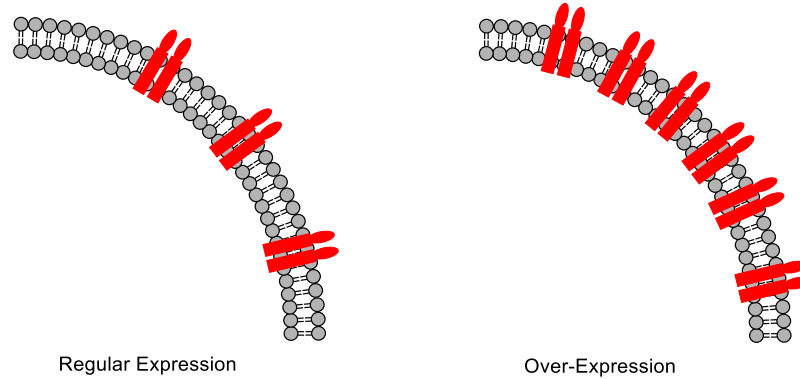


Figure 1.6. Regular expression versus over-expression of a receptor kinase leads to the over activation of downstream pathways

Overexpression of kinases can be seen in several cancers such as lung cancer (MET), breast (FGFR3), melanoma (KIT), and GIST (KIT)^{64–67}.

1.4.4 Fusion

The Philadelphia chromosome, also known as the BCR-ABL1 protein, is created by the translocation between the ABL1 gene of chromosome 9 and the BCR gene of chromosome 22 (Figure 1.7)¹⁶. This BCR-ABL1 is an oncogene that is constitutively active⁶⁸. BCR-ABL1 phosphorylates SRC family kinases such as HCK and LYN and binds to activators of the RAS pathway⁶⁹.

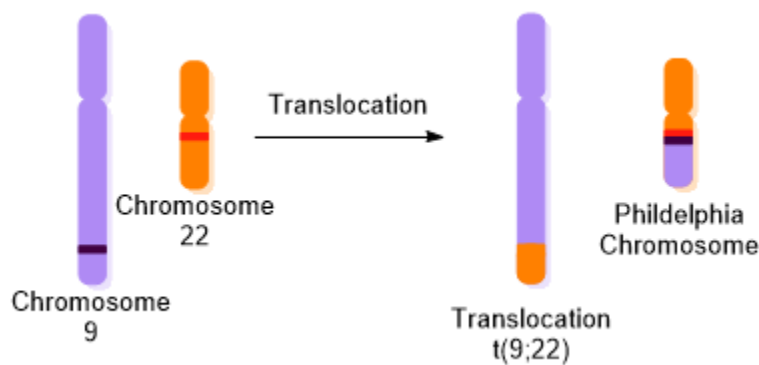


Figure 1.7. Translocation between Chromosome 9 and Chromosome 22 create the Philadelphia Chromosome

A translocation between RET and KIF5B allows for a ligand independent dimerization, which causes activation in other pathways such as the PI3K/AKT pathway and JAK/STAT pathway⁷⁰. This fusion protein has been seen in lung cancers such as NSCLC and lung adenocarcinoma⁷¹.

1.5 Treatment of Cancer with Kinase inhibitors

Mutations in the kinases can cause activations and unregulated and uncontrolled cell responses, which can lead to cancer⁷². Imatinib was the first approved kinase inhibitor for Chronic Myeloid Leukemia in 2001⁷³. Since 2001, there has been a steady increase in kinase inhibitors that has resulted in over 50 approved kinase inhibitors to date (Figure 1.8). These inhibitors target a range of kinases including BCR-ABL1, EGFR, FLT3, and JAK1&2.

There are several different types of kinase inhibitors, which are based on their binding mode to the kinase. Type I kinase inhibitors bind to the active conformation of the kinase at the ATP-binding pocket with the DFG-motif in an “in” conformation⁷⁴. Type I½ binds to the inactive kinase with the DFG-motif in its “in” conformation. Type II inhibitors bind to the inactive DFG- “out” conformation⁷⁴. Type III and Type IV kinase inhibitors are allosteric inhibitors. However, Type III binds next to the ATP site while Type IV are bound elsewhere on the kinase⁷⁴. Type V kinase inhibitors are bivalent inhibitors that span two regions in the kinase⁷⁴. Type VI kinase inhibitors are covalent inhibitors that react with the kinase and form a covalent bond⁷⁴. It is also possible to target the substrate binding site on a kinase⁷⁵⁻⁷⁷. Targeting this site could allow for more selectivity compared to that of targeting the ATP binding site⁷⁸.

As kinase inhibitors are developed and approved, common moieties begin to appear. 4-(pyridin-3-yl) pyrimidine can be seen in both imatinib and nilotinib which are both approved BCR-ABL1 inhibitors (Figure 1.9A). However, imatinib contains a 4-((4-methylpiperazin-1-yl) methyl) benzamide and nilotinib contains a 3-(4-methyl-1H-imidazol-1-yl)-5-(trifluoromethyl)benzamide (Figure 1.9A). Quinazoline are also common core structures and can be seen in gefitinib, erlotinib, and vandetanib (Figure 1.9A). Inhibitors such as ibrutinib also contain a covalent inhibitor moiety, which allows for the compound to form a bond with the kinase, leading to irreversible inhibition (Figure 1.9A).

Many kinase inhibitors also take on similar binding modes. Different parts of a molecule interact with different parts of the active site such as the hinge region of the kinase, hydrophobic

pockets, and solvent regions (Figure 1.9B). Due to the conserved active site among kinases, and similarities in binding modes from inhibitors, there can often be a lack a selectivity which can lead to off target effects and toxicities⁷⁹.

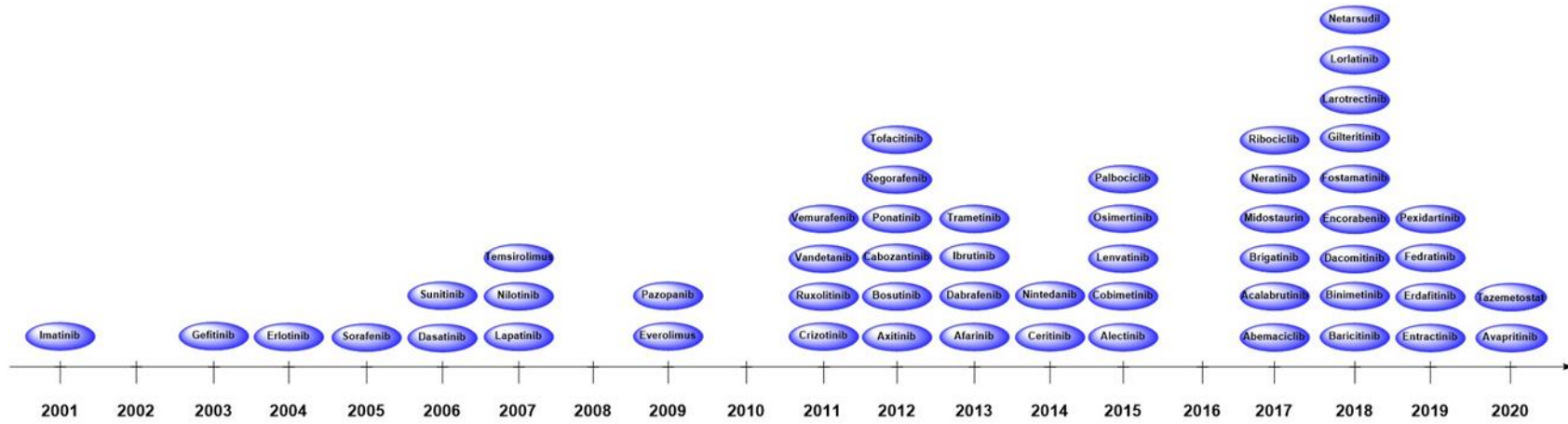


Figure 1.8. Approved kinase inhibitors from 2001-2020

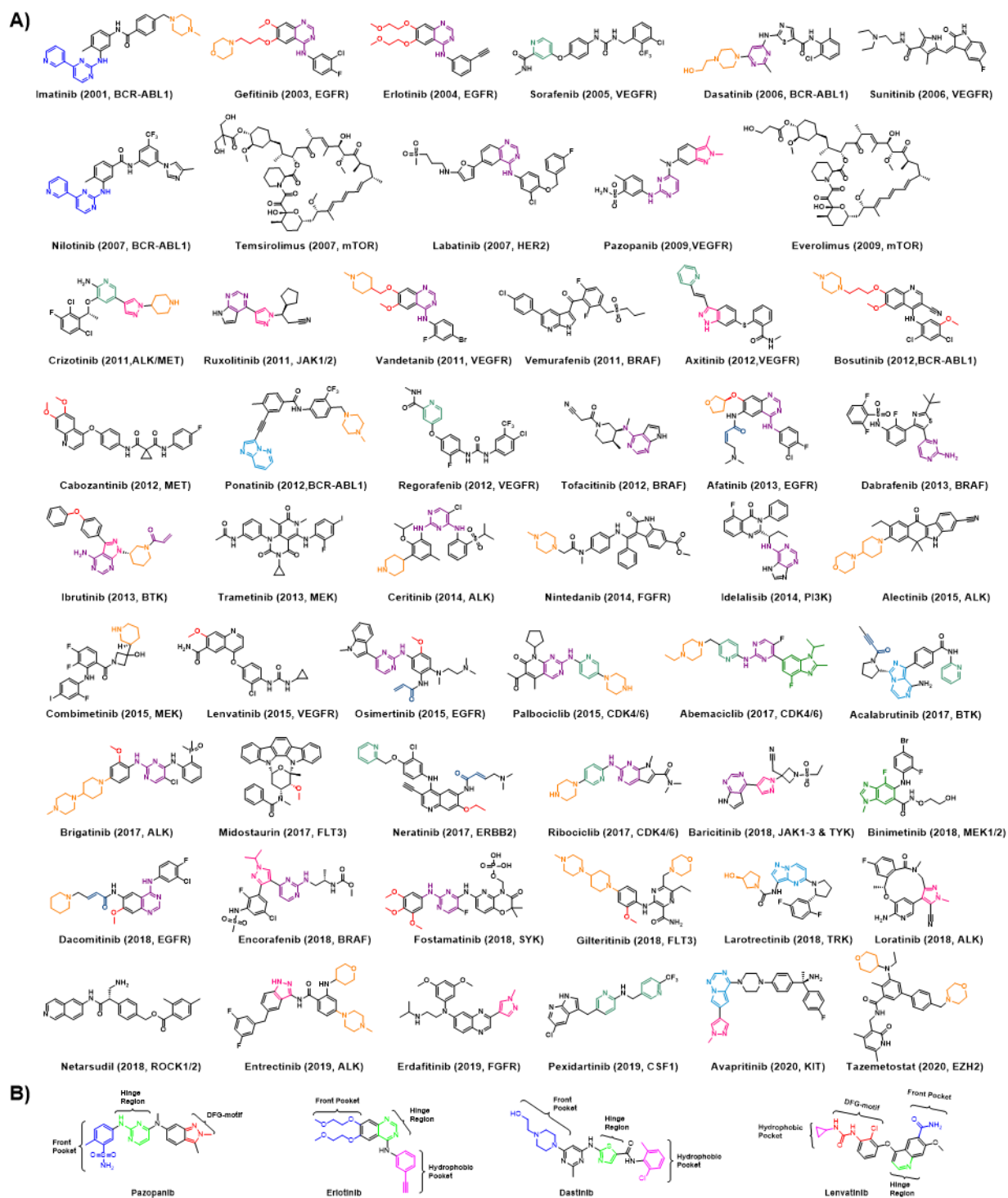


Figure 1.9. A) Structures of all approved kinase inhibitors with similar features colored B) Examples of binding modes of select kinase inhibitors

1.6 Relapse in Cancer Treatment

1.6.1 Epithelial Growth Factor Receptor (EGFR)

EGFR is a receptor tyrosine kinase that is part of the ErbB family⁸⁰. It plays an important role in epithelial cell physiology as well as cell survival, proliferation, and differentiation⁸⁰. Once the ATP phosphorylates the tyrosine and homo- or heterodimerization occurs, the protein becomes activated. Upon this activation is a downstream cascade allowing various cellular processes to occur. EGFR plays a role in the RAS/RAF/ MAPK pathways as well as the PI3K/AKT pathway⁸¹. Dysregulation, amplification and activations of EGFR has been linked to several cancers such as NSCLC, breast, and colon cancer⁸². Despite good initial response so treatment, over the course of time, resistance can be seen in patients.

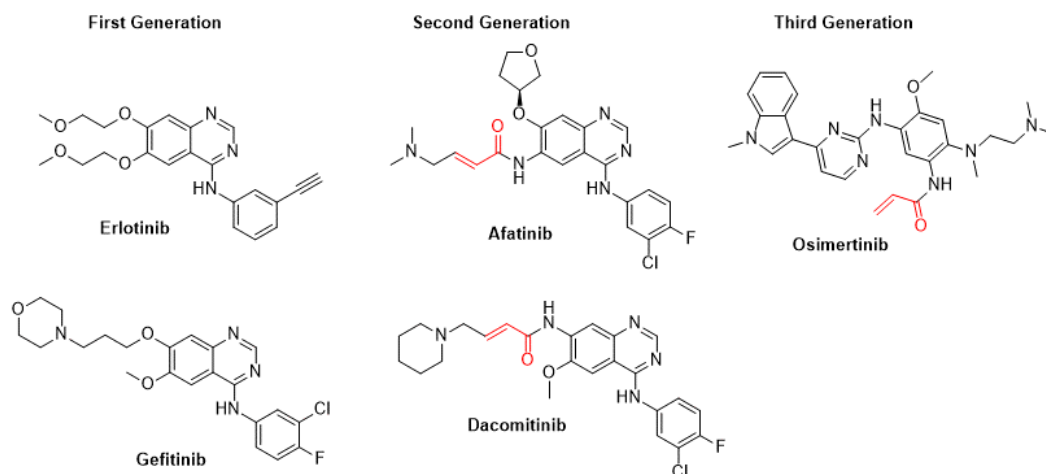


Figure 1.10. Current Approved EGFR inhibitors

The first line of treatment for EGFR driven cancers are erlotinib (approved in 2004) and gefitinib (approved in 2015)^{83,84}. Both compounds are reversible inhibitors of EGFR, which compete with ATP for the binding site. Over time, both drugs start to be less effective due to resistance. One possible mechanism of resistance is the T790M mutation within the binding site⁸⁵. The T790M mutation, also known as a gatekeeper mutation, occurs when the threonine at the 790 position of the kinase is mutated to a methionine at that position⁸⁵. MET is also commonly expressed in several overlapping cancers that EGFR plays a role in⁸⁶.

Second generation TKIs include dacomitinib (2018) and afatinib (2013 with expanded approval in 2018)^{87,88}. Both second-generation inhibitors contain an α , β -unsaturated amide (Figure 1.10). This moiety is a covalent inhibitor, which allows the compounds to irreversibly bind in the ATP-binding pocket⁸⁹. These second-generation compounds bind with the cysteine at the 797 position within the kinase⁹⁰. However, as seen with erlotinib and gefitinib, over time resistance can be seen and a C797S secondary mutation occurs⁹⁰. This changes the cysteine, which was the basis of the covalent binding with the second-generation compounds, to a serine. Osimertinib is a third-generation covalent EGFR inhibitor⁹¹. However, Osimertinib is still ineffective against the C797S mutation⁹¹.

1.6.2 Bruton's Tyrosine Kinase (BTK)

BTK plays a role in B-cell maturation and mast cell activation as well as regulating cell differentiation and signaling⁹². BTK is a serine/threonine kinase that is part of the TEC family and is located at the cell membrane⁹³. SYK kinase initially phosphorylates BTK at the TYR-551 residue⁹⁴. BTK can then undergo autophosphorylation at Tyr-223 to become active⁹⁴. The BTK activation cascade in B-cells leads to proliferation and survival signaling within the cell. BTK is overexpressed in several cancers such as CLL, MCL, and multiple myeloma⁹⁵. Due to its overexpression, it was seen as a possible target for future treatment.

Approved in 2013, ibrutinib is a first generation BTK inhibitor used to treat CLL, MCL and other B-Cell Malignancies⁹⁶. As seen in several EGFR inhibitors previously mentioned, ibrutinib contains an α , β -unsaturated amide to make an irreversible inhibitor (Figure 1.11)⁹⁷. This allows ibrutinib to bind in the ATP binding pocket to the cysteine at 481 and inhibits autophosphorylation⁹⁷.

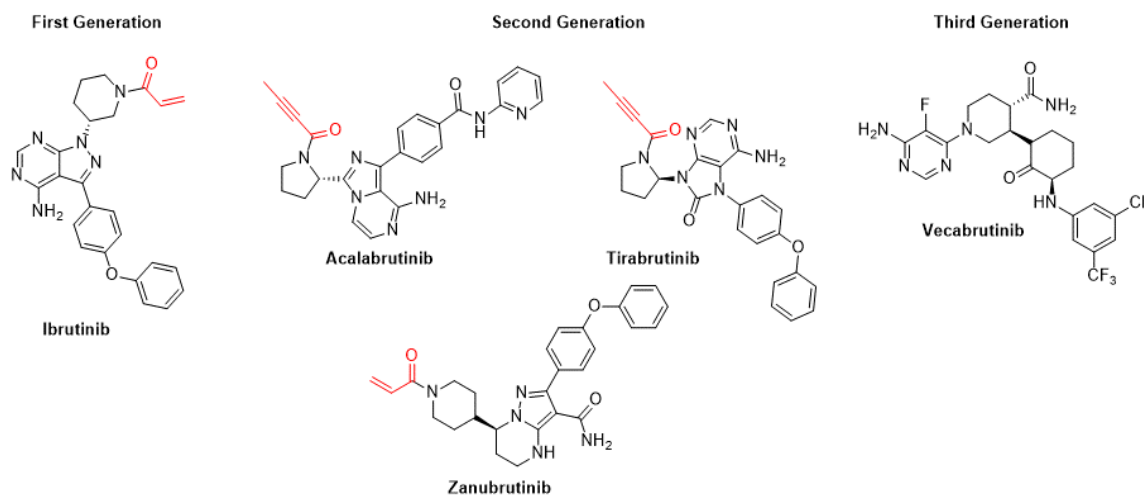


Figure 1.11. Approved BTK inhibitors

Common side effects of ibrutinib include bleeding, rash, and atrial fibrillation as well as off target effects due to additional inhibition of EGFR kinases⁷⁶. Resistance is also seen after prolonged drug use due to a point mutation. A substitution to a serine from a cysteine at the 481 position in the kinase domain disrupts the irreversible inhibition seen in ibrutinib⁹⁸. Acalabrutinib, tirabrutinib and zanubrutinib are irreversible second-generation inhibitors that are either approved or in clinical trial (Figure 1.11)⁹⁹⁻¹⁰¹. Acalabrutinib is more selective compared to ibrutinib, which limits off target toxicities¹⁰². However, similar to ibrutinib it binds to the cysteine at the 481-position suggesting that after prolonged treatment acalabrutinib could become ineffective⁹⁸. Tirabrutinib also works under the same covalent inhibition mechanism and will start to see resistance¹⁰³. Zanubrutinib is also a covalent, irreversible inhibitor to use target BTK driven cancers¹⁰⁴. Vecabrutinib is a third generation, reversible inhibitor that inhibits BTK and is currently in clinical trial¹⁰⁵. Due to its lack of α , β -unsaturated amide, vecabrutinib maintains its potency against the C481S mutation¹⁰⁶. It also does not inhibit EGFR which is where many off target toxicities were from in the previous generation of inhibitors¹⁰⁶.

1.6.3 BCR-ABL1

As previously mentioned, the BCR-ABL1 fusion protein is the kinase driver of chronic myeloid leukemia. The approval of imatinib in 2001 increased the five-year survival rate of CML

from about 30% to over 80%¹⁰⁷. Although imatinib is effective as a first line treatment, resistance does occur over time.

After prolonged imatinib treatment, the protein undergoes a mutation from glutamic acid at the 255 position to a lysine¹⁰⁸. This mutation renders imatinib ineffective (Table 1.4). Several second-generation BCR-ABL1 inhibitors This led to development of second-generation inhibitors dasatinib and nilotinib which are both effective against this mutation (Figure 1.12, Table 1.4)¹⁰⁹. However, a gate-keeper mutation at the 315 position of BCR-ABL1 kinase frequently occurs¹¹⁰. A leucine is substituted for a threonine causing imatinib, dasatinib, and nilotinib to be ineffective¹¹⁰.

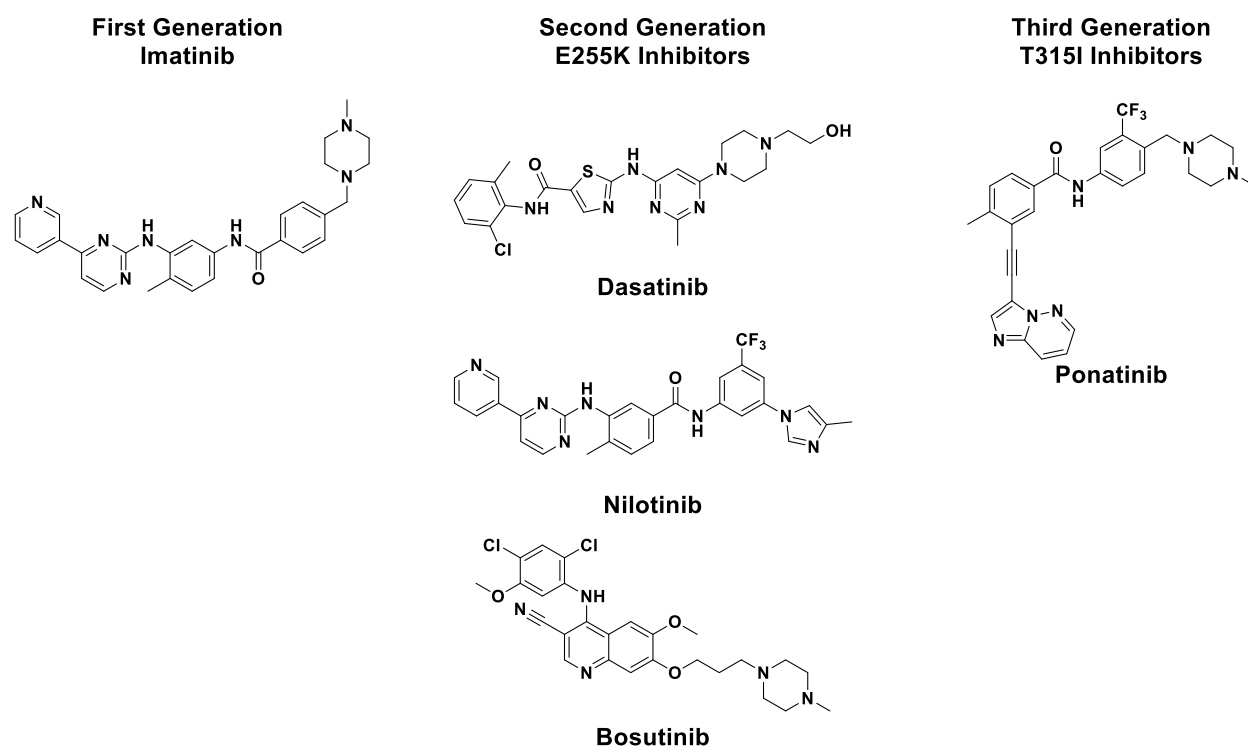


Figure 1.12. Approved BCR-ABL1 inhibitors

Ponatinib is the only approved kinase inhibitor that is active against the BCR-ABL1 T315I mutation (Table 1.4)¹¹¹. This is due to the alkyne linker which allows the molecule to bypass the mutation¹¹². However, ponatinib is a very promiscuous inhibitor and is active against many kinases, which leads to many off target toxicities¹¹³. These off-target effects drive the need for a more selective inhibitor that is also potent against secondary mutations.

Table 1.4. Select kinase IC₅₀ and cell line IC₅₀ data for approved CML inhibitors

Approved Inhibitor	BCR-ABL1 Kinase IC ₅₀ (nM) ¹¹¹			Cell Line IC ₅₀ ¹¹⁴		
	Wild Type	E255K	T315I	K562	KCL22	KCL22-IR
Imatinib	100-500	3174-12,100	76,400-20,000	88.6	83.7	>1 μM
Ponatinib	0.5	14	11	0.60	0.14	0.66
Dasatinib	0.8-1.8	5.6-13	137-1,000	-	-	-
Nilotinib	<10-25	118-566	697-10,000	-	-	-
Bosutinib	41.6	394	1890	-	-	-

1.6.4 FMS-like Tyrosine Kinase 3 (FLT3)

FLT3 is a receptor kinase that is part of the receptor tyrosine kinase class III family¹¹⁵. FLT3 signaling is important for development of progenitor cells and haematopoietic stem cells¹¹⁶. It plays a role in early stage development of myeloid and lymphoid cells¹¹⁷. Upon ligand binding, FLT3 dimerizes, which leads to the exposing of phosphorylation sites in the active site¹¹⁵. FLT3 has downstream pathways including the RAS/MEK/ERK pathway as well as the PI3K/AKT pathway (Figure 1.13)¹¹⁸.

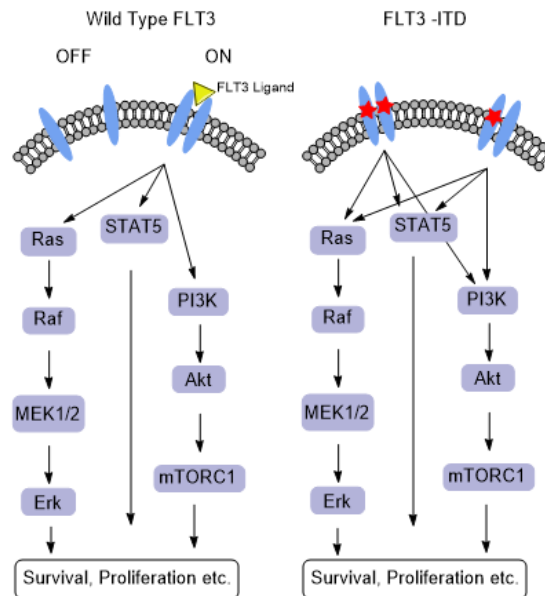


Figure 1.13. When FLT3 is unmutated the kinase requires ligand binding to be turned “on”. However, when the FLT3-ITD is present in either one or both kinases in the dimer, ligand is no longer needed and the receptor is constantly in its active state

Mutations in FLT3 can be seen in about 30% of acute myeloid leukemia cases with the internal tandem duplication (ITD) mutation in roughly 25% of cases¹¹⁹. There is also a possibility of a mutation in the kinase domain seen in about 7-10 % of AML cases (Figure 1.14)¹¹⁹. When the FLT3-ITD mutation is present, ligand binding is no longer necessary to activate downstream signaling (Figure 1.13)¹²⁰.

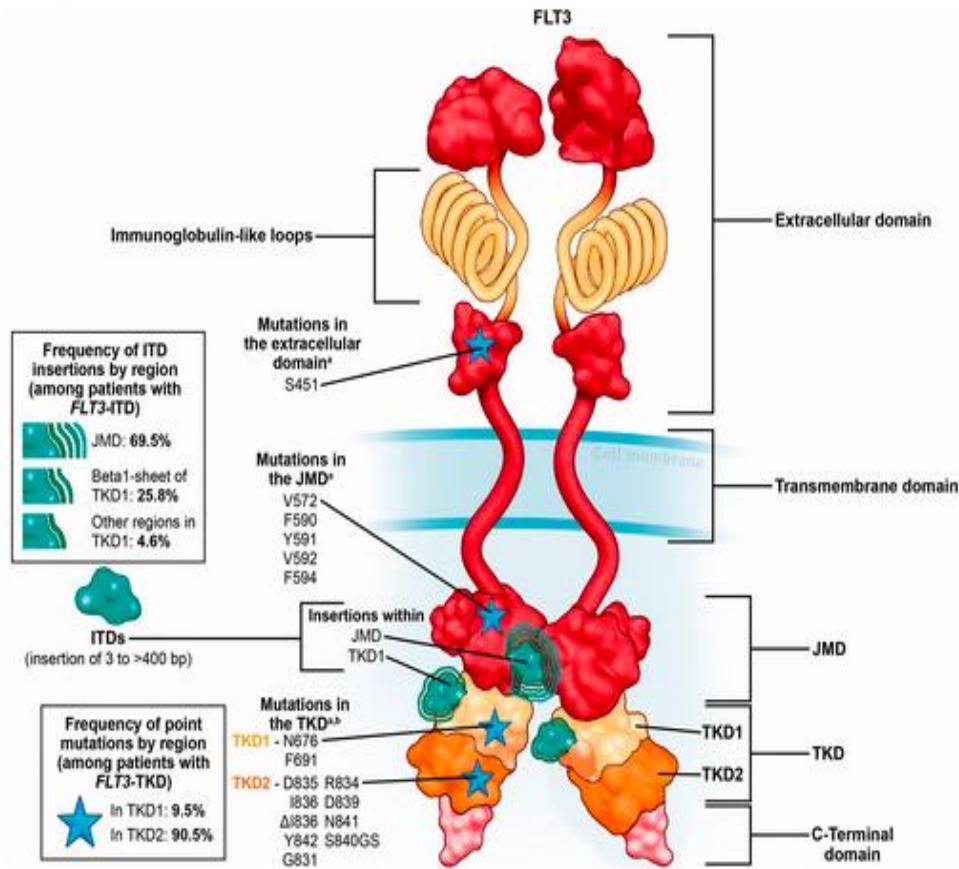


Figure 1.14. FLT3 receptor with main domains shown as well as common mutations. Image provided by Taylor and Francis <https://doi.org/10.1080/10428194.2017.1399312>

Midostaurin was the first FLT3-ITD inhibitor for the treatment of AML (Figure 1.15)¹²¹. However, as seen in many other cancers, after prolonged treatment of midostaurin, mutations can occur¹²². Although, several mutations are seen the most prevalent one is the F691L gatekeeper mutation¹²³. One of the most common mutations seen in the clinic is the addition of a D835Y mutation¹²⁴. This mutation, found at the 835 position in the activation loop of FLT3, mutates an

aspartic acid to a tyrosine (Figure 1.14)¹²⁴. Gilteritinib is currently the only approved to treat patients who contain the FLT3-ITD mutation and the D835Y mutation (Figure 1.15)^{125,126}. The other common mutation seen in the clinic is the F691L gatekeeper mutation¹²⁷. The phenylalanine at the 691 position is mutated to a leucine (Figure 1.14). Quizartinib, which originally showed promise against this mutation was recently denied FDA approval^{128,129}. The FDA did not grant its approval due to factors such as possible cardiotoxicity, lack of robust data, and lack of substantial evidence of overall survival¹³⁰. There are currently no approved drugs that are effective against the F691L mutation which drives a need for new inhibitors that are active against this mutation.

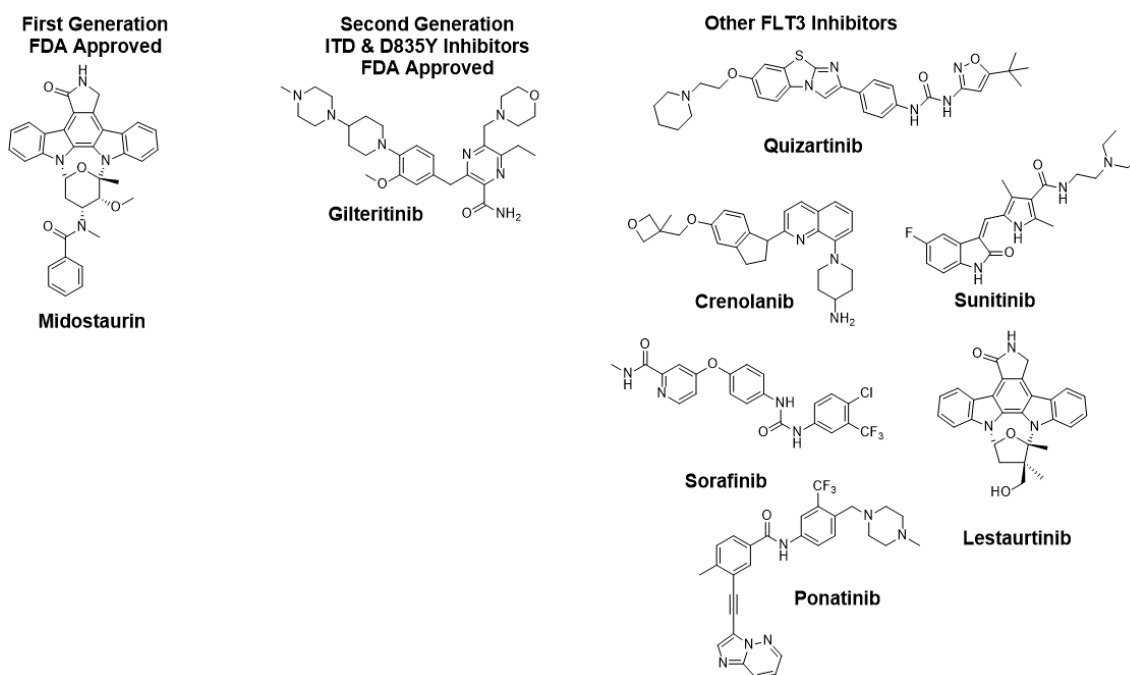


Figure 1.15. Inhibitors that target FLT3 for AML. Midostaurin and gilteritinib are both approved by the FDA. Other have either gone through clinical trail and failed or are currently in clinical trial

Table 1.5. Examples of potency and binding affinity of select FLT3 inhibitors

Inhibitor	IC ₅₀ (nM) ¹³¹				K _d (nM) ¹³²			
	MV4-11 (ITD)	MOLM-14 (ITD)	MOLM-14 (ITD, D835Y)	MOLM-14 (ITD, F691L)	FLT3	FLT3 (ITD)	FLT3 (D835Y)	FLT3 (ITD, F691L)
Midostaurin	18.4	16.1	19.1	30.7	4	4.1	1.6	3.9
Quizartinib	0.4	0.5	23	48.5	1.4	7	7.6	160
Crenolanib	3.1	4.5	6.6	15.6	0.2	0.26	0.19	0.11
Ponatinib	0.1	0.5	52.6	6.8	-	-	-	-

1.7 Summary

Although there are approved kinases inhibitors for several kinase driven cancers, there is still a drive for new and better inhibitors. In my thesis work, I focused on developing compounds that potently inhibit drug resistant ABL1(T315I) and FLT3(F691L or D835Y). These mutant kinases are responsible for CML or AML relapse and there are no potent inhibitors available to tackle these mutant kinases in the clinic.

1.8 References

- 1.Cheng, H.-C., Qi, R. Z., Paudel, H. & Zhu, H.-J. Regulation and Function of Protein Kinases and Phosphatases. *Enzyme Research* vol. 2011 e794089 <https://www.hindawi.com/journals/er/2011/794089/> (2011).
- 2.Lodish, H. *et al.* Receptor Tyrosine Kinases and Ras. *Mol. Cell Biol.* 4th Ed. (2000).
- 3.Milanesi, L. *et al.* Systematic analysis of human kinase genes: a large number of genes and alternative splicing events result in functional and structural diversity. *BMC Bioinformatics* **6**, S20 (2005).
- 4.Robinson, D. R., Wu, Y.-M. & Lin, S.-F. The protein tyrosine kinase family of the human genome. *Oncogene* **19**, 5548–5557 (2000).
- 5.Protein Kinases: Human Protein Kinases Overview | CST. <https://www.cellsignal.com/contents/science-protein-kinases/protein-kinases-human-protein-kinases-overview/kinases-human-protein>.
- 6.Paul, M. K. & Mukhopadhyay, A. K. Tyrosine kinase – Role and significance in Cancer. *Int. J. Med. Sci.* **1**, 101–115 (2004).
- 7.Siveen, K. S. *et al.* Role of Non Receptor Tyrosine Kinases in Hematological Malignances and its Targeting by Natural Products. *Mol. Cancer* **17**, 31 (2018).
8. Roskoski, R. Src protein–tyrosine kinase structure and regulation. *Biochem. Biophys. Res. Commun.* **324**, 1155–1164 (2004).
- 9.Via, A. & Zanzoni, A. *Protein Phosphorylation in Health and Disease*. (Frontiers Media SA, 2016).
- 10.Bahar, I., Jernigan, R. L. & Dill, K. A. *Protein Actions: Principles and Modeling*. (Garland Science, 2017).
- 11.Conformational Analysis of the DFG-Out Kinase Motif and Biochemical Profiling of Structurally Validated Type II Inhibitors. <https://www.ncbi.nlm.nih.gov/pmc/articles/PMC4326797/>.

12. Huse, M. & Kuriyan, J. The Conformational Plasticity of Protein Kinases. *Cell* **109**, 275–282 (2002).
13. McClendon, C. L., Kornev, A. P., Gilson, M. K. & Taylor, S. S. Dynamic architecture of a protein kinase. *Proc. Natl. Acad. Sci.* **111**, E4623–E4631 (2014).
14. Ins and Outs of Kinase DFG Motifs - ScienceDirect. <https://www.sciencedirect.com/science/article/pii/S1074552113002147>.
15. Bhullar, K. S. *et al.* Kinase-targeted cancer therapies: progress, challenges and future directions. *Mol. Cancer* **17**, (2018).
16. Chandrasekhar, C., Kumar, P. S. & Sarma, P. V. G. K. Novel mutations in the kinase domain of BCR-ABL gene causing imatinib resistance in chronic myeloid leukemia patients. *Sci. Rep.* **9**, (2019).
17. Tokarski, J. S. *et al.* The Structure of Dasatinib (BMS-354825) Bound to Activated ABL Kinase Domain Elucidates Its Inhibitory Activity against Imatinib-Resistant ABL Mutants. *Cancer Res.* **66**, 5790–5797 (2006).
18. Zhang, J. *et al.* Targeting Bcr–Abl by combining allosteric with ATP-binding-site inhibitors. *Nature* **463**, 501–506 (2010).
19. Wagner, M. J., Stacey, M. M., Liu, B. A. & Pawson, T. Molecular Mechanisms of SH2- and PTB-Domain-Containing Proteins in Receptor Tyrosine Kinase Signaling. *Cold Spring Harb. Perspect. Biol.* **5**, (2013).
20. Liu, B. A. *et al.* SH2 Domains Recognize Contextual Peptide Sequence Information to Determine Selectivity* □ S. 14.
21. Moran, M. F. *et al.* Src homology region 2 domains direct protein-protein interactions in signal transduction. *Proc. Natl. Acad. Sci. U. S. A.* **87**, 8622–8626 (1990).
22. Kurochkina, N. & Guha, U. SH3 domains: modules of protein–protein interactions. *Biophys. Rev.* **5**, 29–39 (2013).
23. Nars, M. & Vihinen, M. Coevolution of the Domains of Cytoplasmic Tyrosine Kinases. *Mol. Biol. Evol.* **18**, 312–321 (2001).
24. Hall, J. E., Fu, W. & Schaller, M. D. Chapter Five - Focal Adhesion Kinase: Exploring FAK Structure to Gain Insight into Function. in *International Review of Cell and Molecular Biology* (ed. Jeon, K. W.) vol. 288 185–225 (Academic Press, 2011).
25. Lemmon, M. A. & Schlessinger, J. Cell signaling by receptor-tyrosine kinases. *Cell* **141**, 1117–1134 (2010).
26. Krause, D. S. & Van Etten, R. A. Tyrosine Kinases as Targets for Cancer Therapy. *N. Engl. J. Med.* **353**, 172–187 (2005).

27. Hubbard, S. R. & Till, J. H. Protein Tyrosine Kinase Structure and Function. *Annu. Rev. Biochem.* **69**, 373–398 (2000).
28. Maruyama, I. N. Mechanisms of Activation of Receptor Tyrosine Kinases: Monomers or Dimers. *Cells* **3**, 304–330 (2014).
29. Lee, M. J. & Yaffe, M. B. Protein Regulation in Signal Transduction. *Cold Spring Harb. Perspect. Biol.* **8**, (2016).
30. Receptor serine/threonine kinase (RSTK) family | Enzymes | IUPHAR/BPS Guide to PHARMACOLOGY.
<https://www.guidetopharmacology.org/GRAC/FamilyDisplayForward?familyId=303#subfamilies>.
31. Oh, S. A. & Li, M. O. TGF- β : Guardian of T Cell Function. *J. Immunol. Baltim. Md 1950* **191**, 3973–3979 (2013).
32. Rauch, J., Volinsky, N., Romano, D. & Kolch, W. The secret life of kinases: functions beyond catalysis. *Cell Commun. Signal. CCS* **9**, 23 (2011).
33. Role of Non Receptor Tyrosine Kinases in Hematological Malignancies and its Targeting by Natural Products | Molecular Cancer | Full Text. <https://molecular-cancer.biomedcentral.com/articles/10.1186/s12943-018-0788-y>.
34. Wheeler, D. L., Iida, M. & Dunn, E. F. The Role of Src in Solid Tumors. *The Oncologist* **14**, 667–678 (2009).
35. Boggon, T. J. & Eck, M. J. Structure and regulation of Src family kinases. *Oncogene* **23**, 7918–7927 (2004).
36. Roskoski, R. Src protein-tyrosine kinase structure, mechanism, and small molecule inhibitors. *Pharmacol. Res.* **94**, 9–25 (2015).
37. Harrison, S. C. Variation on an Src-like Theme. *Cell* **112**, 737–740 (2003).
38. Fajer, M., Meng, Y. & Roux, B. The Activation of c-Src Tyrosine Kinase: Conformational Transition Pathway and Free Energy Landscape. *J. Phys. Chem. B* **121**, 3352–3363 (2017).
39. Pseudokinases: update on their functions and evaluation as new drug targets | Future Medicinal Chemistry. <https://www.future-science.com/doi/full/10.4155/fmc-2016-0207>.
40. Mendrola, J. M., Shi, F., Park, J. H. & Lemmon, M. A. Receptor Tyrosine Kinases with Intracellular Pseudokinase Domains. *Biochem. Soc. Trans.* **41**, 1029–1036 (2013).
41. Kung, J. E. & Jura, N. Structural basis for the non-catalytic functions of protein kinases. *Struct. Lond. Engl. 1993* **24**, 7–24 (2016).

42. Hinton, S. D. The role of pseudophosphatases as signaling regulators. *Biochim. Biophys. Acta BBA - Mol. Cell Res.* **1866**, 167–174 (2019).
43. Yamaoka, K. *et al.* The Janus kinases (Jaks). *Genome Biol.* **5**, 253 (2004).
44. Byrne, D. P., Foulkes, D. M. & Eyers, P. A. Pseudokinases: update on their functions and evaluation as new drug targets. *Future Med. Chem.* **9**, 245–265 (2017).
45. Kanev, G. K. *et al.* The Landscape of Atypical and Eukaryotic Protein Kinases. *Trends Pharmacol. Sci.* **40**, 818–832 (2019).
46. Casares, D., Escribá, P. V. & Rosselló, C. A. Membrane Lipid Composition: Effect on Membrane and Organelle Structure, Function and Compartmentalization and Therapeutic Avenues. *Int. J. Mol. Sci.* **20**, (2019).
47. Bhattacharya, S., McElhanon, K. E., Gushchina, L. & Weisleder, N. Role of phosphatidylinositol-4,5-bisphosphate 3-kinase signaling in vesicular trafficking. *Life Sci.* **167**, 39–45 (2016).
48. Boucher, J., Kleinridders, A. & Kahn, C. R. Insulin Receptor Signaling in Normal and Insulin-Resistant States. *Cold Spring Harb. Perspect. Biol.* **6**, (2014).
49. Loo, L., Wright, B. D. & Zylka, M. J. Lipid kinases as therapeutic targets for chronic pain. *Pain* **156 Suppl 1**, S2-10 (2015).
50. Hebron, M. & Moussa, C. E.-H. Two sides of the same coin: tyrosine kinase inhibition in cancer and neurodegeneration. *Neural Regen. Res.* **10**, 1767–1769 (2015).
51. Gain-of-Function Mutations of Receptor Tyrosine Kinases in Gastrointestinal Stromal Tumors. <https://www.ncbi.nlm.nih.gov/pmc/articles/PMC2269002/>.
52. Du, Z. & Lovly, C. M. Mechanisms of receptor tyrosine kinase activation in cancer. *Mol. Cancer* **17**, 58 (2018).
53. Lodish, H. *et al.* Proto-Oncogenes and Tumor-Suppressor Genes. *Mol. Cell Biol.* **4th Ed.** (2000).
54. Pines, G., Köstler, W. J. & Yarden, Y. Oncogenic mutant forms of EGFR: lessons in signal transduction and targets for cancer therapy. *FEBS Lett.* **584**, 2699–2706 (2010).
55. Janke, H. *et al.* Activating FLT3 Mutants Show Distinct Gain-of-Function Phenotypes In Vitro and a Characteristic Signaling Pathway Profile Associated with Prognosis in Acute Myeloid Leukemia. *PLoS ONE* **9**, (2014).
56. Chaix, A. *et al.* KIT-D816V oncogenic activity is controlled by the juxtamembrane docking site Y568-Y570. *Oncogene* **33**, 872–881 (2014).

57. Matsuse, M. *et al.* Functional characterization of the novel BRAF complex mutation, BRAFV600delinsYM, identified in papillary thyroid carcinoma. *Int. J. Cancer* **132**, 738–743 (2013).
58. Miller, M., Shirole, N., Tian, R., Pal, D. & Sordella, R. The Evolution of TP53 Mutations: From Loss-of-Function to Separation-of-Function Mutants. *13* (2017).
59. Reference, G. H. TP53 gene. *Genetics Home Reference* <https://ghr.nlm.nih.gov/gene/TP53>.
60. Berggren, P. *et al.* p53 mutations in urinary bladder cancer. *Br. J. Cancer* **84**, 1505–1511 (2001).
61. Silwal-Pandit, L., Langerød, A. & Børresen-Dale, A.-L. TP53 Mutations in Breast and Ovarian Cancer. *Cold Spring Harb. Perspect. Med.* **7**, (2017).
62. Klimovich, B. *et al.* Loss of p53 function at late stages of tumorigenesis confers ARF-dependent vulnerability to p53 reactivation therapy. *Proc. Natl. Acad. Sci.* **116**, 22288–22293 (2019).
63. Prelich, G. Gene Overexpression: Uses, Mechanisms, and Interpretation. *Genetics* **190**, 841–854 (2012).
64. Targeting MET in Lung Cancer: Will Expectations Finally Be MET? | Elsevier Enhanced Reader. <https://reader.elsevier.com/reader/sd/pii/S1556086416311790?token=2A089B38932A02BBB803B386B4F30C0550A124304922D7B562F81DD963A74DD5C23CED38000427A5B20EE52F698E0170> doi:10.1016/j.jtho.2016.10.014.
65. Tomlinson, D., Baldo, O., Harnden, P. & Knowles, M. FGFR3 protein expression and its relationship to mutation status and prognostic variables in bladder cancer. *J. Pathol.* **213**, 91–98 (2007).
66. Smalley, K. S. M. *et al.* Identification of a Novel Subgroup of Melanomas with KIT/Cyclin-Dependent Kinase-4 Overexpression. *Cancer Res.* **68**, 5743–5752 (2008).
67. Lai, S. *et al.* KIT over-expression by p55PIK-PI3K leads to Imatinib-resistance in patients with gastrointestinal stromal tumors. *Oncotarget* **7**, 1367–1379 (2015).
68. Hantschel, O. Structure, Regulation, Signaling, and Targeting of Abl Kinases in Cancer. *Genes Cancer* **3**, 436–446 (2012).
69. Quintás-Cardama, A. & Cortes, J. Molecular biology of bcr-abl1-positive chronic myeloid leukemia. *Blood* **113**, 1619–1630 (2009).
70. Bronte, G. *et al.* Targeting RET-rearranged non-small-cell lung cancer: future prospects. *Lung Cancer Targets Ther.* **10**, 27–36 (2019).
71. Ju, Y. S. *et al.* A transforming KIF5B and RET gene fusion in lung adenocarcinoma revealed from whole-genome and transcriptome sequencing. *Genome Res.* **22**, 436–445 (2012).

72. Sever, R. & Brugge, J. S. Signal Transduction in Cancer. *Cold Spring Harb. Perspect. Med.* **5**, (2015).
73. How Gleevec Transformed Leukemia Treatment. *National Cancer Institute* <https://www.cancer.gov/research/progress/discovery/gleevec> (2015).
74. Classification of small molecule protein kinase inhibitors based upon the structures of their drug-enzyme complexes | Elsevier Enhanced Reader. <https://reader.elsevier.com/reader/sd/pii/S1043661815301298?token=78557ABADD19B528AA6434BFC6CFD9BB38414B6C8A101BDA8CBC5E0EAB7D3DE38E7060AF77AD5EFE4A3C7948C034BD4B> doi:10.1016/j.phrs.2015.10.021.
75. Johnson, L. N., Lowe, E. D., Noble, M. E. M. & Owen, D. J. The structural basis for substrate recognition and control by protein kinases | The previous Datta Lectures were given by: F. Melchers (1st, 1986), N. Sharon (2nd, FEBS Letters 217 (1987) 145–157); B.G. Malmström (3rd, FEBS Letters 250 (1989) 9–21); J.C. Skou (4th, FEBS Letters 268 (1990) 314–324); B.A. Lynch and D.E. Koshland, Jr. (5th, FEBS Letters 307 (1992) 3–9); A.R. Fersht (6th, FEBS Letters 325 (1993) 5–16); E. Sackmann (7th, FEBS Letters 346 (1994) 3–16); P. De Camilli (8th, FEBS Letters 369 (1995) 3–12); C. Weissmann (9th, FEBS Letters 389 (1996) 3–11); Ph. Cohen et al. (10th, FEBS Letters 410 (1997) 3–10). 1. *FEBS Lett.* **430**, 1–11 (1998).
76. Gavrin, L. K. & Saiah, E. Approaches to discover non-ATP site kinase inhibitors. *MedChemComm* **4**, 41–51 (2012).
77. Zhang, J., Yang, P. L. & Gray, N. S. Targeting cancer with small molecule kinase inhibitors. *Nat. Rev. Cancer* **9**, 28–39 (2009).
78. Breen, M. E. & Soellner, M. B. Small Molecule Substrate Phosphorylation Site Inhibitors of Protein Kinases: Approaches and Challenges. *ACS Chem. Biol.* **10**, 175–189 (2015).
79. Ward, R. A. & Goldberg, F. W. *Kinase Drug Discovery: Modern Approaches*. (Royal Society of Chemistry, 2018).
80. Wieduwilt, M. J. & Moasser, M. M. The epidermal growth factor receptor family: Biology driving targeted therapeutics. *Cell. Mol. Life Sci. CMLS* **65**, 1566–1584 (2008).
81. Wee, P. & Wang, Z. Epidermal Growth Factor Receptor Cell Proliferation Signaling Pathways. *Cancers* **9**, (2017).
82. Prabhakar, C. N. Epidermal growth factor receptor in non-small cell lung cancer. *Transl. Lung Cancer Res.* **4**, 110–118 (2015).
83. Johnson, J. R. *et al.* Approval Summary for Erlotinib for Treatment of Patients with Locally Advanced or Metastatic Non-Small Cell Lung Cancer after Failure of at Least One Prior Chemotherapy Regimen. *Clin. Cancer Res.* **11**, 6414–6421 (2005).

84. Kazandjian, D. *et al.* FDA Approval of Gefitinib for the Treatment of Patients with Metastatic EGFR Mutation-Positive Non-Small Cell Lung Cancer. *Clin. Cancer Res.* **22**, 1307–1312 (2016).
85. Morgillo, F., Della Corte, C. M., Fasano, M. & Ciardiello, F. Mechanisms of resistance to EGFR-targeted drugs: lung cancer. *ESMO Open* **1**, (2016).
86. Matsubara, D. *et al.* Co-Activation of Epidermal Growth Factor Receptor and c-MET Defines a Distinct Subset of Lung Adenocarcinomas. *Am. J. Pathol.* **177**, 2191–2204 (2010).
87. Research, C. for D. E. and. FDA approves dacomitinib for metastatic non-small cell lung cancer. *FDA* (2019).
88. Research, C. for D. E. and. FDA broadens afatinib indication to previously untreated, metastatic NSCLC with other non-resistant EGFR mutations. *FDA* (2019).
89. Jackson, P. A., Widen, J. C., Harki, D. A. & Brummond, K. M. Covalent Modifiers: A Chemical Perspective on the Reactivity of α,β -Unsaturated Carbonyls with Thiols via Hetero-Michael Addition Reactions. *J. Med. Chem.* **60**, 839–885 (2017).
90. Schwartz, P. A. *et al.* Covalent EGFR inhibitor analysis reveals importance of reversible interactions to potency and mechanisms of drug resistance. *Proc. Natl. Acad. Sci. U. S. A.* **111**, 173–178 (2014).
91. Takeda, M. & Nakagawa, K. First- and Second-Generation EGFR-TKIs Are All Replaced to Osimertinib in Chemo-Naive EGFR Mutation-Positive Non-Small Cell Lung Cancer? *Int. J. Mol. Sci.* **20**, (2019).
92. Gilfillan, A. M. & Rivera, J. The tyrosine kinase network regulating mast cell activation. *Immunol. Rev.* **228**, 149–169 (2009).
93. Wang, Q., Pechersky, Y., Sagawa, S., Pan, A. C. & Shaw, D. E. Structural mechanism for Bruton's tyrosine kinase activation at the cell membrane. *Comput. Biol.* **10**.
94. Lin, L. *et al.* Activation Loop Phosphorylation Modulates Bruton's Tyrosine Kinase (Btk) Kinase Domain Activity. *Biochemistry* **48**, 2021–2032 (2009).
95. Pal Singh, S., Dammeijer, F. & Hendriks, R. W. Role of Bruton's tyrosine kinase in B cells and malignancies. *Mol. Cancer* **17**, 57 (2018).
96. AbbVie Announces U.S. FDA Approval of IMBRUVICA® (ibrutinib) Plus Obinutuzumab (GAZYVA®) - First Chemotherapy-Free, Anti-CD20 Combination Regimen Approved for Chronic Lymphocytic Leukemia/Small Lymphocytic Lymphoma (CLL/SLL) in Previously Untreated Patients | AbbVie News Center. <https://news.abbvie.com/news/abbvie-announces-us-fda-approval-imbruvica-ibrutinib-plus-obinutuzumab-gazyva--first-chemotherapy-free-anti-cd20-combination-regimen-approved-for-chronic-lymphocytic-leukemiasmall-lymphocytic-lymphoma-cllsll-in-previously-untreated-pati.htm>.

97. Avendaño, C. & Menéndez, J. C. Drugs That Inhibit Signaling Pathways for Tumor Cell Growth and Proliferation. in *Medicinal Chemistry of Anticancer Drugs* 391–491 (Elsevier, 2015). doi:10.1016/B978-0-444-62649-3.00010-7.
98. Hamasy, A. *et al.* Substitution scanning identifies a novel, catalytically active ibrutinib-resistant BTK cysteine 481 to threonine (C481T) variant. *Leukemia* **31**, 177–185 (2017).
99. Research, C. for D. E. and. Project Orbis: FDA approves acalabrutinib for CLL and SLL. *FDA* (2019).
100. Dose Escalation and Dose Expansion Study of Tirabrutinib in Combination With Other Targeted Anti-cancer Therapies in Adults With B-cell Malignancies - Full Text View - ClinicalTrials.gov. <https://clinicaltrials.gov/ct2/show/NCT02457598>.
101. FDA grants accelerated approval to zanubrutinib for mantle cell lymphoma | FDA. <https://www.fda.gov/drugs/resources-information-approved-drugs/fda-grants-accelerated-approval-zanubrutinib-mantle-cell-lymphoma>.
102. Barf, T. *et al.* Acabrutinib (ACP-196): A Covalent Bruton Tyrosine Kinase Inhibitor with a Differentiated Selectivity and In Vivo Potency Profile. *J. Pharmacol. Exp. Ther.* **363**, 240–252 (2017).
103. Biochemical characterization of tirabrutinib and other irreversible inhibitors of Bruton's tyrosine kinase reveals differences in on - and off - target inhibition | Elsevier Enhanced Reader. <https://reader.elsevier.com/reader/sd/pii/S0304416520300210?token=BC84F1B3F684FCA96CD4FC99E90CE4E0B590CE77F8724E691331634E9D75419BA0FE6C53CA17414B09CFDC96B8A83FAB> doi:10.1016/j.bbagen.2020.129531.
104. Guo, Y. *et al.* Discovery of Zanubrutinib (BGB-3111), a Novel, Potent, and Selective Covalent Inhibitor of Bruton's Tyrosine Kinase. *J. Med. Chem.* **62**, 7923–7940 (2019).
105. Safety, PK, PD, and Antitumor Activity of Vecabrutinib (SNS-062) in B Lymphoid Cancers - Full Text View - ClinicalTrials.gov. <https://clinicaltrials.gov/ct2/show/NCT03037645>.
106. Bond, D. A. & Woyach, J. A. Targeting BTK in CLL: Beyond Ibrutinib. *Curr. Hematol. Malig. Rep.* **14**, 197–205 (2019).
107. Druker, B. J. *et al.* Five-Year Follow-up of Patients Receiving Imatinib for Chronic Myeloid Leukemia. *N Engl J Med* **10** (2006).
108. Yamamoto, M., Kurosu, T., Kakahana, K., Mizuchi, D. & Miura, O. The two major imatinib resistance mutations E255K and T315I enhance the activity of BCR/ABL fusion kinase. *Biochem. Biophys. Res. Commun.* **319**, 1272–1275 (2004).
109. Cang, S. & Liu, D. P-loop mutations and novel therapeutic approaches for imatinib failures in chronic myeloid leukemia. *J. Hematol. Oncol. J Hematol Oncol* **1**, 15 (2008).

110. Mian, A. A. *et al.* The gatekeeper mutation T315I confers resistance against small molecules by increasing or restoring the ABL-kinase activity accompanied by aberrant transphosphorylation of endogenous BCR, even in loss-of-function mutants of BCR/ABL. *Leukemia* **23**, 1614–1621 (2009).
111. Rossari, F., Minutolo, F. & Orciuolo, E. Past, present, and future of Bcr-Abl inhibitors: from chemical development to clinical efficacy. *J. Hematol. Oncol. J Hematol Oncol* **11**, 84 (2018).
112. Liu, X., Kung, A., Malinoski, B., Prakash, G. K. S. & Zhang, C. Development of Alkyne-Containing Pyrazolopyrimidines To Overcome Drug Resistance of Bcr-Abl Kinase. *J. Med. Chem.* **58**, 9228–9237 (2015).
113. Gainor, J. F. & Chabner, B. A. Ponatinib: Accelerated Disapproval. *The Oncologist* **20**, 847–848 (2015).
114. Larocque, E. A., Naganna, N., Opoku-Temeng, C., Lambrecht, A. M. & Sintim, H. O. Alkynylnicotinamide-Based Compounds as ABL1 Inhibitors with Potent Activities against Drug-Resistant CML Harboring ABL1(T315I) Mutant Kinase. *ChemMedChem* **13**, 1172–1180 (2018).
115. Grafone, T., Palmisano, M., Nicci, C. & Storti, S. An overview on the role of FLT3-tyrosine kinase receptor in acute myeloid leukemia: biology and treatment. *Oncol. Rev.* **6**, (2012).
116. Volpe, G. *et al.* Regulation of the Flt3 Gene in Haematopoietic Stem and Early Progenitor Cells. *PLOS ONE* **10**, e0138257 (2015).
117. Greenblatt, S. & Small, D. FLT3 in lineage specification and plasticity. *Oncotarget* **3**, 576–580 (2012).
118. Takahashi, S. Downstream molecular pathways of FLT3 in the pathogenesis of acute myeloid leukemia: biology and therapeutic implications. *J. Hematol. Oncol. J Hematol Oncol* **4**, 13 (2011).
119. Daver, N., Schlenk, R. F., Russell, N. H. & Levis, M. J. Targeting FLT3 mutations in AML: review of current knowledge and evidence. *Leukemia* **33**, 299–312 (2019).
120. Larrosa-Garcia, M. & Baer, M. R. FLT3 inhibitors in acute myeloid leukemia: Current status and future directions. *Mol. Cancer Ther.* **16**, 991–1001 (2017).
121. Research, C. for D. E. and. Midostaurin. *FDA* (2019).
122. Daver, N. *et al.* Secondary mutations as mediators of resistance to targeted therapy in leukemia. *Blood* **125**, 3236–3245 (2015).
123. Staudt, D. *et al.* Targeting Oncogenic Signaling in Mutant FLT3 Acute Myeloid Leukemia: The Path to Least Resistance. *Int. J. Mol. Sci.* **19**, (2018).

124. Nguyen, B. *et al.* FLT3 activating mutations display differential sensitivity to multiple tyrosine kinase inhibitors. *Oncotarget* **8**, 10931–10944 (2017).
125. Zimmerman, E. I. *et al.* Crenolanib is active against models of drug-resistant FLT3-ITD-positive acute myeloid leukemia. *Blood* **122**, 3607–3615 (2013).
126. Research, C. for D. E. and. FDA approves gilteritinib for relapsed or refractory acute myeloid leukemia (AML) with a FLT3 mutation. *FDA* (2019).
127. Minson, K. A., DeRyckere, D. & Graham, D. K. The Current State of FLT3 Inhibition in Acute Myeloid Leukemia – Pitfalls and Promises. *J. Cell Signal.* **2**, (2017).
128. Fletcher, L., Joshi, S. K. & Traer, E. Profile of Quizartinib for the Treatment of Adult Patients with Relapsed/Refractory FLT3-ITD-Positive Acute Myeloid Leukemia: Evidence to Date. *Cancer Manag. Res.* **12**, 151–163 (2020).
129. Quizartinib FDA Approval Status. *Drugs.com*
<https://www.drugs.com/history/quizartinib.html>.
130. May 14, 2019: Meeting of the Oncologic Drugs Advisory Committee Meeting Announcement - 05/14/2019 - 05/14/2019. *FDA* <http://www.fda.gov/advisory-committees/advisory-committee-calendar/may-14-2019-meeting-oncologic-drugs-advisory-committee-meeting-announcement-05142019-05142019> (2019).
131. Naganna, N. *et al.* Amino alkynylisoquinoline and alkynyl naphthyridine compounds potently inhibit acute myeloid leukemia proliferation in mice. *EBioMedicine* **40**, 231–239 (2019).
132. Jones, L. M. *et al.* Targeting AML-associated FLT3 mutations with a type I kinase inhibitor. <https://www.jci.org/articles/view/127907/table/1> (2020) doi:10.1172/JCI127907.

CHAPTER 2. ALKYNILNICOTINAMIDE-BASED COMPOUNDS AS ABL1 INHIBITORS WITH POTENT ACTIVITIES AGAINST DRUG-RESISTANT CML HARBORING ABL1(T315I) MUTANT KINASE

This chapter was reprinted with permission from John Wiley and Sons. Original article can be found at Larocque, E. A., Naganna, N., Opoku-Temeng, C., Lambrecht, A. M. & Sintim, H. O. Alkynylnicotinamide-Based Compounds as ABL1 Inhibitors with Potent Activities against Drug-Resistant CML Harboring ABL1(T315I) Mutant Kinase. *ChemMedChem* **13**, 1172–1180 (2018).

2.1 Abstract

The introduction of imatinib into the clinical scene revolutionized the treatment of chronic myelogenous leukemia (CML). The overall eight-year survival rate for CML has increased from about 6% in the 1970s to over 90% in the imatinib era. However, about 20% of CML patients harbor primary or acquired resistance to tyrosine kinase inhibitors. ABL1 point mutations in the BCR-ABL1 fusion protein, such as ABL1(T315I), typically emerge after prolonged kinase inhibitor treatment. Ponatinib (AP24534) is currently the only approved CML drug that is active against the ABL1(T315I) mutation. However, ponatinib has severe cardiovascular toxicities; hence, there have been efforts to find safer CML drugs that work against ABL1 secondary mutations. We reveal that isoquinoline- or naphthyridine-based compounds, such as HSN431, HSN576, HSN459, and HSN608 potently inhibit the enzymatic activities of ABL1, ABL1(T315I), and ABL1(E255K). These compounds inhibit the proliferation of ABL1-driven CML cell lines, K652 and KCL22 as well as the drug-resistant cell line, KCL22-IR, which harbors the secondary mutated ABL1(T315I) kinase.

2.2 Introduction

When a pluripotent hematopoietic stem cell acquires the Philadelphia (Ph) chromosome, which encodes BCR fused to the ABL1 kinase protein (designated as BCR-ABL1 fusion oncoprotein), the cells gain proliferative advantage over normal stem cells, and the uncontrolled expansion of the leukemic stem cells leads to chronic myelogenous leukemia (CML)¹. The overactive BCR-ABL1 protein promotes the expansion of granulocytes, which are most commonly seen in CML². Approved in 2001, imatinib has had tremendous success in increasing the life expectancy of CML patients. Before 1975, the eight-year survival rate for newly diagnosed CML

patient was about 6% but this has steadily increased to over 90% in the imatinib/tyrosine kinase era³. Imatinib binds to the inactive conformation of the BCR-ABL protein and it has a good selectivity profile against human kinases; hence it is relatively nontoxic⁴. Various kinases adopt similar active conformations but have very different inactive conformations. Therefore, inhibitors that bind to the inactive conformer of kinases, but not the active conformer, can achieve selective kinase binding⁵. Other FDA-approved kinase inhibitors that target BCR-ABL include nilotinib (Tasigna, Novartis), dasatinib (Sprycelm, Bristol-Myers Squibb), and bosutinib (Bosulif, Pfizer) (Figure 2.1)⁶⁻⁹. Unfortunately, ABL1(T315I) and other kinase domain mutations, which are resistant to imatinib, emerge upon prolonged drug treatment¹⁰. In the mutant BCR-ABL1(T315I) kinase, a polar uncharged threonine side chain becomes a hydrophobic and more sterically hindering isoleucine. The T315I mutation is the most problematic due to its altering of the three-dimensional structure of the BCR-ABL1 kinase into the “DFG-in” A-loop conformation, causing a decrease in the sensitivity of most kinase inhibitor drugs that bind the inactive conformer of BCR-ABL1, including imatinib^{11,12}.

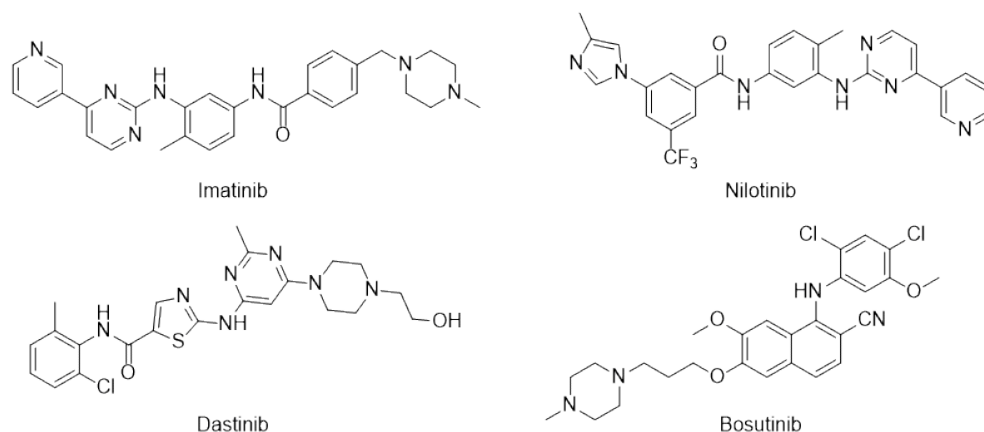


Figure 2.1. Current first- and second-generation CML drugs

Ponatinib (AP24534), a pan-kinase inhibitor, is currently the only approved CML drug that is able to potently inhibit the BCR-ABL1(T315I) mutant kinase¹³. Over the course of ponatinib’s clinical trials 17.1% of patients taking ponatinib reported both serious and non-serious thrombotic events (this is defined as cardiovascular, cerebrovascular, and peripheral vascular events)¹⁴. [14] Five deaths in the study (n=499) were linked to the use of ponatinib¹⁴. The accumulation of these adverse effects caused the trial to be put on hold and then canceled¹⁴. Due to these risks, ponatinib

is now used as a last resort drug¹⁵. Because of the adverse events associated with ponatinib, there is a motivation to develop other potent BCR-ABL1(T315I) inhibitors. Unfortunately, most preclinical studies use mouse models that may not adequately predict clinical success in humans so the search for safer BCR-ABL1(T315I) inhibitors is a non-trivial task^{16,17}.

Our group has been interested in developing alkynyl aminoisoquinolines and alkynylaminonaphthyridine as FLT3 inhibitors for the treatment of acute myeloid leukemia^{18,19}. Some of our FLT3 inhibitors, such as HSN286 and compound 1 (see Figure 2.2) contain aryl alkynyl benzamide moiety, which is also found in ponatinib. Because ponatinib also inhibits ABL1, in addition to FLT3, we wondered if our compounds were also ABL1 inhibitors. We however found out that the mere presence of a piperazine-containing alkynylbenzamide in a molecule did not make such compound an ABL1 inhibitor. For example, ponatinib shares the same piperazine-containing alkynylbenzamide moiety with HSN285, yet 500 nM ponatinib inhibited 99% of the enzymatic activity of ABL1 whereas at the same concentration HSN285 only inhibited ABL1 at 8%. Also, compounds 1, 6, and 8 each contain piperidine-containing amide, yet at 500 nM concentration compound 1 inhibited ABL1 at 90 %, compound 8 inhibited ABL1 at 96%, whereas compound 6 inhibited ABL1 at only 69 %. Based on the excellent ABL1 inhibition profile of compounds 1 and 8, which contain aminoisoquinoline or aminonaphthyridine moieties, and ponatinib, which contains a piperazine-containing alkynylbenzamide moiety, we focused on making more analogues of 1 and 8 or analogues of HSN356 (which combine the aminonaphthyridine moiety found in 8 and methyl piperazine found in ponatinib). Herein we report alkynyl aminoisoquinolines and aminonaphthyridines analogues that are active against the BCR-ABL1 enzyme, as well as ABL1 with T315I and E255K point mutations. these compounds also inhibit the proliferation of CML cell lines K562, KCL22, and KCL22-IR, the latter of which is an imatinib-resistant cell line²⁰⁻²².

2.3 Results and Discussion

2.3.1 Structural analysis of alkynyl aminoisoquinolines and alkynylaminonaphthyridine:

We have previously reported that alkynyl aminoisoquinoline and aminonaphthyridine analogues are privileged kinase inhibitors with potent activities against FLT3-driven acute myeloid leukemia^{18,19}. Our success in developing alkynyl aminoisoquinolines and aminonaphthyridines as

FLT3 inhibitors prompted us to evaluate our compounds against other kinases and to endow the compounds with moieties that are commonly found in drugs (Figure 2.3).

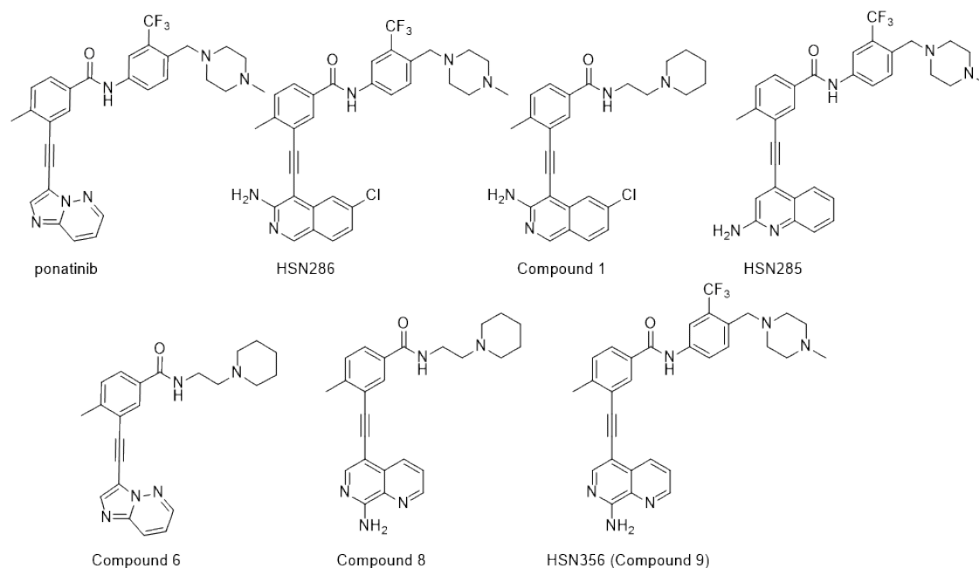


Figure 2.2. Initial Alkynyl compounds, which inspired the synthesis of new ABL1 inhibitors (see Figure 2.6)

To optimize our library, we wanted to change several aspects of the first-generation compounds, compound 1 and compound 9 (HSN356), to make compounds that bind better to ABL1 and also to improve upon the drug likeness (see Figure 2.3). Docking of compound **9** (HSN356) and ponatinib to ABL1 protein, using GOLD software, indicated that both compounds bound in the same mode (see Figure 2.4)²³. Importantly, the docking of ponatinib to ABL1 recapitulated the bound pose in the crystallized structure, thereby giving confidence to the docking pose. The imidazo[1,2*b*] pyridazine moiety found in ponatinib interacts with the hinge region at the back of the binding pocket of ABL1 (Figure 2.4A). Similarly, according to the docking results, the aminonaphthyridine core found in compound 9 (HSN356) also binds to this hinge region (Figure 2.4B). the 4-methyl benzamide ring in our first-generation compounds and also in ponatinib could pose a possible metabolic liability, whereby the benzylic hydrogens are oxidized. Ponatinib was found to be hydroxylated by liver enzymes, and some of this hydroxylation could occur at the 4-methyl position²⁴. We therefore explored the possibility of removing this potential metabolic liability with a halogen or a bulkier alkyl group such as ethyl

(compounds 9-16, Figure 2.6). In addition, to improve upon the aqueous solubility of the compounds we added nitrogen to the benzamide ring.

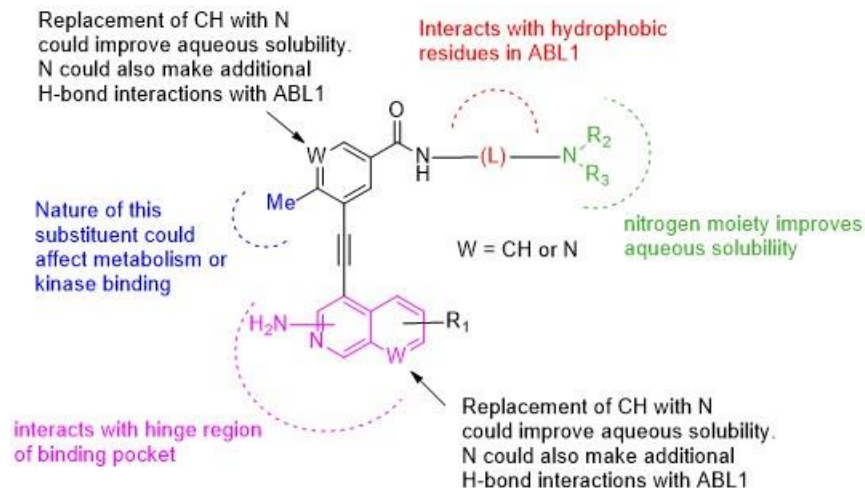


Figure 2.3. Optimization strategy to improve drug-like properties and potency of first-generation compounds HSN356 and HSN286

The linker (either the CF₃-bearing aromatic or the aliphatic chain) can interact with the hydrophobic residues in the active site of ABL1 (Figure 2.5). The CF₃ group however adds 69 gmol⁻¹ to the molecular weight of the compounds. We therefore investigated if other groups, such as CH₃ (compound 20), Cl (compound 21), or F (compound 22) could replace the CF₃ group without a great penalty to binding (see Figure 2.6). Due to the lack of activity of the compounds with an aliphatic chain to mutated ABL1(T315I), these analogues were no longer pursued (see below). The N-methylpiperazine group in ponatinib and our compounds mainly acts as an aqueous solubilizing moiety but adds significant mass unit to the molecule. We explored if this group could be replaced by lower mass unit groups, such as morpholine (compound 17), pyrrolidine (compound 18) and a dimethylamine (compound 19). These units also contain basic nitrogen and could also improve upon the aqueous solubility of the compounds.

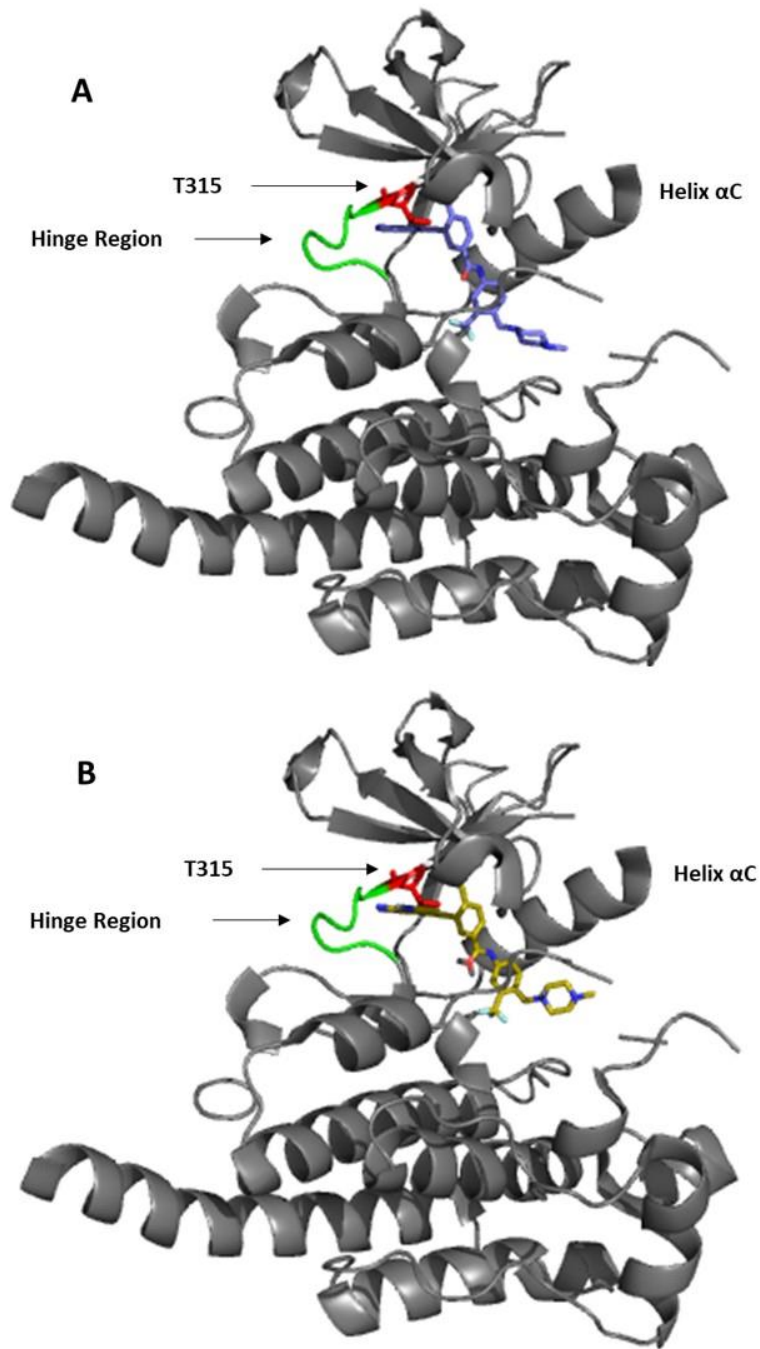


Figure 2.4. Ponatinib and compound 9 bound to the ABL kinase domain. A) docked ponatinib bound to the ABL kinase domain. B) Docked compound 9 bound to the ABL kinase domain. All compounds were docked against PDBID: 3OXZ using GOLD software [23]. The hinge region is shown in green, the key T315 is colored red

Compounds were readily synthesized via an established Sonogashira coupling protocol¹⁸. With a vast library of compounds that contain various aromatic and aliphatic side chains, initial screening was done at compound concentration of 500 nM against ABL1, ABL1(T315I), and ABL1(E255K).

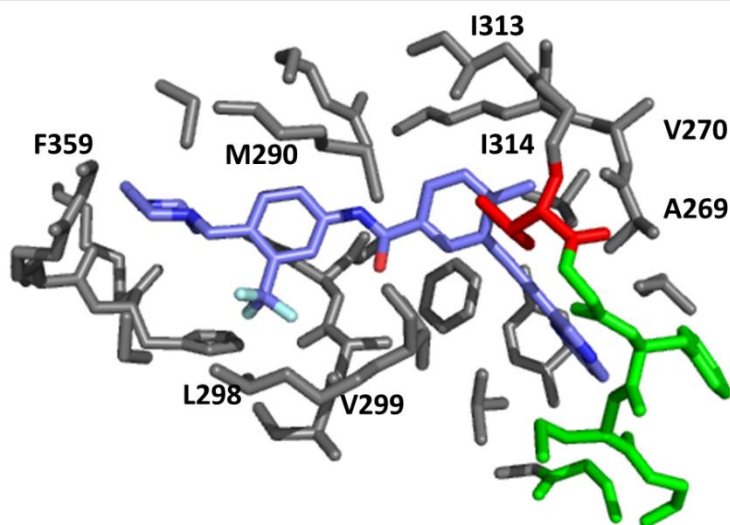


Figure 2.5. ABL residues within 6 Å of the bound ponatinib (blue). Key hydrophobic residues are labeled. T315 is colored red, while residues that are part of the hinge region are green

Analogs that contained an aliphatic side chain (1-8) showed similar inhibition against aBL1 to that of their aromatic side chain counterparts. However, these compounds were poor inhibitors of ABL1(T315I) and ABL1 (E255K) (Figure 2.7A). Compounds containing 1-amino- or 3-aminoisoquinoline or aminonaphthyridine rings were generally good inhibitors of ABL1 (Figure 2.7A). Compound which contained the 4-((4-methylpiperazin-1-yl)methyl)-3-trifluoromethylphenylamine moiety displayed potent enzymatic inhibition against ABL1 kinase (at 500 nM, these compounds inhibited over 90% of the enzymatic activity of the ABL1 enzyme). The 4-((4-methylpiperazin-1-yl)methyl)-3-trifluoromethylphenylamine-containing compounds were also potent inhibitors of ABL1(T315I) and ABL1(E255K) mutant kinases (Figure 2.7).

the importance of the trifluoromethyl group. All of the compounds in this series, 19–22, significantly inhibited wild-type ABL1. However, with regard to ABL1(E255K), compounds 19 (trifluoro methyl) and 21 (chloro), but not 20 or 22, were able to moderately inhibit this mutant version of ABL1. All four compounds 19–22 were found to be poor inhibitors of ABL1(T315I). Interestingly, the only difference between compound 19 and 15 is that 19 contains a dimethyl amine, which we originally thought functioned as a mere aqueous solubilizing group whereas 15 contains a dimethyl piperazine group, which we also thought functioned as a mere solubilizing group. It appears that these groups, which were put into the molecules to increase aqueous solubility also affect binding to mutant ABL1 kinase, providing a cautionary tale that moieties added to potential drugs could have unintended functions.

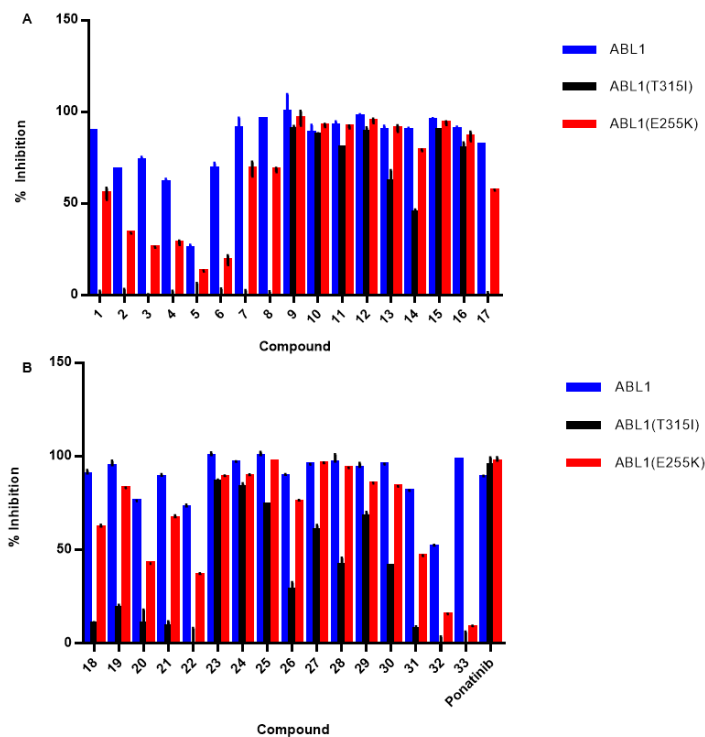


Figure 2.7. Enzymatic inhibition against ABL1 wild-type and common mutations T315I and E255K. Screening of compounds was done as a service at Reaction Biology Corporation

2.3.2 IC₅₀ determination of select analogues against ABL1 and ABL1(T315I):

Compounds 16 (HSN608), 15 (HSN459), 28 (HSN431), and 29 (HSN576) were chosen as representative isoquinoline or naphthyridine compounds for further characterization. These compounds were chosen due to their good activities against the wild-type and mutant ABL1 enzymes. Secondly, these compounds contain the water-soluble nicotinamide moiety (and not the benzamide moiety that is found in ponatinib), which made them more appealing for possible translation. All four compounds and ponatinib inhibit ABL1 wild type with IC₅₀ values less than 5 nM (Figure 2.8A). For mutant ABL1(T315I), however, only ponatinib and compound 15 (HSN459) potently inhibited with IC₅₀ less than 10 nM (1.6 nM and 4.7 nM, respectively). Compound 29 (HSN576) and compound 16 (HSN608) inhibited ABL1(T315I) with IC₅₀ values of 32.8 nM and 40.7 nM, respectively. Compound 28 (HSN431) was the least sensitive of the four analogues toward ABL1(T315I), with an IC₅₀ value of 507 nM (Figure 2.8B).

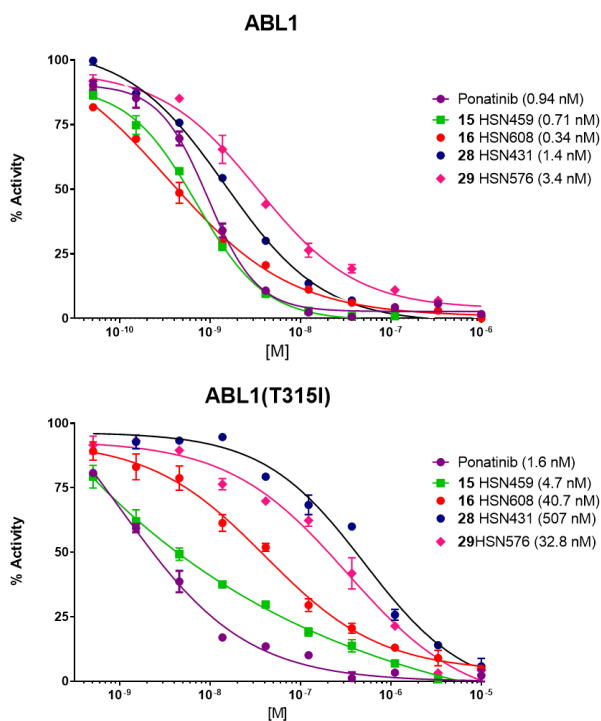


Figure 2.8. Compounds 16 (HSN608), 15 (HSN459), 28 (HSN431), and 29 (HSN576) inhibit A) ABL1 and B) ABL1(t315I) at nanomolar IC₅₀ values

2.3.3 Aminoisoquinolines and aminonaphthyridines potently inhibit the proliferation of ABL1-driven CML cell lines:

Having established that the compounds were good ABL1 inhibitors, we proceeded to test the activities of our library against three CML cell lines, K562, KCL22 and KCL22-IR. K562 is a CML line which is positive for the Bcr-Abl1 fusion gene. KCL22 is an imatinib-sensitive CML cell line and KCL22-IR is an imatinib-resistant cell line, containing the T315I mutation²².

In general, there is a positive correlation between the percent inhibition of ABL1 enzymatic activity and BCR-ABL-driven CML cell line proliferation inhibition. The 4-((4-methylpiperazin-1-yl)methyl)-3-trifluoromethylphenylamine-containing compounds are all potent inhibitors of CML cell lines with IC₅₀ values in the sub-nanomolar or single-digit nanomolar range. Excitingly, many compounds (9–13, 15, 16, 19, 23, 25, 27–29) maintained good potency (IC₅₀<10 nM) against the KCL22-IR cell line, which contains the T315I mutation (Table 2.1). A few compounds did not display potent inhibition against ABL1(T315I) in vitro yet inhibited the proliferation of KCL22-IR cell line with reasonably low IC₅₀ values. For example, in vitro, the IC₅₀ value of compound 28 against ABL1(T315I) enzyme is 507 nM (Figure 2.8B) and thus did not appear to be a potent inhibitor of ABL1(T315I). However, compound 28 inhibited the fusion kinase BCR-ABL(T315I) in cells with an IC₅₀ of 54.7 nM, (see below), which is an order of magnitude less than the IC₅₀ against ABL1(T315I) kinase domain in vitro. Caution must be taken in directly assuming that IC₅₀ values obtained in vitro will translate directly into cellular assays. The in vitro IC₅₀ value will depend on the enzyme and ATP concentrations used in the in vitro assay, which may be different in the cellular context. IC₅₀ values should therefore really be used in ranking order. Also, the ABL1 kinase, which is used in the in vitro experiment, does not contain the fusion BCR partner whereas ABL1 is fused to BCR to form BCR-ABL1 fusion protein in CML cells. Therefore, conformational differences between the isolated ABL1 kinase domain and the BCR-ABL fusion protein that is found in the cell could give rise to differences in compound sensitivities. In fact, others have also noted differences in sensitivities between ABL1 and the fusion protein against other inhibitors^{25–27}. There are also BCR-ABL1-independent mechanisms that makes KCL22-IR and other imatinib-resistant CML cell lines resistant to imatinib and it is possible that some of our compounds are also affecting these pathways. Unfortunately, the BCR-ABL1-independent mechanisms of resistance in CML have been poorly characterized^{28–31}. Finally the activity of a compound against a cell line does not depend only on the isolated activity against an enzyme target but also depends

on cellular permeation, cellular compartment localization, stability of the compound in cells and promiscuity of compound toward binding to other cellular proteins (both kinase and non-kinase targets). A compound that potently inhibits ABL1 but also binds to other cellular macromolecules and/or localizes into compartments that BCR-ABL1 does not reside will not display the same potency against the target protein as was seen in an in vitro assay. Compounds 16 (HSN608) and 15 (HSN459) are of interest because in addition to potent activity against drug-resistant CML cell line, KCL22-IR, they have lower logP values (2.3 and 2.7, respectively) than the rest of the active compounds and therefore are more drug-like in comparison.

Table 2.1. Calculated logP and antiproliferative activities of alkynyl analogs

		IC ₅₀ (mean ±SD, nM)					IC ₅₀ (mean ±SD, nM)		
Compound	LogP ^[a]	K562	KCL22	KCL22-IR	Compound	LogP ^[a]	K562	KCL22	KCL22-IR
1 (HSN248)	4.4	7.01 ± 0.07	6.45 ± 0.13	> 1 μm	19 (HSN534)	2.8	0.388 ± 0.001	0.459 ± 0.016	3.8 ± 0.1
2	4.2	25.7 ± 1.7	35.5 ± 1.69	> 1 μm	20	2.4	56.9 ± 0.6	16.6 ± 0.4	> 1 μm
3	5.3	30.05 ± 1.9	ND	ND	21	2.6	11.4 ± 0.1	3.79 ± 0.07	> 1 μm
4	4.3	10.1 ± 0.8	111 ± 1.35	> 1 μm	22	2.1	75.5 ± 0.4	29.09 ± 0.82	> 1 μm
5	4.4	161 ± 10.8	ND	ND	23	4.9	0.234 ± 0.004	2.19 ± 0.11	3.2 ± 0.2
6	3	43.5 ± 1.4	ND	ND	24	3.6	1.44 ± 0.06	1.45 ± 0.02	13.3 ± 0.5
7	4.9	94.5 ± 0.8	ND	ND	25	5	0.216 ± 0.002	0.426 ± 0.001	0.25 ± 0.07
8 (HSL45)	3.9	25.3 ± 0.5	17.16 ± 0.3	> 1 μm	26	5.2	8.44 ± 0.05	2.25 ± 0.03	50.1 ± 2.23
9 (HSN356)	3.9	1.85 ± 0.03	0.18 ± 0.004	0.74 ± 0.004	27	4.2	1.75 ± 0.02	0.652 ± 0.002	7.3 ± 0.07
10	4.2	0.587 ± 0.004	0.606 ± 0.606	3.27 ± 0.09	28 (HSN431)	2.9	0.485 ± 0.002	0.325 ± 0.007	4.4 ± 0.05
11	4.5	0.856 ± 0.006	0.699 ± 0.003	2.12 ± 0.09	29 (HSN576)	2.6	0.688 ± 0.003	0.444 ± 0.008	4.1 ± 0.03
12	4.7	0.292 ± 0.005	1.05 ± 0.02	1.52 ± 0.08	30	5.7	6.59 ± 0.01	2.59 ± 0.04	23.3 ± 0.6
13	4.8	1.18 ± 0.05	1.85 ± 0.04	5.49 ± 0.14	31	3.4	6.8 ± 0.08	60.6 ± 0.9	> 1 μm
14	3.9	0.833 ± 0.005	1.48 ± 0.05	16.3 ± 0.7	32	2.5	> 1 μm	> 1 μm	> 1 μm
15 (HSN459)	2.7	1.75 ± 0.04	0.303 ± 0.002	2.67 ± 0.07	33	2.3	> 1 μm	731 ± 0.09	> 1 μm
16 (HSN608)	2.3	0.765 ± 0.005	1.02 ± 0.04	4.14 ± 0.11	Ponatinib	4.2	0.6003 ± 0.0023	0.142 ± 0.003	0.66 ± 0.005
17	2.6	20.4 ± 0.3	5.71 ± 0.04	198 ± 11.8	Imatinib	4.36	88.6 ± 0.6	83.7 ± 0.7	> 1 μm
18	3.2	6.26 ± 0.02	1.6 ± 0.4	ND					

[a] Calculated using online software at www.molinspiration.com. [b] Values are the mean ± SD of n=3 technical replicates; ND: not determined; see Experimental Section for procedural details

Compound series 19–22 allowed investigation into the role of the CF₃ group in the inhibition of ABL1 and CML cell proliferation. Compound 19 (contains CF₃ group) inhibited imatinib sensitive K562 and KCL22 with IC₅₀ values of 0.388 nM and 0.459 nM respectively. Compound 19 also inhibited KCL22-IR with a respectable IC₅₀ of 3.8 nM. Replacing the CF₃ group with Cl, Me or F decreased the sensitivity of both K562 and KCL22 by two orders of magnitude. For the ABL1(T315I) harboring cell line, compounds 20–22 were inactive against this cell line (IC₅₀>1000 nM). It therefore appears that the trifluoromethyl group is critical for the potency of these new alkynyl isoquinoline or naphthyridine compounds.

Compound 25 has an impressive potency against all three CML cell lines tested (sub-nanomolar IC₅₀ values for all cell lines). The logP value for compound 25 is 5, and therefore is not as ideal as other tested compounds.

Changing the 6-methylnicotinamide moiety found in compound 15 (HSN459) or 24 (HSN461) into 1-methyl-1H-pyrazole-3-carboxamide (compounds 23 and 24) decreased affinity for the tested ABL1 enzymes. In line with the lower inhibition of ABL1 wild-type and mutant forms, both compounds 31 and 32 were & 50 to 100 times less potent than the 6-methylnicotinamide analogues at inhibiting the ABL1-driven CML cell lines.

When the N-(3-(trifluoromethyl)phenyl) group was replaced with aliphatic side chains (compounds 1–8), there was a dramatic decrease in activity against the drug-resistant CML cell line KCL22-IR (IC₅₀>1000 nM). The low activity of the aforementioned compounds against KCL22-IR is not surprising because these compounds are poor inhibitors of ABL1(T315I) enzyme (Figure 2.7A).

Compound 15 (HSN459), compound 16 (HSN608), compound 28 (HSN431) and compound 29 (HSN576) inhibit ABL1 and ABL1(T315I) activities in KCL22 and KCL22-IR cell lines, respectively.

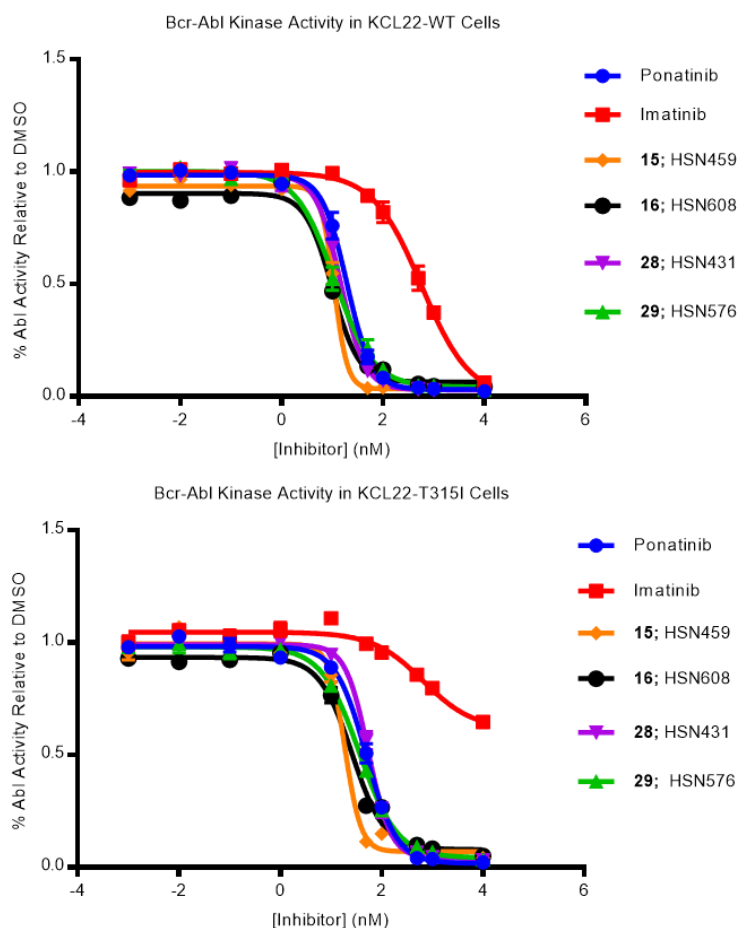


Figure 2.9. Dose-response curves for inhibition of ABL1 and ABL1(T315I) in KCL22 and KCL22-IR, respectively, by imatinib, ponatinib, HSN431, HSN459, HSN576, and HSN608. IC₅₀ values were determined by KinaSense (West Lafayette, IN, USA)

We proceeded to investigate the effects of approved drugs, imatinib and ponatinib, and four of the compounds in this study (HSN431, HSN459, HSN576 and HSN608) on ABL1 activity in imatinib-sensitive (KCL22-WT) and imatinib-resistant (KCL22-T315I) cell lines. For this investigation, KinaSense (West Lafayette, IN, USA) performed the cellular ABL1 kinase phosphorylation assay, using their novel phosphorylation detection platform. All tested compounds were able to inhibit the phosphorylation of ABL1 in KCL22-WT but imatinib was the least potent, followed by ponatinib (see Figure 2.9 and Table 2.2). For the drug resistant CML cell line, KCL22-IR (harboring ABL1(T315I)), imatinib was ineffective whereas ponatinib inhibited ABL1 phosphorylation inside KCL22-IR cells with IC₅₀ of 50 nM. Impressively three of our

compounds, HSN459, HSN576, and HSN608 inhibited KCL22-IR better than ponatinib (Table 2.2; compare IC₅₀ of HSN459 (19 nM) with ponatinib (50 nM)). These compounds are therefore good candidates to evaluate further for possible clinical translation against drug-resistant CML.

Table 2.2: Inhibition of cellular ABL1 activity by imatinib, ponatinib, and HSN compounds

Compound	IC ₅₀ (nM) ^[a]	
	KCL22	KCL22-IR
ponatinib	19.3 ± 1.1	49.7 ± 1.1
imatinib	574 ± 1.2	ND
15: HSN459	10.9 ± 1.1	18.9 ± 1.1
16: HSN608	9.9 ± 1.1	26.0 ± 1.1
28: HSN431	14.6 ± 1.0	54.7 ± 1.0
29: HSN576	11.1 ± 1.1	36.4 ± 1.1

[a] Values are the mean±SD of n=3 technical replicates; ND: not determined.

2.4 Conclusion

Here we have reported a new library of compounds that are potent against the ABL1, ABL1(T315I) and ABL1(E255K) enzymes. These compounds also inhibit the proliferation of CML cell lines K562, KCL22, and KCL22-IR with IC₅₀ values that are competitive with the FDA-approved ponatinib, the only inhibitor currently approved for CML harboring ABL1(T315I) mutation. Because ponatinib has some toxicity liability and hence not appropriate for patients who have a history of cardiovascular disease, new compounds that are as potent as ponatinib but with less toxic profile are welcomed. Unfortunately, due to the nature of drug development, whereby preclinical studies are done on animal models, which may not be accurate models for humans, many of these side effects cannot be predicted until a drug reaches clinical trials^{16,17}. Therefore, one has to be cognizant of the fact that until such new inhibitors pass the muster of clinical testing, one would never be certain if they are indeed less toxic than ponatinib but the importance of finding a less toxic compound than ponatinib should provide the impetus to persevere in the endeavor of finding new BCR-ABL1(T315I) inhibitors. Future work, beyond the scope of this report, will investigate the safety profiles and in vivo efficacies of the reported compounds to ascertain their translational potential. These future studies will be reported in due course.

2.5 Experimental Section:

2.5.1 Molecular docking with GOLD software:

For docking, PDB ID: 3OXZ was obtained from RCSB Protein Data Bank (www.rcsb.org). Ponatinib and HSN356 were drawn using ChemDraw Professional software version 16.0 and Chem3D software version 16.0 (PerkinElmer Informatics) to minimize the energy; then saved as a mol2 file. The Hermes visualizer was used for protein preparation and docking, the wizard option added hydrogens, deleted waters and crystalized the ligand. Ponatinib and HSN356 were then docked to the binding site using the default 10 genetic algorithm and the ChemPLP scoring function. PyMOL visualization software (The PyMOL Molecular Graphics System, Version 2.0 Schrödinger, LLC) was then used to form images.

2.5.2 General aromatic amide coupling procedure:

A solution of benzoic acid (1 equiv) and HATU (1.1 equiv) in DMF (5 mL) was cooled to 0°C. DIPEA (3 equiv) was then added followed by the amine compound (1 equiv). The temperature was increased to 50°C and allowed to stir 12 h. The reaction was diluted with EtOAc (50 mL) and washed with water (3x20 mL). and brine solution (20 mL). Combined organic layers were dried over anhydrous sodium sulfate, filtered and concentrated in vacuo. The pure product was then obtained via flash column chromatography.

2.5.3 General aliphatic amide coupling procedure:

A solution of benzoic acid (1 equiv) and HCTU (1.1 equiv) in dry CH₂Cl₂ (5 mL) was cooled to 0°C. DIPEA (3 equiv) was then added followed by the amine compound (1 equiv). The temperature was increased to room temperature and allowed to stir 12 h. The reaction was diluted with CH₂Cl₂ (50 mL) and washed with water (3x20 mL). and brine solution (20 mL). Combined organic layers were dried over anhydrous sodium sulfate, filtered and concentrated in vacuo. The pure product was then obtained via flash column chromatography.

2.5.4 General Sonogashira Coupling:

A solution of aromatic halogen compound (1 equiv), Pd(PPh₃)₂Cl₂ (10 mol%), CuI (5 mol%) and triphenylphosphine (5 mg) in triethylamine (30 equiv) was de-oxygenated with argon gas. A de-oxygenated solution of alkyne (1.2 equiv) in DMF (3 mL) was added slowly over a period of 10 minutes to the triethylamine solution. After the addition, the reaction temperature was increased to 55°C and allowed to stir for 12 h. The reaction was quenched by addition of NH₄Cl (5 mL) at room temperature. The crude compound was extracted using EtOAc (3x30 mL). Combined organic layers were dried over anhydrous sodium sulfate, filtered and concentrated in vacuo. The final compound was purified via flash column chromatography.

2.5.5 Cell Culture

KCL22-WT and KCL22-T315I cells were cultured in Roswell Park Memorial Institute (RPMI) 1640 medium. K562 was routinely cultured in Iscove's modified Dulbecco's medium (IMDM). Media were supplemented with 10% fetal bovine serum and 1X penicillin-streptomycin solution.

2.5.6 Cellular proliferation assays:

Cells were seeded into 96-well tissue culture-treated plates for up to 24 h. After seeding, DMSO stock solutions of compounds were serially diluted in a 1:3 ratio, first in DMSO. Then, subsequently into appropriate cell culture medium before being added to the cultures, with 10 mM being the highest tested concentration. The plates were incubated for 72 h as above. The CellTiter Blue assay (Promega, Madison, WI, USA) was then added to the cultures and incubated an additional 4 h before the fluorescence measured following the manufacturers recommendations. The fluorescence data from compounds were normalized to that DMSO and the resulting data fitted to a nonlinear regression equation to obtain IC₅₀ using GraphPad Prism 5.0 Software. Data was done with either duplicate or triplicate.

2.5.7 Evaluation of compounds activity against ABL1 and ABL1(T315I) in CML cell lines KCL22 and KCL22-IR (by KinaSense, West Lafayette, IN, USA)

To evaluate cellular ABL activity, KCL22-WT or KCL22-T315I cells were seeded at 600000 cells per well and final volume of 750 μ L of media into 1 mL per well (AcroPrep Advance 96 Filter Plates, Pall Corporation). Cells were dosed with the indicated kinase inhibitor or vehicle control (0.001% v/v DMSO) and incubated for 2 h at 37°C in a 5% CO₂ humidified atmosphere. Following incubation with TKI, ABL substrate was added and incubated for 10 minutes at 37 °C in a 5% CO₂ humidified atmosphere. Following incubation with substrate, cell media were removed from the filter plate using a vacuum manifold, and the filter plate was stacked on top of a NeutravidinQ coated 96-well capture plate (Thermo Fisher Scientific) containing 100 μ L blocking buffer per well (TBST+1% BSA). In the upper filter plate, 50 μ L of modified RIPA buffer containing protease inhibitor cocktail (Roche), phosphatase inhibitors, and 4 mM EDTA was added to each well. The plate stack was incubated on a short orbital plate shaker at room temperature for 5 min. Following lysis buffer incubation, the plate stack was centrifuged at 1500 rpm for 5 min to collect lysate in the NeutravidinQ capture plate. After lysate collection, the filter plate was removed, and the capture plate was incubated with shaking for 1 h at room temperature. The plate was then washed with TBST. 100 μ L of mouse 4G10 antibody (Millipore, 1:5000 in wash buffer) was added to each well and the plate incubated for 1 h at room temperature with shaking as described above. Following incubation with 4G10 antibody, the plate was washed with TBST and 100 μ L of anti-mouse IgG conjugated to HRP (1:10000 in wash buffer) was added to each well and incubated for 1 h at room temperature with shaking. The plate was washed three times with TBST followed by two washes with phosphate buffer (50 mM Na₂PO₄, pH 7.5). 100 μ L of developing reagent (50 mM Na₂HPO₄, 2.3 mM H₂O₂, 98 mM Amplex RedQ reagent, pH 7.4) was added to each well and incubated for 30 min with shaking as described above. The plate was read using a Biotek Synergy H1 plate reader using 532 nm excitation and 590 nm emission wavelengths. Each concentration was normalized to vehicle control and were plotted in GraphPad Prism software. IC₅₀ values were calculated by fitting an unconstrained log(inhibitor) vs. response with variable slope (four parameters) curve. Each cell line was treated using 10 concentrations of control (imatinib and ponatinib) and experimental compounds, ranging from 0.001–10000 nM in four technical replicates. As expected, BCR-ABL activity in the KCL22-WT cell line responded to all inhibitors. The IC₅₀ values derived for ponatinib (IC₅₀: 19.3 nM) and imatinib (IC₅₀: 574 nM)

are in line with known potencies for both in vitro biochemical activity assays as well as growth inhibition phenotypic assays. Biochemical IC₅₀ values of ponatinib for the wild-type ABL protein was reported as 0.37 nM and growth inhibition assay at 6 nM in the K562 CML model after a 42-h exposure. Biochemical IC₅₀ values of imatinib for the wild-type ABL protein was reported as 600 nM and growth inhibition assay at 1 μM in K562 cells following 72-h imatinib exposure. Agreement between the ABL activity assay results and reported IC₅₀ values indicate reliable assay performance.

2.6 Acknowledgements:

E. Larocque synthesized compounds 3-8 and compounds 10-14, did docking studies and performed cell viability experiments. The manuscript was written by E. Larocque. N. Naganna (a postdoc in the Sintim laboratory) synthesized the remaining compounds.

NMR and MS data were acquired by facilities supported by the US National Institutes of Health (NIH) grant P30 CA023168. We thank Prof. Robert Kirken (University of Texas at El Paso) for generously providing KCL22 and KCL22-IR cell lines.

2.7 Conflict of Interest:

HOS is a co-founder of KinaRx LLC, a start-up company interested in developing therapies for malignant neoplastic diseases.

2.8 References:

1. Pricl, S. T315I-mutated Bcr-Abl in chronic myeloid leukemia and imatinib: insights from a computational study. *Mol. Cancer Ther.* **4**, 1167–1174 (2005).
2. Zhou, H. & Xu, R. Leukemia stem cells: the root of chronic myeloid leukemia. *Protein Cell* **6**, 403–412 (2015).
3. Woessner, D. W., Lim, C. S. & Deininger, M. W. Development of an Effective Therapy for CML. *Cancer J. Sudbury Mass* **17**, (2011).
4. Lydon, N. Attacking cancer at its foundation. *Nat. Med.* **15**, 1153–1157 (2009).
5. Miller, G. D., Bruno, B. J. & Lim, C. S. Resistant mutations in CML and Ph(+)-ALL - role of ponatinib. *Biol. Targets Ther.* **8**, 243–254 (2014).

6. Druker, B. J. *et al.* Five-Year Follow-up of Patients Receiving Imatinib for Chronic Myeloid Leukemia. *N Engl J Med* **10** (2006).
7. Saglio, G. *et al.* Nilotinib versus Imatinib for Newly Diagnosed Chronic Myeloid Leukemia. *N. Engl. J. Med.* **362**, 2251–2259 (2010).
8. Kantarjian, H. *et al.* Dasatinib versus Imatinib in Newly Diagnosed Chronic-Phase Chronic Myeloid Leukemia. *N. Engl. J. Med.* **362**, 2260–2270 (2010).
9. Brümmendorf, T. H. *et al.* Bosutinib *versus* imatinib in newly diagnosed chronic-phase chronic myeloid leukaemia: results from the 24-month follow-up of the BELA trial. *Br. J. Haematol.* **168**, 69–81 (2015).
10. Gainor, J. F. & Shaw, A. T. Emerging paradigms in the development of resistance to tyrosine kinase inhibitors in lung cancer. *J. Clin. Oncol. Off. J. Am. Soc. Clin. Oncol.* **31**, 3987–3996 (2013).
11. Pemovska, T. *et al.* Axitinib effectively inhibits BCR-ABL1(T315I) with a distinct binding conformation. *Nature* **519**, 102–105 (2015).
12. Ai, J. & Tiu, R. V. Practical management of patients with chronic myeloid leukemia who develop tyrosine kinase inhibitor-resistant BCR-ABL1 mutations. *Ther. Adv. Hematol.* **5**, 107–120 (2014).
13. Gibbons, D. L., Pricl, S., Kantarjian, H., Cortes, J. & Quintás-Cardama, A. The rise and fall of gatekeeper mutations? The BCR-ABL1 T315I paradigm. *Cancer* **118**, 293–299 (2012).
14. Cortes, J. E. *et al.* A Phase 2 Trial of Ponatinib in Philadelphia Chromosome-Positive Leukemias. *N. Engl. J. Med.* **369**, 1783–1796 (2013).
15. Gainor, J. F. & Chabner, B. A. Ponatinib: Accelerated Disapproval. *The Oncologist* **20**, 847–848 (2015).
16. Giacomini, K. M. *et al.* When good drugs go bad. *Nature* **446**, 975–977 (2007).
17. Challenges in Drug discovery: Can We Improve Drug Development. *J. Bioanal. Biomed.* **01**, (2009).
18. Ma, X. *et al.* Identification of New FLT3 Inhibitors That Potently Inhibit AML Cell Lines via an Azo Click-It/Staple-It Approach. *ACS Med. Chem. Lett.* **8**, 492–497 (2017).
19. Larocque, E. A., Naganna, N., Opoku-Temeng, C., Lambrecht, A. M. & Sintim, H. O. Alkynylnicotinamide-Based Compounds as ABL1 Inhibitors with Potent Activities against Drug-Resistant CML Harboring ABL1(T315I) Mutant Kinase. *ChemMedChem* **13**, 1172–1180 (2018).

20. Colavita, I. *et al.* Gaining insights into the Bcr-Abl activity-independent mechanisms of resistance to imatinib mesylate in KCL22 cells: a comparative proteomic approach. *Biochim. Biophys. Acta* **1804**, 1974–1987 (2010).
21. Yuan, H. *et al.* BCR-ABL Gene Expression Is Required for Its Mutations in a Novel KCL-22 Cell Culture Model for Acquired Resistance of Chronic Myelogenous Leukemia. *J. Biol. Chem.* **285**, 5085–5096 (2010).
22. Oaxaca, D. M. *et al.* Sensitivity of imatinib-resistant T315I BCR-ABL CML to a synergistic combination of ponatinib and forskolin treatment. *Tumor Biol.* **37**, 12643–12654 (2016).
23. Jones, G., Willett, P., Glen, R. C., Leach, A. R. & Taylor, R. Development and validation of a genetic algorithm for flexible docking. *J. Mol. Biol.* **267**, 727–748 (1997).
24. Ye, Y. E., Woodward, C. N. & Narasimhan, N. I. Absorption, metabolism, and excretion of [14C]ponatinib after a single oral dose in humans. *Cancer Chemother. Pharmacol.* **79**, 507–518 (2017).
25. De Keersmaecker, K., Versele, M., Cools, J., Superti-Furga, G. & Hantschel, O. Intrinsic differences between the catalytic properties of the oncogenic NUP214-ABL1 and BCR-ABL1 fusion protein kinases. *Leukemia* **22**, 2208–2216 (2008).
26. Hantschel, O. & Superti-Furga, G. Regulation of the c-Abl and Bcr-Abl tyrosine kinases. *Nat. Rev. Mol. Cell Biol.* **5**, 33–44 (2004).
27. Rausch, J. L. *et al.* Opposing roles of KIT and ABL1 in the therapeutic response of gastrointestinal stromal tumor (GIST) cells to imatinib mesylate. *Oncotarget* **8**, 4471–4483 (2016).
28. Mahon, F.-X. *et al.* MDR1 gene overexpression confers resistance to imatinib mesylate in leukemia cell line models. *Blood* **101**, 2368–2373 (2003).
29. Lee, F., Fandi, A. & Voi, M. Overcoming kinase resistance in chronic myeloid leukemia. *Int. J. Biochem. Cell Biol.* **40**, 334–343 (2008).
30. Quintás-Cardama, A., Kantarjian, H. M. & Cortes, J. E. Mechanisms of Primary and Secondary Resistance to Imatinib in Chronic Myeloid Leukemia. *Cancer Control* **16**, 122–131 (2009).
31. Colavita, I. *et al.* Identification of Annexin A1 interacting proteins in chronic myeloid leukemia KCL22 cells. *Proteomics* **13**, 2414–2418 (2013).

CHAPTER 3. NICOTINAMIDE-PONATINIB ANALOGS AS POTENT ANTI-CML AND ANIT-AML COMPOUNDS

Reproduced with permission from *ACS Omega* 2020, 5,6,2690-2698 Copyright 2020 American Chemical Society. Publication can be found at <https://pubs.acs.org/doi/abs/10.1021/acsomega.9b03223>. Further permission related to publication should be directed to the ACS

3.1 Abstract

Ponatinib is a multikinase inhibitor that is used to treat chronic myeloid leukemia patients harboring mutated ABL1(T315I) kinase. Due to the potent inhibition of FLT3, RET and FGFRs, it is also being evaluated against AML, biliary, and lung cancers. The multikinase inhibition profile of ponatinib may also account for its toxicity, thus, analogs with improved kinase selectivity or different kinase inhibition profile could be better tolerated. The introduction of nitrogen into drug compounds can enhance efficacy and drug properties (a concept called “necessary nitrogen”). Here we introduce additional nitrogen into the benzamide moiety of ponatinib to arrive at nicotinamide analogs. A nicotinamide analog of ponatinib, HSN748, retains activity against FLT3, ABL1, RET and PDGFR α/β but loses activity against c-Src and P38 α . MNK1 and 2 are key kinases that phosphorylate eIF4E to regulate the protein translation complex. MNK also modulates mTORC1 signaling and contributes to rapamycin resistance. Inhibitors of MNK1 and 2 are being evaluated for anticancer therapy. Ponatinib is not a potent inhibitor of MNK1 or 2 but the nicotinamide analogs are potent inhibitors of MNKs. This illustrates a powerful demonstration of the “necessary nitrogen” concept to alter both the potency and selectivity of drugs.

3.2 Introduction

Ponatinib, developed by Ariad pharmaceuticals as a multikinase inhibitor, was approved by the Food and Drug Administration (FDA) in 2012¹. It targets many of the various cancer-driver kinases. These include kinases such as ABL1, FLT3, FGFR1-4, and RET. Due to its impressive kinase inhibition profile it has been shown to potently inhibit various cancers, including CML, AML, various FGFR and RET-driven cancers (such as non-small cell lung cancer² and thyroid cancer³). Currently, ponatinib is the only FDA approved drug for imatinib-resistant CML that

harbors the T315I mutation⁴. It is also undergoing various clinical trials for AML, lung and other cancers (NCT02428543; Ponatinib for FLT3-ITD Acute Myelogenous Leukemia (PONATINIB-AML)⁵, NCT02265341; Advanced Biliary Cancer with FGFR2 Fusions⁶, NCT01813734; Ponatinib in advanced NSCLC with RET Translocations⁷).

Despite these impressive arrays of cancer types that ponatinib is currently being evaluated against, the drug is relatively toxic and is associated with cardiovascular adverse events⁸. Patients taking Ponatinib have also shown side effects of hypertension, platelet dysfunction and peripheral arterial occlusive disease⁹. Other more serious side effects such as myocardial infraction, stroke, and liver failure have occurred in patients taking ponatinib¹⁰. The unfavorable toxicity profile associated with ponatinib could be due to the simultaneous inhibition of cardiovascular-related kinases¹¹. Herein we disclose that a nicotinamide analog of ponatinib (HSN748), whereby the benzamide moiety in ponatinib is replaced with a nicotinamide analog, shows a different kinase inhibition profile to ponatinib. Additionally, the nicotinamide analog of ponatinib is a better inhibitor of AML cell lines harboring secondary mutations, such as FLT3-ITD, D835Y and FLT3-ITD, F691L, which appear upon prolonged treatment with other FLT3 inhibitors and lead to drug resistance¹².

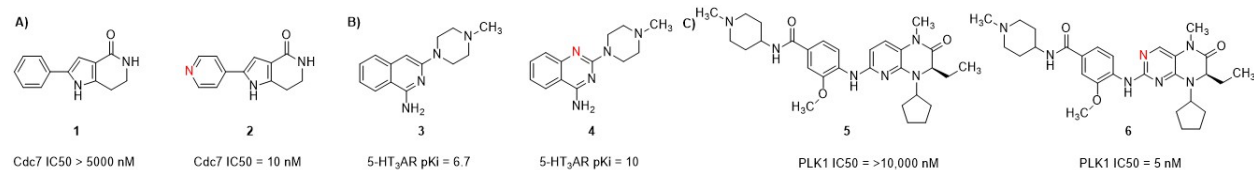


Figure 3.1. Examples of the necessary nitrogen concept. Introduction of nitrogen into initial hits led to remarkable activity enhancement as seen in A) cell division cycle 7 (Cdc7) kinase inhibitors; B) 5-HT₃AR inhibitors; C) PLK1 inhibitors.

3.3 Results and Discussion

3.3.1 The necessary nitrogen, a high-level medicinal chemistry design strategy:

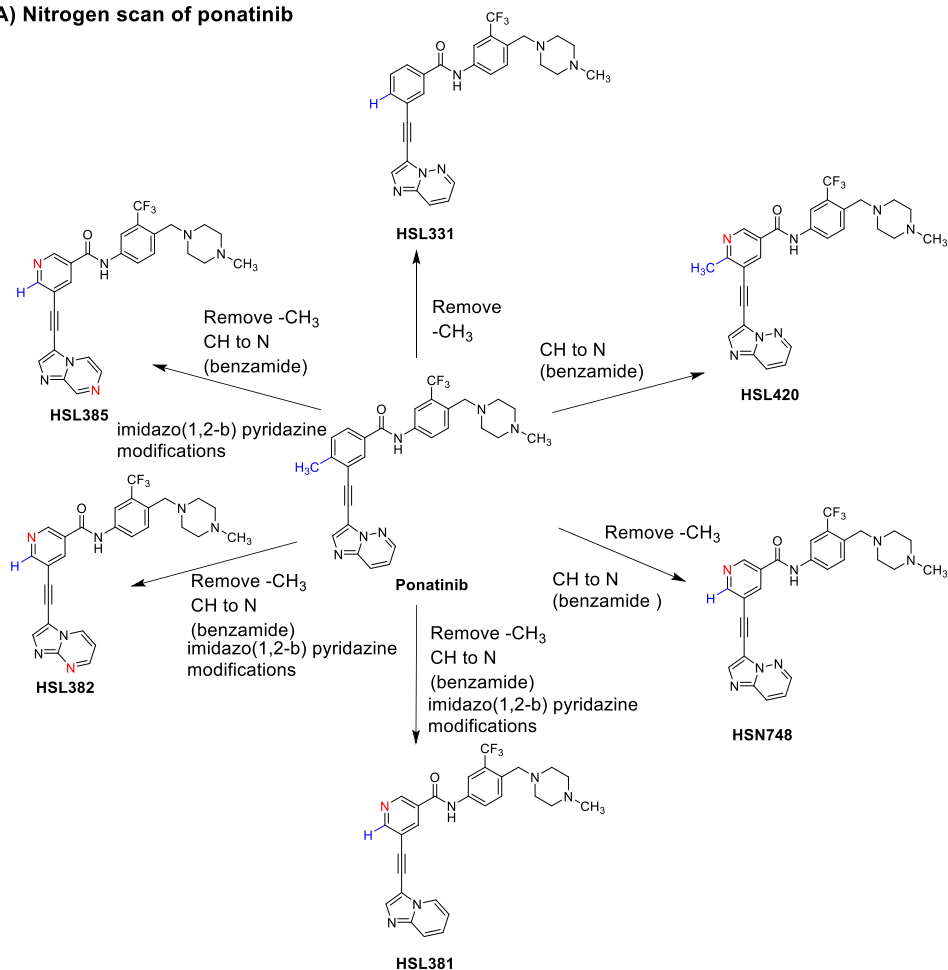
The substitution of a -CH group in a hit compound with a N atom in aromatic and heteroaromatic ring systems is a small modification but has potentially large effects on pharmacological profiles. This is due to large changes in molecular and physicochemical properties and intra- and intermolecular interactions. The methyl group scanning is also a high-level medicinal chemistry design strategy, and this has been extensively reviewed¹³. Whereas the

-CH to -Me or -Me to -CH switch is not accompanied by a big desolvation penalty, a -CH to N switch is accompanied by a large desolvation penalty¹⁴. Despite this penalty, the strategic placement of nitrogen into compounds can lead to dramatic improvement in both potency and drug properties and this has been extensively documented (Figure 3.1)¹⁵⁻¹⁷. A ring nitrogen can form new and stabilizing hydrogen bonding interactions with protein residues, backbone or even form network interactions with water molecules that interact with the protein's residues or backbone. For a few illustrative examples, Vanotti et al. revealed that a strategic replacement of a phenyl group with a 4-pyridyl group in a cell division cycle 7 (Cdc7) kinase inhibitor improved biochemical activity by > 500-fold (compound 1 to 2, Figure 3.1). This large effect was attributed to “necessary nitrogen” in the 4-pyridyl substitution making a key hydrogen bonding interaction with the protein backbone (Figure 3.1A)¹⁵.

Esch et al. performed a N-scan on the isoquinoline 5-HT3AR inhibitor 3 (Figure 1.1B), with pKi = 6.7, and arrived at the quinazoline 4 (Figure 3.1B) with pKi = 10 against 5-HT3AR (4300-fold enhancement)¹⁶. The newly installed N atom was not predicted to engage in any favorable electrostatic interactions for the ligand docking pose in a homology model of the 5-HT3AR binding site (acetylcholine binding protein (AChBP)] yet compound 4 is greater than two orders of magnitude more potent than 3. Recently Remillard et al. showed that the replacement of CH in compound 5 to N in compound 6 increased PLK1 binding (Figure 3.1C)¹⁷.

These examples and others prompted us to perform a “nitrogen scan” on ponatinib as well as remove the methyl group on the benzamide core of ponatinib and test the analogs (Figure 3.2) for inhibition against various kinases and cancers.

A) Nitrogen scan of ponatinib



B) Other analogs

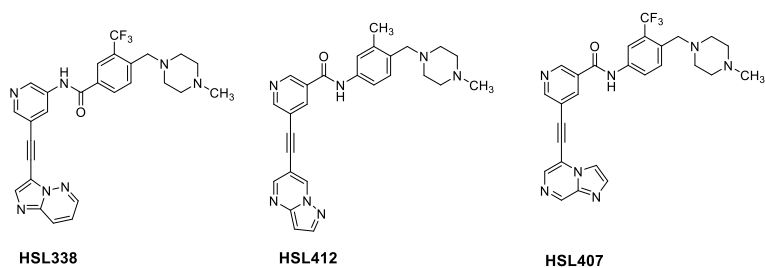


Figure 3.2. A) nitrogen and methyl scan of ponatinib B) other ponatinib analogs.

3.3.2 Synthesis of Ponatinib Analogs:

HSN748 and other analogs (Figure 3.2) were synthesized in two linear steps from 5-ethynynicotinic acid (Figure 3.3)¹⁸⁻²². By introducing a nitrogen into the benzamide ring (to make a nicotinamide), the calculated LogP changed from 4.29 (ponatinib) to 3.62 (HSN420). Removing the methyl group on HSN420 reduced the cLogP even further to 3.23 (HSN748)²³. The ranking of

LogP values can be derived from retention times of compounds on C18 columns²⁴. In concordance with the calculated LogP values, the HPLC retention times of the analogs showed corresponding trends (Table 3.1).

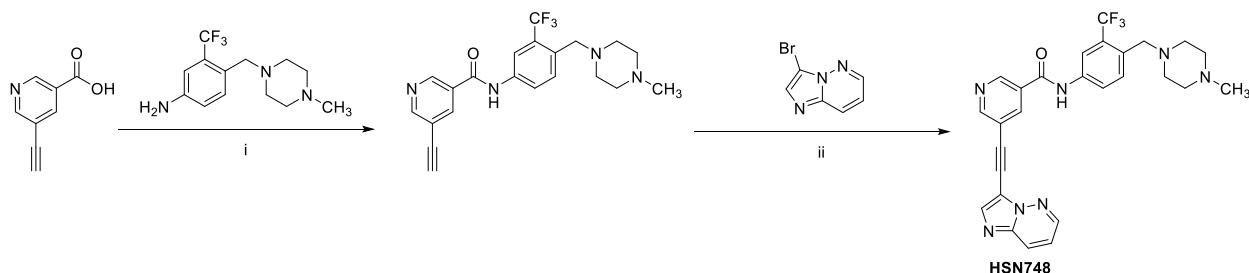


Figure 3.3. Representative synthesis of analogs (HSN748). Conditions: i: HATU, DIPEA, DMF, 45 °C, overnight. Yield = 85%; ii: Pd(PPh₃)₂Cl₂, PPh₃, CuI, DMF, TEA, 45 °C, overnight. Yield = 53%. See SI for details about other analogs.

Table 3.1. Calculated LogP values and HPLC retention times

	Calculated LogP ^a	HPLC Retention Time (min) ^b
HSN748	3.28	10.86
HSL331	3.98	11.56
HSN338	3.32	11.63
HSN382	3.22	12.33
HSN385	3.13	12.70
HSN407	3.14	12.73
HSN412	3.24	12.96
HSN381	3.82	13.31
HSN420	3.62	13.46
Ponatinib	4.29	13.90

^aUsing SWISSADME for calculations; ^bHPLC details: Agilent Eclipse instrument; C18 column (3 μm, 4.6x100 mm); method: 0 → 15 min, 50% B → 100% B, (A: 0.1% NH₄OH in H₂O, B: MeOH), 25 °C. Compound concentration is 100 μM in MeOH

3.3.3 Anticancer activities of nicotinamide analogs and ponatinib:

With compounds in hand, we proceeded to evaluate the effects of compounds on CML cell lines as well as FLT3, ABL1 and c-Src kinases, which are known to be targets of ponatinib²⁵. Although ponatinib is not an effective inhibitor of MAPK-interacting kinases (MNK1 and 2), we also evaluated the inhibition of the compounds on MNK1 and MNK2. An unrelated project, using alkynyl nicotinamide compounds, had taught us that alkynyl nicotinamide-containing compounds were MNK2 inhibitors (unpublished work), prompting us to also evaluate the inhibition of ponatinib analogs against MNK enzymes. The mechanistic Target Of Rapamycin (mTOR) is an important drug target as mTOR integrates many stimuli and coordinates the adaptive response of many cellular processes²⁶. Rapamycin is an inhibitor of mTOR. MNK contributes to rapamycin resistance by sustaining mTORC1 activity upon rapamycin treatment in cancer cells²⁶. MNKs modulate mTORC1 but not mTORC2 (which includes Rictor, rapamycin-insensitive companion of mTOR) signaling^{27,28}. Thus, concurrent inhibition of MNK1 and/or MNK2 and any of cancer-driver kinases, such as FLT3, ABL1, RET, BRAF, c-Kit, PDGFR α , and PDGFR β could lead to more sustained inhibition of cancer growth. MNK1 and 2 modulate the function of eIF4E (a key player in translational control), which is elevated in human cancers. MNK1 and 2 phosphorylate a conserved serine (Ser209) of eIF4E to modulate function. The inhibition of both MNK1 and 2 has been shown to lead to growth inhibition in cancers²⁶.

Table 3.2. IC₅₀ of library against CML cell lines

	IC ₅₀ (nM) ^a		
	K562	KCL22	KCL22-IR
HSN748	0.80 ± 0.003	1.32 ± 0.05	0.23 ± 0.013
HSL420	0.06 ± 0.002	0.06 ± 0.002	0.46 ± 0.01
HSL381	0.57 ± 0.003	0.89 ± 0.005	4.24 ± 0.05
HSL382	ND ^b	> 100 nM	> 100 nM
HSL385	0.94 ± 0.002	2.62 ± 0.06	17.2 ± 0.86
HSL338	0.45 ± 0.002	1.40 ± 0.02	4.24 ± 0.05
HSL331	0.26 ± 0.002	0.63 ± 0.002	2.86 ± 0.04
HSL412	28.13 ± 0.60	28.06 ± 0.37	> 100 nM
HSL407	1.83 ± 0.02	2.93 ± 0.04	49.7 ± 2.5
Ponatinib	0.60 ± 0.002	0.14 ± 0.003	0.66 ± 0.005

^aExperiments done in triplicate. ^bNot determined.

With ponatinib as the standard of care for imatinib-resistant CML harboring ABL1(T315I), we were initially interested in how our compounds compared in the imatinib resistant CML line, KCL22-IR. The compounds were active against the BCR-ABL1 cell lines, K562 and KCL22, with varying activity against KCL22-IR. Removing the methyl and substituting CH with N on the benzamide ring (ponatinib to HSN748) did not affect anticancer properties against the tested CML cell lines. In addition, reversing the amide bond in HSN748 (HSL338) did not result in a change in anti-cancer activity. Modification of the imidazo[1,2-*b*] pyridazine moiety resulted in attenuation of CML growth inhibition. Ponatinib, HSN748, HSL338, and HSL420 all share the imidazo[1,2-*b*] pyridazine ring system and they all inhibited the CML cell lines K562, KCL22 and KCL22-IR with similar efficacies (Table 3.2). However, when the imidazo[1,2-*b*] pyridazine was changed into imidazo[1,2-*a*] pyridine (HSL381) or imidazo[1,2-*a*] pyrazine (HSL385), there was a decrease in potency against the CML cell lines with the biggest difference seen in KCL22-IR. The imidazo[1,2-*a*] pyrimidine-containing compound (HSL382), was inactive against all of the three tested cell lines. Interestingly, when the ring system was changed to imidazol[1,2-*a*] pyrazine (HSL407), activity against K562 and KCL22 were maintained but a decrease in activity against KCL22-IR was seen.

3.3.4 Compounds exhibited potent inhibition against key kinases

Similar trends that were present against the cell lines were also seen when the compounds were profiled against several kinases. Ponatinib had less than 40% inhibition against FLT3(ITD) at 4 nM. However, several of the nicotinamide compounds had inhibition at over 80% such as HSN748 (86%), HSL381 (91%) and HSL338 (84%) at the same concentration. There was also an increase in FLT3(D835Y) inhibition in compounds containing the nicotinamide. Ponatinib had a 39% inhibition against FLT3(D835Y). When the nitrogen was added to make a nicotinamide ring (HSL420), there was no significant change in inhibition. When the methyl was then removed (HSN748), FLT3(D835Y) inhibition increased to 87%. This shows that even small modifications to a kinase inhibitor can result in drastic changes in kinase profiling. Inhibition of c-Src saw the opposite effect. At 111 nM, ponatinib had a 98% inhibition against c-Src. The methyl nicotinamide analog (HSL420), inhibited c-Src at 32%, whereas HSN748 had less than 10% inhibition. For ABL1(T315I) inhibition, it appears that a benzamide to nicotinamide switch had no effect on inhibition. At 123 nM, both HSL420 and ponatinib had similar inhibition against ABL1 (T315I)

at 83% and 90% respectively. Analogs that contained the imidazo[1,2-*b*]pyridazine (ponatinib, HSN748, HSL338, HSL420) system were generally more potent than analogs that did not against ABL1(T315I). Interestingly, when the imidazo[1,2-*b*]pyridazine was substituted with imidazo[1,2-*a*] pyridine (HSL381) potency against ABL1(T315I) was maintained at 73%. The compounds had differential activities against MNKs. At 123 nM, ponatinib inhibited MNK2 at 32% whereas HSN420 and HSN748 inhibited MNK2 at 51% and 85% respectively. MNK2 inhibition could tolerate minimal changes to the imidazo[1,2-*a*] pyridine as seen in HSL381 (imidazo[1,2-*a*] pyridine, 84% inhibition) and HSL385 (imidazo[1,2 – *a*] pyrazine, 72% inhibition).

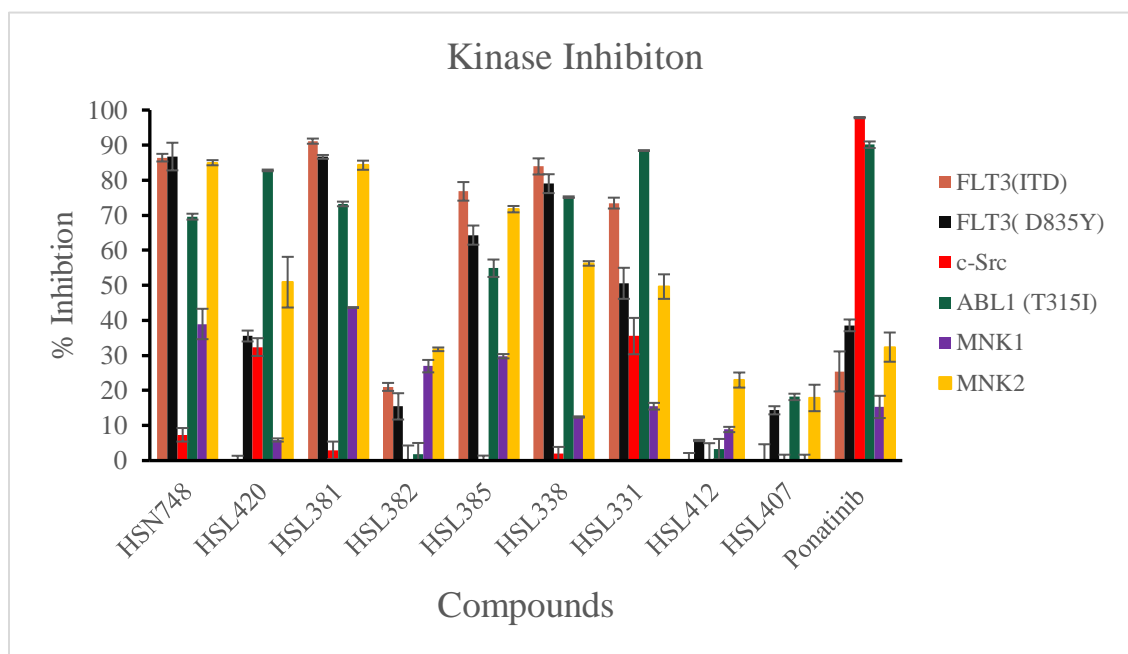


Figure 3.4. Kinase inhibition against key kinases. Compounds were screened at the following concentrations; FLT3(ITD) – 4 nM, FLT3(D835Y) and c-Src - 111 nM, ABL1(T315I), MNK1&2 at 123 nM. Percent inhibition is with respect to DMSO control, which is 0% inhibition. Data provided by Reaction Biology Corp.

3.3.5 Ponatinib is a more promiscuous kinase inhibitor than HSN748

The initial work with ponatinib analogs indicated that HSN748 and HSN381 had the best combined ABL1, FLT3 and MNK2 inhibitions. HSN748 was chosen for further studies because it had a lower cLogP and HPLC retention time than HSN381 (see Table 3.1). Therefore, we obtained IC₅₀ for ponatinib and HSN748 against various cancer-associated kinases (Table 3.3). Interestingly, as already established in the single concentration assay (Figure 3.4), the inhibition profile of

HSN748 against ABL1 (T315I) and FLT3-ITD were similar to ponatinib but there were some notable differences with other kinases (Table 3.3).

Table 3.3. IC₅₀ of ponatinib and HSN748 against several kinases

Kinase	IC ₅₀ (nM) ^a		
	HSN748	Ponatinib	Staurosporine
ABL1	1.1 ± 0.38	0.87 ± 0.05	379 ± 36.8
ABL1 (T315I)	11.1 ± 3.83	2.5 ± 0.13	310 ± 29.5
c-Kit	96 ± 4.21	30 ± 7.5	70.31 ± 39.42
c-SRC	>1000	4.6 ± 0.57	7.06 ± 1.16
FGFR1	24.4 ± 3.75	6.9 ± 0.29	20.1 ± 6.09
FGFR2	11.7 ± 0.97	6.0 ± 0.61	8.54 ± 2.97
FGFR3	96.4 ± 3.03	25.0 ± 1.68	35.4 ± 5.86
FGFR4	125.1 ± 0.92	46.8 ± 8.64	217 ± 63.1
FLT3 (D835Y)	13.8 ± 1.64	176 ± 3.11	0.06 ± 0.02
FLT3 (ITD)	1.5 ± 0.02	10.03 ± 0.11	1.81 ± 0.34
P38α/MAPK14	382.7 ± 17.4	86.6 ± 6.31	- ^b
p70S6K/RPS6KB1	273.1 ± 8.5	200.1 ± 17.5	0.80 ± 0.14
PDGFRα	10.7 ± 5.8	3.8 ± 0.29	3.88 ± 0.79
PDGFRβ	10.2 ± 1.02	7.01 ± 0.57	3.33 ± 0.67
RET	0.65 ± 0.05	0.88 ± 0.07	5.54 ± 0.09
MNK1	202 ± 13.4	3930 ± 707	108 ± 2.95
MNK2	9.36 ± 0.69	268 ± 84.1	27.88 ± 11.05

^aIC₅₀ was determined at Reaction Biology (Malvern, PA). [ATP] = 100 μM, experiments done in duplicates. ^bSB202190 (IC₅₀ = 55.5 ± 47.3) was used as the control for P38a/MAPK14.

HSN748 was inactive against c-Src kinase (IC₅₀ > 1 μM) while ponatinib potently inhibited c-Src (IC₅₀ of 4.6 nM), Table 3.3. Src has been shown to play various roles in heart function. For example, Src plays critical roles in maintaining the structure of myocyte²⁹. Despite the oncogenic role played by Src in various cancers, its inhibition could also come with the dysregulation of normal cells and platelets³⁰. It is therefore noteworthy that HSN748 does not inhibit Src while ponatinib does. c-Kit is an important player in hematopoiesis and substantial inhibition of c-kit causes myelosuppression³¹. The IC₅₀ for ponatinib against c-Kit is three times lower than HSN748.

Ponatinib has been shown to inhibit FGFRs and it is currently undergoing clinical trials for the treatment of biliary cancer with FGFR2 fusion⁷. Although many drugs that target FGFRs are currently undergoing clinical trials, FGFRs have important cardiac and liver functions and so their

inhibitions could lead to adverse events. Hyperphosphatemia is one major complication that is associated with FGFR inhibition due to interruption to FGF23 signaling³². Pan-FGFR inhibition has been linked to cardiovascular dysfunction³³. On the other hand, FGFR signaling also promotes AML resistance to drugs³⁴. Thus, some inhibition of FGFR signaling might enhance the efficacy of AML therapeutics. Ponatinib is slightly more active against FGFR1-4 than HSN748.

ABL1 and FLT3 are mutated in CML and AML respectively. Ponatinib and HSN748 have similar activities against ABL1, ABL1 (T315I) and FLT3-ITD. Interestingly HSN748 has a significantly lower IC₅₀ against FLT3 (D835Y) kinase than ponatinib (compare IC₅₀ of 14 nM for HSN748 versus 173 nM for ponatinib, see Table 3.1 and Figure 3.3). Most FLT3 inhibitors used in the clinic show initial efficacy but within months some patients relapse due to kinase mutation, which reduces the efficacy of treatment³⁵. The D835Y mutation is one of the most frequent mutations observed at in a study using the TKI quizartinib³⁶. Thus, for drug-resistant AML (due to kinase mutation), HSN748 could be a better treatment option than ponatinib.

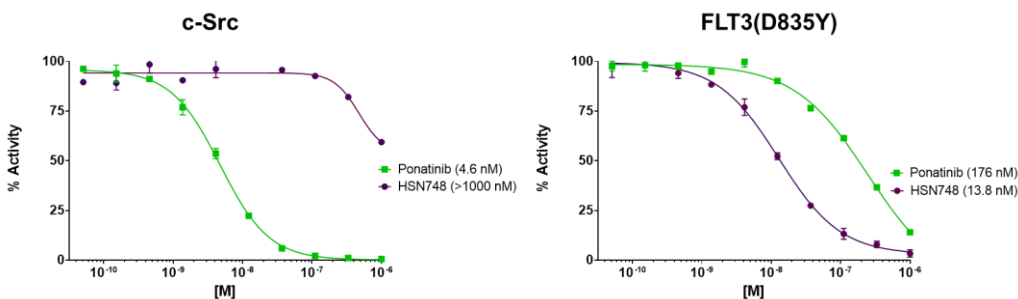


Figure 3.5. Dose response curves of ponatinib and HSN748 against Src and FLT3 (D835Y).

It is interesting that a -CH to -N switch in the benzamide of ponatinib can lead to such dramatic kinase selectivity's and potencies. Analyses of the crystal structures of ponatinib bound to several kinases (Figure 3.6) did not reveal an obvious hydrogen bonding interaction between the introduced nitrogen and active site residue, which would enhance binding. We however do not discount a role for an uncharacterized active site water molecule to mediate such interactions. In a beautiful work by Boxer at al. it was shown that the cyano moiety in bosutinib engaged in water-mediated hydrogen network³⁷. Future work, which solves the crystal structures of target kinases bound to HSN748, will help clarify how the nicotinamide nitrogen enhances binding.

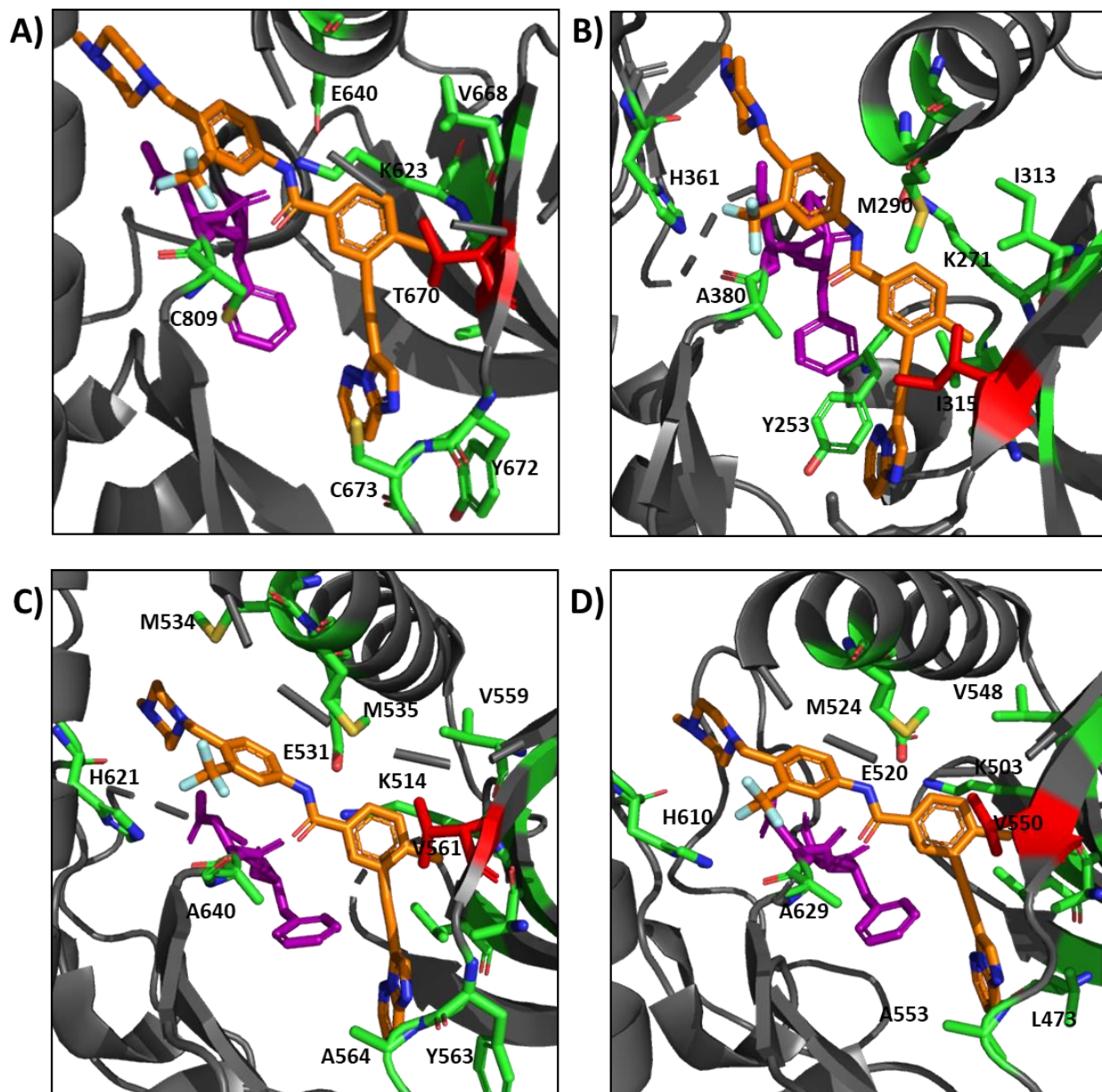


Figure 3.6: Active sites of various kinases with bound ponatinib (orange). Gatekeeper residues of each kinase are shown in red, DGF- motifs are shown in purple, amino acid residues within 4 Å of ponatinib are shown in green. A) KIT, PDBID: 4V0I; B) ABL1 with the T315I mutation PDBID: 3IK3; C) FGFR1, PDBID: 4V0I; D) FGFR4, PDBID: 4UXQ

Table 3.4: Activities of HSN748 and ponatinib against FLT3, ABL1, FGFR and RET-driven cancers.

Cell Line	IC ₅₀ (nM)	
	HSN748	Ponatinib
MV-4-11	0.07	0.09
MOLM13-res	1.73	24.1
MOLM14	0.25	0.45
MOLM14-D835Y	0.69	52.6
MOLM14-F691L	0.18	6.8
K562	0.8	0.6
KCL22	1.32	0.14
KCL22-IR	0.23	0.66
LC2/Ad	41	35.1
H520	838.6	128.2

We proceeded to test whether the degree of inhibition of FLT3, ABL1, RET and FGFR-driven cancers by ponatinib and HSN748 mirrored the order of kinase inhibition. The IC₅₀ for growth inhibition by both compounds against MV4-11 (FLT3), K562 (ABL1) and LC2/ad (RET) were similar. HSN748 was better at inhibiting quizartinib-resistant AML (MOLM14-D835Y cell line) than ponatinib (compare IC₅₀ of 0.69 nM for HSN748 and 52.6 nM for ponatinib). For gilteritinib-resistant AML cell line, Molm14 (ITD, F691L), HSN748 was also more potent than ponatinib (IC₅₀ of 0.18 nM for HSN748 and 6.8 nM for ponatinib).

3.4 Conclusion:

We have shown that the replacement of the benzamide moiety of ponatinib with nicotinamide results in enhanced activity against drug-resistant AML while reducing the inhibition of off-target kinases, such as Src, Kit and FGFRs. HSN748 is a lead compound that warrants further consideration as an antileukemia compound, with potentially less toxic profile than ponatinib. We are aware that idiosyncratic toxicities in real patient populations cannot be predicted based on *in vitro* kinase selectivity alone. Nonetheless, the fact that some level of kinase selectivity has been achieved is in the right direction towards a safer ponatinib analog. Ongoing

work will conduct further preclinical toxicity experiments on this new ponatinib analog, with an eye towards clinical translation.

3.5 Experimental Section:

Solvents and starting materials were purchased from commercial sources and used without further purifications.

3.5.1 General Cell Culture Procedure:

The human cell lines were cultured using RPMI-1640 (Gibco) supplemented with 10 % fetal bovine serum (FBS) (Atlanta Biologicals), 1% glutaMAX, and 1 % penicillin/streptomycin. Cells were seeded with 2×10^3 cells in each well of a 96 well plate and incubated for 24 h. Cells were then treated for 72 h with serial dilutions of the desired compound. After the 72 h, cells were treated with CellTiter- Blue Cell Viability Assay. The cells were then incubated for 3 h and absorbance at 570 nm was measured using a microplate reader. IC₅₀ values were then determined with GraphPad Prism.

3.5.2 General Kinase Assay Procedure (provided by Reaction Biology):

Reaction buffer: 20 mM Hepes (pH 7.5) 10 mM MgCl₂, 1 mM EGTA, 0.02% Brij35, 0.02 mg/mL BSA, 0.1 mM Na₃VO₄, 2 mM DTT, 1 % DMSO.

Reaction Procedure: To the kinase and corresponding substrate (see SI, Table S1 for details) in reaction buffer was added compounds (100% DMSO stock solution) via Acoustic technology (Echo500; nanoliter range). The mixture was incubated at room temperature for 20 min, after which ³³P-ATP was added to the mixture (final ATP concentration of 100 μM) to start the reaction. The reaction mixture was incubated at room temperature for 2 h and the degree of substrate phosphorylation was measured via the P81 filter-binding method.

3.5.3 General Sonogashira Coupling:

*5-(imidazo[1,2-*b*]pyridazin-3-ylethynyl)-6-methyl-N-(4-((4-methylpiperazin-1-yl)methyl)-3-(trifluoromethyl)phenyl)nicotinamide, HSL420*: Reaction was preformed using standard

sonagashira coupling procedure. Pd(PPh₃)₂Cl₂ (10 mol%) was used as catalyst. Yield = 38%. ¹H NMR (500 MHz, DMSO-*d*₆) δ 10.69 (s, 1H), 8.99 (d, *J* = 2.2 Hz, 1H), 8.73 (dd, *J* = 4.3, 2.2 Hz, 1H), 8.49 (d, *J* = 2.3 Hz, 1H), 8.28 – 8.24 (m, 2H), 8.19 (d, *J* = 2.5 Hz, 1H), 8.04 (d, *J* = 8.4 Hz, 1H), 7.70 (d, *J* = 8.5 Hz, 1H), 7.40 (ddd, *J* = 9.1, 4.5, 1.9 Hz, 1H), 3.56 (s, 2H), 2.80 (s, 3H), 2.41 (s, 8H), 2.21 (s, 3H). ¹³C NMR (126 MHz, DMSO-*d*₆) δ 163.8, 162.7, 148.4, 145.6, 140.3, 139.1, 138.4, 137.7, 132.8, 131.8, 127.8, 126.7, 124.0, 119.8, 117.8, 111.8, 95.2, 83.7, 57.8, 55.0, 52.8, 45.8, 24.0. HRMS (ESI⁺): calcd. for C₂₈H₂₇F₃N₇O (M + H⁺) 534.2224, found 534.2219.

*5-(imidazo[1,2-*a*]pyridin-3-ylethynyl)-N-(4-((4-methylpiperazin-1-yl)methyl)-3-(trifluoromethyl)phenyl)nicotinamide, HSL381* Reaction was preformed using standard sonagashira coupling procedure. Pd(PPh₃)₂Cl₂ (10 mol%) was used as catalyst. Yield = 24%. ¹H NMR (500 MHz, DMSO-*d*₆) δ 10.81 (s, 1H), 9.11 – 9.02 (m, 2H), 8.80 (d, *J* = 6.7 Hz, 1H), 8.62 (d, *J* = 2.2 Hz, 1H), 8.21 (d, *J* = 2.2 Hz, 1H), 8.09 (s, 1H), 8.05 (dd, *J* = 8.5, 2.2 Hz, 1H), 7.73 (t, *J* = 9.4 Hz, 2H), 7.46 (dd, *J* = 9.0, 6.7 Hz, 1H), 7.17 (t, *J* = 6.7 Hz, 1H), 3.58 (s, 2H), 2.48 (s, *J* = 1.7 Hz, 8H), 2.25 (s, 3H). ¹³C NMR (126 MHz, DMSO-*d*₆) δ 164.0, 153.9, 148.4, 139.5, 138.3, 137.4, 132.8, 131.8, 130.3, 128.1, 127.8, 127.5, 126.7, 125.8, 124.0, 123.6, 119.4, 118.0, 117.7, 114.5, 96.0, 81.4, 57.7, 54.8, 52.5, 45.5; HRMS (ESI⁺): calcd. for C₂₈H₂₆F₃N₆O (M + H⁺) 519.2115, found 519.2111.

*5-(imidazo[1,2-*a*]pyrimidin-3-ylethynyl)-N-(4-((4-methylpiperazin-1-yl)methyl)-3-(trifluoromethyl)phenyl)nicotinamide, HSL382:* Reaction was preformed using standard sonagashira coupling procedure. Pd(PPh₃)₂Cl₂ (10 mol%) was used as catalyst. Yield = 29%. ¹H NMR (500 MHz, DMSO-*d*₆) δ 10.92 (s, 1H), 9.28 (dd, *J* = 6.8, 2.0 Hz, 1H), 9.12 (d, *J* = 2.2 Hz, 1H), 9.06 (d, *J* = 2.0 Hz, 1H), 8.71 (dt, *J* = 4.2, 2.4 Hz, 2H), 8.24 (d, *J* = 2.2 Hz, 2H), 8.08 (dd, *J* = 8.5, 2.2 Hz, 1H), 7.72 (d, *J* = 8.5 Hz, 1H), 7.30 (dd, *J* = 6.7, 4.2 Hz, 1H), 3.57 (s, 2H), 2.42 (s, 8H), 2.22 (s, 3H). ¹³C NMR (126 MHz, DMSO-*d*₆) δ 163.9, 153.9, 152.6, 149.0, 148.7, 140.4, 138.4, 137.8, 135.3, 132.8, 131.8, 130.2, 128.0, 124.1, 123.6, 119.1, 117.8, 110.8, 106.4, 95.7, 80.6, 57.8, 54.9, 52.7, 45.7. HRMS (ESI⁺): calcd. for C₂₇H₂₅F₃N₇O (M + H⁺) 520.2067, found 520.2063.

*5-(imidazo[1,2-*a*]pyrazin-3-ylethynyl)-N-(4-((4-methylpiperazin-1-yl)methyl)-3-(trifluoromethyl)phenyl)nicotinamide, HSL385:* Reaction was preformed using standard

sonagashira coupling procedure. Pd(PPh₃)₂Cl₂ (10 mol%) was used as catalyst. Yield = 39%. ¹H NMR (500 MHz, DMSO-*d*₆) δ 10.85 (s, 1H), 9.21 (d, *J* = 1.5 Hz, 1H), 9.11 (dd, *J* = 18.4, 2.1 Hz, 2H), 8.88 (dd, *J* = 4.5, 1.5 Hz, 1H), 8.69 (d, *J* = 2.2 Hz, 1H), 8.28 (s, 1H), 8.21 (d, *J* = 2.2 Hz, 1H), 8.14 (d, *J* = 4.5 Hz, 1H), 8.05 (dd, *J* = 8.4, 2.2 Hz, 1H), 7.72 (d, *J* = 8.5 Hz, 1H), 3.57 (s, 2H), 2.48 – 2.28 (m, 8H), 2.23 (s, 3H). ¹³C NMR (126 MHz, DMSO-*d*₆) δ 163.9, 154.1, 148.9, 143.7, 140.9, 140.4, 138.3, 137.9, 132.9, 131.8, 131.3, 130.3, 127.8, 124.0, 123.6, 119.9, 118.8, 117.8, 108.9, 96.7, 79.8, 57.8, 54.9, 52.7, 45.7. HRMS (ESI⁺): calcd. for C₂₇H₂₅F₃N₇O (M + H⁺) 520.2067, found 520.2072.

N-(5-(imidazo[1,2-*b*]pyridazin-3-ylethynyl)pyridin-3-yl)-4-((4-methylpiperazin-1-yl)methyl)-3-(trifluoromethyl)benzamide, HSL338: Reaction was performed using standard sonagashira coupling procedure. Pd(PPh₃)₂Cl₂ (10 mol%) was used as catalyst. Yield = 29%. ¹H NMR (500 MHz, DMSO-*d*₆) δ 10.76 (s, 1H), 8.97 – 8.90 (m, 1H), 8.71 (dd, *J* = 4.4, 1.5 Hz, 1H), 8.57 – 8.51 (m, 1H), 8.45 (t, *J* = 2.2 Hz, 1H), 8.28 (d, *J* = 1.8 Hz, 1H), 8.25 (ddd, *J* = 8.4, 5.4, 1.7 Hz, 3H), 7.95 (d, *J* = 8.1 Hz, 1H), 7.40 (dd, *J* = 9.2, 4.4 Hz, 1H), 3.69 (s, 2H), 2.50 – 2.37 (m, 8H), 2.26 (s, 3H). ¹³C NMR (126 MHz, DMSO) δ 165.1, 146.5, 145.5, 142.0, 139.2, 135.9, 133.5, 132.2, 131.3, 129.2, 128.0, 127.7, 126.6, 125.6, 123.5, 119.8, 119.0, 111.8, 95.3, 80.2, 57.8, 54.8, 52.7, 45.6. HRMS (ESI⁺): calcd. for C₂₈H₂₅F₃N₇O (M + H⁺) 520.2067, found 520.2067.

3-(imidazo[1,2-*b*]pyridazin-3-ylethynyl)-*N*-(4-((4-methylpiperazin-1-yl)methyl)-3-(trifluoromethyl)phenyl)benzamide, HSL331: Reaction was performed using standard sonagashira coupling procedure. Pd(PPh₃)₂Cl₂ (10 mol%) was used as catalyst. Yield = 36%. ¹H NMR (500 MHz, DMSO-*d*₆) δ 10.64 (s, 1H), 8.71 (dd, *J* = 4.4, 1.6 Hz, 1H), 8.25 (dd, *J* = 9.2, 1.6 Hz, 1H), 8.23 – 8.20 (m, 3H), 8.07 – 8.00 (m, 2H), 7.82 (dt, *J* = 7.7, 1.4 Hz, 1H), 7.70 (d, *J* = 8.5 Hz, 1H), 7.64 (t, *J* = 7.8 Hz, 1H), 7.39 (dd, *J* = 9.2, 4.4 Hz, 1H), 3.56 (s, 2H), 2.39 (s, 8H), 2.18 (s, 3H). ¹³C NMR (126 MHz, DMSO-*d*₆) δ 165.2, 145.4, 139.0, 138.6, 135.4, 134.6, 132.6, 131.7, 130.5, 129.8, 129.1, 127.8, 126.6, 125.9, 124.0, 123.7, 122.4, 119.6, 117.8, 97.9, 78.0, 57.8, 55.0, 52.8, 45.8. HRMS (ESI⁺): calcd. for C₂₈H₂₆F₃N₆O (M + H⁺) 519.2113, found 519.2114.

N-(4-((4-methylpiperazin-1-yl)methyl)-3-(trifluoromethyl)phenyl)-5-(pyrazolo[1,5-*a*]pyrimidin-6-ylethynyl)nicotinamide, HSL412: Reaction was performed using standard sonagashira coupling procedure. Pd(PPh₃)₂Cl₂ (10 mol%) was used as catalyst. Yield = 32%. ¹H NMR (500 MHz,

DMSO-*d*₆) δ 10.86 (s, 1H), 9.58 (d, *J* = 2.0 Hz, 1H), 9.13 (d, *J* = 2.2 Hz, 1H), 8.97 (d, *J* = 2.0 Hz, 1H), 8.71 (d, *J* = 2.1 Hz, 1H), 8.55 (t, *J* = 2.2 Hz, 1H), 8.34 (d, *J* = 2.3 Hz, 1H), 8.21 (d, *J* = 2.2 Hz, 1H), 8.05 (dd, *J* = 8.5, 2.2 Hz, 1H), 7.72 (d, *J* = 8.5 Hz, 1H), 6.84 (d, *J* = 2.2 Hz, 1H), 3.58 (s, 2H) 2.50 – 2.34 (m, 8H), 2.28 (s, 3H). ¹³C NMR (126 MHz, DMSO-*d*₆) δ 163.8, 154.4, 151.3, 149.0, 147.1, 147.0, 139.2, 138.3, 138.1, 132.8, 131.9, 130.3, 127.8, 125.8, 124.0, 119.0, 117.8, 104.5, 98.0, 89.2, 87.6, 57.7, 54.7, 52.4, 45.3. HRMS (ESI⁺): calcd. for C₂₈H₂₆F₃N₆O (M + H⁺) 520.2067, found 520.2063.

*5-(imidazo[1,2-*a*]pyrazin-5-ylethynyl)-N-(4-((4-methylpiperazin-1-yl)methyl)-3-(trifluoromethyl)phenyl)nicotinamide, HSL407*: Reaction was preformed using standard sonagashira coupling procedure. Pd(PPh₃)₂Cl₂ (10 mol%) was used as catalyst. Yield = 86%. ¹H NMR (500 MHz, DMSO-*d*₆) δ 10.87 (s, 1H), 9.17 (d, *J* = 2.0 Hz, 3H), 8.76 (q, *J* = 2.5 Hz, 1H), 8.57 (s, 1H), 8.32 (s, 1H), 8.21 (d, *J* = 2.2 Hz, 1H), 8.07 – 8.00 (m, 2H), 7.72 (d, *J* = 8.5 Hz, 1H), 3.57 (s, 2H), 2.47 – 2.27 (m, 8H), 2.22 (s, 3H). ¹³C NMR (126 MHz, DMSO-*d*₆) δ 163.8, 154.8, 149.7, 143.7, 140.0, 138.7, 138.3, 136.8, 134.2, 133.0, 131.8, 130.4, 128.1, 125.8, 124.0, 117.9, 117.7, 115.4, 114.9, 96.8, 82.9, 57.8, 54.9, 52.7, 45.7, 40.5, 40.3, 40.1, 40.0, 39.8, 39.6. ¹³C NMR (126 MHz, DMSO-*d*₆) δ 163.7, 154.8, 149.7, 143.7, 140.0, 138.7, 138.3, 136.7, 134.2, 132.9, 131.8, 130.4, 128.1, 124.0, 123.6, 117.9, 117.7, 115.4, 114.9, 96.8, 82.9, 57.8, 54.9, 52.7, 45.7. HRMS (ESI⁺): calcd. for C₂₇H₂₅F₃N₇O (M + H⁺) 520.2067, found 520.2062.

3.6 Supporting Information:

The Supporting Information is available free of charge on the ACS Publications website.

¹H and ¹³C NMR spectra, HPLC traces of compounds

3.7 Author Information:

Corresponding Author:

E-mail: hsintim@purdue.edu

ORCID

Herman O. Sintim: 0000-0002-2280-9359

Present Address: Institute for Drug Discovery, Purdue University, 720 Clinic Drive, West Lafayette, IN 47907, USA

Notes:

HOS is a co-founder of KinaRx LLC, a start-up company interested in developing therapies for malignant neoplastic diseases.

3.8 Acknowledgement:

N. Naganna (a postdoc in the Sintim laboratory) synthesized HSN748. E. Larocque synthesized compounds HSL331, HSL420, HSL385, HSL382, HSL381, HSL 338, HSL412, HSL417. E. Larocque and E. Chu (a graduate student in Sintim laboratory) performed cell viability studies. E. Chu performed HPLC experiments. The manuscript was written by E. Larocque.

We thank Prof. Neil Shah for providing drug-resistant AML cell lines MOLM14 (ITD, D835Y) and MOLM14 (ITD, F691L)- Shah. We also thank Prof. Robert Kirken (University of Texas at El Paso) for donating KCL22 and KCL22-IR.

3.9 Funding Sources:

We thank Purdue University, Purdue University Center for Cancer Research and Elks Foundation for financial support. NMR and MS data were acquired by the NMR and MS facilities supported by NIH P30 CA023168.

3.10 Contributions:

H.O.S. designed the project. E.L. E. F. Y. C. and N.N. performed experiments. H.O.S. and E.L. wrote the manuscript. All authors reviewed the manuscript.

3.11 References

1. Ponatinib (marketed as Iclusig) Informaton. *FDA* (2018).
2. Ren, M. *et al.* Novel FGFR inhibitor ponatinib suppresses the growth of non-small cell lung cancer cells overexpressing FGFR1. *Oncol. Rep.* **29**, 2181–2190 (2013).
3. De Falco, V. *et al.* Ponatinib (AP24534) is a novel potent inhibitor of oncogenic RET mutants associated with thyroid cancer. *J. Clin. Endocrinol. Metab.* **98**, E811-819 (2013).
4. Gibbons, D. L., Pricl, S., Kantarjian, H., Cortes, J. & Quintás-Cardama, A. The rise and fall of gatekeeper mutations? The BCR-ABL1 T315I paradigm. *Cancer* **118**, 293–299 (2012).

5. Ponatinib for FLT3-ITD Acute Myelogenous Leukemia - Full Text View - ClinicalTrials.gov. <https://clinicaltrials.gov/ct2/show/NCT02428543>.
6. Ponatinib Hydrochloride in Treating Patients With Advanced Biliary Cancer With FGFR2 Fusions - Full Text View - ClinicalTrials.gov. <https://clinicaltrials.gov/ct2/show/NCT02265341>.
7. Ponatinib in Advanced NSCLC w/ RET Translocations - Full Text View - ClinicalTrials.gov. <https://clinicaltrials.gov/ct2/show/NCT01813734>.
8. Aghel, N., Delgado, D. H. & Lipton, J. H. Cardiovascular toxicities of BCR-ABL tyrosine kinase inhibitors in chronic myeloid leukemia: preventive strategies and cardiovascular surveillance. *Vasc. Health Risk Manag.* **13**, 293–303 (2017).
9. Pasvolsky, O. *et al.* Tyrosine kinase inhibitor associated vascular toxicity in chronic myeloid leukemia. *Cardio-Oncol.* **1**, 5 (2015).
10. Banavath, H. N., Sharma, O. P., Kumar, M. S. & Baskaran, R. Identification of novel tyrosine kinase inhibitors for drug resistant T315I mutant BCR-ABL: a virtual screening and molecular dynamics simulations study. *Sci. Rep.* **4**, (2014).
11. Moslehi, J. J. & Deininger, M. Tyrosine Kinase Inhibitor-Associated Cardiovascular Toxicity in Chronic Myeloid Leukemia. *J. Clin. Oncol. Off. J. Am. Soc. Clin. Oncol.* **33**, 4210–4218 (2015).
12. Baker, S. D. *et al.* Emergence of polyclonal FLT3 tyrosine kinase domain mutations during sequential therapy with sorafenib and sunitinib in FLT3-ITD-positive acute myeloid leukemia. *Clin. Cancer Res. Off. J. Am. Assoc. Cancer Res.* **19**, (2013).
13. Barreiro, E. J., Kümmerle, A. E. & Fraga, C. A. M. The Methylation Effect in Medicinal Chemistry. *Chem. Rev.* **111**, 5215–5246 (2011).
14. Pennington, L. D. & Moustakas, D. T. The Necessary Nitrogen Atom: A Versatile High-Impact Design Element for Multiparameter Optimization. *J. Med. Chem.* **60**, 3552–3579 (2017).
15. Vanotti, E. *et al.* Cdc7 Kinase Inhibitors: Pyrrolopyridinones as Potential Antitumor Agents. 1. Synthesis and Structure–Activity Relationships. *J. Med. Chem.* **51**, 487–501 (2008).
16. Verheij, M. H. P. *et al.* Design, Synthesis, and Structure–Activity Relationships of Highly Potent 5-HT₃ Receptor Ligands. *J. Med. Chem.* **55**, 8603–8614 (2012).
17. Remillard, D. *et al.* Dual Inhibition of TAF1 and BET Bromodomains from the BI-2536 Kinase Inhibitor Scaffold. *ACS Med. Chem. Lett.* **10**, 1443–1449 (2019).
18. Ma, X. *et al.* Identification of New FLT3 Inhibitors That Potently Inhibit AML Cell Lines via an Azo Click-It/Staple-It Approach. *ACS Med. Chem. Lett.* **8**, 492–497 (2017).

19. Larocque, E. *et al.* Aminoisoquinoline benzamides, FLT3 and Src-family kinase inhibitors, potently inhibit proliferation of acute myeloid leukemia cell lines. *Future Med. Chem.* **9**, 1213–1225 (2017).
20. Larocque, E. A., Naganna, N., Opoku-Temeng, C., Lambrecht, A. M. & Sintim, H. O. Alkynylnicotinamide-Based Compounds as ABL1 Inhibitors with Potent Activities against Drug-Resistant CML Harboring ABL1(T315I) Mutant Kinase. *ChemMedChem* **13**, 1172–1180 (2018).
21. Naganna, N. *et al.* Amino alkynylisoquinoline and alkynyl naphthyridine compounds potently inhibit acute myeloid leukemia proliferation in mice. *EBioMedicine* **40**, 231–239 (2019).
22. Wang, M., Naganna, N. & Sintim, H. O. Identification of nicotinamide aminonaphthyridine compounds as potent RET kinase inhibitors and antitumor activities against RET rearranged lung adenocarcinoma. *Bioorganic Chem.* **90**, 103052 (2019).
23. Daina, A., Michielin, O. & Zoete, V. SwissADME: a free web tool to evaluate pharmacokinetics, drug-likeness and medicinal chemistry friendliness of small molecules. *Sci. Rep.* **7**, (2017).
24. Zheng, B. & West, L. M. Estimating the Lipophilicity of Natural Products using a Polymeric Reversed Phase HPLC Method. *J. Liq. Chromatogr. Relat. Technol.* **33**, 118–132 (2009).
25. Tan, F. H., Putoczki, T. L., Stylli, S. S. & Luwor, R. B. Ponatinib: a novel multi-tyrosine kinase inhibitor against human malignancies. *Oncotargets Ther.* **12**, 635–645 (2019).
26. Hou, J., Lam, F., Proud, C. & Wang, S. Targeting Mnks for cancer therapy. *Oncotarget* **3**, 118–131 (2012).
27. Brown, M. C. & Gromeier, M. MNK Controls mTORC1:Substrate Association through Regulation of TELO2 Binding with mTORC1. *Cell Rep.* **18**, 1444–1457 (2017).
28. Lineham, E., Spencer, J. & Morley, S. J. Dual abrogation of MNK and mTOR: a novel therapeutic approach for the treatment of aggressive cancers. *Future Med. Chem.* **9**, 1539–1555 (2017).
29. Destaing, O. *et al.* The Tyrosine Kinase Activity of c-Src Regulates Actin Dynamics and Organization of Podosomes in Osteoclasts. *Mol. Biol. Cell* **19**, 394–404 (2008).
30. Turro, E. *et al.* A dominant gain-of-function mutation in universal tyrosine kinase SRC causes thrombocytopenia, myelofibrosis, bleeding, and bone pathologies. *Sci. Transl. Med.* **8**, 328ra30 (2016).
31. Galanis, A. & Levis, M. Inhibition of c-Kit by tyrosine kinase inhibitors. *Haematologica* **100**, e77-79 (2015).

32. Hierro, C., Rodon, J. & Tabernero, J. Fibroblast Growth Factor (FGF) Receptor/FGF Inhibitors: Novel Targets and Strategies for Optimization of Response of Solid Tumors. *Semin. Oncol.* **42**, 801–819 (2015).
33. Yanocho, G. M. *et al.* Pan-FGFR Inhibition Leads to Blockade of FGF23 Signaling, Soft Tissue Mineralization, and Cardiovascular Dysfunction. *Toxicol. Sci.* **135**, 451–464 (2013).
34. Karajannis, M. A. *et al.* Activation of FGFR1 β signaling pathway promotes survival, migration and resistance to chemotherapy in acute myeloid leukemia cells. *Leukemia* **20**, 979–986 (2006).
35. Daver, N. *et al.* Secondary mutations as mediators of resistance to targeted therapy in leukemia. *Blood* **125**, 3236–3245 (2015).
36. Levis, M. FLT3 mutations in acute myeloid leukemia: what is the best approach in 2013? *Hematol. Educ. Program Am. Soc. Hematol. Am. Soc. Hematol. Educ. Program* **2013**, 220–226 (2013).
37. Levinson, N. M. & Boxer, S. G. A conserved water-mediated hydrogen bond network defines bosutinib's kinase selectivity. *Nat. Chem. Biol.* **10**, 127–132 (2014).

CHAPTER 4. PYRIDO[3,4-*b*]PYRAZINE BASED COMPOUNDS AS POTENTIAL ANTICANCER AGENTS

4.1 Abstract

Many cancers are driven by aberrantly expressed or mutated kinases. Therefore, driving drug discovery efforts to focus on the development of kinase inhibitors for the potential treatments of cancers. Since 2001, when imatinib (one of the first kinase inhibitors, KIs, to be approved for human use) entered the market for the treatment of BCR-ABL1 driven chronic myeloid leukemia, an additional 54 kinase inhibitors have been approved by the FDA for the treatment of cancer. However, despite the availability of many kinase inhibitor treatment options, it is now well observed that after prolonged use, many KIs become ineffective. This is commonly due to secondary mutations and/or the upregulations of other compensatory pathways. Thus, the development of novel chemotypes, which could inhibit secondary mutated kinases that are commonly found in relapsed cancer patients, is hotly pursued by both academia and industry. Previously, we reported that alkynylisoquinolines or naphthyridines are potent inhibitors of drug resistant FLT3, ABL1 and RET kinases. Here we disclose that the analogous pyrido[3,4-*b*]pyrazine, containing additional nitrogen's, are also potent inhibitors of cancers driven by drug-resistant FLT3 and ABL1

4.2 Introduction

Imatinib was approved in 2001 to treat chronic myeloid leukemia harboring the BCR-ABL1 fusion protein¹. Since this approval, kinases have been the target of many new treatment options against several different types of cancer. However, it has become clear that many of the developed kinase inhibitors become ineffective after prolonged use, most after only a few years, due to tumor resistance. Although many classic resistance mechanisms, such as drug efflux, drug degradation or modification account for a significant fraction of resistance mechanisms, kinase target modification(s) and/or upregulation of other kinase signaling pathways are often at play to reduce drug's efficacy². For example, gefitinib is used for treatment of EGFR-driven lung cancer but after prolonged use a T790M mutation occurs, which abrogates binding of gefitinib to EGFR³.

Another example is idelalisib, a PI3K inhibitor, which loses potency via an ill understood mechanism⁴.

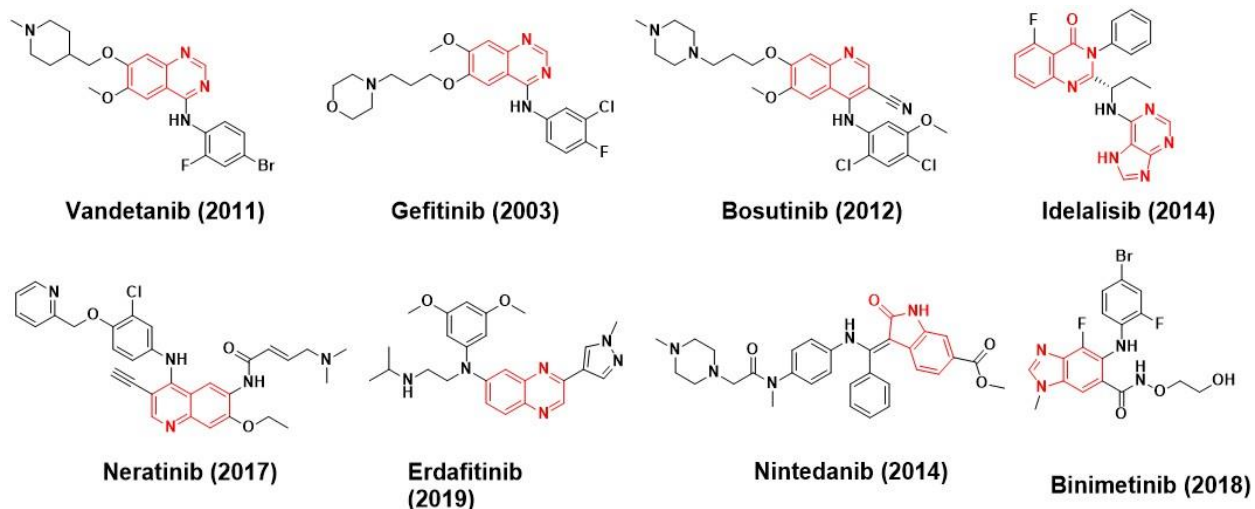


Figure 4.1. Approved kinase inhibitors that contained isoquinolines, quinolines, indazoles, quinazolines, quinazolinones, quinoxalines, and oxindole

Many kinase inhibitors contain privileged nitrogen-containing bicyclic systems such as quinoline (bosutinib and neratinib), isoquinoline (fasudil and netarsudil), indazole (axitinib), quinazolines (vandetanib and gefitinib), quinazolinone (idelalisib), quinoxaline (erdafitinib), and oxindole (nintedanib), Figure 4.1. We recently reported that alkynyl isoquinolines or naphthyridines are excellent kinase inhibitors, displaying subnanomolar activities against various cancer-driver kinases, such as FLT3, ABL1 and RET⁵⁻¹⁰. Nitrogen is considered an essential atom in drug discovery and many reports have demonstrated that the addition of nitrogen into lead compounds can improve drug potency by enhancing both target engagement and drugness (typically via solubility enhancement)¹¹. The introduction of methyl group into lead compounds is also considered a “high value” medicinal chemistry strategy. Often the introduction of a methyl group (and to some extent an ethyl or isopropyl groups) to lead molecules improves compound potency and drugness (Figure 4.2)^{12,13}.

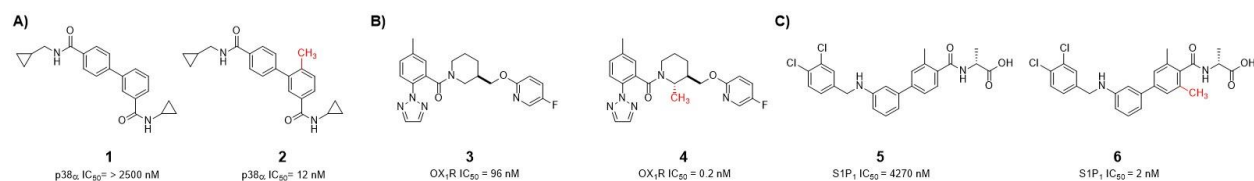


Figure 4.2. Examples of increased potency with the addition of a strategic methyl group (additional methyl groups shown in red). Increase in potency can be seen in inhibition of A) p38 α B) OX₁R and C) S1P₁

Schönherr et al. demonstrated that by strategically placing methyl groups on lead compounds the activity can significantly improve¹³. For example, against p38 α , compound 1 has an IC_{50} of over 2500 nM (Figure 4.2A)¹³. When a methyl is introduced there is an increase in potency to an IC_{50} 12 nM (Figure 4.2A). There is also an increase in potency shown with methyl addition against OX₁R and S1P₁ (Figure 4.2B and Figure 4.2C)¹³. The approach to activity cliffs via methyl group introduction is poorly understood. Thus, we decided to prepare analogs of our previously reported alkynyl isoquinolines or naphthyridines, whereby an additional nitrogen has been introduced into the bicyclic moiety to arrive at the analogous pyrido[3,4-b]pyrazines (see Figure 4.3).

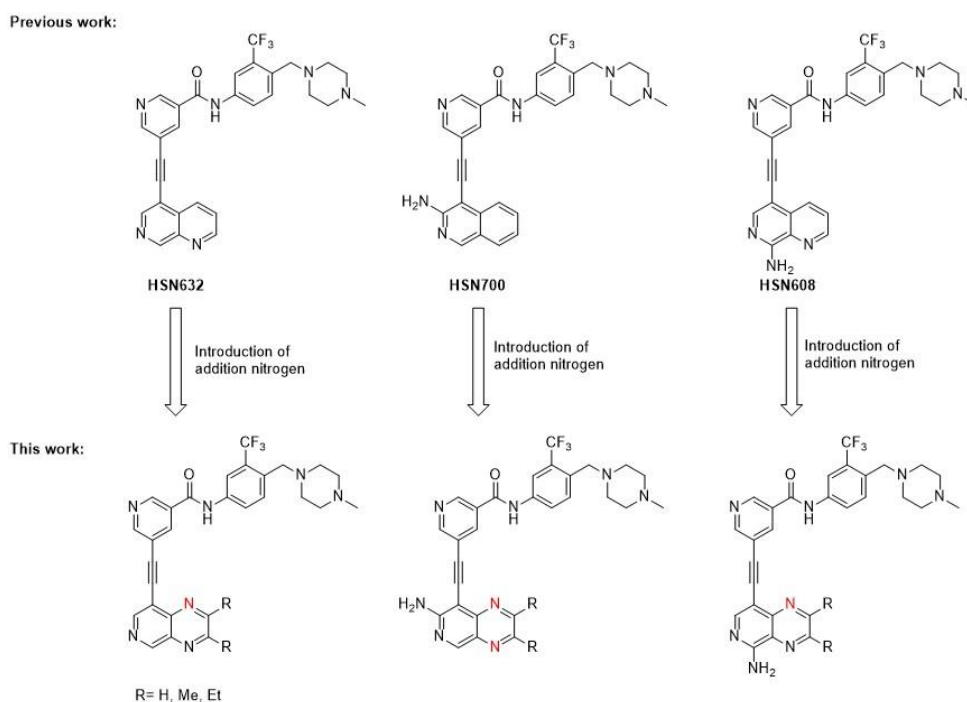


Figure 4.3. Previous analogs synthesized by the Sintim Lab that feature fused six-membered ring systems. HSN608 was reported as a potent inhibitor of ABL1⁷.

4.3 Results and Discussion

4.3.1 Synthesis of pyrido[3,4-*b*]pyrazine based analogs

The synthesis of pyrido[3,4-*b*]pyrazine motifs bearing a bromo- or iodo- unit, essential for the subsequent Sonogashira coupling, involves one to three steps depending on the presence and/or location of the amine (see Figure 4.4). For the synthesis of bromopyrido[3,4-*b*]pyrazine analogs, the requisite haloarene starting material (8-bromopyrido[3,4-*b*]pyrazine analogs) for the Sonogashira reaction, was synthesized via the reaction of 5-bromopyridine-3,4-diamine with a diketone in ethanol (see Figure 4.4A). 8-Iodopyrido[3,4-*b*]pyrazin-7-amine analogs were synthesized in a similar manner starting with the reaction of pyridine-2,4,5-triamine with the desired diketone in ethanol (Figure 4.4B). The reaction gave rise to pyrido[3,4-*b*]pyrazin-7-amine derivatives. These were then transformed into the desired 8-iodopyrido[3,4-*b*]pyrazin-7-amine after iodine addition, using NIS as reagent in methanol at 0°C (Figure 4.4B). The synthesis of the 8-bromopyrido[3,4-*b*]pyrazin-5-amine was a three-step process (see Figure 4.4C). The first step was the reaction of 2,5-dibromopyridine-3,4-diamine with the desired diketone to give rise to 5,8-dibromopyrido[3,4-*b*]pyrazine analogs. 5,8-Dibromopyrido[3,4-*b*]pyrazine analogs were then heated with tertbutylamine in ethanol at 110°C to afford 8-bromo-*N*-(tert-butyl)pyrido[3,4-*b*]pyrazin-5-amines. Cleavage of the *t*-butyl group with HCl at 80°C resulted in the final 8-bromopyrido[3,4-*b*]pyrazin-5-amine analogs (Figure 4.4C).

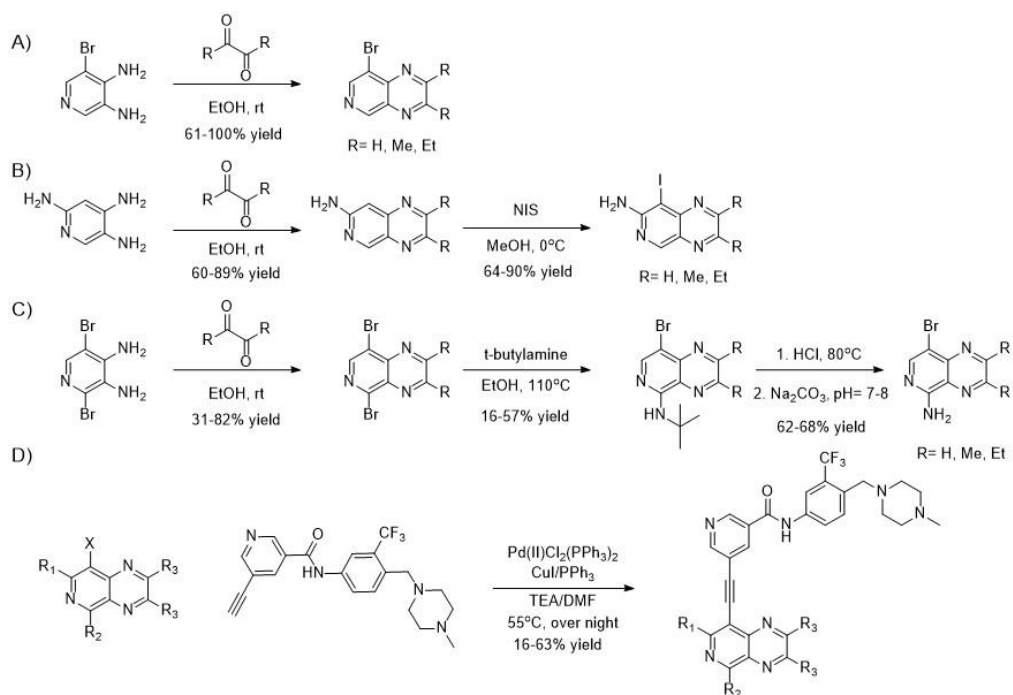


Figure 4.4. Synthetic pathways for pyrido[3,4-*b*]pyrazine analogs

Once the pyrido[3,4-*b*]pyrazine analogs were synthesized they then underwent Sonagashira coupling to afford the compound library (Figure 4.4D and Figure 4.5).

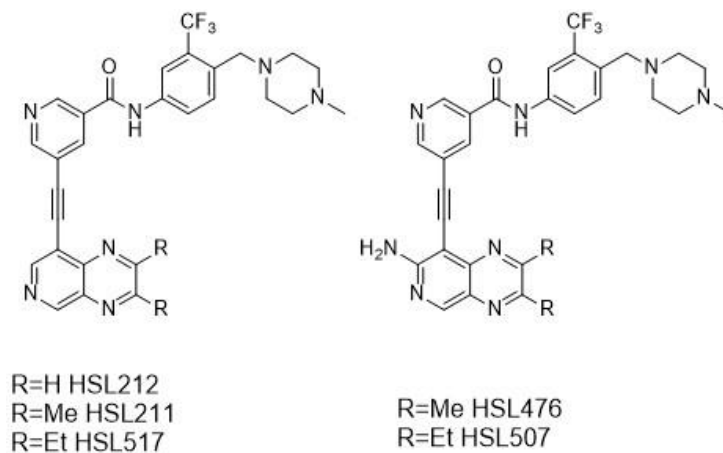


Figure 4.5. pyrido[3,4-*b*]pyrazine compound library

4.3.2 Compounds potently inhibit AML and CML cell lines

With compounds in hand they were then screened against several AML and CML cell lines. MOLM14 is an AML cell line that contains the FLT3-ITD mutation. All pyrido[3,4-*b*]pyrazine analogs showed subnanomolar inhibition. The most potent pyrido[3,4-*b*]pyrazine analog, HSL476, contained an 2,3-dimethylpyrido[3,4-*b*]pyrazin-7-amine and had an IC₅₀ of 0.08 nM against MOLM14. This is comparable to previously synthesized analogs, HSN632 which contains a 1,7-naphthyridine and HSN608 which contains a 1,7-naphthyridin-8-amine (Table 4.1).

Compounds were also then screened against cell lines that contained both the FLT3-ITD mutation as well as common point mutations seen in the clinic (D835Y and F691L). Against MOLM14-D835Y compounds lost potency but were still able to inhibit cell growth at a low IC₅₀. For example, HSL211 and HSL476, which both contain the 2,3-dimethylpyrido[3,4-*b*]pyrazine moiety, had IC₅₀'s of 1.17 nM and 2 nM respectively against MOLM14-D835Y. HSN700 and HSN608, which contain different heterocycles (isoquinoline and naphthyridine cores respectively) inhibited the same cell line (MOLM14-D835Y) with IC₅₀ values of 7.4 nM and 6.96 nM respectively. These values are similar to the IC₅₀ values of the 3-dimethylpyrido[3,4-*b*]pyrazine-containing HSL211 and HSL476. However, HSL212, which contains the pyrido[3,4-*b*]pyrazine and hence more similar to HSL211 than HSN608 or 700, inhibited MOLM14-D835Y with IC₅₀ value of 19 nM (a fold less than HSL211). HSN632, which is similar to HSL212 but lacks an additional heterocyclic nitrogen, inhibited MOLM14-D835Y with IC₅₀ value of 21 nM. It appears that the introduction of an additional nitrogen into a naphthyridine to arrive at pyrido[3,4-*b*]pyrazine did not drastically affect the inhibition potential of MOLM14-D835Y. HSL517 and HSL507 containing 2,3-diethylpyrido[3,4-*b*]pyrazine and amino 2,3-diethylpyrido[3,4-*b*]pyrazine respectively, had IC₅₀'s of 8.64 nM and 5 nM respectively against the MOLM14-D835Y (Table 4.1), indicating that an additional exocyclic NH₂ group did not impact antileukemia activity.

Against MOLM14-F691L, all compounds were potent inhibitors (IC₅₀'s less than 10 nM), in contrast to the trends against MOLM14-D835Y. The 2,3-dimethylpyrido[3,4-*b*]pyrazine, HSL211 and HSL476 displayed subnanomolar IC₅₀'s against this cell line (Table 4.1).

Table 4.1. Antiproliferation activity of compound library against AML and CML cell lines

Compound	LogP ^b	IC ₅₀ (nM) ^a					
		MOLM14	MOLM14-D835Y	MOLM14-F691L	K562	KCL22	KCL22-IR
HSN632	3.88	0.04	21.3	1.38	nd	1.26	nd
HSL212	3.19	0.54	19.12	nd	nd	3.13	> 100 nM
HSL211	3.87	0.13	1.17	0.64	1.07	0.55	7.95
HSL517	4.49	0.89	8.64	3.78	30.2	11.03	> 100 nM
HSN700	4.13	0.33	7.4	0.96	nd	1.5	2.6
HSL476	3.53	0.08	2.13	0.53	0.25	0.16	1.3
HSL507	4.11	0.28	5.03	2.15	8.76	4.46	37
HSN608	3.43	0.07	6.96	0.4	0.76	1	4.14

^aIC₅₀'s were determined in triplicate ^bLogP are consensus LogP calculated by SwissADME nd= not determined

K562 and KCL22 are both imatinib sensitive cell lines, which only contain the BCR-ABL1 mutation while KCL22-IR is an imatinib resistant cell line which contains the T315I mutation¹⁴⁻¹⁶. When screened against the imatinib sensitive cell lines, compounds maintained potency but were not as potent compared to the AML lines. HSL211 and HSL476 were most efficacious at subnanomolar or subnanomolar concentrations. HSL517 and HSL507 (2,3-diethylpyrido[3,4-b]pyrazine) were less potent with IC₅₀'s of 30.2 nM and 8.76 nM respectively against K562. HSN608 maintains its potency against K562 with and IC₅₀ of 0.76 nM (Table 4.1). Similar trends were observed in KCL22 and KCL22-IR. HSL211 and HSL476 remained the most potent with subnanomolar IC₅₀'s against KCL22. HSL507 and HSL517 did not have as drastic decrease in potency compared to K562 but were still less potent compared to rest of the compound library. HSL212 and HSL517 had IC₅₀'s greater than 100 nM against KCL22-IR and HSL507 increased to 37 nM (Table 4.1). HSL211 and HSL476 did have a decrease in potency against KCL22-IR to 7.95 nM and 1.3 nM respectively.

The 2,3-dimethylpyrido[3,4-b]pyrazine analogs (HSL211 and HSL476) maintained their potency more effectively compared to the other pyrido[3,4-b]pyrazine analogs. As previously mentioned, the addition of methyl groups is a common medicinal chemistry strategy that can drastically improve compound efficacy¹². This trend was observed in the pyrido[3,4-b]pyrazine

analogs. While both HSL211 and HSL476 are more potent, HSL476 contains exocyclic amine (NH₂), which could allow for better binding in the active site as it is both a proton acceptor and donor (Figure 4.6).

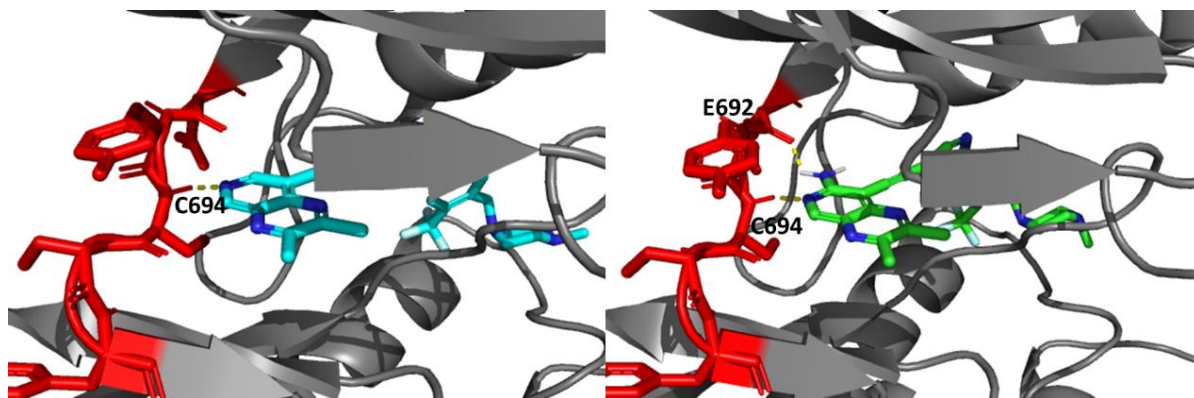


Figure 4.6. Docking of HSL211 (left) and HSL476 (right) with FLT3 (PDBID: 4RT7). Both compounds have nitrogen that binds to the cystine at the 694 position in the hinge region (red). The free amine allows for an extra polar contact with the glutamic acid in the hinge region.

4.4 Conclusion

Herein we report the synthesis and biological activity of novel pyrido[3,4-b]pyrazine compounds. These compounds potently inhibit AML and CML driven cell lines at subnanomolar concentrations. These compounds are also active against cell lines that include secondary point mutations that are often seen in the clinic.

4.5 References

1. How Gleevec Transformed Leukemia Treatment. *National Cancer Institute* <https://www.cancer.gov/research/progress/discovery/gleevec> (2015).
2. Housman, G. *et al.* Drug Resistance in Cancer: An Overview. *Cancers* **6**, 1769–1792 (2014).
3. Morgillo, F., Della Corte, C. M., Fasano, M. & Ciardiello, F. Mechanisms of resistance to EGFR-targeted drugs: lung cancer. *ESMO Open* **1**, (2016).
4. Scheffold, A. *et al.* IGF1R as druggable target mediating PI3K-d inhibitor resistance in a murine model of chronic lymphocytic leukemia. 14.
5. Ma, X. *et al.* Identification of New FLT3 Inhibitors That Potently Inhibit AML Cell Lines via an Azo Click-It/Staple-It Approach. *ACS Med. Chem. Lett.* **8**, 492–497 (2017).

6. Larocque, E. *et al.* Aminoisoquinoline benzamides, FLT3 and Src-family kinase inhibitors, potently inhibit proliferation of acute myeloid leukemia cell lines. *Future Med. Chem.* **9**, 1213–1225 (2017).
7. Larocque, E. A., Naganna, N., Opoku-Temeng, C., Lambrecht, A. M. & Sintim, H. O. Alkynylnicotinamide-Based Compounds as ABL1 Inhibitors with Potent Activities against Drug-Resistant CML Harboring ABL1(T315I) Mutant Kinase. *ChemMedChem* **13**, 1172–1180 (2018).
8. Naganna, N. *et al.* Amino alkynylisoquinoline and alkynyl naphthyridine compounds potently inhibit acute myeloid leukemia proliferation in mice. *EBioMedicine* **40**, 231–239 (2019).
9. Wang, M., Naganna, N. & Sintim, H. O. Identification of nicotinamide aminonaphthyridine compounds as potent RET kinase inhibitors and antitumor activities against RET rearranged lung adenocarcinoma. *Bioorganic Chem.* **90**, 103052 (2019).
10. Larocque, E., Chu, E. F. Y., Naganna, N. & Sintim, H. O. Nicotinamide–Ponatinib Analogues as Potent Anti-CML and Anti-AML Compounds. *ACS Omega* **5**, 2690–2698 (2020).
11. Pennington, L. D. & Moustakas, D. T. The Necessary Nitrogen Atom: A Versatile High-Impact Design Element for Multiparameter Optimization. *J. Med. Chem.* **60**, 3552–3579 (2017).
12. Barreiro, E. J., Kümmerle, A. E. & Fraga, C. A. M. The Methylation Effect in Medicinal Chemistry. *Chem. Rev.* **111**, 5215–5246 (2011).
13. Schönherr, H. & Cernak, T. Profound Methyl Effects in Drug Discovery and a Call for New C-H Methylation Reactions. *Angew. Chem. Int. Ed.* **52**, 12256–12267 (2013).
14. Colavita, I. *et al.* Gaining insights into the Bcr-Abl activity-independent mechanisms of resistance to imatinib mesylate in KCL22 cells: a comparative proteomic approach. *Biochim. Biophys. Acta* **1804**, 1974–1987 (2010).
15. Yuan, H. *et al.* BCR-ABL Gene Expression Is Required for Its Mutations in a Novel KCL-22 Cell Culture Model for Acquired Resistance of Chronic Myelogenous Leukemia. *J. Biol. Chem.* **285**, 5085–5096 (2010).
16. Oaxaca, D. M. *et al.* Sensitivity of imatinib-resistant T315I BCR-ABL CML to a synergistic combination of ponatinib and forskolin treatment. *Tumor Biol.* **37**, 12643–12654 (2016).

APPENDIX A. CHAPTER 2 SUPPORTIVE INFORMATION

This appendix was reprinted with permission from John Wiley and Sons. Original article can be found at Larocque, E. A., Naganna, N., Opoku-Temeng, C., Lambrecht, A. M. & Sintim, H. O. Alkynylnicotinamide-Based Compounds as ABL1 Inhibitors with Potent Activities against Drug-Resistant CML Harboring ABL1(T315I) Mutant Kinase. *ChemMedChem* **13**, 1172–1180 (2018).

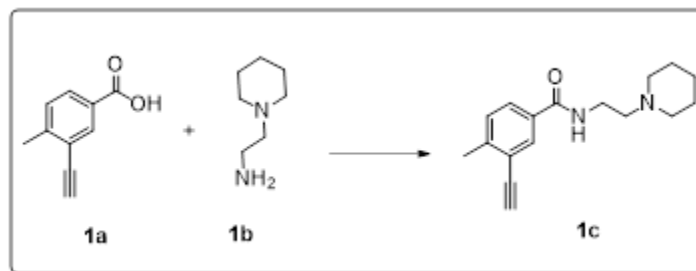
Compound 1,2, and 9 and Compounds 15-33 were synthesized by N. Naganna and for experimental details and characterization see Larocque, E. A., Naganna, N., Opoku-Temeng, C., Lambrecht, A. M. & Sintim, H. O. Alkynylnicotinamide-Based Compounds as ABL1 Inhibitors with Potent Activities against Drug-Resistant CML Harboring ABL1(T315I) Mutant Kinase. *ChemMedChem* **13**, 1172–1180 (2018).

General Methods

Unless stated otherwise, all Sonogashira reactions were performed with anhydrous and deoxygenated solvents. Commercially available chemicals were used without further purification. All the reactions were monitored by thin-layer chromatography (TLC). TLC was performed using Merck silica gel 60 F254 precoated plastic plates and visualized by UV fluorescence quenching. Normal phase prepacked Silica gel columns (Cat. No: 69-2203-312) was used for flash chromatography. ¹H NMR spectra were recorded on Brukar AV 500 MHz spectrometer. Data for ¹H NMR are reported as follows: chemical shift (δ ppm) (multiplicity, coupling constant (Hz), integration). Multiplicities are reported as follows: s = singlet, d = doublet, t = triplet, q = quartet, p = pentet, sept = septuplet, m = multiplet, br s = broad singlet, ¹³C NMR spectra were recorded on a Brukar AV 500 MHz spectrometer (125 MHz) Highresolution mass spectra (HRMS) were obtained on Agilent high resolution 6550 quadrupole time-of-flight (Q-TOF). Analytical RP-HPLC was carried out on a Agilent Eclipse system using water (0.1% NH₄OH) and Methanol as the mobile phase and a Agilent Eclipse plus C18 column, 3.5 μ m, 4.6 \times 100 mm column as the stationary phase. The compounds were injected at a concentration of 500 μ M solution. The following compounds were purchased from commercial sources and used without purification: Sigma, US: 8a (3-ethynylbenzoic acid), 26a (4-ethynylbenzaldehyde) 26b (2-methylpropane- 1,2-diamine) Enamine LLC, US: 14a (5-ethynylnicotinic acid), 15 (4-(morpholinomethyl)-3-(trifluoromethyl)aniline), 7a (5-bromo-1,7-naphthyridin-8-amine), 16b (4-(pyrrolidin-1-ylmethyl)-3-(trifluoromethyl)aniline), 17b (4-((dimethylamino)methyl)-3-(trifluoromethyl)aniline), 18b (4-((dimethylamino)methyl)-3-methylaniline), 19b (3-chloro-4-

((dimethylamino)methyl)aniline), 20b (4-((dimethylamino)methyl)-3-fluoroaniline), 4b (2-(4-methylpiperazin-1-yl)ethan-1-amine), 1b (2-(piperidin-1-yl)ethan-1-amine) Oxchem Corporation, US: 22a (1-methylisoquinolin-3-amine), 23a (6-fluoroisoquinoline-3-amine), 9a (3-bromo-4-fluorobenzoic acid), 5a (3-bromoimidazo[1,2-b]pyridazine) Ark Pham, Inc., US: 8b (4-((4-methylpiperazin-1-yl)methyl)-3-(trifluoromethyl)aniline), 6a (4-bromoisoquinolin-1-amine), 24b (3-(4-methyl-1H-imidazol-1-yl)-5-(trifluoromethyl)aniline) 10a (3-bromo-4-chlorobenzoic acid), 11a (3-bromo-4-ethylbenzoic acid), 3b (2-morpholinoethan-1-amine), 2d (6-chloroisoquinolin-3-amine) Asta Tech Inc., US: 13a (5-bromo-6-methylnicotinic acid), 25a (5-bromo-1-methyl-1H-pyrrole-3-carboxylic acid), 26d (4-chloro-6,7-dimethoxyquinazolin-2-amine), 12a (3-bromo-4-cyanobenzoic acid) Aurum Pharmatech, US: 1a (3-ethynyl-4-methylbenzoic acid)

Synthesis and analytical data of compounds



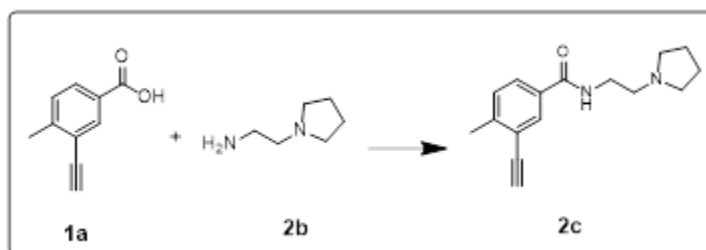
3-ethynyl-4-methyl-N-(2-(piperidin-1-yl)ethyl)benzamide (1c): Compound 1a (200mg, 1.25 mol, 1 eq) and HCTU (240 mg, 1.5 mol, 1.2 eq) were added to a round bottom flask, air vacuumed out and protected with a balloon of argon. Dry DCM (10 mL) was then added and allowed to dissolve compound 1a. The round bottom was then placed on ice and temperature allowed to reach 0°C. DIPEA (0.68 mL, 3.75 mol, 3 eq) was then added to the DCM solution. Compound 1b (240 mg, 1.9 mol, 1.5 eq) was then added to the flask. Temperature was then raised to room temperature and allowed to run over night. The crude compound was extracted using water (3 × 40 mL). Combined organic layers were dried over anhydrous sodium sulphate, filtered and concentrated in vacuo. The pure product 1c was then obtained via flash column chromatography. Yield = 70%

¹H NMR (500 MHz, DMSO-d₆) δ 8.87 (s, 1H), 8.70 (s, 1H), 7.93 (d, J = 1.9 Hz, 1H), 7.77 (dd, J = 8.0, 2.0 Hz, 1H), 7.41 (d, J = 8.0 Hz, 1H), 4.48 (s, 1H), 3.64 – 3.46 (m, 4H), 3.20 (s, 2H), 2.91

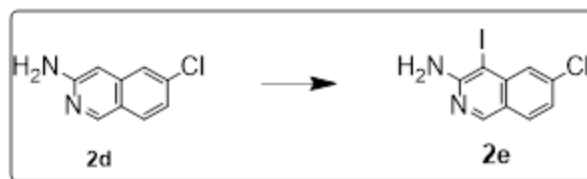
(d, $J = 11.3$ Hz, 2H), 2.42 (s, 3H), 1.82 (d, $J = 14.4$ Hz, 2H), 1.73 – 1.54 (m, 3H), 1.37 (s, 1H); ^{13}C NMR (126 MHz, DMSO) δ 166.28, 144.12, 132.02, 131.17, 130.24, 128.29, 122.08, 85.82, 82.02, 55.51, 52.76, 34.64, 22.99, 21.66, 20.64 HRMS (ESI+) calculated for $\text{C}_{17}\text{H}_{22}\text{N}_2\text{O}$ 271.1805 found 462.2058

Compound 1: Synthesis and characterization of this compound can be found at Larocque, E. *et al.* Aminoisoquinoline benzamides, FLT3 and Src-family kinase inhibitors, potently inhibit proliferation of acute myeloid leukemia cell lines. *Future Med. Chem.* **9**, 1213–1225 (2017).

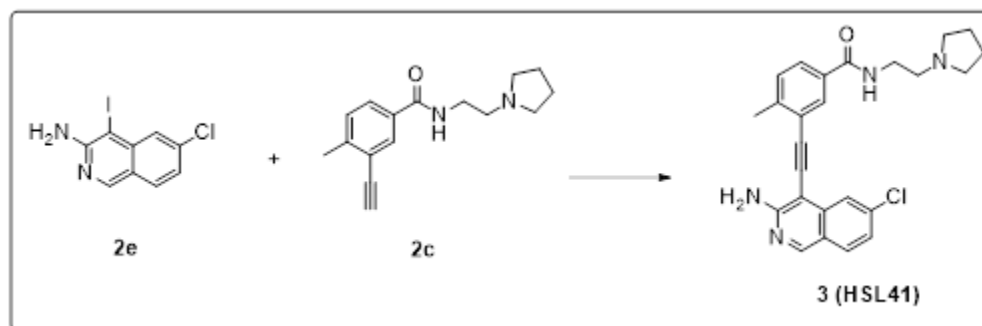
Compound 2: Synthesis and characterization of this compound can be found at Larocque, E. *et al.* Aminoisoquinoline benzamides, FLT3 and Src-family kinase inhibitors, potently inhibit proliferation of acute myeloid leukemia cell lines. *Future Med. Chem.* **9**, 1213–1225 (2017).



3-ethynyl-4-methyl-N-(2-(pyrrolidin-1-yl)ethyl)benzamide (2c): Compound 1a (250 mg, 1.56 mol, 1 eq) and HCTU (709 mg, 1.72 mol, 1.1 eq) were added to a round bottom flask, air vacuumed out and protected with a balloon of argon. Dry DCM was then added and allowed to dissolve compound 8a. The round bottom was then placed on ice and temperature allowed to reach 0°C . DIPEA (815 mg, 4.68 mol, 3 eq) was then added to the DCM solution. Compound 2b (178 mg, 1.56 mol, 1 eq) was then added to the flask. Temperature was then raised to room temperature and allowed to run over night. The crude compound was extracted using water (3×40 mL). Combined organic layers were dried over anhydrous sodium sulphate, filtered and concentrated in vacuo. The pure product 2c was then obtained via flash column chromatography. Yield = 62.74 % (10 % MeOH/DCM) ^1H NMR (500 MHz, DMSO- d_6) δ 8.48 (t, $J = 5.7$ Hz, 1H), 7.91 (d, $J = 2.0$ Hz, 1H), 7.75 (dd, $J = 8.0, 2.0$ Hz, 1H), 7.36 (d, $J = 8.0$ Hz, 1H), 4.45 (s, 1H), 3.36 (q, $J = 6.7$ Hz, 2H), 2.60 (t, $J = 7.0$ Hz, 2H), 2.40 (s, 3H), 1.67 (t, $J = 3.6$ Hz, 4H); ^{13}C NMR (126 MHz, DMSO) δ 165.47, 143.57, 132.63, 131.10, 130.08, 128.16, 121.97, 85.55, 82.15, 55.21, 54.09, 38.89, 23.56, 20.59 HRMS (ESI+): calc [M+H]: 257.1648 found: 257.1650

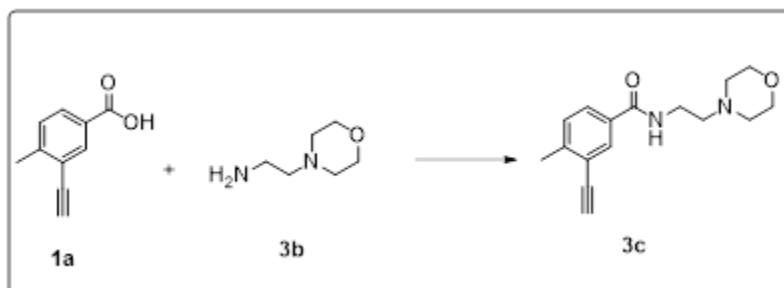


6-chloro-4-iodoisoquinolin-3-amine (2e): To a solution of 6-chloroisoquinolin-3-amine 2d (1g, 5.6 mmol, 1 equiv) in MeOH (45 mL) at 0 °C was added N-Iodo succenamide (1.38g, 6.5 mmol, 1.2 equiv) slowly over a period of 10 min. The reaction was allowed to stir 15 min., concentrated. The product 2e was purified by flash column chromatography. Yield 71% (1:1 EtOAc:Hexane)
¹H NMR (500 MHz, DMSO-d₆) δ 8.80 (s, 1H), 7.89 (d, J = 8.6 Hz, 1H), 7.61 (d, J = 2.0 Hz, 1H), 7.26 (dd, J = 8.6, 2.0 Hz, 1H), 6.40 (s, 2H); ¹³C NMR (126 MHz, DMSO) δ 157.40, 152.78, 140.70, 137.85, 131.58, 126.78, 123.48, 122.12; HRMS (ESI⁺): calcd. for C₉H₇ClI₂N₂ (MH⁺) 304.9337, found 304.9339

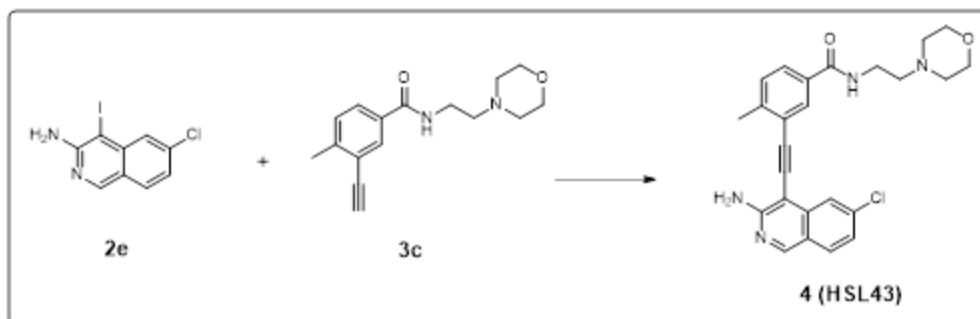


Compound 3: 3-((3-amino-6-chloroisoquinolin-4-yl)ethynyl)-4-methyl-N-(2-(pyrrolidin-1-yl)ethyl)benzamide: A solution of Iodo compound 2e (60 mg, 0.198 mmol, 1 equiv), Pd(PPh₃)₂Cl₂ (5 mol%), CuI (5 mol%) and Triphenylphosphine (10 mg, 0.04 mmol, 0.1 equiv) in Triethylamine (1 mL, 7.2 mmol, 22 equiv) was de-oxygenated using steam of Argon gas. A de-oxygenated solution of alkyne 2c (61 mg, 0.237 mmol, 1.2 equiv) in DMF (3 mL) was added slowly over a period of 10 min to the solution and the reaction temperature was increased to 50 °C and allowed to stir 12 h. The reaction was quenched by addition of NH₄Cl (5 mL) at room temperature. The crude compound was extracted using EtOAc (3 × 40 mL). Combined organic layers were dried over anhydrous sodium sulphate, filtered and concentrated in vacuo. The pure product 3 was then obtained via flash column chromatography. Yield = 43% TLC R_f = 0.2 (10 %

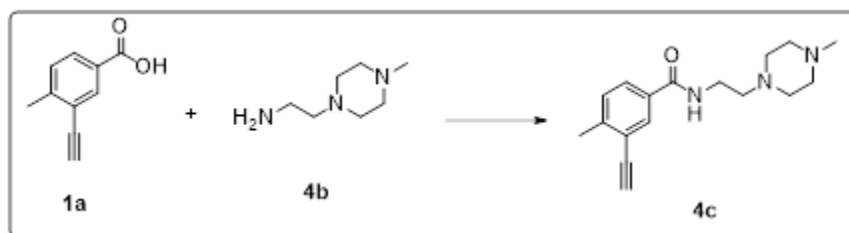
MeOH/CH₂Cl₂)¹H NMR (500 MHz, DMSO-d₆) δ 8.91 (s, 1H), 8.45 (t, J = 5.7 Hz, 1H), 8.20 (d, J = 1.9 Hz, 1H), 7.96 (d, J = 8.6 Hz, 1H), 7.86 (d, J = 2.0 Hz, 1H), 7.75 (dt, J = 7.9, 1.8 Hz, 1H), 7.42 (d, J = 8.0 Hz, 1H), 7.28 (dd, J = 8.6, 2.0 Hz, 1H), 6.74 (s, 2H), 3.40 – 3.36 (m, 2H), 3.36 – 3.31 (m, 2H), 2.59 (s, 3H), 2.59 – 2.52 (m, 4H), 1.67 – 1.64 (m, 4H); ¹³C NMR (126 MHz, DMSO) δ 165.85, 158.48, 153.11, 142.40, 138.71, 137.35, 132.90, 131.64, 131.02, 130.01, 128.15, 127.57, 123.50, 123.22, 121.32, 120.68, 98.35, 88.91, 88.18, 85.55, 55.39, 54.15, 23.61, 21.16, 20.59; HRMS (ESI⁺) calculated for C₂₅H₂₅ClN₄O: 433.1795 found: 433.1786



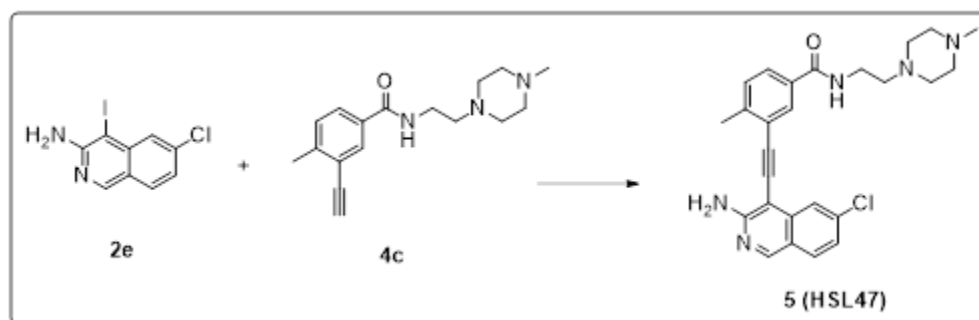
3-ethynyl-4-methyl-N-(2-morpholinoethyl)benzamide (3c): Compound 1a (100 mg, 0.684 mol, 1 eq) and HCTU (311 mg, 0.752 mol, 1.1 eq) were added to a round bottom flask, air vacuumed out and protected with a balloon of argon. Dry DCM was then added and allowed to dissolve compound 1a. The round bottom was then placed on ice and temperature allowed to reach 0°C. DIPEA (264 mg, 2.05 mol, 3 eq) was then added to the DCM solution. Compound 3b (89.05 mg, 0.684 mol, 1 eq) was then added to the flask. Temperature was then raised to room temperature and allowed to run over night. The crude compound was extracted using water (3 × 40 mL). Combined organic layers were dried over anhydrous sodium sulphate, filtered and concentrated in vacuo. The pure product 3c was then obtained via flash column chromatography. Yield = 71 % TLC (10 % MeOH: DCM) ¹H NMR (500 MHz, Chloroform-d) δ 7.84 (d, J = 2.0 Hz, 1H), 7.67 (dd, J = 7.9, 2.0 Hz, 1H), 7.28 (dt, J = 8.0, 0.7 Hz, 1H), 6.74 (s, 1H), 3.74 (t, J = 4.7 Hz, 4H), 3.58 – 3.51 (m, 2H), 3.33 (s, 1H), 2.60 (t, J = 6.0 Hz, 2H), 2.51 (t, J = 4.5 Hz, 7H). ¹³C NMR (126 MHz, CDCl₃) δ 166.51, 144.36, 132.17, 130.90, 129.80, 127.33, 122.32, 81.87, 81.66, 66.93, 56.93, 53.34, 36.03, 20.66; HRMS (ESI⁺): calc [M+H]: 273.1597 found: 273.1597



Compound 4 : 3-((3-amino-6-chloroisoquinolin-4-yl)ethynyl)-4-methyl-N-(2-morpholinoethyl)benzamide: A solution of Iodo compound 2e (60 mg, 0.198 mmol, 1 equiv), Pd(PPh₃)₂Cl₂ (5 mol%), CuI (5 mol%) and Triphenylphosphine (10 mg, 0.04 mmol, 0.1 equiv) in Triethylamine (1 mL, 7.2 mmol, 22 equiv) was de-oxygenated using steam of Argon gas. A de-oxygenated solution of alkyne 3c (64.55mg, 0.237 mmol, 1.2 equiv) in DMF (3 mL) was added slowly over a period of 10 min to the solution and the reaction temperature was increased to 50 °C and allowed to stir 12 h. The reaction was quenched by addition of NH₄Cl (5 mL) at room temperature. The crude compound was extracted using EtOAc (3 × 40 mL). Combined organic layers were dried over anhydrous sodium sulphate, filtered and concentrated in vacuo. The pure product 4 was then obtained via flash column chromatography. Yield: 38 % TLC R_f = 0.1 (5 % MeOH/CH₂Cl₂) ¹H NMR (500 MHz, DMSO-d₆) δ 8.92 (s, 1H), 8.44 (t, J = 5.8 Hz, 1H), 8.20 (s, 1H), 7.96 (d, J = 8.6 Hz, 1H), 7.86 (d, J = 2.0 Hz, 1H), 7.74 (dd, J = 8.0, 2.0 Hz, 1H), 7.43 (d, J = 8.0 Hz, 1H), 7.28 (dd, J = 8.6, 2.0 Hz, 1H), 6.74 (s, 2H), 3.57 (d, J = 9.5 Hz, 4H), 3.40 (q, J = 6.6 Hz, 2H), 2.59 (s, 3H), 2.50 (s, 6H), 2.43 (s, 4H); ¹³C NMR (126 MHz, DMSO) δ 165.94, 158.48, 153.11, 142.44, 138.71, 137.35, 132.90, 131.64, 131.01, 130.03, 127.55, 123.50, 123.24, 121.31, 120.68, 98.34, 88.90, 88.20, 66.62, 57.82, 53.75, 37.01, 21.16; HRMS (ESI+) calculated for C₂₅H₂₅ClN₄O₂ found 449.1740

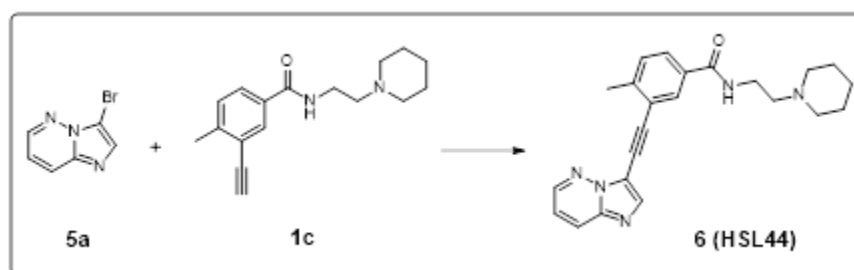


3-ethynyl-4-methyl-N-(2-(4-methylpiperazin-1-yl)ethyl)benzamide (4c): Compound 1a (500 mg, 3.13 mol, 1 eq) and HCTU (1.4 g, 3.44 mmol, 1.1 eq) were added to a round bottom flask, air vacuumed out and protected with a balloon of argon. Dry DCM was then added and allowed to dissolve compound 1a. The round bottom was then placed on ice and temperature allowed to reach 0°C. DIPEA (1.2 g, 9.4 mol, 3 eq) was then added to the DCM solution. Compound 4b (447.55 mg, 3.13 mol, 1 eq) was then added to the flask. Temperature was then raised to room temperature and allowed to run over night. The crude compound was extracted using water (3 × 40 mL). Combined organic layers were dried over anhydrous sodium sulphate, filtered and concentrated in vacuo. The pure product 4c was then obtained via flash column chromatography. Yield = 50 % (10 % MeOH: DCM) ¹H NMR (500 MHz, Chloroform-d) δ 7.85 (d, J = 2.0 Hz, 1H), 7.66 (dd, J = 7.9, 2.0 Hz, 1H), 7.25 (d, J = 8.0 Hz, 1H), 6.94 (d, J = 5.1 Hz, 1H), 3.70 – 3.46 (m, 2H), 3.31 (s, 1H), 2.68 – 2.52 (m, 10H), 2.46 (s, 3H), 2.34 (s, 3H); ¹³C NMR (126 MHz, CDCl₃) δ 166.56, 144.30, 132.10, 131.01, 129.74, 127.33, 122.27, 81.83, 81.67, 56.38, 54.63, 52.31, 45.59, 36.27, 20.64; HRMS (ESI+): calc [M+H]: 286.1914 found: 286.1913



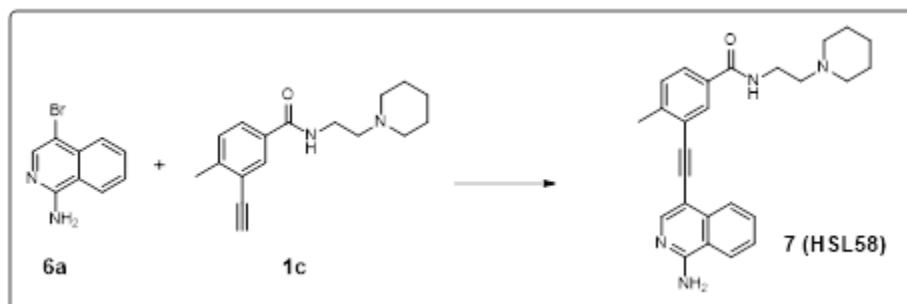
Compound 5: 3-((3-amino-6-chloroisoquinolin-4-yl)ethynyl)-4-methyl-N-(2-(4-methylpiperazin-1-yl)ethyl)benzamide: A solution of Iodo compound 5e (60 mg, 0.198 mmol, 1 equiv), Pd(PPh₃)₂ Cl₂ (5 mol%), CuI (5 mol%) and Triphenylphosphine (10 mg, 0.04 mmol, 0.1 equiv) in Triethylamine (1 mL, 7.2 mmol, 22 equiv) was de-oxygenated using steam of Argon gas. A de-oxygenated solution of alkyne 4c (61 mg, 0.237 mmol, 1.2 equiv) in DMF (3 mL) was added slowly over a period of 10 min to the solution and the reaction temperature was increased to 50 °C and allowed to stir 12 h. The reaction was quenched by addition of NH₄Cl (5 mL) at room temperature. The crude compound was extracted using EtOAc (3 × 40 mL). Combined organic layers were dried over anhydrous sodium sulphate, filtered and concentrated in vacuo. The pure

product 5 was then obtained via flash column chromatography. Yield = 10 % TLC Rf = 0.1 (10 % MeOH/CH₂Cl₂) ¹H NMR (500 MHz, DMSO-d₆) δ 8.92 (s, 1H), 8.41 (t, J = 5.7 Hz, 1H), 8.19 (d, J = 1.8 Hz, 1H), 7.96 (d, J = 8.6 Hz, 1H), 7.86 (d, J = 2.0 Hz, 1H), 7.73 (dd, J = 8.0, 1.9 Hz, 1H), 7.42 (d, J = 8.0 Hz, 1H), 7.28 (dd, J = 8.6, 2.0 Hz, 1H), 6.74 (s, 2H), 3.37 (q, J = 6.6 Hz, 2H), 3.31 (s, 2H), 2.59 (s, 3H), 2.31 (s, 8H), 2.13 (s, 3H); ¹³C NMR (126 MHz, DMSO) δ 165.92, 158.46, 153.11, 142.42, 138.70, 137.37, 132.91, 131.64, 130.98, 130.04, 127.54, 123.51, 123.22, 121.30, 120.68, 98.34, 88.91, 88.17, 57.36, 55.11, 53.05, 46.09, 39.78, 37.36, 21.15; HRMS (ESI+) calculated for C₂₆H₂₈ClN₅O 462.2061 found 462.2058

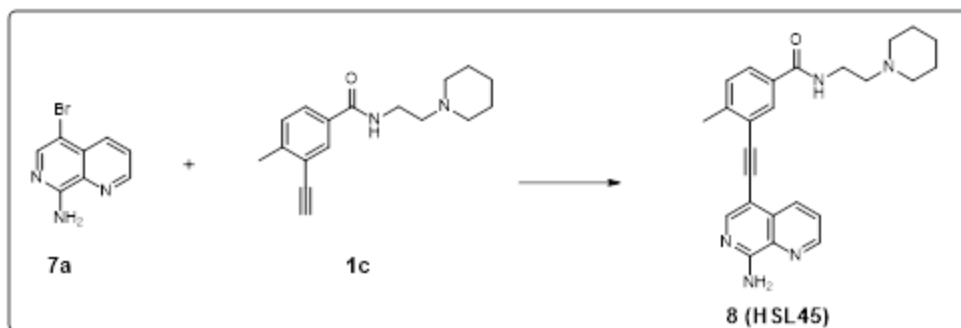


Compound 6: 3-(imidazo[1,2-b]pyridazin-3-ylethynyl)-4-methyl-N-(2-(piperidin-1-yl)ethyl)benzamide: A solution of Bromo compound 5a (60 mg, 0.303 mmol, 1 equiv), Pd(PPh₃)₂Cl₂ (5 mol%), CuI (5 mol%) and Triphenylphosphine (10 mg, 0.04 mmol, 0.1 equiv) in Triethylamine (1 mL, 7.2 mmol, 22 equiv) was de-oxygenated using steam of Argon gas. A de-oxygenated solution of alkyne 1c (98 mg, 0.363 mmol, 1.2 equiv) in DMF (3 mL) was added slowly over a period of 10 min to the solution and the reaction temperature was increased to 50 °C and allowed to stir 12 h. The reaction was quenched by addition of NH₄Cl (5 mL) at room temperature. The crude compound was extracted using EtOAc (3 × 40 mL). Combined organic layers were dried over anhydrous sodium sulphate, filtered and concentrated in vacuo. The pure product 6 was then obtained via flash column chromatography. Yield = 83 % TLC Rf = 0.2 (10 % MeOH/CH₂Cl₂) ¹H NMR (500 MHz, DMSO-d₆) δ 8.70 (dd, J = 4.5, 1.5 Hz, 1H), 8.49 (t, J = 5.6 Hz, 1H), 8.24 (dd, J = 9.2, 1.6 Hz, 1H), 8.20 (s, 1H), 8.02 (d, J = 1.8 Hz, 1H), 7.79 (dd, J = 8.0, 1.9 Hz, 1H), 7.44 (d, J = 8.1 Hz, 1H), 7.37 (dd, J = 9.2, 4.4 Hz, 1H), 3.36 (q, J = 6.6 Hz, 2H), 2.55 (s, 3H), 2.42 (m, 2H), 2.41 – 2.32 (m, 4H), 1.47 (q, J = 5.6 Hz, 4H), 1.36 (t, J = 5.9 Hz, 2H); ¹³C NMR (126 MHz, DMSO) δ 165.45, 145.50, 142.99, 140.08,

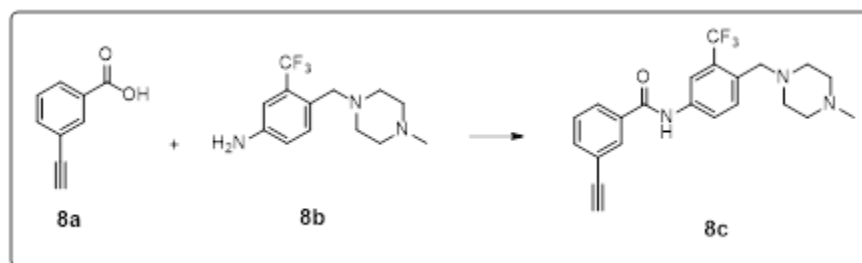
138.63, 132.89, 130.32, 130.22, 128.37, 126.56, 122.03, 119.50, 112.22, 97.02, 81.27, 58.09, 54.53, 37.43, 26.00, 24.45, 20.75; HRMS (ESI+) calculated for C₂₃H₂₅N₅O 388.2137 found: 388.2134



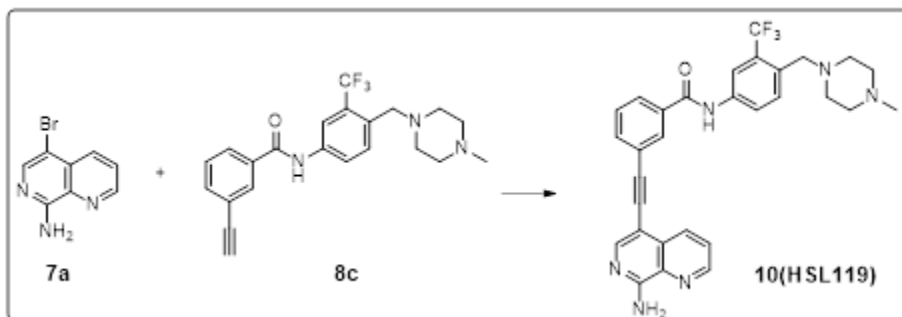
Compound 7: 3-((1-aminoisoquinolin-4-yl)ethynyl)-4-methyl-N-(2-(piperidin-1-yl)ethyl)benzamide: A solution of Bromo compound 6a (60 mg, 0.198 mmol, 1 equiv), Pd(PPh₃)₂Cl₂ (5 mol%), CuI (5 mol%) and Triphenylphosphine (10 mg, 0.04 mmol, 0.1 equiv) in Triethylamine (1 mL, 7.2 mmol, 22 equiv) was de-oxygenated using steam of Argon gas. A de-oxygenated solution of alkyne 1c (61 mg, 0.49 mmol, 1.5 equiv) in DMF (3 mL) was added slowly over a period of 10 min to the solution and the reaction temperature was increased to 50 °C and allowed to stir 12 h. The reaction was quenched by addition of NH₄Cl (5 mL) at room temperature. The crude compound was extracted using EtOAc (3 × 40 mL). Combined organic layers were dried over anhydrous sodium sulphate, filtered and concentrated in vacuo. The pure product 7 was then obtained via flash column chromatography. Yield = 11 %; TLC R_f = 0.1 (10 % MeOH/CH₂Cl₂)
¹H NMR (500 MHz, DMSO-d₆) δ 8.44 (t, J = 5.6 Hz, 1H), 8.33 – 8.24 (m, 1H), 8.16 (s, 1H), 8.08 (dd, J = 8.2, 1.1 Hz, 1H), 8.01 (d, J = 1.9 Hz, 1H), 7.79 (ddd, J = 8.2, 6.9, 1.2 Hz, 1H), 7.72 (dd, J = 7.9, 2.0 Hz, 1H), 7.57 (ddd, J = 8.3, 6.9, 1.3 Hz, 1H), 7.41 (d, J = 8.1 Hz, 1H), 7.36 (s, 2H), 2.56 (s, 3H) 2.44 – 2.41 (m, 3H), 2.37 (s, 4H), 1.47 (q, J = 5.5 Hz, 4H), 1.36 (s, 2H); ¹³C NMR (126 MHz, DMSO) δ ¹³C NMR (126 MHz, DMSO) δ 165.78, 158.08, 147.52, 142.38, 136.35, 132.80, 131.59, 130.13, 127.31, 126.79, 124.97, 124.74, 123.46, 103.27, 91.84, 91.49, 58.09, 54.52, 40.41, 40.24, 40.08, 39.91, 39.74, 39.57, 39.41, 37.38, 29.45, 25.97, 24.44, 21.06; HRMS (ESI+) calculated for C₂₆H₂₈N₄O 413.2342 found 413.2339



Compound 8: 3-((8-amino-1,7-naphthyridin-5-yl)ethynyl)-4-methyl-N-(2-(piperidin-1-yl)ethyl)benzamide: A solution of Bromo compound 7a (60 mg, 0.267 mmol, 1 equiv), Pd(PPh₃)₂Cl₂ (5 mol%), CuI (5 mol%) and Triphenylphosphine (10 mg, 0.04 mmol, 0.1 equiv) in Triethylamine (1 mL, 7.2 mmol, 22 equiv) was de-oxygenated using steam of Argon gas. A de-oxygenated solution of alkyne 1c (86.78 mg, 0.321 mmol, 1.2 equiv) in DMF (3 mL) was added slowly over a period of 10 min to the solution and the reaction temperature was increased to 50 °C and allowed to stir 12 h. The reaction was quenched by addition of NH₄Cl (5 mL) at room temperature. The crude compound was extracted using EtOAc (3 × 40 mL). Combined organic layers were dried over anhydrous sodium sulphate, filtered and concentrated in vacuo. The pure product 8 was then obtained via flash column chromatography. Yield = 22%; TLC R_f = 0.2 (10 % MeOH/CH₂Cl₂)¹H NMR (500 MHz, DMSO-d₆) δ 8.88 (dd, J = 4.2, 1.6 Hz, 1H), 8.44 (dd, J = 8.4, 1.6 Hz, 1H), 8.06 (s, 1H), 7.84 (dd, J = 8.3, 4.2 Hz, 1H), 7.75 (dd, J = 8.0, 2.0 Hz, 1H), 7.52 (s, 2H), 7.42 (d, J = 8.0 Hz, 1H), 3.41 (s, 4H), 2.56 (s, 3H), 1.53 (s, 6H), 1.39 (s, 4H);¹³C NMR (126 MHz, DMSO) δ 165.84, 158.52, 149.71, 148.08, 142.58, 133.10, 132.69, 131.35, 130.42, 130.15, 127.52, 127.05, 123.22, 102.21, 91.87, 90.17, 21.07; HRMS (ESI⁺) calculated for C₂₅H₂₇N₅O 414.2294 found 414.2290

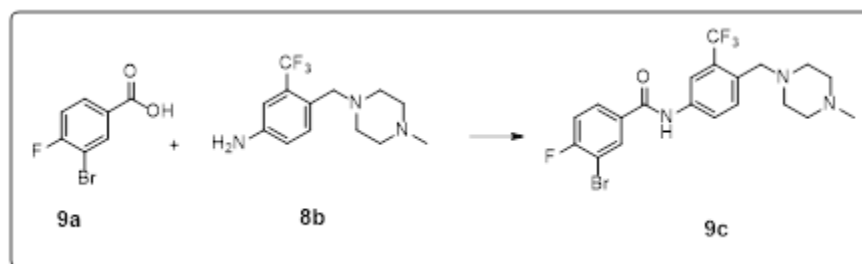


Compound 8c: 3-ethynyl-N-(4-((4-methylpiperazin-1-yl)methyl)-3-(trifluoromethyl)phenyl)benzamide: Compound 8a (150 mg, 1.02 mmol, 1 eq.) and HATU (468.33 mg, 1.23 mmol, 1.2 eq.) were added to a round bottom flask, air vacuumed out and protected with a balloon of argon. DMF was then added and allowed to dissolve compound 1a. The round bottom was then placed on ice and temperature allowed to reach 0°C. DIPEA (476.93 mg, 3.69 mol, 3 eq.) was then added to the DMF solution. Compound 8b (278.76 mg, 1.02 mmol, 1 eq.) was then added to the flask. Temperature was then raised to 55 °C and allowed to run over night. The crude compound was extracted using EtOAc (3 × 40 mL). Combined organic layers were dried over anhydrous sodium sulphate, filtered and concentrated in vacuo. The pure product 8c was then obtained via flash column chromatography. Yield = 74 % ¹H NMR (500 MHz, DMSO-d₆) δ 10.55 (s, 1H), 8.18 (d, J = 2.3 Hz, 1H), 8.08 (t, J = 1.8 Hz, 1H), 8.02 (dd, J = 8.5, 2.3 Hz, 1H), 7.97 (dt, J = 7.9, 1.4 Hz, 1H), 7.69 (ddd, J = 8.3, 3.2, 1.8 Hz, 2H), 7.55 (t, J = 7.7 Hz, 1H), 4.32 (s, 1H), 3.54 (s, 3H), 2.36 (s, 10H); ¹³C NMR (126 MHz, DMSO) δ 165.18, 138.52, 135.29, 135.25, 132.67, 131.67, 131.09, 129.51, 128.83, 123.96, 122.38, 117.72, 117.67, 83.19, 82.20, 57.90, 55.19, 53.16, 46.18; HRMS (ESI+): calc [M+H]: 402.1787 found: 402.1787



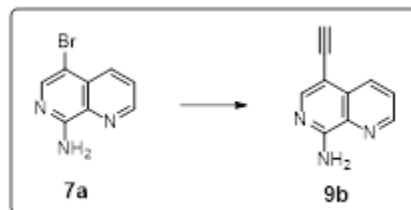
Compound 10: 3-((8-amino-1,7-naphthyridin-5-yl)ethynyl)-N-(4-((4-methylpiperazin-1-yl)methyl)-3-(trifluoromethyl)phenyl)benzamide: A solution of bromo compound 7a (60 mg, 0.267 mmol, 1 equiv), Pd(PPh₃)₂Cl₂ (5 mol%), CuI (5 mol%) and Triphenylphosphine (6.8 mg, 0.026 mmol, 0.1 equiv) in Triethylamine (1 mL, 7.2 mmol, 26.9 equiv) was de-oxygenated using steam of Argon gas. A de-oxygenated solution of alkyne 8c (127.92 mg, 0.321 mmol, 1.2 equiv) in DMF (3 mL) was added slowly over a period of 10 min to the solution and the reaction temperature was increased to 50 °C and allowed to stir 12 h. The reaction was quenched by addition of NH₄Cl (5 mL) at room temperature. The crude compound was extracted using EtOAc (3 × 40

mL). Combined organic layers were dried over anhydrous sodium sulphate, filtered and concentrated in vacuo. The pure product 10 was then obtained via flash column chromatography. Yield = 16%, TLC Rf = 0.4 (10 % MeOH/CH₂Cl₂) ¹H NMR (500 MHz, DMSO-d₆) δ 10.62 (s, 1H), 8.88 (dd, J = 4.3, 1.6 Hz, 1H), 8.50 (dd, J = 8.3, 1.6 Hz, 1H), 8.22 (d, J = 1.9 Hz, 3H), 8.06 (dd, J = 8.5, 2.2 Hz, 1H), 7.95 (dt, J = 7.8, 1.4 Hz, 1H), 7.86 – 7.81 (m, 2H), 7.70 (d, J = 8.5 Hz, 1H), 7.60 (t, J = 7.8 Hz, 1H), 7.52 (s, 2H), 3.56 (s, 2H), 2.37 (s, 8H), 2.15 (s, 3H); ¹³C NMR (126 MHz, DMSO) δ 165.46, 158.58, 149.72, 148.13, 138.61, 135.40, 134.59, 133.31, 132.59, 132.51, 131.72, 131.46, 130.42, 129.52, 128.07, 127.00, 124.01, 123.70, 123.60, 117.77, 101.87, 92.97, 86.69, 57.87, 55.08, 52.98, 45.99; HRMS (ESI⁺): calcd. for C₃₀H₂₇F₃N₆O (MH⁺) 545.2271, found 545.2275



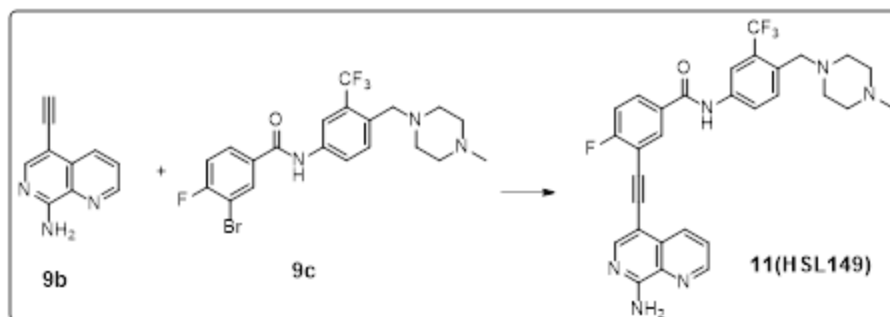
3-bromo-4-fluoro-N-(4-((4-methylpiperazin-1-yl)methyl)-3-(trifluoromethyl)phenyl)benzamide (9c): Compound 9a (250 mg, 1.15 mmol, 1 eq.) and HATU (524 mg, 1.38 mmol, 1.2 eq.) were added to a round bottom flask, air vacuumed out and protected with a balloon of argon. DMF was then added and allowed to dissolve compound 3a. The round bottom was then placed on ice and temperature allowed to reach 0°C. DIPEA (445 mg, 3.45 mmol, 3 eq.) was then added to the DMF solution. Compound 8b (314 mg, 1.15 mmol, 1 eq.) was then added to the flask. Temperature was then raised to 55 °C and allowed to run over night. The crude compound was extracted using EtOAc (3 × 40 mL). Combined organic layers were dried over anhydrous sodium sulphate, filtered and concentrated in vacuo. The pure product 9c was then obtained via flash column chromatography. Yield = 71 (10 % MeOH:DCM) ¹H NMR (500 MHz, DMSO-d₆) δ 10.55 (s, 1H), 8.32 (dd, J = 6.7, 2.3 Hz, 1H), 8.14 (d, J = 2.3 Hz, 1H), 8.03 – 7.96 (m, 2H), 7.69 (d, J = 8.5 Hz, 1H), 7.54 (t, J = 8.6 Hz, 1H), 3.54 (s, 3H), 2.37 (s, 8H); ¹³C NMR (126 MHz, DMSO) δ 163.75, 161.77, 159.78, 138.37, 133.46, 132.76, 132.73, 131.70, 130.31, 130.25, 124.00, 117.45, 117.27,

108.74, 108.56, 57.88, 55.15, 53.09, 46.11; HRMS (ESI+): calc [M+H] 474.0798/476.0780 found: 474.0798/476.0778

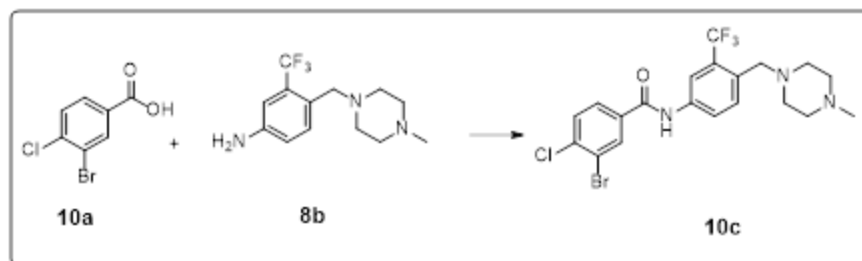


5-ethynyl-1,7-naphthyridin-8-amine (9b): A solution of 5-bromo-1,7-naphthyridin-8-amine 7a (640 mg, 2.9 mmol, 1 equiv), Pd(PPh₃)₂Cl₂ (10 mol%), CuI (5 mol%) and Triphenylphosphine (10 mg), triethylamine (5 mL) and DMF (10 mL) was de-oxygenated using steam of Argon gas. A de-oxygenated solution of ethynyltrimethylsilane (5 mL) was added slowly over a period of 10 min. to the solution and the reaction temperature was increased to 90 °C and allowed to stir 12 h. The reaction was quenched by addition of NH₄Cl (10 mL) at room temperature and diluted with ethyl acetate (300 mL). The organic layer was washed with water (5 × 100 mL) and washed with brine (1 × 50 mL). Combined organic layers were filtered using celite, dried over anhydrous sodium sulphate, filtered and concentrated in vacuo.

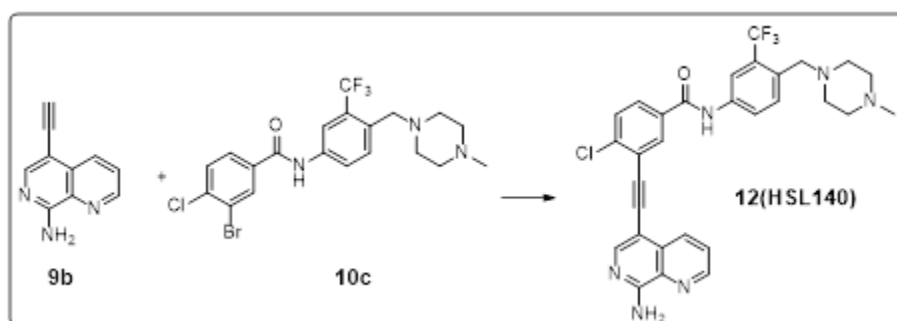
To the crude product obtained was added TBAF (3 mL) at 0 °C. The reaction was allowed to stir 30 min., concentrated. The reaction crude was diluted with EtOAc (200 mL) and was washed with water (5 × 50 mL) and washed with brine (1 × 50 mL). The product 9b was purified by flash column chromatography. Yield 61 % (5% MeOH/DCM) ¹H NMR (500 MHz, DMSO-d₆) δ 8.84 (dd, J = 4.2, 1.6 Hz, 1H), 8.27 (dd, J = 8.4, 1.7 Hz, 1H), 8.09 (s, 1H), 7.78 (dd, J = 8.4, 4.2 Hz, 1H), 7.43 (s, 2H), 4.37 (s, 1H); ¹³C NMR (126 MHz, DMSO) δ 158.49, 149.60, 148.25, 132.94, 132.42, 131.70, 126.93, 101.61, 84.72, 79.69; HRMS (ESI+): calcd. for C₁₀H₈N₃ (MH⁺) 170.0713, found 170.0713



Compound 11: 3-((8-amino-1,7-naphthyridin-5-yl)ethynyl)-4-fluoro-N-(4-(4-methylpiperazin-1-yl)methyl)-3-(trifluoromethyl)phenylbenzamide: A solution of bromo compound 9c (139.5 mg, 0.295 mmol, 1 equiv), Pd(PPh₃)₂Cl₂ (5 mol%), CuI (5 mol%) and Triphenylphosphine (7.6 mg, 0.029 mmol, 0.1 equiv) in triethylamine (1 mL, 7.2 mmol, 24.4 equiv) was de-oxygenated using a stream of argon gas. A de-oxygenated solution of alkyne 9b (55 mg, 0.325 mmol, 1.2 equiv) in DMF (3 mL) was added slowly over 10 minutes to the solution and the reaction temperature was increased to 50 °C and allowed to run for 12 h. The reaction was then quenched by the addition of NH₄Cl (5 mL) at room temperature. The crude compound was extracted using EtOAc (3 × 40 mL). Combined organic layers were dried over anhydrous sodium sulphate, filtered and concentrated in vacuo. The pure product 11 was then obtained via flash column chromatography. Yield = 12 % TLC R_f = 0.2 (10 % MeOH/CH₂Cl₂) ¹H NMR (500 MHz, DMSO-d₆) δ 10.60 (s, 1H), 8.88 (dd, J = 4.3, 1.6 Hz, 1H), 8.43 (dd, J = 8.3, 1.7 Hz, 1H), 8.33 (dd, J = 6.8, 2.4 Hz, 1H), 8.23 (s, 1H), 8.20 (d, J = 2.2 Hz, 1H), 8.03 (tdd, J = 7.4, 5.8, 2.3 Hz, 2H), 7.86 (dd, J = 8.4, 4.2 Hz, 1H), 7.70 (d, J = 8.5 Hz, 1H), 7.61 (s, 2H), 7.53 (t, J = 8.9 Hz, 1H), 3.55 (s, 2H), 2.37 (s, 8H), 2.15 (s, 3H); ¹³C NMR (126 MHz, DMSO) δ 164.45, 158.83, 149.81, 148.42, 138.51, 132.92, 132.87, 132.65, 132.47, 131.74, 131.61, 131.38, 127.15, 124.01, 117.73, 116.60, 116.43, 111.97, 111.84, 101.36, 91.93, 86.25, 57.86, 55.07, 52.97, 45.99; HRMS (ESI⁺): calcd. for C₃₀H₂₆F₄N₆O (MH⁺) 563.2176 found: 562.2177

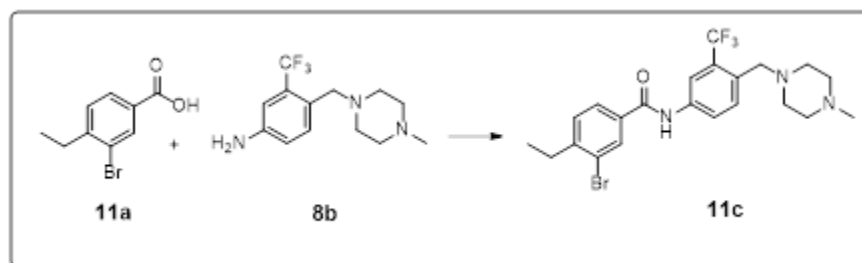


3-bromo-4-chloro-N-(4-((4-methylpiperazin-1-yl)methyl)-3-(trifluoromethyl)phenyl)benzamide (10c): Compound 10a (200 mg, 0.849 mmol, 1 eq.) and HATU (387.3 mg, 1.02 mmol, 1.2 eq.) were added to a round bottom flask, air vacuumed out and protected with a balloon of argon. DMF was then added and allowed to dissolve compound 10a. The round bottom was then placed on ice and temperature allowed to reach 0°C. DIPEA (328.5 mg, 2.5 mol, 3 equiv.) was then added to the DMF solution. Compound 8b (231 mg, 0.849 mmol, 1 eq.) was then added to the flask. Temperature was then raised to 55 °C and allowed to run over night. The crude compound was extracted using EtOAc (3 × 40 mL). Combined organic layers were dried over anhydrous sodium sulphate, filtered and concentrated in vacuo. The pure product 10c was then obtained via flash column chromatography. Yield = 86 % (10 % MeOH:DCM) ¹H NMR (500 MHz, Chloroform-d) δ 8.34 (s, 1H), 8.10 (d, J = 2.1 Hz, 1H), 7.85 – 7.80 (m, 2H), 7.73 (dd, J = 8.4, 1.9 Hz, 2H), 7.51 (d, J = 8.3 Hz, 1H), 3.61 (s, 2H), 2.51 (s, 8H), 2.33 (s, 3H); ¹³C NMR (126 MHz, MeOD) δ 164.65, 137.72, 137.61, 134.67, 132.84, 132.77, 131.18, 130.27, 127.71, 123.58, 122.05, 117.74, 57.47, 54.56, 52.21, 44.51; HRMS (ESI+): calc [M+H]: 490.0503/492.0482 found: 490.0504/492.0484



Compound 12: 3-((8-amino-1,7-naphthyridin-5-yl)ethynyl)-4-chloro-N-(4-((4-methylpiperazin-1-yl)methyl)-3-(trifluoromethyl)phenyl)benzamide: A solution of bromo compound 10c (132.5

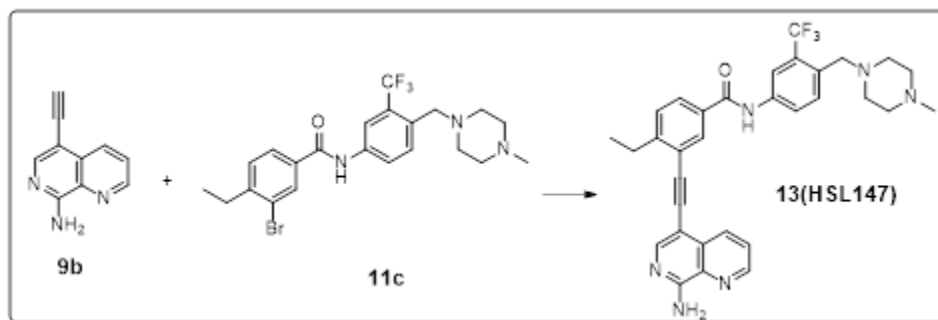
mg, 0.271 mmol, 1 equiv), Pd(PPh₃)₂Cl₂ (5 mol%), CuI (5 mol%) and Triphenylphosphine (7.1 mg, 0.027 mmol, 0.1 equiv) in triethylamine (1 mL, 7.2 mmol, 26.56 equiv) was de-oxygenated using a stream of argon gas. A de-oxygenated solution of alkyne 9b (55 mg, 0.325 mmol, 1.2 equiv) in DMF (3 mL) was added slowly over 10 minutes to the solution and the reaction temperature was increased to 50 °C and allowed to run for 12 h. The reaction was then quenched by the addition of NH₄Cl (5 mL) at room temperature. The crude compound was extracted using EtOAc (3 × 40 mL). Combined organic layers were dried over anhydrous sodium sulphate, filtered and concentrated in vacuo. The pure product 12 was then obtained via flash column chromatography. Yield = 5 %; TLC R_f = 0.2 (5 % MeOH/CH₂Cl₂) ¹H NMR (500 MHz, DMSO-d₆) δ 10.64 (s, 1H), 8.89 (dd, J = 4.2, 1.6 Hz, 1H), 8.51 (dd, J = 8.3, 1.7 Hz, 1H), 8.32 (d, J = 2.2 Hz, 1H), 8.25 (s, 1H), 8.19 (d, J = 2.2 Hz, 1H), 8.04 (dd, J = 8.5, 2.2 Hz, 1H), 7.94 (dd, J = 8.4, 2.2 Hz, 1H), 7.87 (dd, J = 8.4, 4.2 Hz, 1H), 7.79 (d, J = 8.4 Hz, 1H), 7.71 (d, J = 8.5 Hz, 1H), 7.63 (s, 2H), 3.56 (s, 2H), 2.38 (s, 8H), 2.17 (s, 3H); ¹³C NMR (126 MHz, DMSO) δ 164.66, 158.70, 149.97, 148.41, 138.28, 137.68, 133.80, 133.01, 132.71, 132.41, 132.08, 131.81, 131.41, 130.10, 129.29, 127.28, 124.13, 123.16, 117.86, 101.61, 92.03, 89.97, 57.72, 54.80, 52.57, 45.58; HRMS (ESI⁺): calcd. for C₃₀H₂₆ClF₃N₆O (MH⁺) 579.1881 found 579.1885



3-bromo-4-ethyl-N-(4-(4-methylpiperazin-1-yl)methyl)-3-(trifluoromethyl)phenylbenzamide (11c): Compound 11a (110 mg, 0.48 mmol, 1 eq.) and HATU (218.8 mg, 0.576 mmol, 1.2 eq.) were added to a round bottom flask, air vacuumed out and protected with a balloon of argon. DMF was then added and allowed to dissolve compound. The round bottom was then placed on ice and temperature allowed to reach 0 °C. DIPEA (185.76 mg, 1.44 mol, 3 equiv) was then added to the DMF solution. Compound 8b (131.04 mg, 0.0480 mmol, 1 eq.) was then added to the flask. Temperature was then raised to 55 °C and allowed to run over night. The crude compound was extracted using EtOAc (3 × 40 mL). Combined organic layers were dried over anhydrous sodium

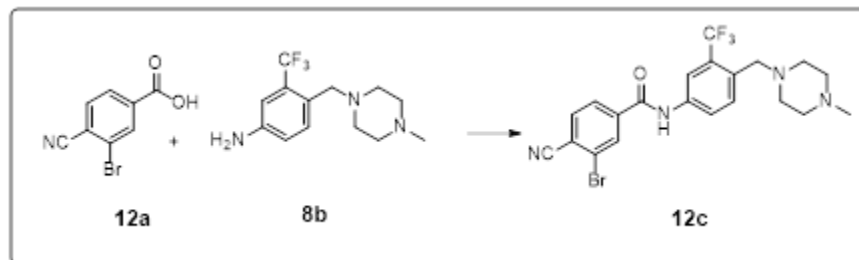
sulphate, filtered and concentrated in vacuo. The pure product 11c was then obtained via flash column chromatography. Yield= 82% (10 % MeOH/DCM)

^1H NMR (500 MHz, Chloroform-d) δ 8.04 (d, J = 1.9 Hz, 1H), 7.91 (s, 1H), 7.90 – 7.82 (m, 3H), 7.81 – 7.72 (m, 2H), 7.35 (d, J = 7.9 Hz, 1H), 3.64 (d, J = 1.6 Hz, 2H), 2.82 (q, J = 7.6 Hz, 2H), 2.33 (s, 3H), 1.26 (t, J = 7.5 Hz, 3H); ^{13}C NMR (126 MHz, CDCl_3) δ 164.30, 147.83, 136.46, 133.79, 133.58, 131.45, 131.37, 129.77, 126.17, 124.72, 123.28, 117.66, 57.77, 55.13, 52.85, 45.87, 29.46, 13.90, 1.03; HRMS (ESI+): calc $[\text{M}+\text{H}]$: 484.1206, found: 484.1207

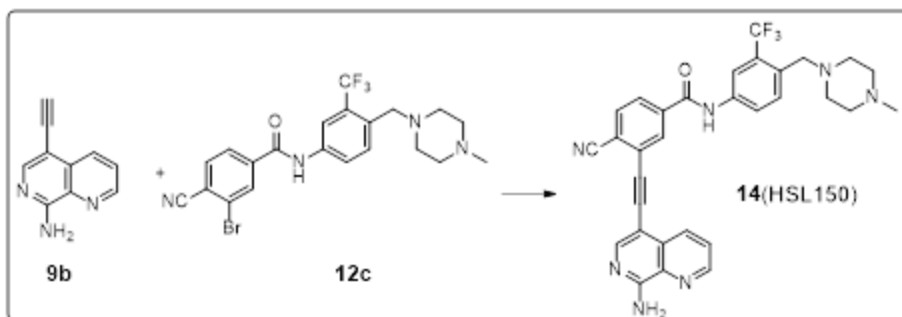


Compound 13: 3-((8-amino-1,7-naphthyridin-5-yl)ethynyl)-4-ethyl-N-(4-methylpiperazin-1-yl)methyl-3-(trifluoromethyl)phenylbenzamide: A solution of bromo compound 11c (142.8 mg, 0.295 mmol, 1 equiv), $\text{Pd}(\text{PPh}_3)_2\text{Cl}_2$ (5 mol%), CuI (5 mol%) and Triphenylphosphine (7.6 mg, 0.029 mmol, 0.1 equiv) in triethylamine (1 mL, 7.2 mmol, 24.4 equiv) was de-oxygenated using a stream of argon gas. A de-oxygenated solution of alkyne 9b (60 mg, 0.354 mmol, 1.2 equiv) in DMF (3 mL) was added slowly over 10 minutes to the solution and the reaction temperature was increased to 50 °C and allowed to run for 12 h. The reaction was then quenched by the addition of NH_4Cl (5 mL) at room temperature. The crude compound was extracted using EtOAc (3×40 mL). Combined organic layers were dried over anhydrous sodium sulphate, filtered and concentrated in vacuo. The pure product 13 was then obtained via flash column chromatography. Yield = 4 %; TLC R_f = 0.3 (10 % MeOH/ CH_2Cl_2) ^1H NMR (500 MHz, DMSO-d_6) δ 10.53 (s, 1H), 8.88 (dd, J = 4.2, 1.6 Hz, 1H), 8.43 (dd, J = 8.3, 1.7 Hz, 1H), 8.24 – 8.18 (m, 3H), 8.05 (dd, J = 8.5, 2.2 Hz, 1H), 7.90 (dd, J = 8.0, 2.0 Hz, 1H), 7.86 (dd, J = 8.4, 4.2 Hz, 1H), 7.70 (d, J = 8.5 Hz, 1H), 7.55 – 7.48 (m, 3H), 3.55 (s, 2H), 2.97 (q, J = 7.5 Hz, 2H), 2.37 (s, 8H), 2.15 (s, 3H), 1.31 (t, J = 7.5 Hz, 3H); ^{13}C NMR (126 MHz, DMSO) δ 165.40, 158.56, 149.74, 149.22, 148.17, 138.67, 133.00, 132.82, 132.52, 131.73, 131.38, 131.16, 128.94, 128.32, 127.09, 123.98, 122.70, 117.72, 102.13,

91.41, 90.01, 57.88, 55.10, 53.00, 46.01, 27.83, 15.10; HRMS (ESI+): calcd. for C₃₂H₃₁F₃N₆O (MH⁺) 573.2584 found 573.2584



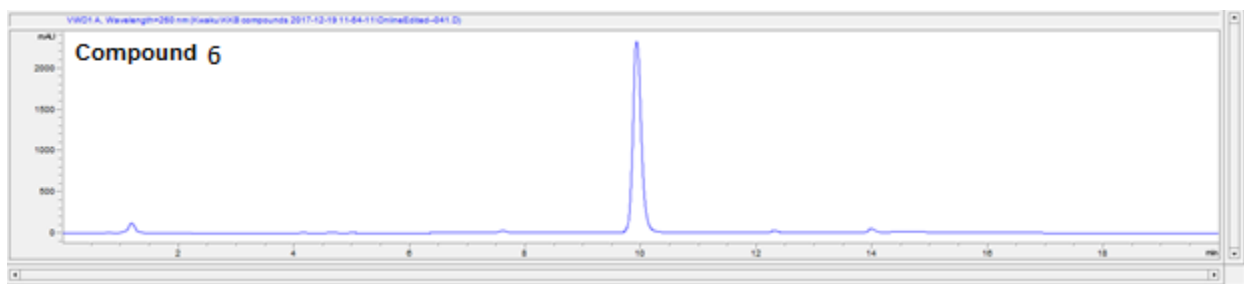
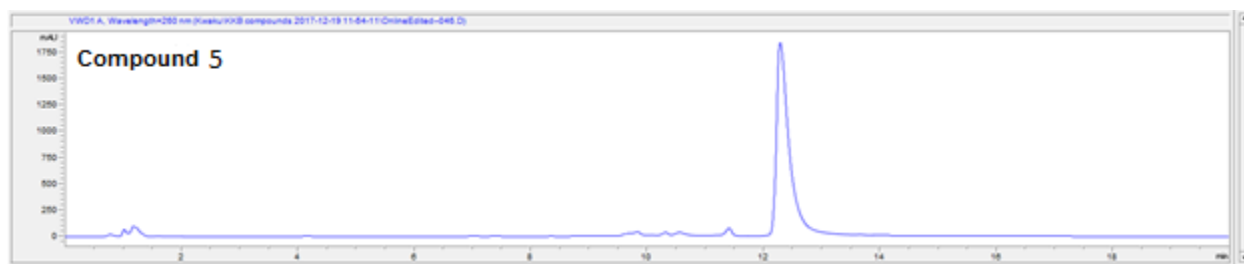
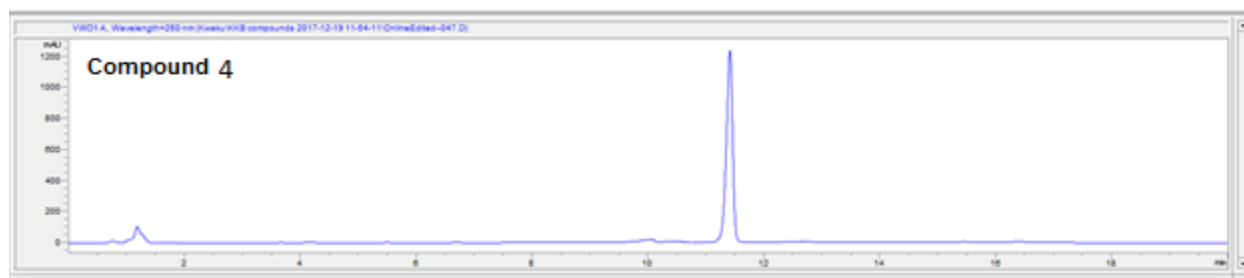
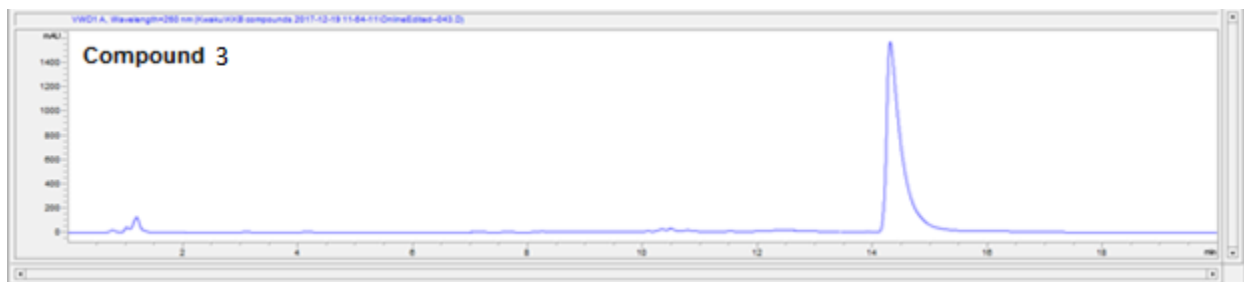
3-bromo-4-cyano-N-(4-((4-methylpiperazin-1-yl)methyl)-3-(trifluoromethyl)phenyl)benzamide (12c): Compound 12a (750 mg, 3.32 mmol, 1 eq.) and HATU (1.5 g, 3.98 mmol, 1.2 eq.) were added to a round bottom flask, air vacuumed out and protected with a balloon of argon. DMF was then added and allowed to dissolve compound. The round bottom was then placed on ice and temperature allowed to reach 0°C. DIPEA (1.2 mL, 9.96 mmol, 3 eq.) was then added to the DMF solution. Compound 8b (906 mg, 3.32 mmol, 1 eq.) was then added to the flask. Temperature was then raised to 55 °C and allowed to run over night. The crude compound was extracted using EtOAc (3 × 40 mL). Combined organic layers were dried over anhydrous sodium sulphate, filtered and concentrated in vacuo. The pure product 12c was then obtained via flash column chromatography. Yield= 7.26 % (10 % MeOH/DCM) ¹H NMR (500 MHz, DMSO-d₆) δ 10.75 (s, 1H), 8.39 (d, J = 1.6 Hz, 1H), 8.15 (d, J = 2.3 Hz, 1H), 8.13 (d, J = 8.1 Hz, 1H), 8.08 (dd, J = 8.0, 1.6 Hz, 1H), 8.00 (dd, J = 8.5, 2.2 Hz, 1H), 7.71 (d, J = 8.5 Hz, 1H), 3.55 (s, 2H), 2.36 (s, 8H), 2.15 (s, 3H); ¹³C NMR (126 MHz, DMSO) δ 163.45, 140.31, 138.07, 135.60, 133.20, 132.29, 131.79, 128.04, 127.79, 125.15, 124.10, 117.82, 117.48, 117.30, 57.87, 55.14, 53.09, 46.11; HRMS (ESI⁺): calc [M+H]: 481.0845/483.0827 found: 481.0847/483.0830

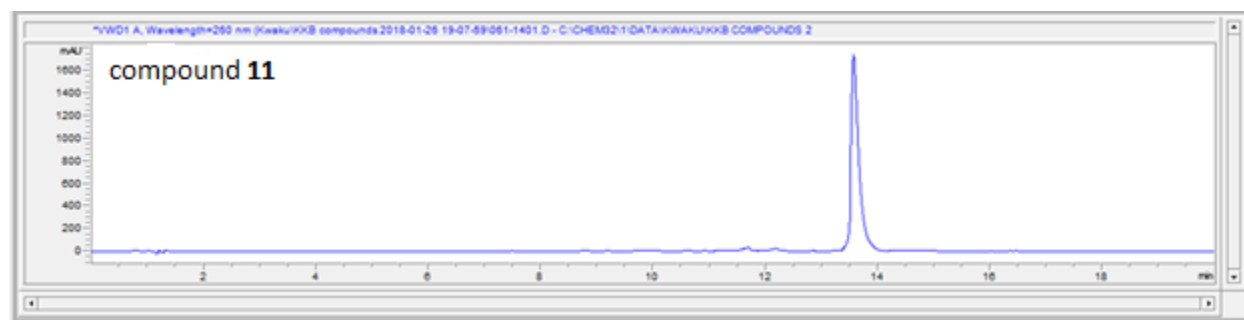
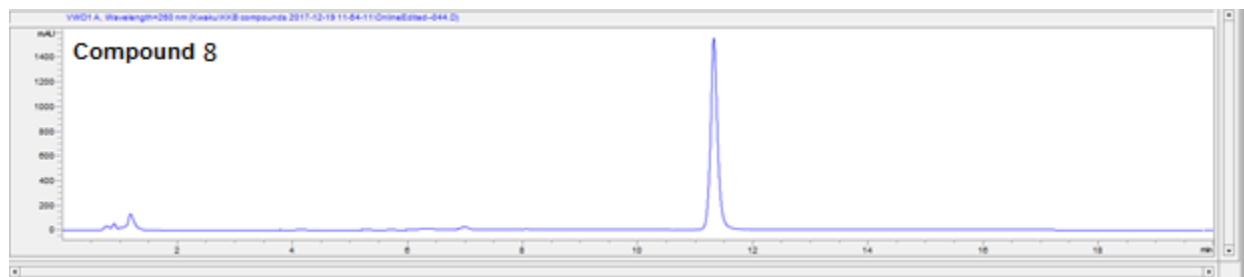
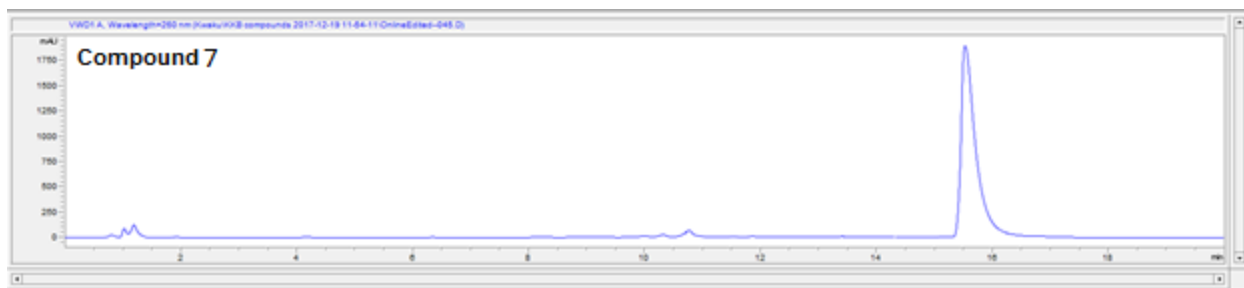


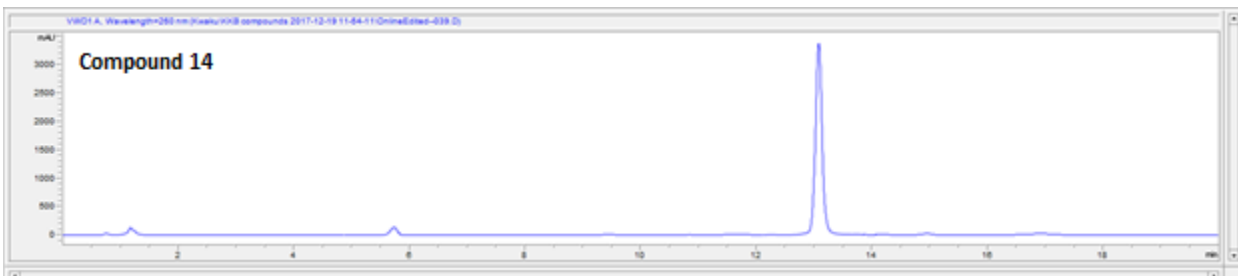
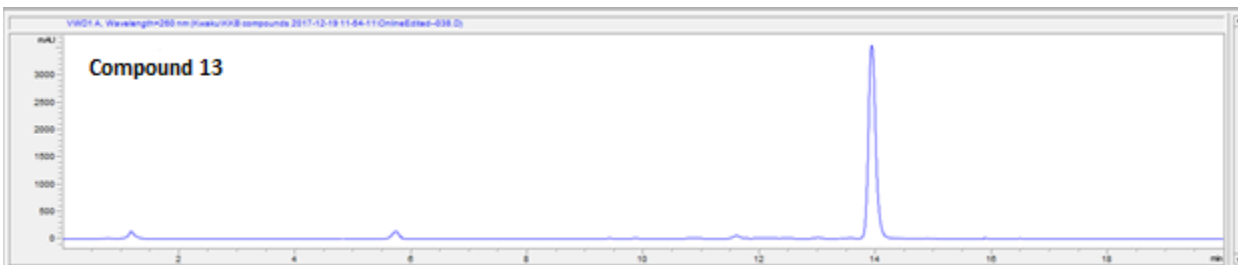
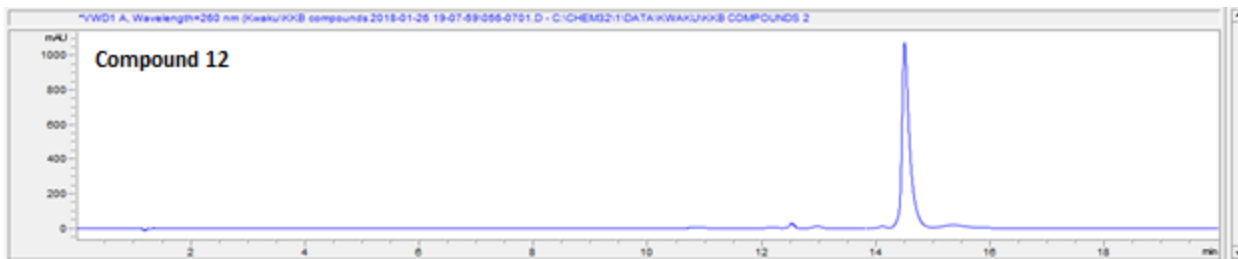
Compound 14: 3-((8-amino-1,7-naphthyridin-5-yl)ethynyl)-4-cyano-N-(4-((4-methylpiperazin-1-yl)methyl)-3-(trifluoromethyl)phenyl)benzamide: A solution of bromo compound 12c (115 mg, 0.239 mmol, 1 equiv), Pd(PPh₃)₂Cl₂ (5 mol%), CuI (5 mol%) and Triphenylphosphine (6.3 mg, 0.024 mmol, 0.1 equiv) in triethylamine (1 mL, 7.2 mmol, 30.1 equiv) was de-oxygenated using a stream of argon gas. A de-oxygenated solution of alkyne 9b (48.6 mg, 0.287 mmol, 1.2 equiv) in DMF (3 mL) was added slowly over 10 minutes to the solution and the reaction temperature was increased to 50 °C and allowed to run for 12 h. The reaction was then quenched by the addition of NH₄Cl (5 mL) at room temperature. The crude compound was extracted using EtOAc (3 × 40 mL). Combined organic layers were dried over anhydrous sodium sulphate, filtered and concentrated in vacuo. The pure product 14 was then obtained via flash column chromatography. Yield = 21 %; TLC R_f = 0.2 (10 % MeOH/CH₂Cl₂) ¹H NMR (500 MHz, DMSO-d₆) δ 10.78 (s, 1H), 8.89 (dd, J = 4.2, 1.6 Hz, 1H), 8.59 (dd, J = 8.4, 1.6 Hz, 1H), 8.35 (d, J = 1.7 Hz, 1H), 8.28 (s, 1H), 8.19 (d, J = 2.2 Hz, 1H), 8.13 (d, J = 8.1 Hz, 1H), 8.04 (ddd, J = 8.2, 4.0, 1.9 Hz, 2H), 7.84 (dd, J = 8.4, 4.2 Hz, 1H), 7.73 (d, J = 2.1 Hz, 2H), 3.56 (s, 2H), 2.37 (s, 8H), 2.14 (s, 3H); ¹³C NMR (126 MHz, DMSO) δ 164.23, 159.19, 149.92, 149.48, 139.04, 138.20, 133.85, 133.10, 132.94, 132.43, 131.79, 131.38, 130.81, 128.00, 127.36, 127.14, 124.09, 118.08, 117.80, 115.82, 100.70, 93.53, 90.07, 57.88, 55.14, 53.09, 46.12; HRMS (ESI⁺): calcd. for C₃₁H₂₆F₃N₇O (MH⁺) 570.2224 found 570.2224

HPLC traces of compounds

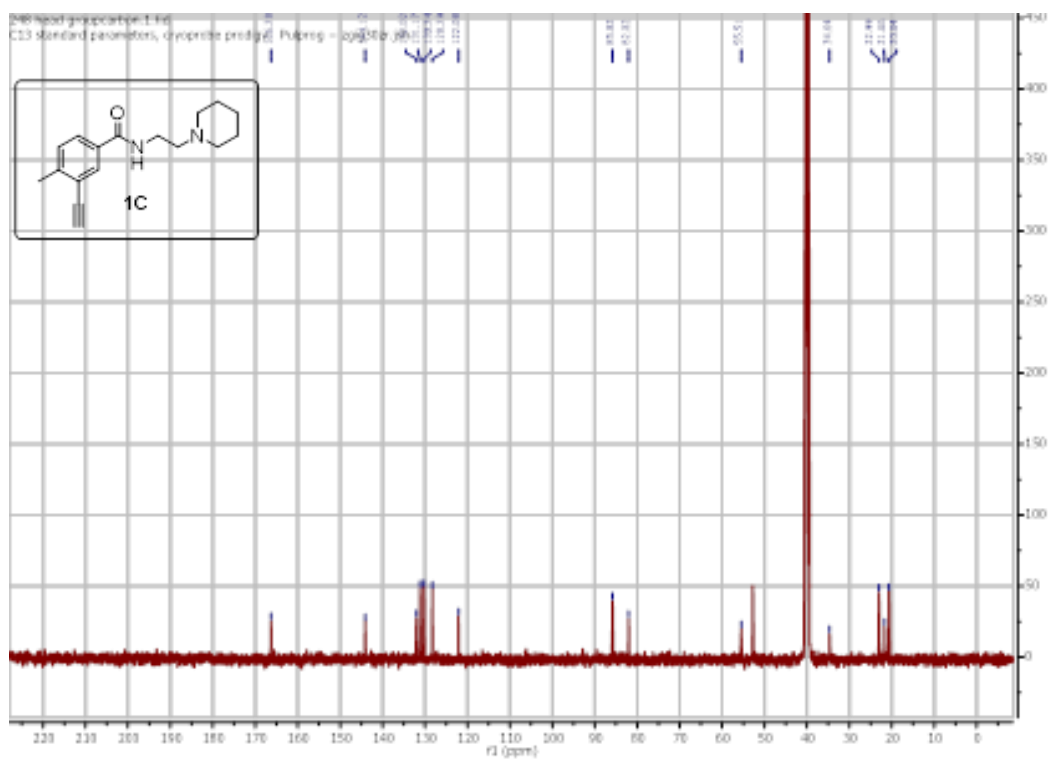
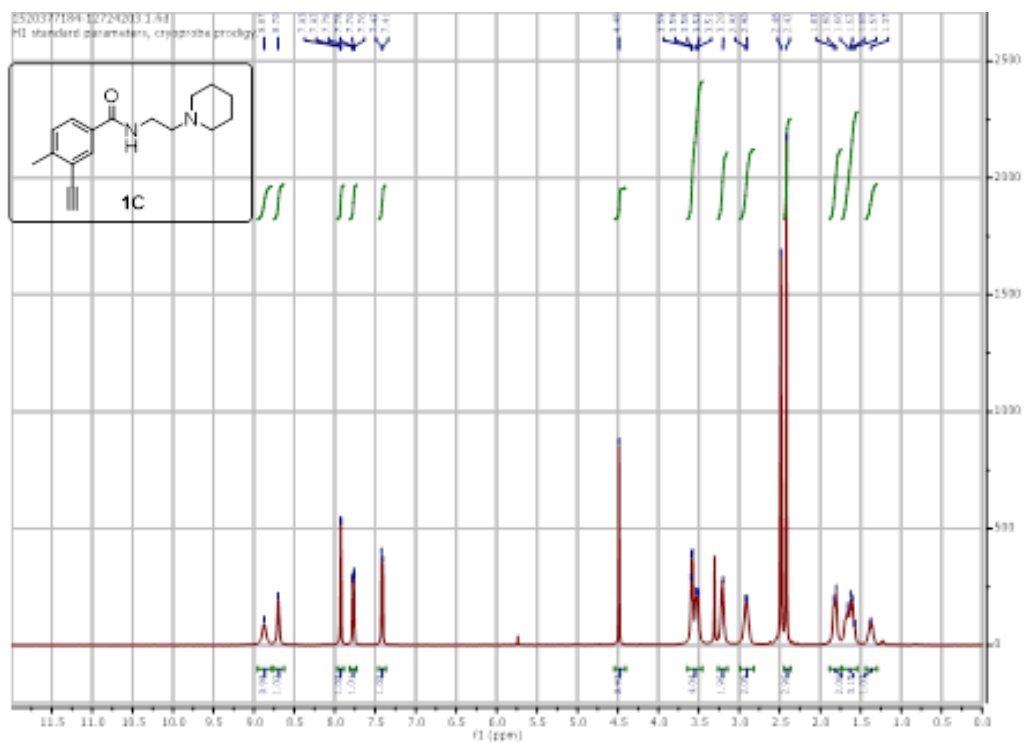
Conditions: Agilent Eclipse plus C18 column, 3,5 μm , 4.6 \times 100 mm, 0 \rightarrow 15 min, 50% B \rightarrow 100% B (A: 0.1% NH_4OH in H_2O , B: MeOH), 50 $^\circ\text{C}$. Compound concentrations are 500 μM in DMSO. HPLC of the compounds **1**, **2**, **23**, and **25** can be found at Larocque, E. *et al.* Aminoisoquinoline benzamides, FLT3 and Src-family kinase inhibitors, potently inhibit proliferation of acute myeloid leukemia cell lines. *Future Med. Chem.* **9**, 1213–1225 (2017).

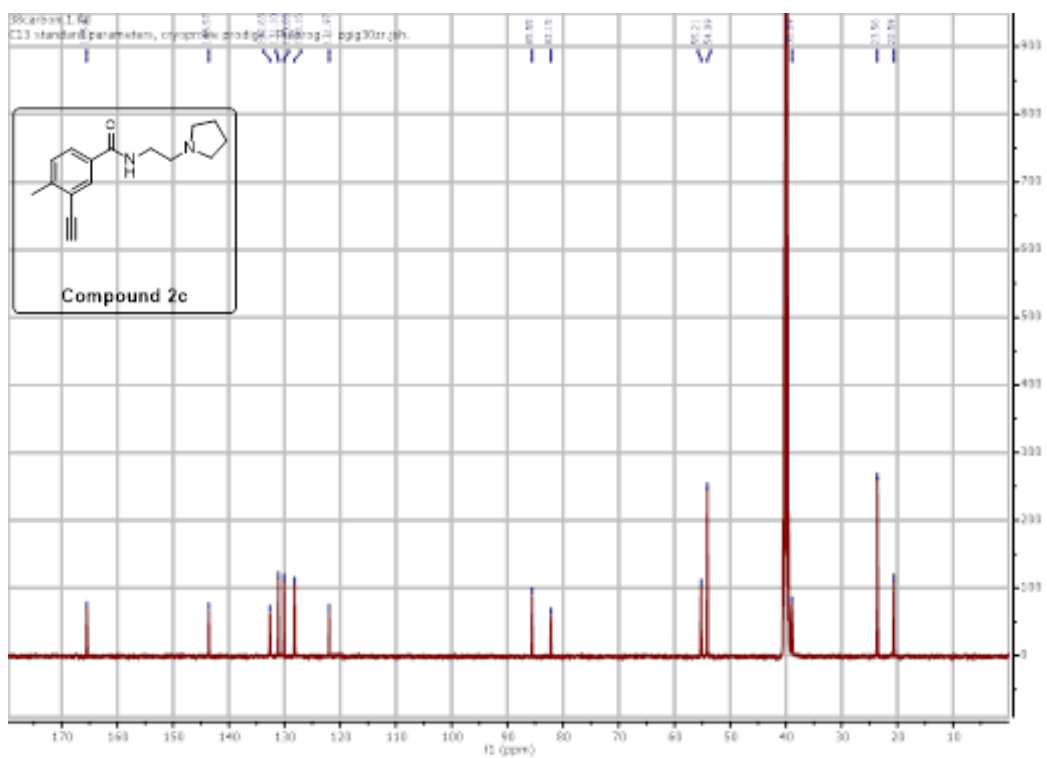
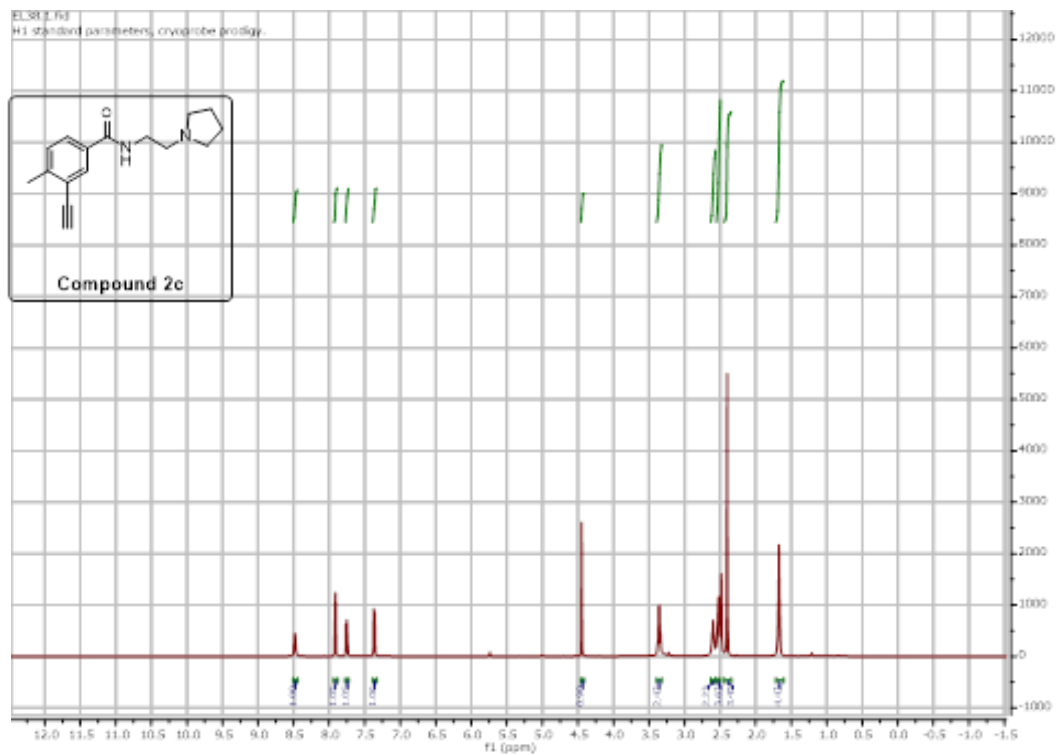


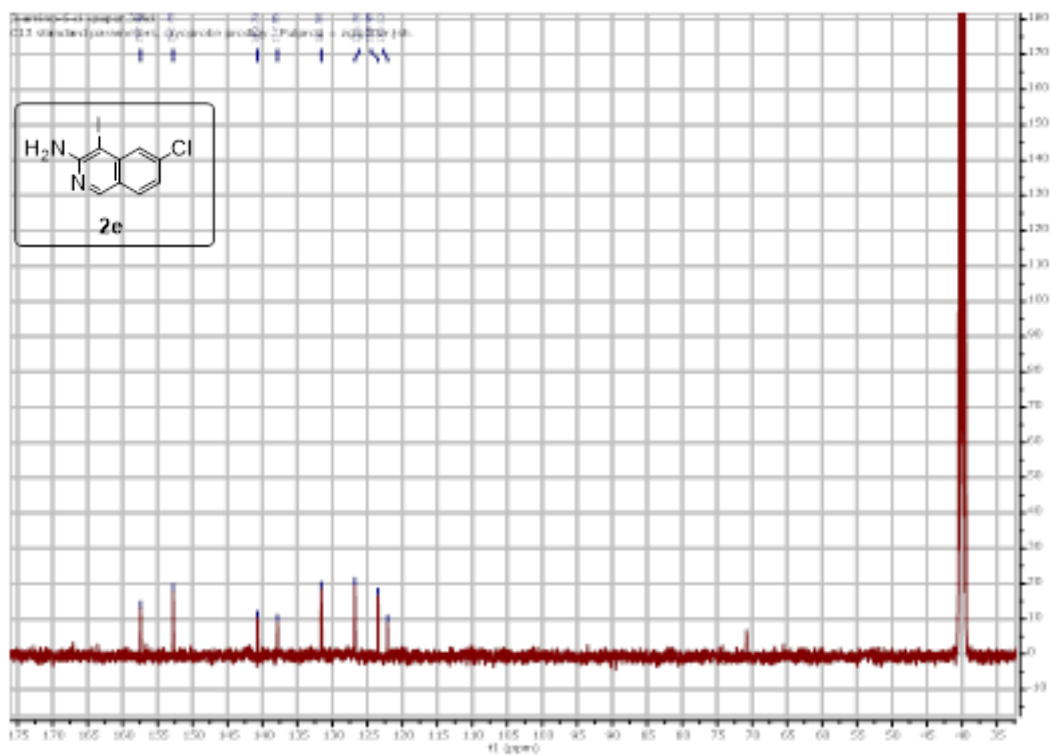
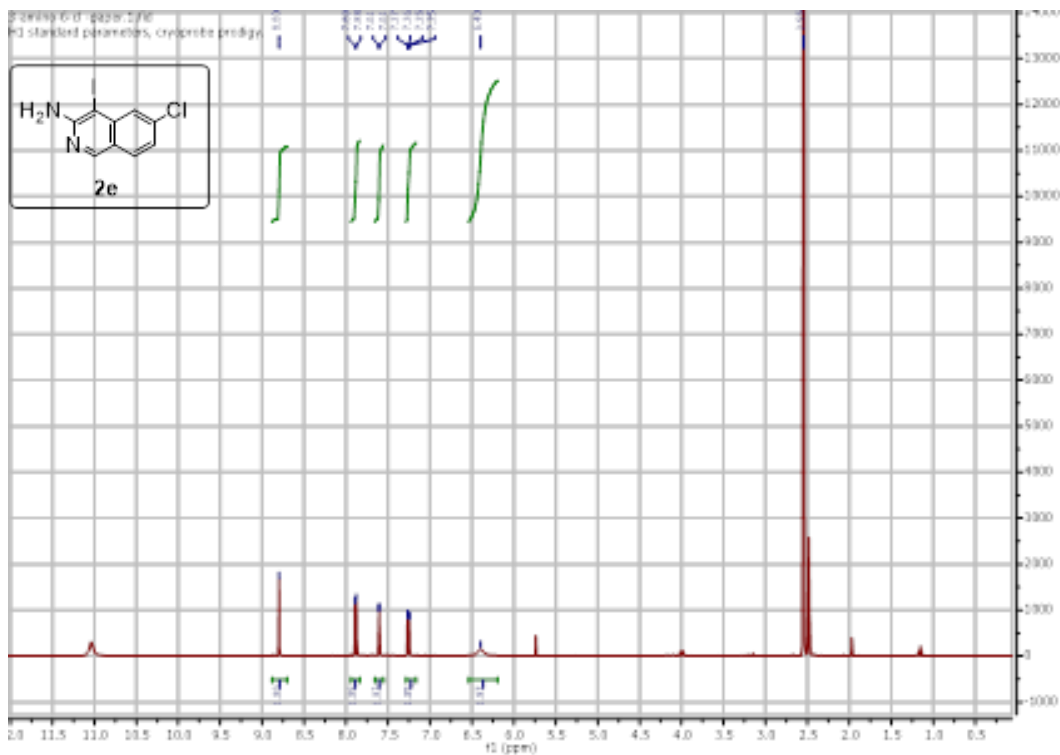


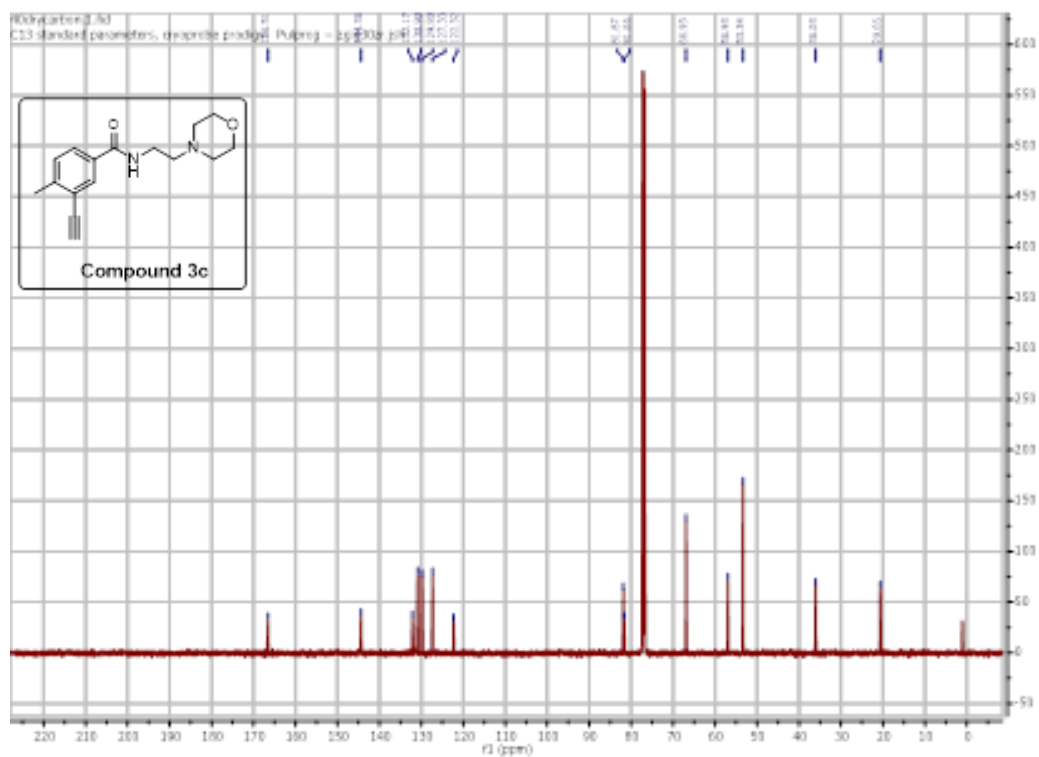
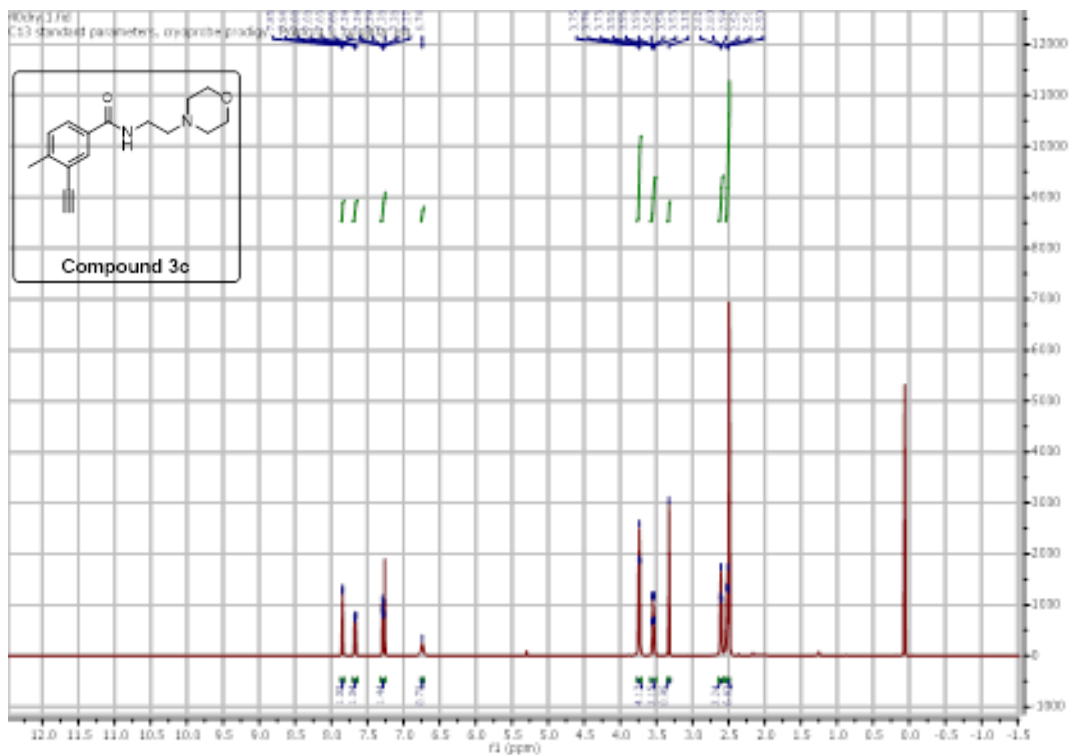


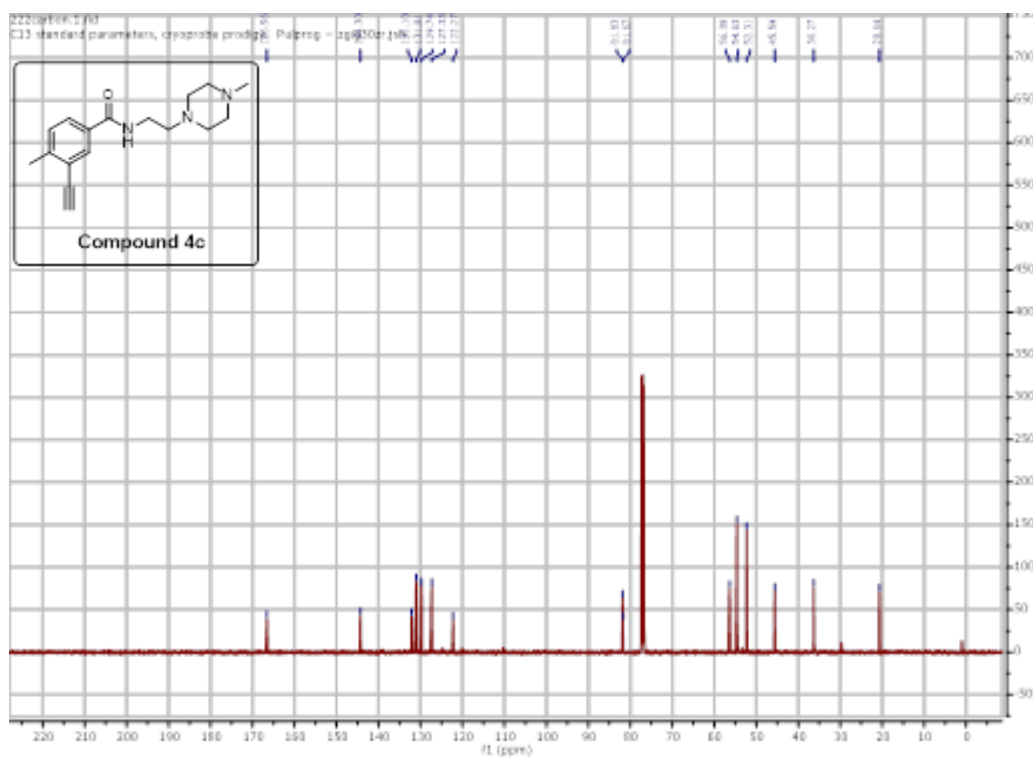
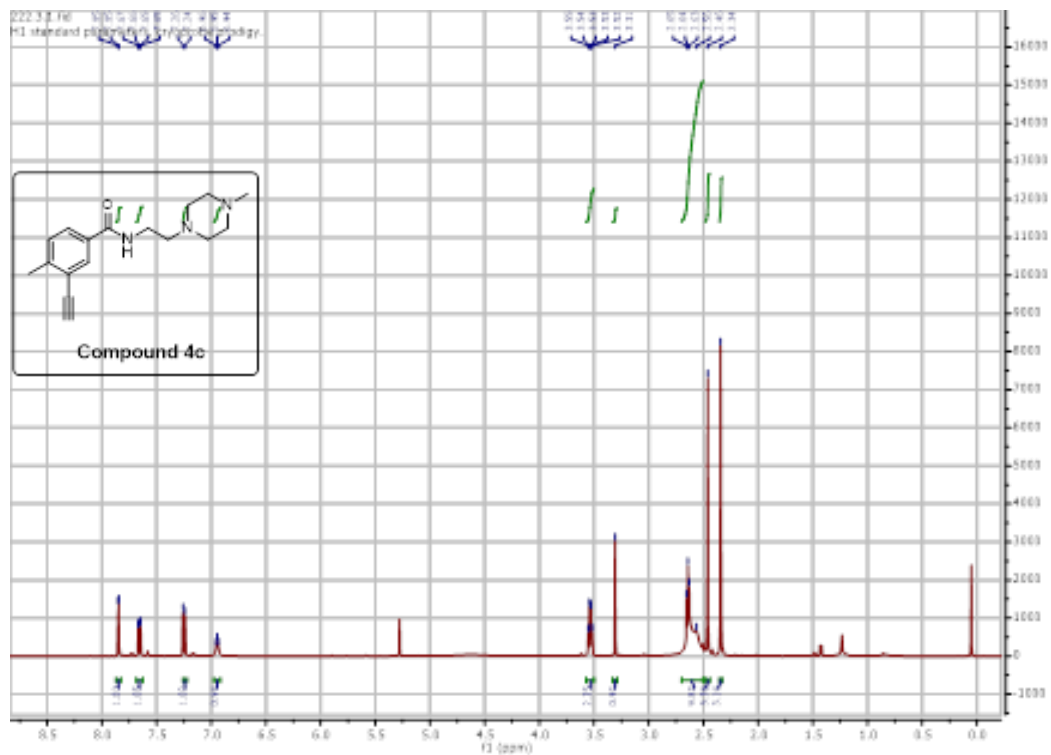
NMR spectra of compounds

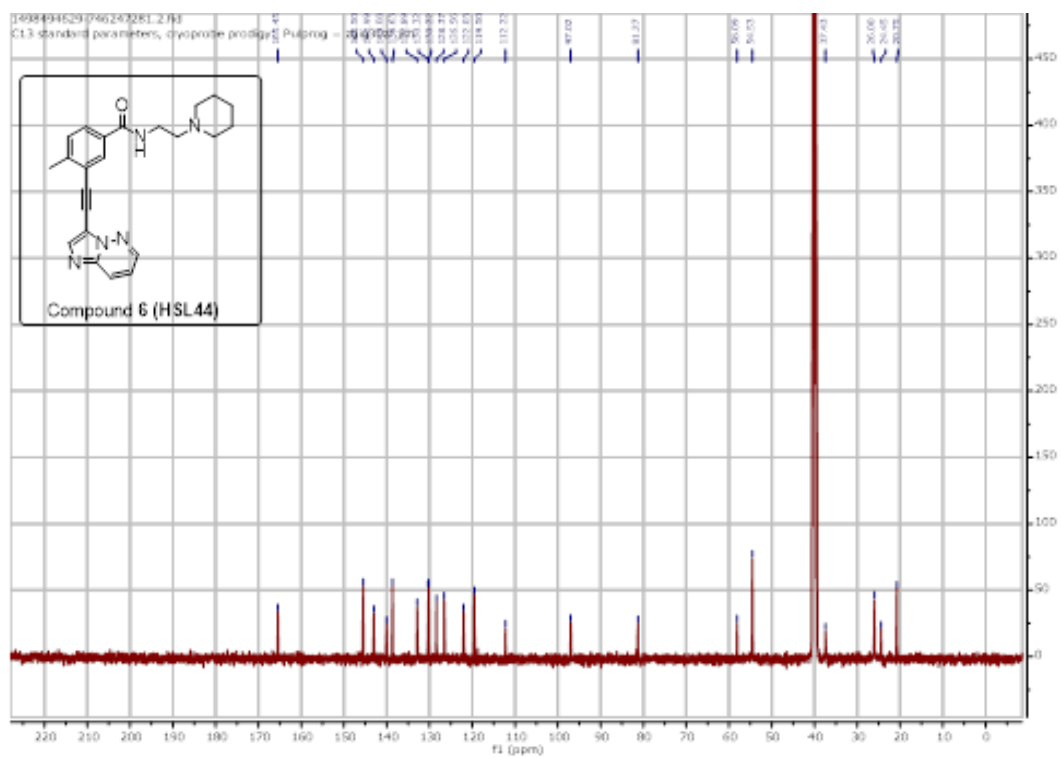
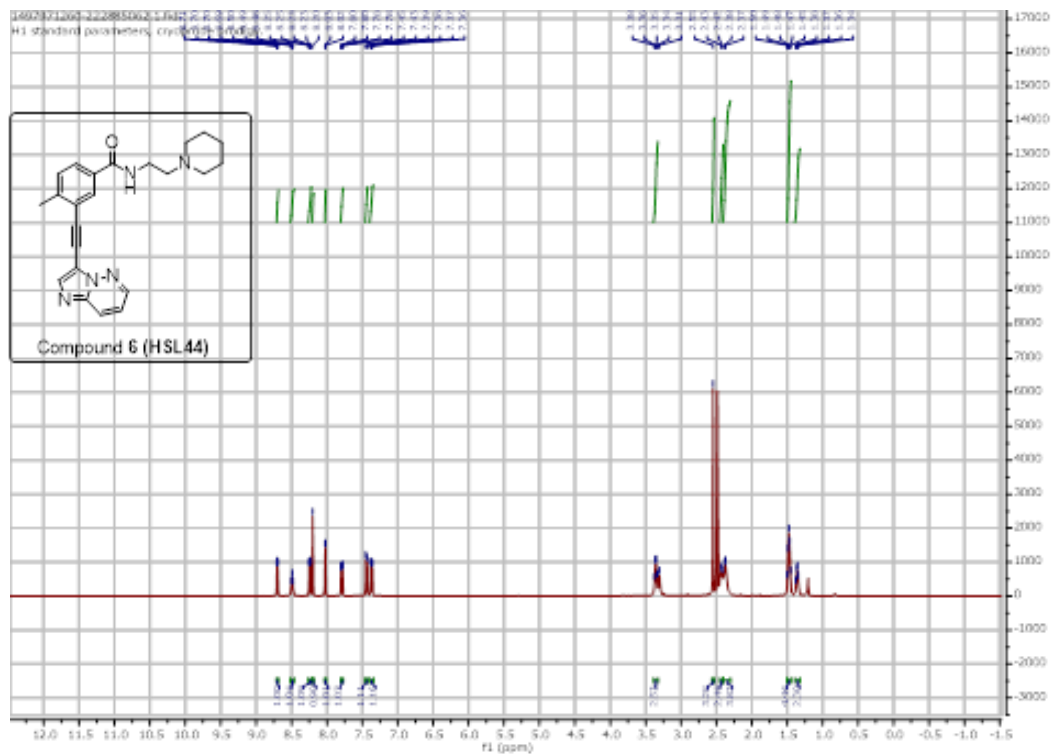


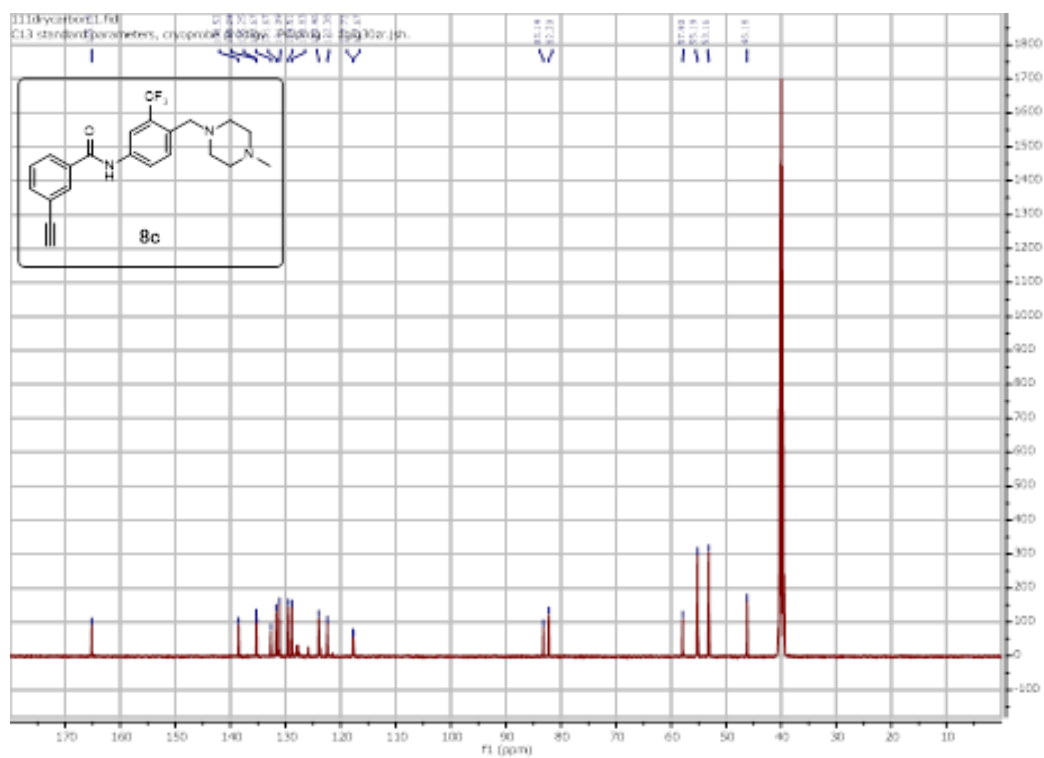
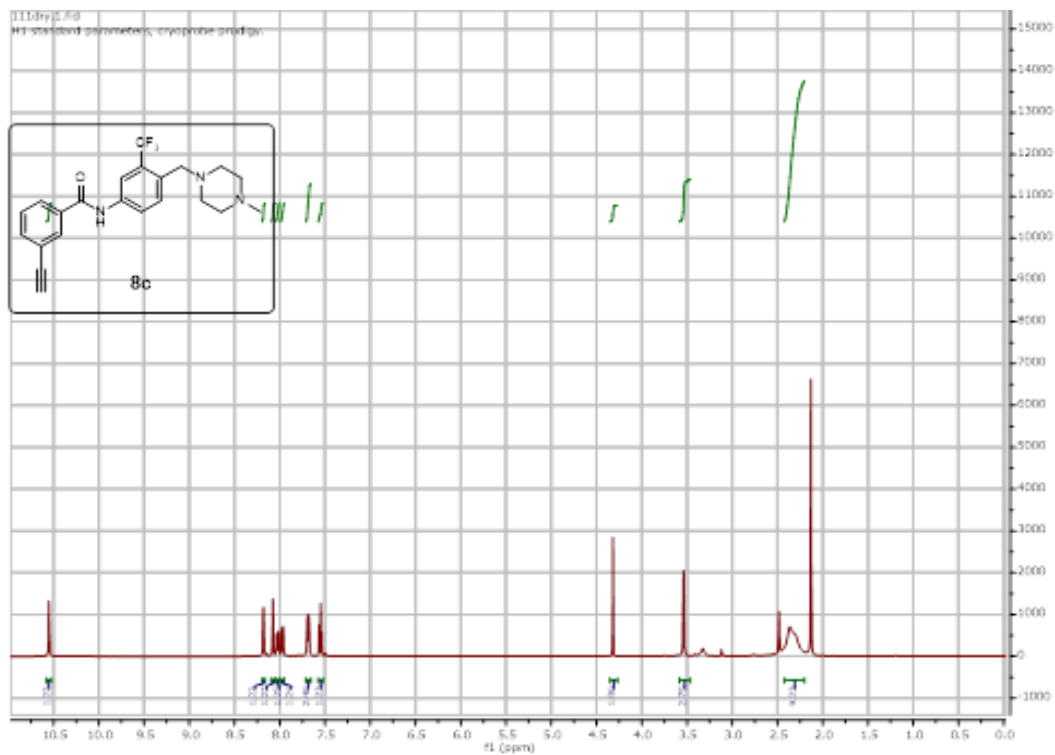


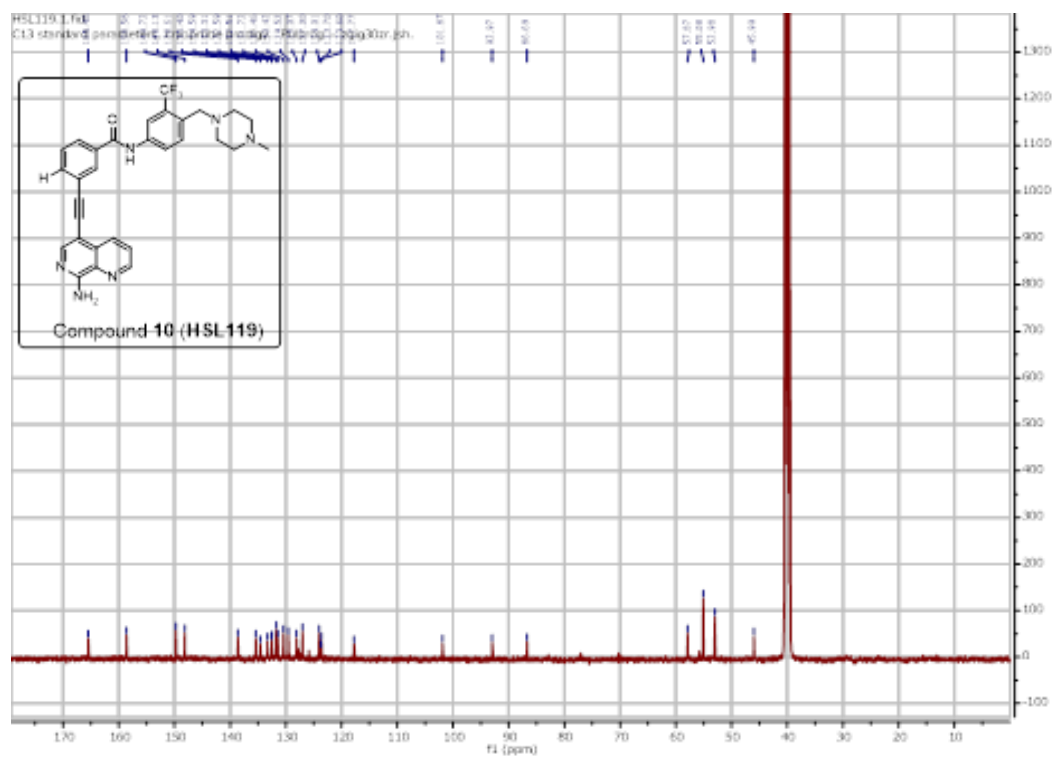
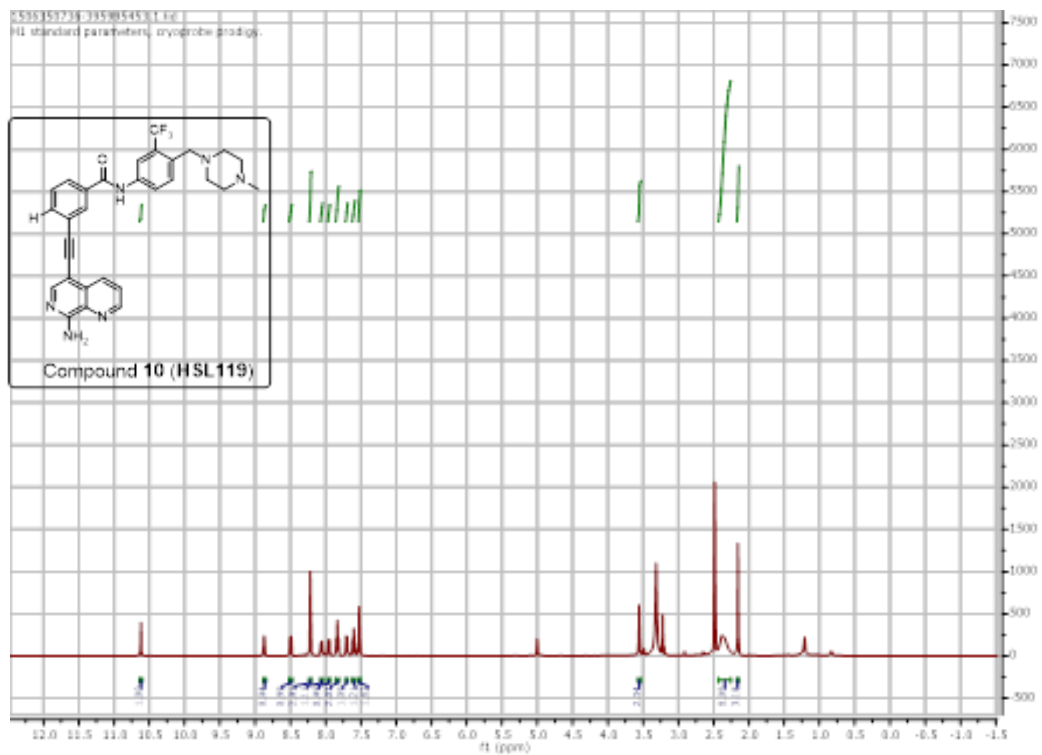


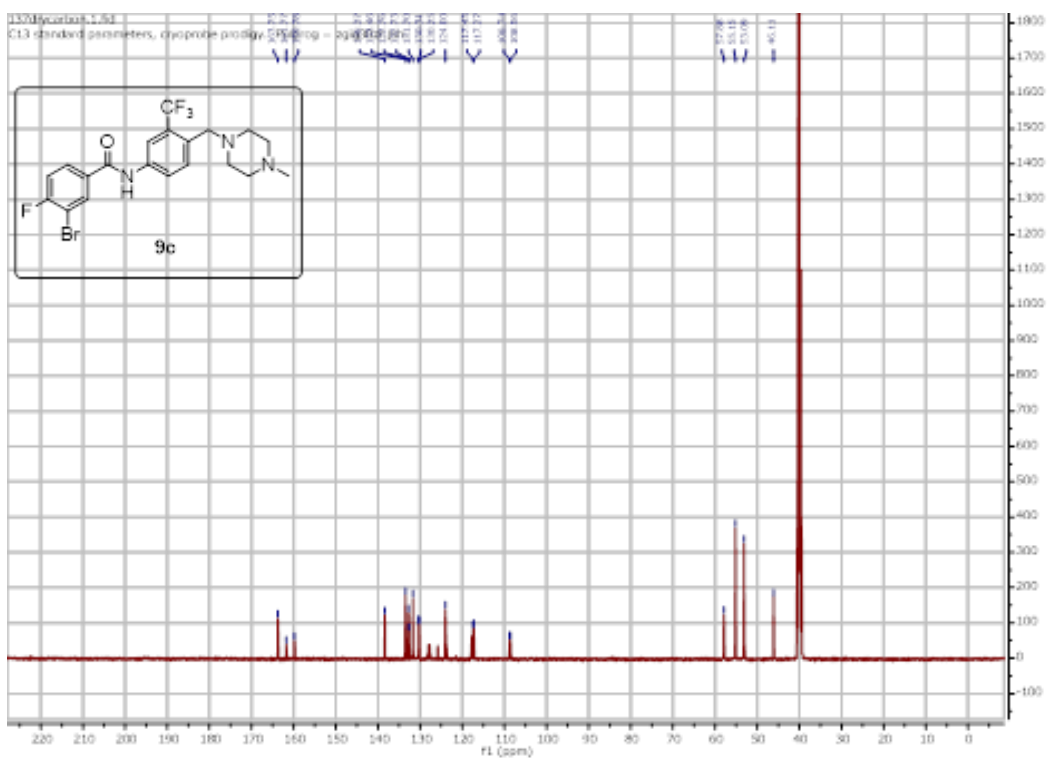
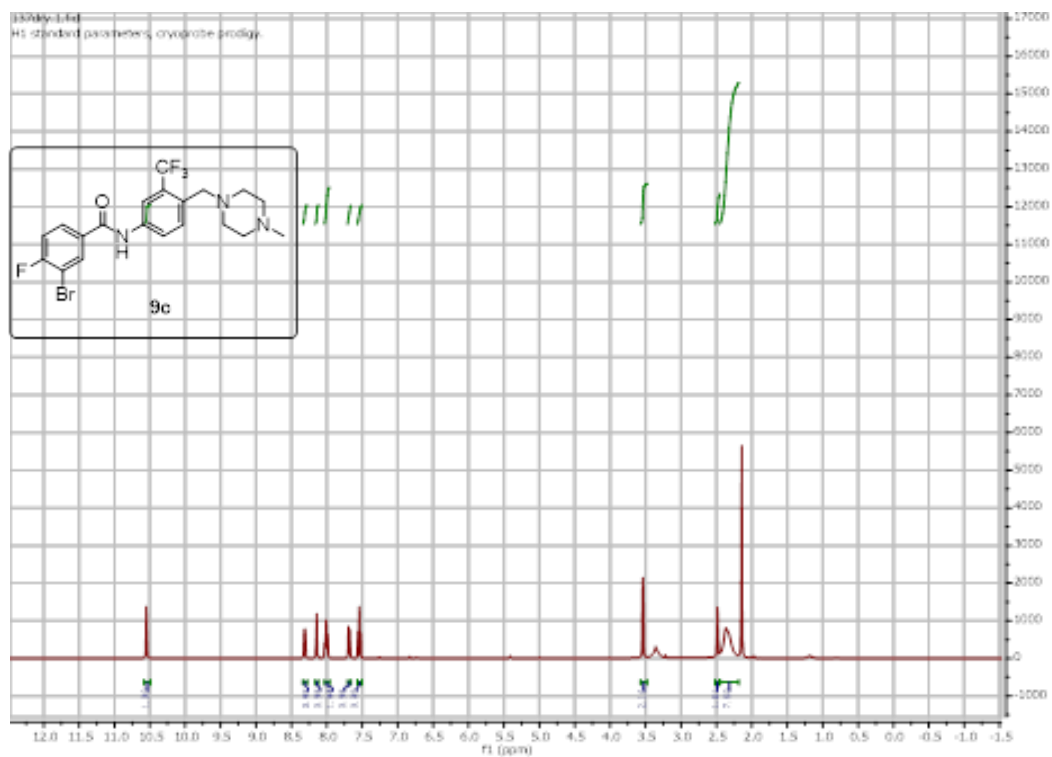


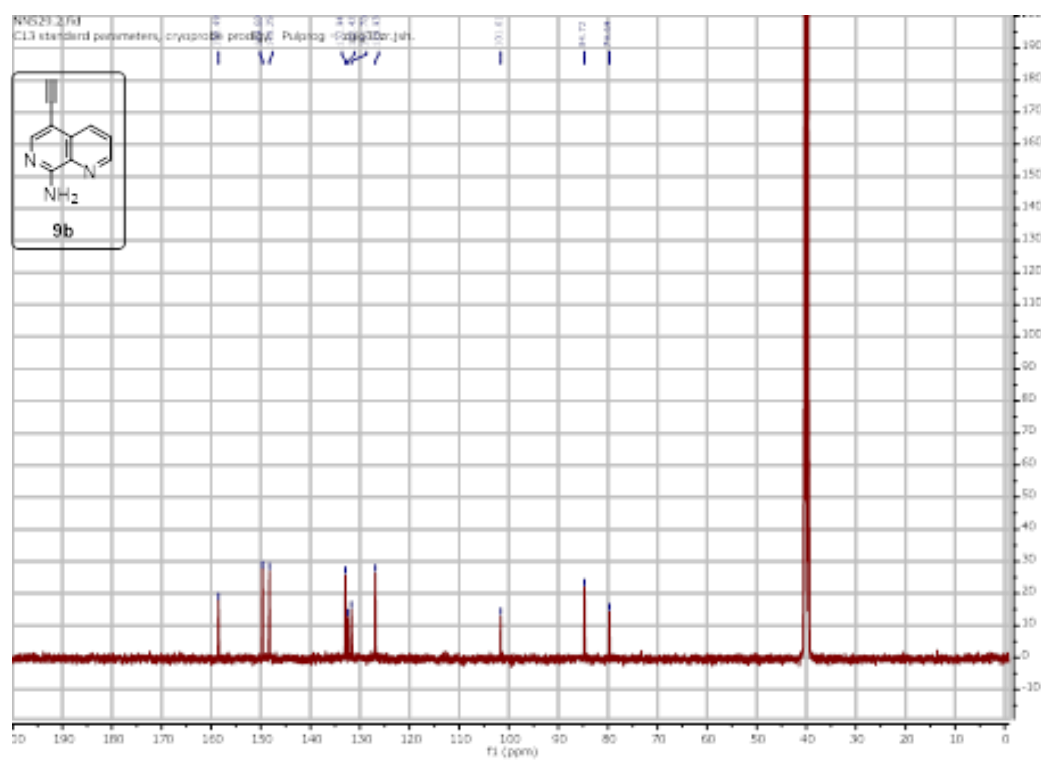
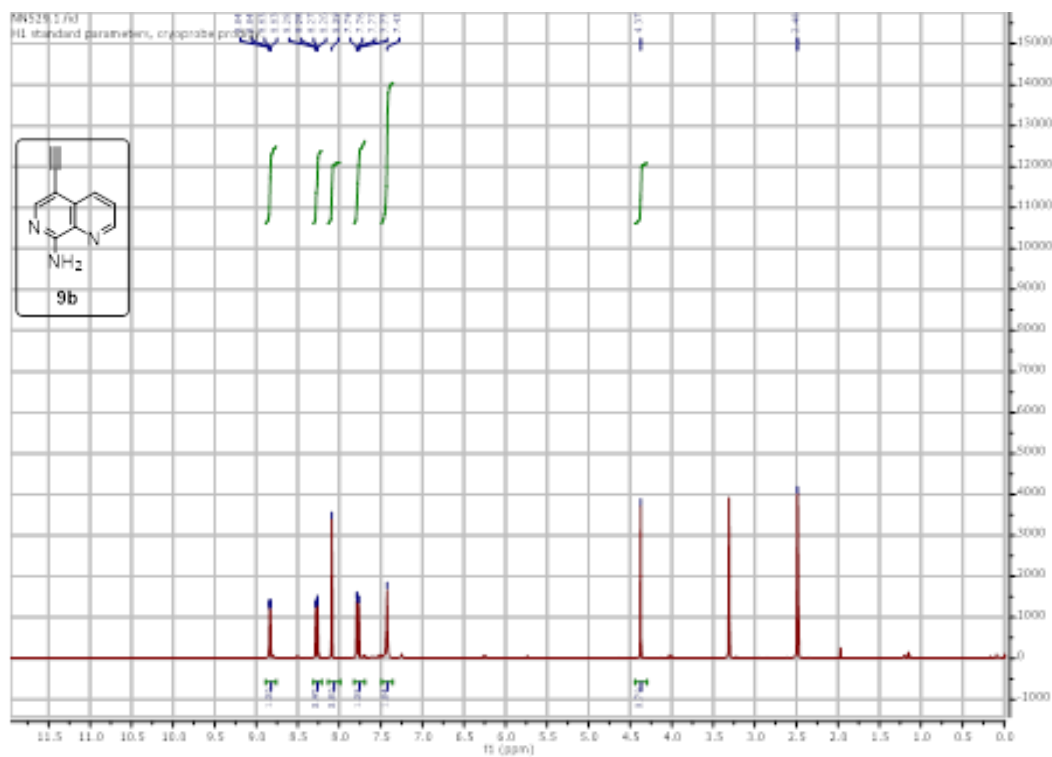


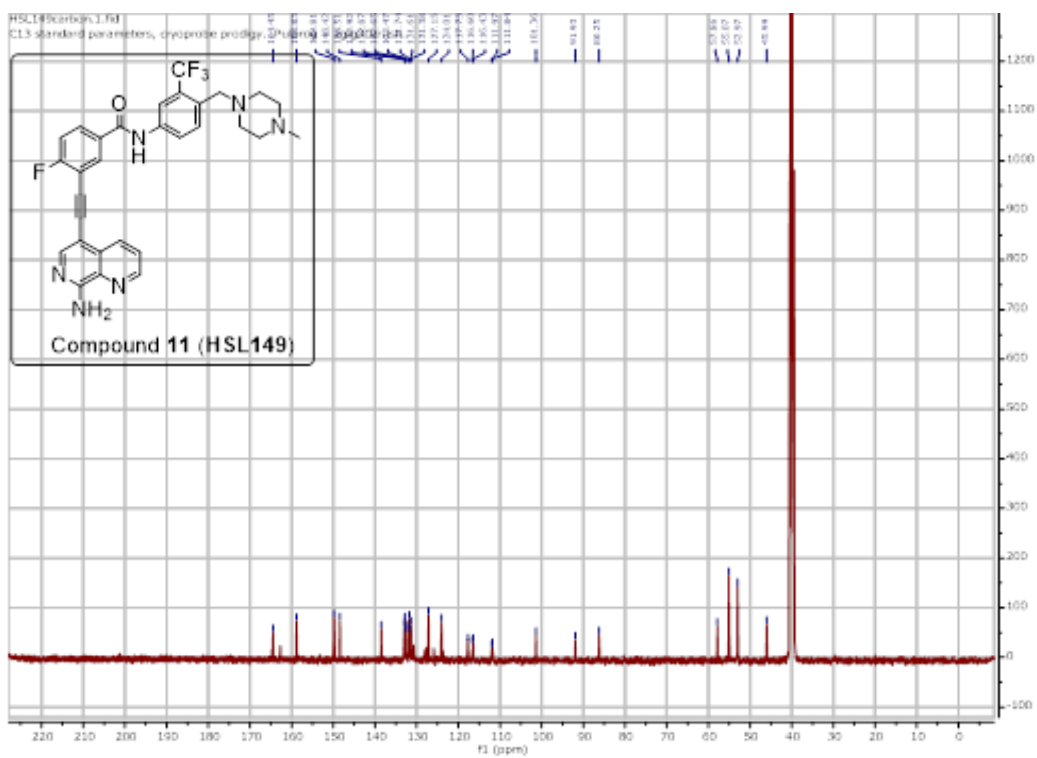
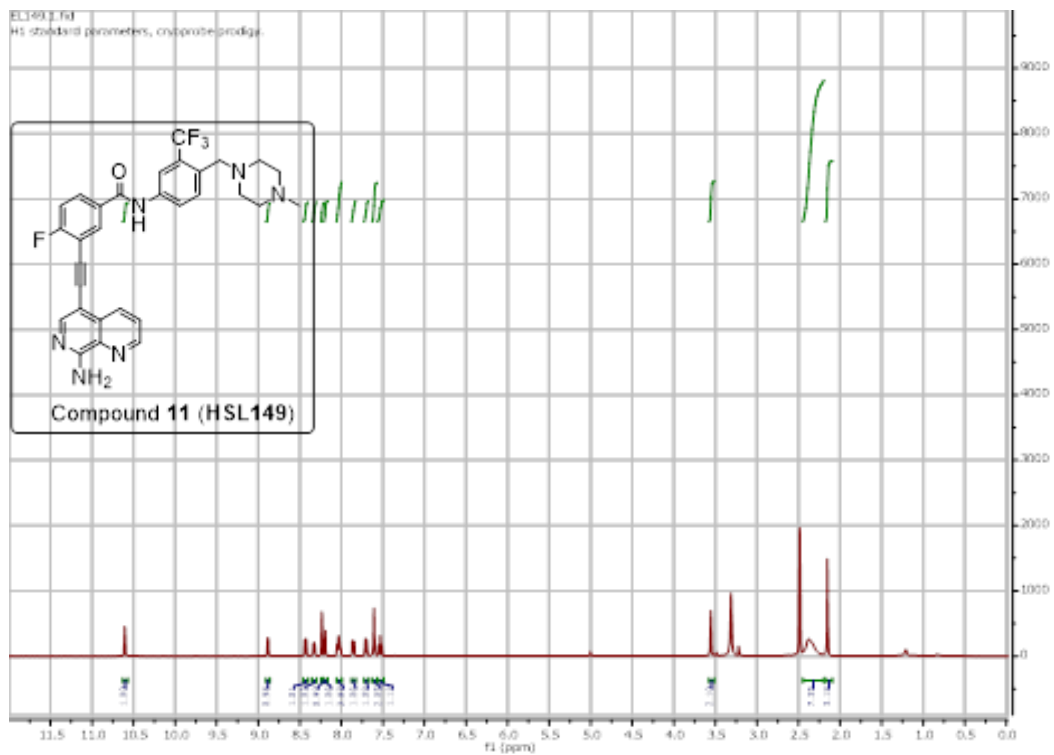


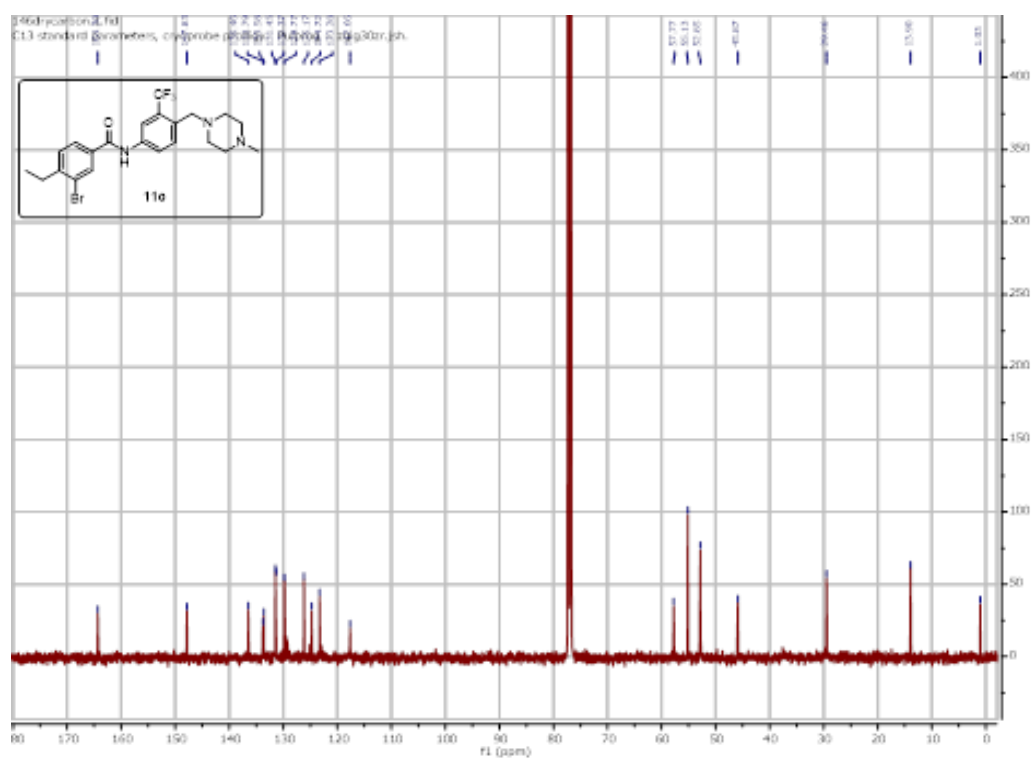
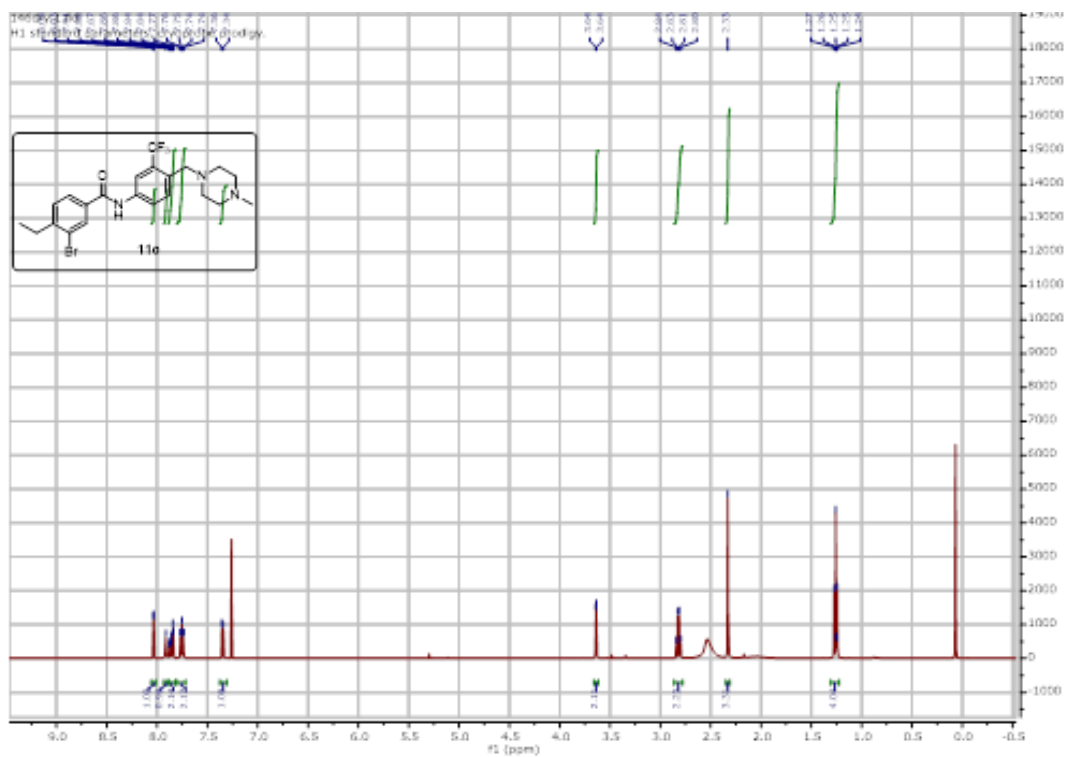


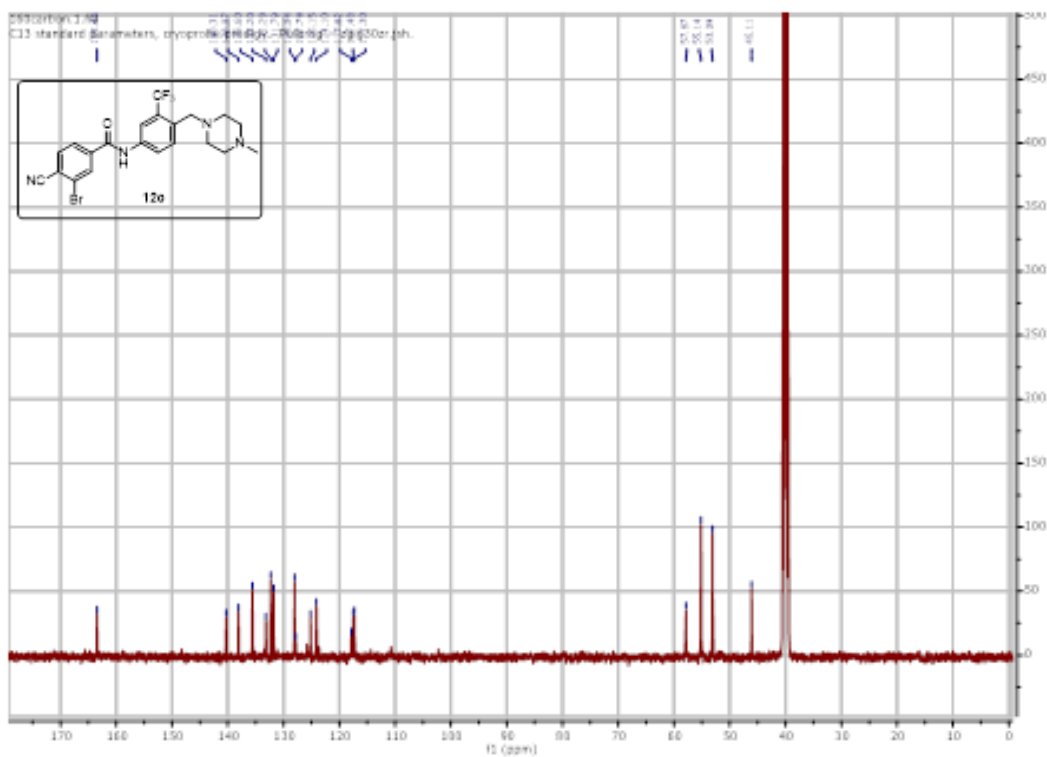
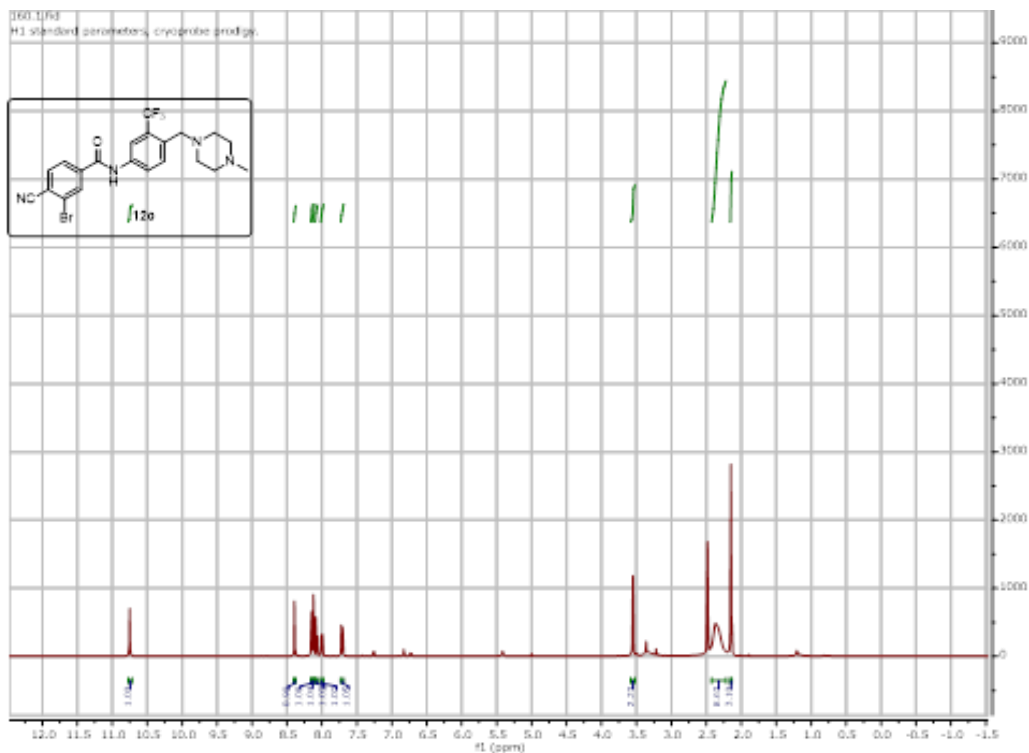










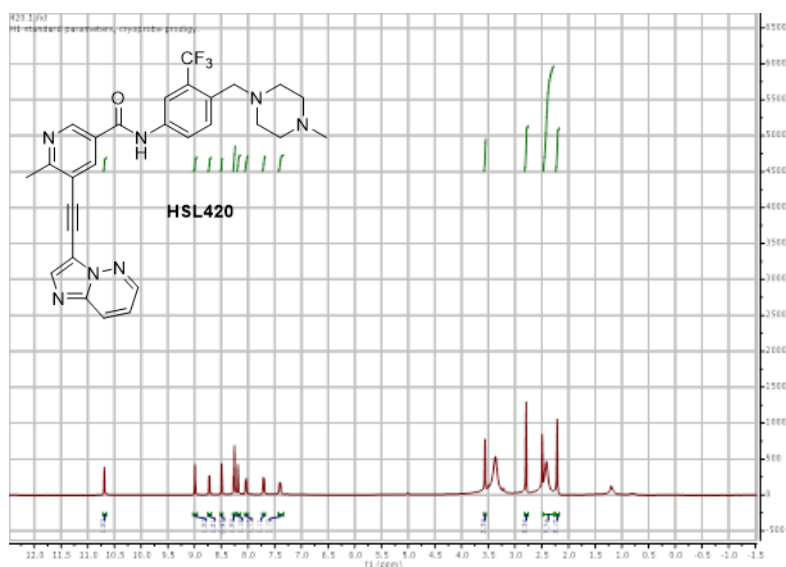


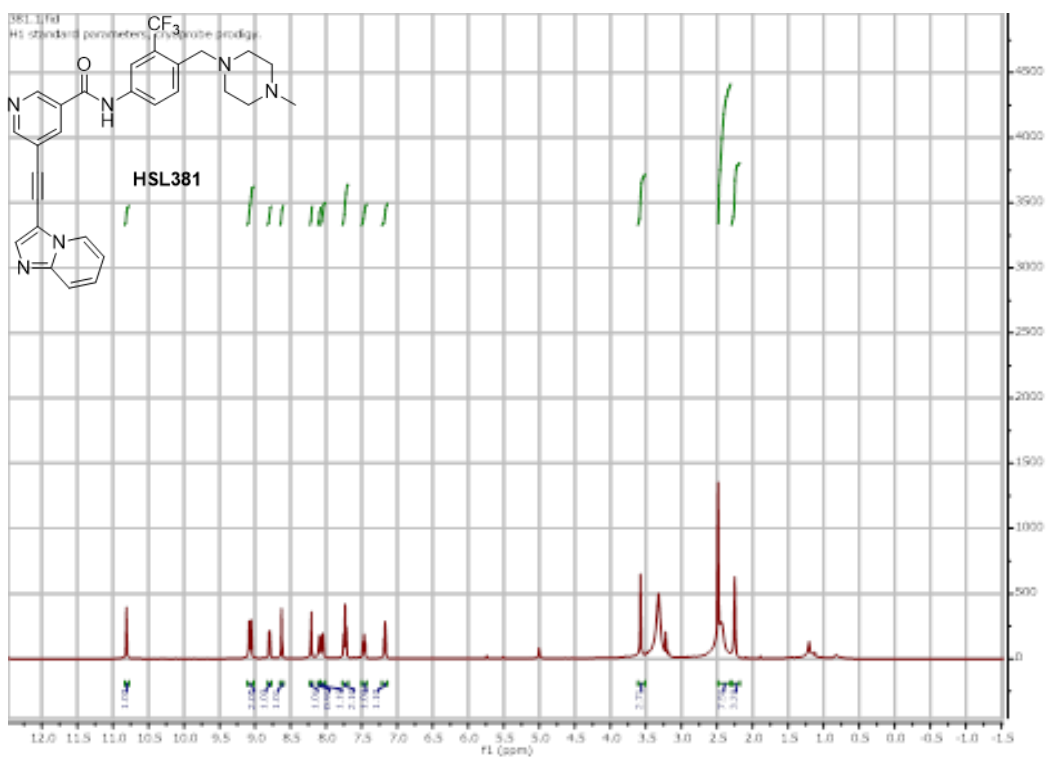
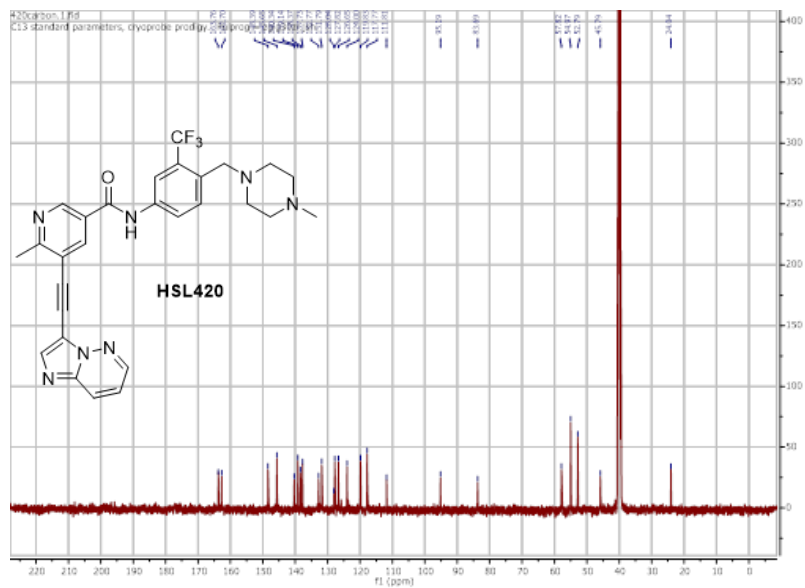
APPENDIX B. CHAPTER 3 SUPPORTIVE INFORMATION

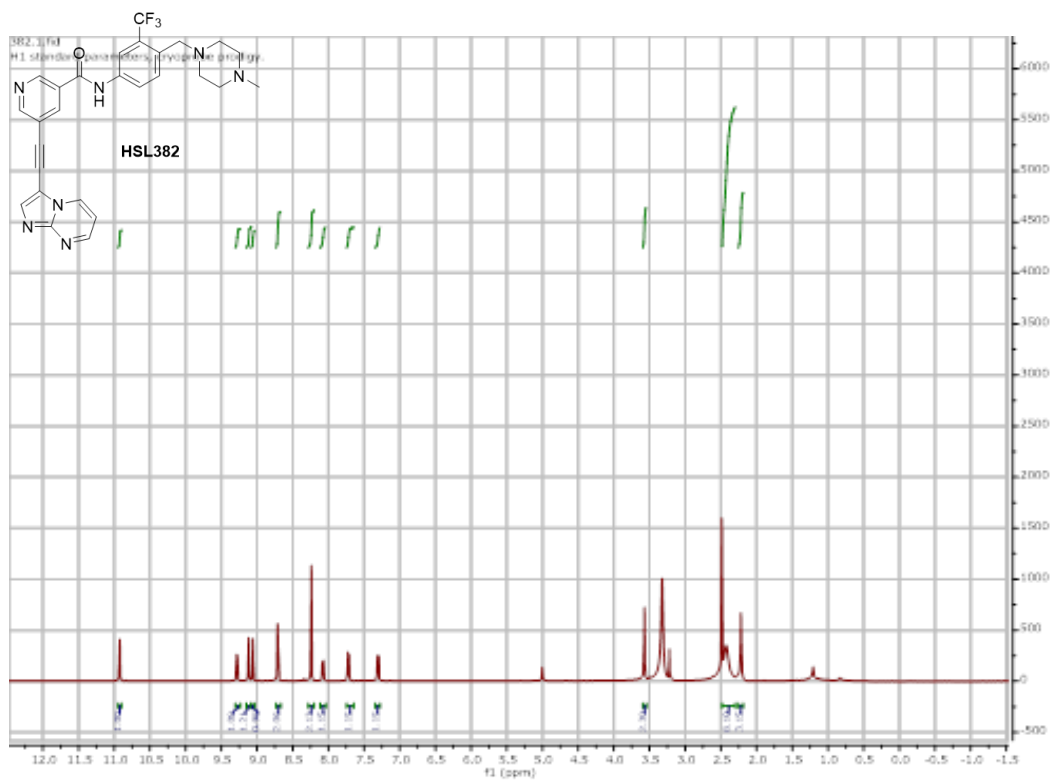
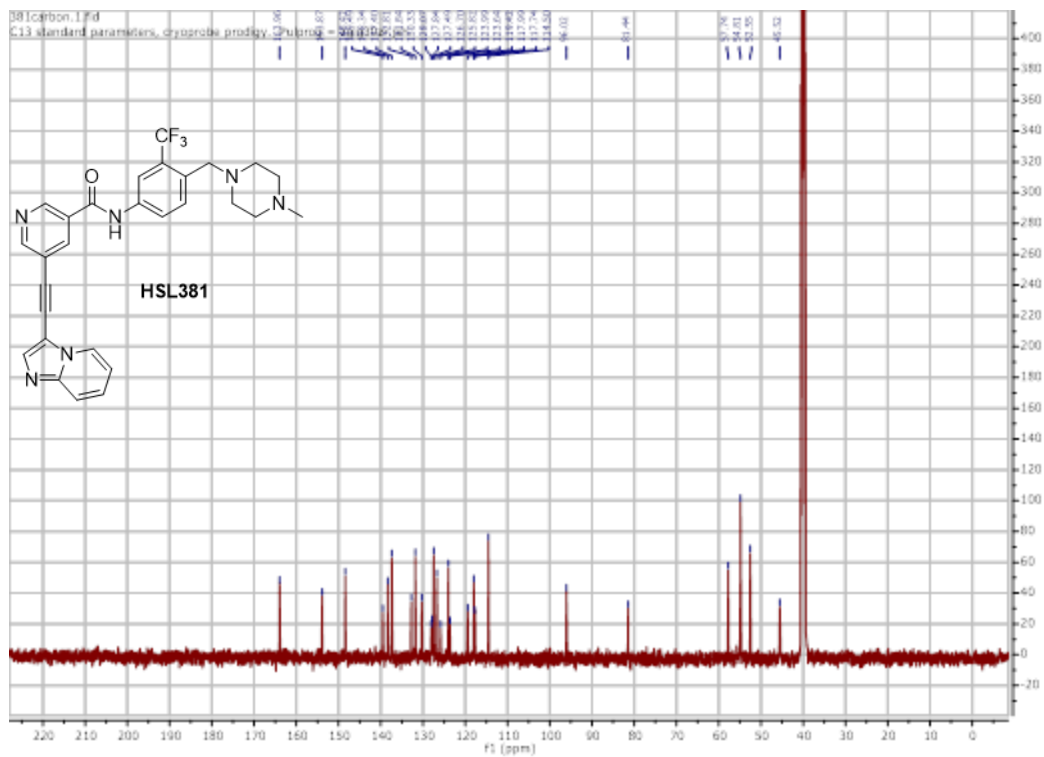
Reproduced with permission from *ACS Omega* 2020, 5,6,2690-2698 Copyright 2020 American Chemical Society. Publication can be found at <https://pubs.acs.org/doi/abs/10.1021/acsomega.9b03223>. Further permission related to publication should be directed to the ACS

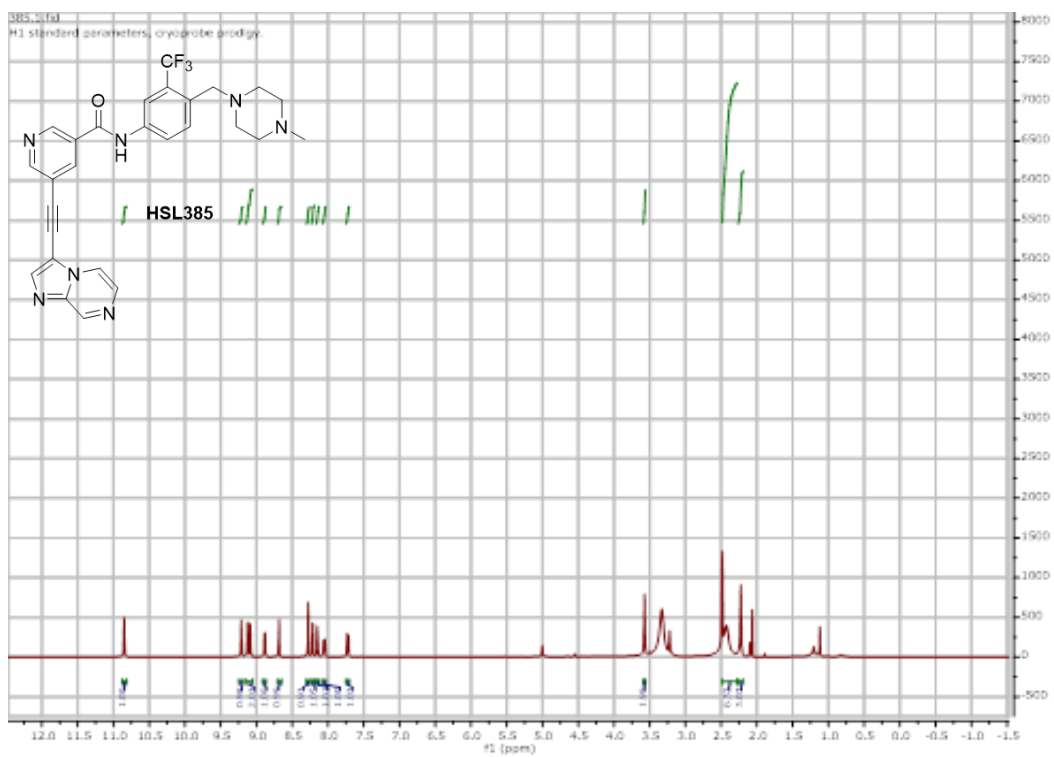
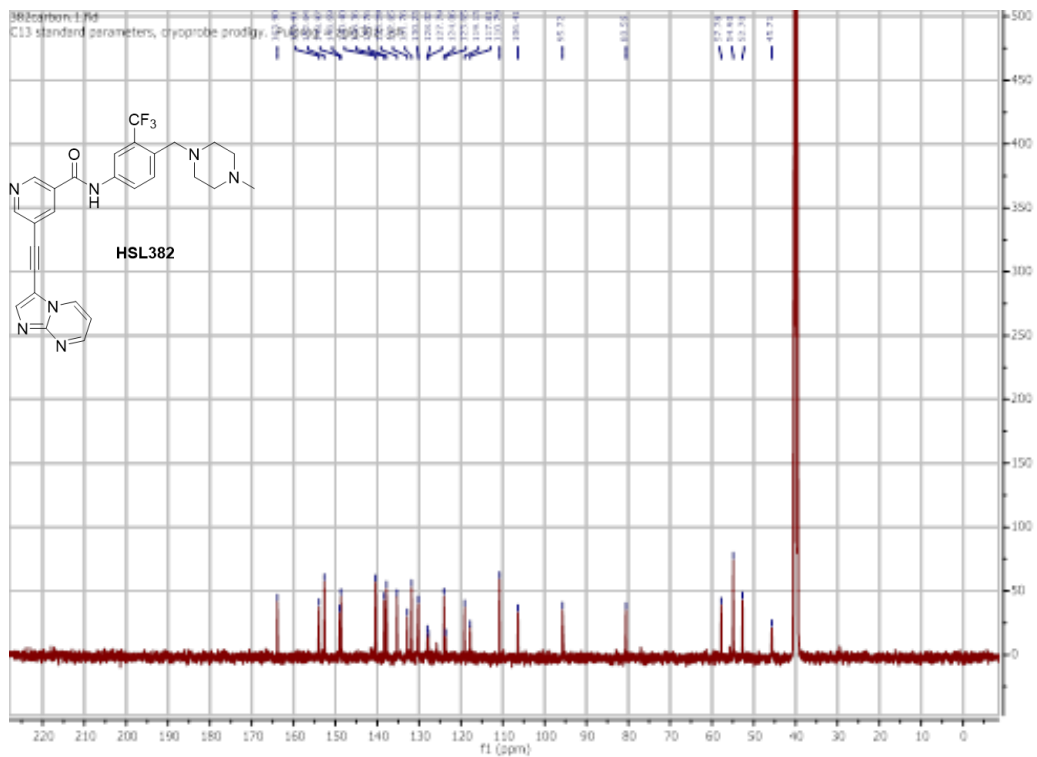
HSN748 and 5-ethynyl-N-(4-((4-methylpiperazin-1-yl)methyl)-3-(trifluoromethyl)phenyl)nicotinamide WERE synthesized by N. Naganna for experimental details and characterization see Larocque, E., Chu, E. F. Y., Naganna, N. & Sintim, H. O. Nicotinamide–Ponatinib Analogues as Potent Anti-CML and Anti-AML Compounds. *ACS Omega* 5, 2690–2698 (2020).

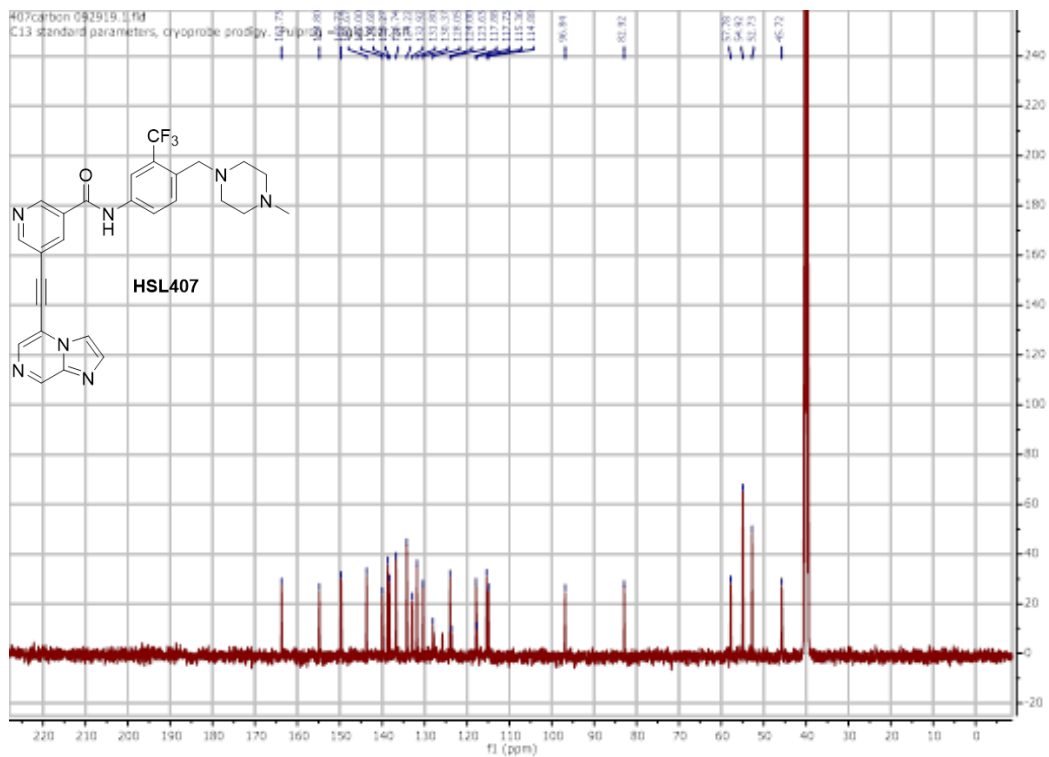
NMR spectra







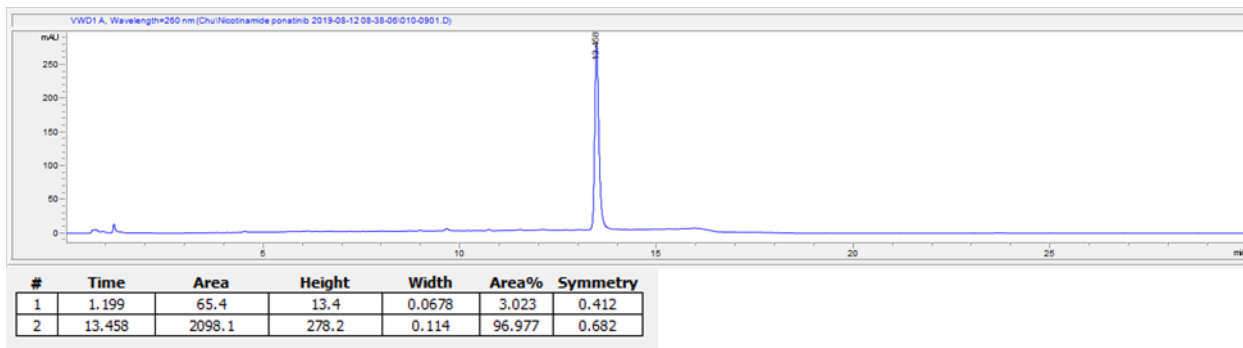




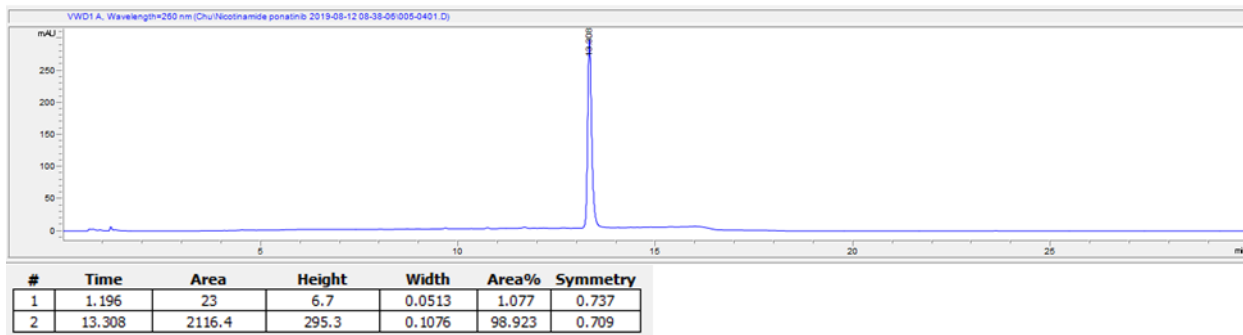
HPLC traces of compounds

Conditions: Agilent Eclipse plus C18, 3 μm , 4.6x100 mm, 0 \rightarrow 15 min, 50% B \rightarrow 100% B, (A: 0.1% NH_4OH in H_2O , B: MeOH), 25 $^\circ\text{C}$. Compound concentration are 100 μM in MeOH.

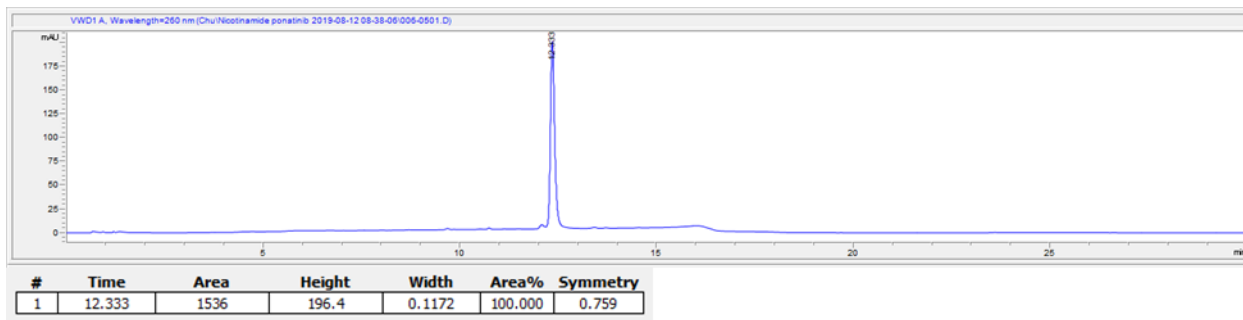
HPLC trace of HSL420



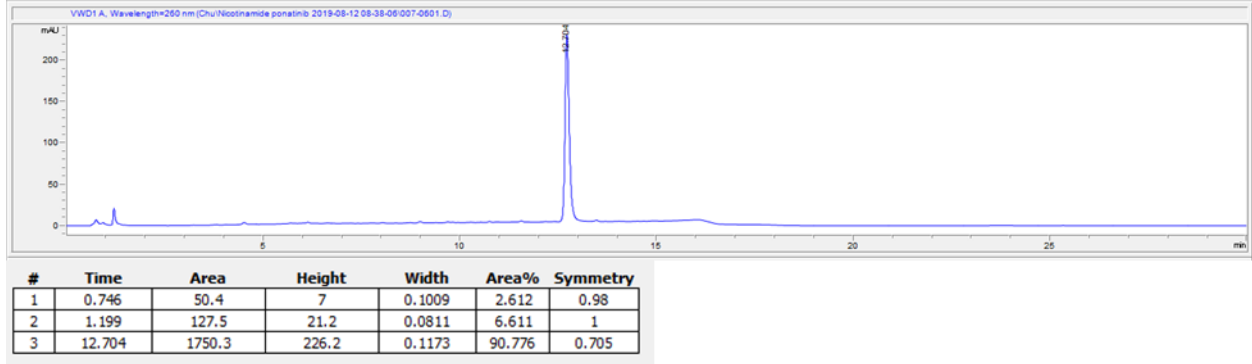
HPLC trace of HSL381



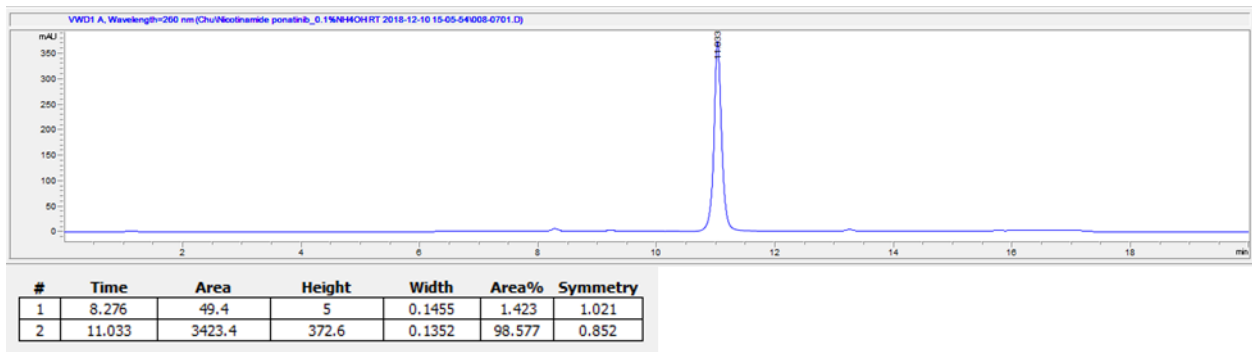
HPLC trace of HSL382



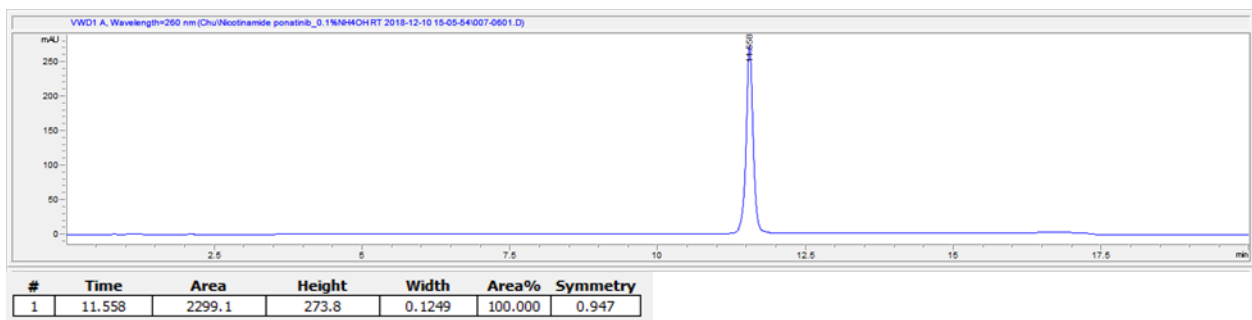
HPLC trace of HSL385



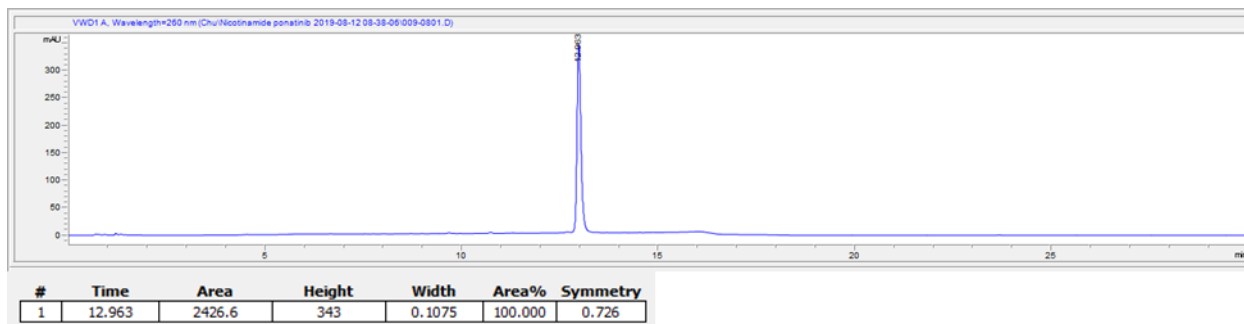
HPLC trace of HSL338



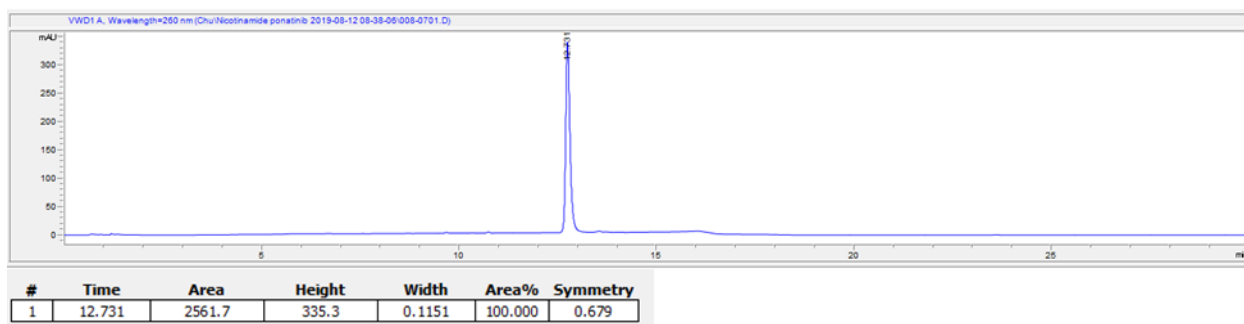
HPLC trace of HSL331



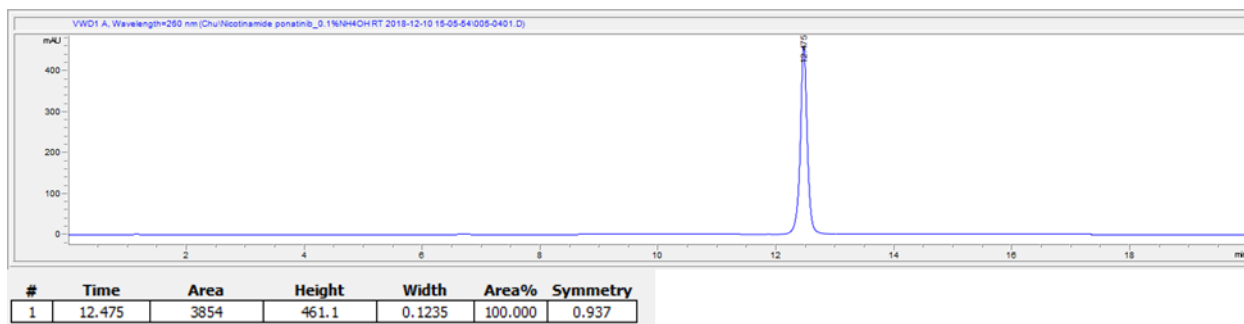
HPLC trace of HSL412



HPLC trace of HSL407



HPLC trace of Ponatinib



HPLC analysis conditions

Initial Events For All Signals:

Integration Events	Value
Tangent Skim Mode	New Exponential
Tail Peak Skim Height Ratio	5.00
Front Peak Skim Height Ratio	5.00
Skim Valley Ratio	20.00
Baseline Correction	Advanced
Peak to Valley Ratio	500.00

Specific Events For Signal:

VWD Default

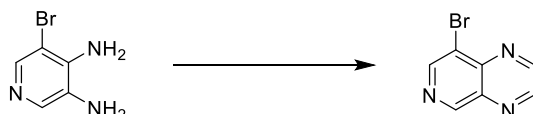
Time	Integration Events	Value
Initial	Slope Sensitivity	1
Initial	Peak Width	0.02
Initial	Area Reject	1
Initial	Height Reject	5
Initial	Shoulders	OFF

Kinases	Kinase Cat#	Kinase Provider	Kinase in RXN (nM)	ATP (uM)	Substrate	Sub in RXN (uM)	Sub Cat#	Sub Provider
ABL1	PR4348B	Invitrogen	0.1	100	ABLtide	20	94851_7	GenScript
ABL1 (T315I)	PV3866	Invitrogen	4	100	ABLtide	20	94851_7	GenScript
c-Kit	PV3589	Invitrogen	200	100	pEY + Mn	0.2	P7244-250MG	Sigma
c-Src	PR4336E	Invitrogen	0.6	100	pEY	0.2	P7244-250MG	Sigma
FGFR1	PV3146	Invitrogen	1.75	100	pEY + Mn	0.2	P7244-250MG	Sigma
FGFR2	PV3368	Invitrogen	0.45	100	pEY + Mn	0.2	P7244-250MG	Sigma
FGFR3	PV3145	Invitrogen	5	100	pEY + Mn	0.2	P7244-250MG	Sigma
FGFR4	P3054	Invitrogen	2.5	100	pEY + Mn	0.2	P7244-250MG	Sigma
FLT3 (D835Y)	PV3967	Invitrogen	0.5	100	ABLtide	20	94851_7	GenScript
FLT3 (ITD)	0778-0000-1	ProQinase	100	100	ABLtide	20	94851_7	GenScript
P38a/MAPK14	PV3304	Invitrogen	20	100	MBP	20	102641	Active Motif
p70S6K/RPS6 KB1	PV3815	Invitrogen	3	100	S6K/Rsk2 peptide 2	20	36009_7	GenScript
PDGFRa	PV3811	Invitrogen	2	100	pEY + Mn	0.2	P7244-250MG	Sigma
PDGFRb	P3082	Invitrogen	15	100	pEY + Mn	0.2	P7244-250MG	Sigma
RET	PV3819	Invitrogen	3	100	CHKtide	20	U6834CD140_1	GenScript
MNK1	PR8046A	Invitrogen	30	100	MBP	20	102641	Active Motif
MNK2	PR9138A	Invitrogen	200	100	MBP	20	102641	Active Motif

APPENDIX C. CHAPTER 4 SUPPLEMENTAL INFORMATION

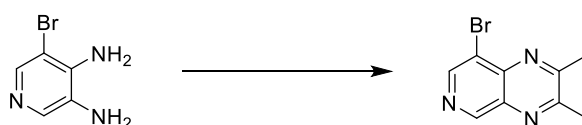
Synthesis and analytical data of compounds

Full characterization of some compounds was not done because of shutdown of laboratory from March 25th due to the COVID-19 pandemics. Future students who proceed with this project are encouraged to complete the characterization



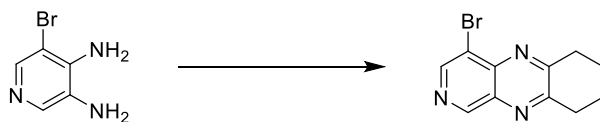
HSL215: 8-bromopyrido[3,4-b]pyrazine

To a reaction vial, 5-bromopyridine-3,4-diamine (250 mg, 1.33 mmol, 1 equiv.) and ethanol (10 mL) were added. Oxalaldehyde (77 mg, 1.33 mmol, 1 equiv.) was then added. The reaction was then allowed to stir at room temperature for 6 hours. Upon reaction completion, crude mixture was concentrated under reduced pressure. Pure compound was obtained via column chromatography (10 % MeOH/CH₂Cl₂). Yield = 85 % TLC R_f = 0.76 (10 % MeOH/CH₂Cl₂) ¹H NMR (500 MHz, DMSO-d₆) δ 9.48 (s, 1H), 9.27 (d, J = 1.8 Hz, 1H), 9.17 (d, J = 1.7 Hz, 1H), 9.12 (s, 1H). ¹³C NMR (126 MHz, DMSO) δ 154.2, 151.6, 149.1, 148.9, 143.0, 138.9, 120.2.



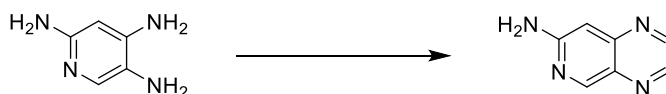
HSL176: 8-bromo-2,3-dimethylpyrido[3,4-b]pyrazine

To a reaction vial, 5-bromopyridine-3,4-diamine (100 mg, 0.532 mmol, 1 equiv.) and ethanol (10 mL) were added. Biacetyl (45.8 mg, 0.532 mmol, 1 equiv.) was then added. The reaction was then allowed to stir at room temperature for 2 hours. Upon reaction completion, crude mixture was concentrated under reduced pressure. Pure compound was obtained via column chromatography (10 % MeOH/CH₂Cl₂). Yield = quantitative TLC R_f = 0.4 (CH₂Cl₂) ¹H NMR (500 MHz, DMSO-d₆) δ 9.21 (s, 1H), 8.90 (s, 1H), 2.73 (s, 3H), 2.71 (s, 3H). ¹³C NMR (126 MHz, DMSO) δ 161.3, 158.3, 152.4, 147.8, 141.4, 137.2, 119.3, 23.9, 23.2.



HSL452: 8-bromo-2,3-diethylpyrido[3,4-b]pyrazine

To a reaction vial, 5-bromopyridine-3,4-diamine (100 mg, 0.531 mmol, 1 equiv.) and MeOH (10 mL) were added. Hexane-3,4-dione (60.6 mg, 0.531 mmol, 1 equiv.) was then added. The reaction was then allowed to stir at room temperature for 2.5 hours. Upon reaction completion, crude mixture was concentrated under reduced pressure. Pure compound was obtained via column chromatography (10 % MeOH/CH₂Cl₂). Yield = 61 % TLC R_f = 0.8 (10 % MeOH/CH₂Cl₂) ¹H NMR (500 MHz, DMSO-*d*₆) δ 9.30 (s, 1H), 8.96 (s, 1H), 3.11 (dq, *J* = 11.1, 7.3 Hz, 4H), 1.36 (dt, *J* = 11.0, 7.3 Hz, 6H).



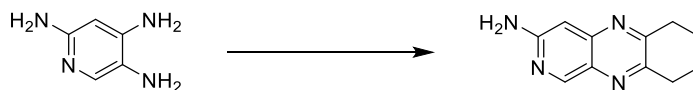
HSL404: pyrido[3,4-b]pyrazin-7-amine

To a reaction vial, pyridine-2,4,5-triamine (80 mg, 0.645 mmol, 1 equiv.) and ethanol (5 mL) were added. Oxalaldehyde (37.41 mg, 0.645 mmol, 1 equiv.) was then added. The reaction was then allowed to stir at room temperature for 6 hours. Upon reaction completion, crude mixture was concentrated under reduced pressure. Pure compound was obtained via column chromatography (DMC). Yield = 60 % TLC R_f = 0.3 (10 % MeOH/CH₂Cl₂) ¹H NMR (500 MHz, DMSO-*d*₆) δ 8.94 (d, *J* = 0.8 Hz, 1H), 8.75 (d, *J* = 1.8 Hz, 1H), 8.49 (d, *J* = 1.8 Hz, 1H), 6.69 (d, *J* = 0.8 Hz, 1H), 6.58 (s, 2H). ¹³C NMR (126 MHz, DMSO) δ 160.1, 154.0, 150.5, 147.7, 142.1, 132.3, 97.3.



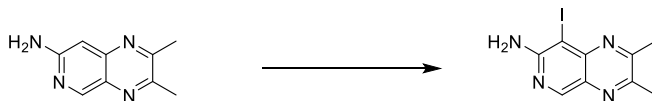
HSL405: 2,3-dimethylpyrido[3,4-b]pyrazin-7-amine

To a reaction vial, pyridine-2,4,5-triamine (80 mg, 0.645 mmol, 1 equiv.) and ethanol (5 mL) were added. Biacetyl (55.54 mg, 0.645 mmol, 1 equiv.) was then added. The reaction was then allowed to stir at room temperature for 2 hours. Upon reaction completion, crude mixture was concentrated under reduced pressure. Pure compound was obtained via column chromatography (DCM). Yield = 89 % TLC Rf = 0.45 (10 % MeOH/CH₂Cl₂). ¹H NMR (500 MHz, DMSO-*d*₆) δ 8.75 (s, 1H), 6.60 (d, *J* = 0.8 Hz, 1H), 6.28 (s, 2H), 2.56 (s, 3H), 2.53 (s, 3H). ¹³C NMR (126 MHz, DMSO) δ 159.4, 159.2, 151.9, 150.3, 146.2, 130.6, 97.5, 23.7, 22.8.



HSL498: 2,3-diethylpyrido[3,4-b]pyrazin-7-amine

To a reaction vial, pyridine-2,4,5-triamine (150 mg, 0.797 mmol, 1 equiv.) and ethanol (10 mL) were added. Hexane-3,4-dione (90 mg, 0.645 mmol, 1 equiv.) was then added. The reaction was then allowed to stir for 2.5 hours at room temperature. An additional equivalent of hexane-3,4-dione was added 2.5 hours later. The reaction was then allowed to stir for an additional 1.5 hours. Upon reaction completion, crude mixture was concentrated under reduced pressure. Pure compound was obtained via column chromatography (DCM). Yield = 80 % TLC Rf = 0.8 (10 % MeOH/CH₂Cl₂). ¹H NMR (500 MHz, DMSO-*d*₆) δ 8.78 (d, *J* = 0.8 Hz, 1H), 6.63 (d, *J* = 0.8 Hz, 1H), 6.27 (s, 2H), 2.89 (dq, *J* = 14.7, 7.4 Hz, 4H), 1.25 (td, *J* = 7.4, 0.9 Hz, 6H). ¹³C NMR (126 MHz, DMSO) δ 162.2, 159.5, 153.6, 152.1, 145.9, 130.4, 97.7, 39.3, 39.1, 28.1, 27.3, 12.0, 11.7.



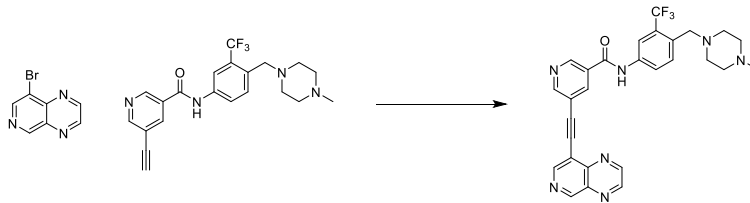
HSL415: 8-iodo-2,3-dimethylpyrido[3,4-b]pyrazin-7-amine

2,3-dimethylpyrido[3,4-b]pyrazin-7-amine (94.1 mg, 0.540 mmol, 1 equiv) were added to a reaction vial with methanol (10 mL). The reaction was then cooled to 0°C and NIS (133.8 mg, 0.594 mol, 1.1 equiv) was slowly added over 10 minutes. The reaction was then allowed to run at 0°C for 15 minutes. Crude mixed was concentrated down under reduced pressure. Pure product was obtained via column chromatography (1:1 EA/HEX). Yield = 90.2 % TLC Rf = 0.9 (10 % MeOH/CH₂Cl₂). ¹H NMR (500 MHz, DMSO-*d*₆) δ 8.71 (s, 1H), 2.64 (s, 3H), 2.58 (s, 3H).



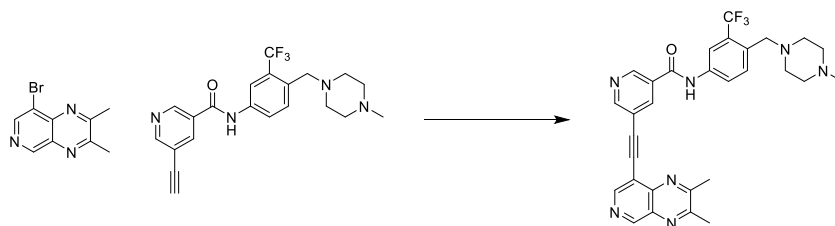
HSL501: 2,3-diethyl-8-iodopyrido[3,4-b]pyrazin-7-amine

2,3-diethylpyrido[3,4-b]pyrazin-7-amine (100 mg, 0.500 mmol, 1 equiv) were added to a reaction vial with methanol (5 mL). The reaction was then cooled to 0°C and NIS (112 mg, 0.500 mol, 1.1 equiv) was slowly added over 10 minutes. The reaction was then allowed to run at 0°C for 10 minutes. Crude mixed was concentrated down under reduced pressure. Pure product was obtained via column chromatography (1:1 EA/HEX). Yield = 64 % TLC Rf = 0.6 (1:1 EA/HEX). ¹H NMR (500 MHz, DMSO-*d*₆) δ 8.73 (s, 1H), 6.49 (s, 2H), 2.99 (q, *J* = 7.3 Hz, 2H), 2.93 (q, *J* = 7.4 Hz, 2H), 1.34 (t, *J* = 7.2 Hz, 3H), 1.28 (t, *J* = 7.4 Hz, 3H). ¹³C NMR (126 MHz, DMSO) δ 163.0, 159.1, 154.7, 151.8, 145.4, 131.1, 74.4, 27.9, 26.9, 11.9, 11.3.



HSL212: N-(4-((4-methylpiperazin-1-yl)methyl)-3-(trifluoromethyl)phenyl)-5-(pyrido[3,4-b]pyrazin-8-ylethynyl)nicotinamide

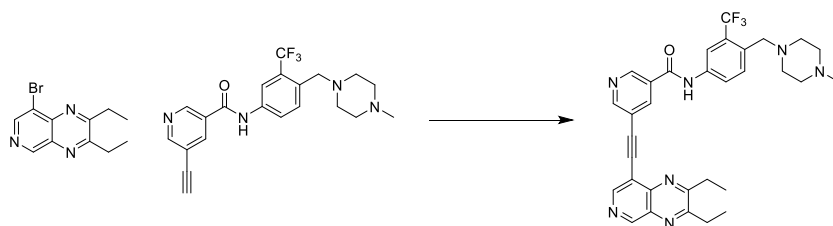
A solution of 8-bromopyrido[3,4-b]pyrazine (100 mg, 0.476 mmol, 1 equiv), Pd(PPh₃)₂ Cl₂ (10 mol%), CuI (5 mol%) and Triphenylphosphine (10 mg) in Triethylamine (1 mL) was de-oxygenated using argon gas for 10 minutes. A de-oxygenated solution of alkyne (101 mg, 0.252 mmol, 0.53 equiv) in DMF (4 mL) was added slowly over a period of 10 min to the TEA solution. The reaction temperature was increased to 55°C and allowed to stir for 7 hours. The crude compound was extracted using EtOAc (3 × 40 mL) and washed with brine (1 x 100 mL). Combined organic layers were dried over anhydrous sodium sulphate, filtered and concentrated under reduced pressure. The pure product obtained via flash column chromatography (10 % MeOH/CH₂Cl₂). Yield = 16.49 % TLC R_f = 0.2 (10 % MeOH + 1 % NH₄OH/CH₂Cl₂). ¹H NMR (500 MHz, DMSO-*d*₆) δ 10.80 (s, 1H), 9.55 (s, 1H), 9.30 (d, *J* = 1.7 Hz, 1H), 9.20 (d, *J* = 1.7 Hz, 1H), 9.16 (s, 1H), 9.14 (d, *J* = 2.0 Hz, 1H), 9.04 (s, 1H), 8.61 (t, *J* = 2.1 Hz, 1H), 8.19 (d, *J* = 2.0 Hz, 1H), 8.04 (dd, *J* = 8.5, 1.7 Hz, 1H), 7.72 (d, *J* = 8.5 Hz, 1H), 3.56 (s, 2H), 2.39 (s, 8H), 2.17 (s, 3H).



HSL211: 5-((2,3-dimethylpyrido[3,4-b]pyrazin-8-yl)ethynyl)-N-(4-((4-methylpiperazin-1-yl)methyl)-3-(trifluoromethyl)phenyl)nicotinamide

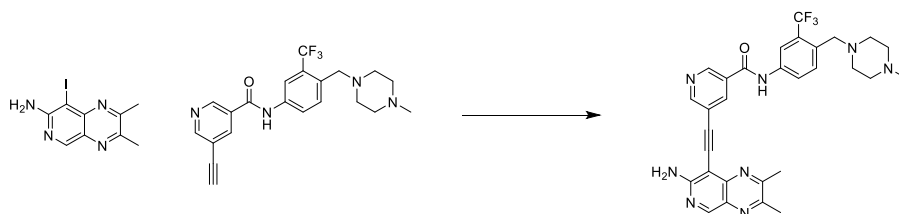
A solution of 8-bromo-2,3-dimethylpyrido[3,4-b]pyrazine (100 mg, 0.420 mmol, 1 equiv), Pd(PPh₃)₂ Cl₂ (10 mol%), CuI (5 mol%) and Triphenylphosphine (10 mg) in Triethylamine (1 mL) was de-oxygenated using argon gas for 10 minutes. A de-oxygenated solution of alkyne (115 mg,

0.286 mmol, 0.68 equiv) in DMF (4 mL) was added slowly over a period of 10 min to the TEA solution. The reaction temperature was increased to 55°C and allowed to stir for 7 hours. The crude compound was extracted using EtOAc (3 × 40 mL) and washed with brine (1 x 100 mL). Combined organic layers were dried over anhydrous sodium sulphate, filtered and concentrated under reduced pressure. The pure product obtained via flash column chromatography (10 % MeOH/CH₂Cl₂). Yield = 22.4 % TLC R_f = 0.2 (10 % MeOH + 1 % NH₄OH/CH₂Cl₂). ¹H NMR (500 MHz, DMSO-*d*₆) δ 10.80 (s, 1H), 9.37 (s, 1H), 9.13 (s, 1H), 9.02 (d, *J* = 7.8 Hz, 2H), 8.59 (t, *J* = 2.0 Hz, 1H), 8.20 (d, *J* = 1.9 Hz, 1H), 8.07 – 8.00 (m, 1H), 7.72 (d, *J* = 8.5 Hz, 1H), 3.56 (s, 2H), 2.80 (s, 3H), 2.75 (s, 3H), 2.38 (s, 8H), 2.16 (s, 3H). ¹³C NMR (126 MHz, DMSO) δ 163.8, 161.1, 158.1, 154.6, 153.6, 150.2, 149.1, 143.5, 138.3, 138.0, 135.8, 133.0, 131.8, 130.4, 124.0, 119.3, 117.7, 116.1, 93.2, 88.3, 57.9, 55.1, 53.1, 46.1, 40.5, 24.2, 23.5.



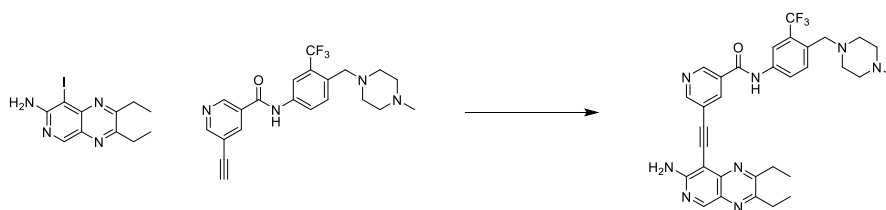
HSL517:5-((2,3-diethylpyrido[3,4-b]pyrazin-8-yl)ethynyl)-N-(4-((4-methylpiperazin-1-yl)methyl)-3-(trifluoromethyl)phenyl)nicotinamide

A solution of 8-bromo-2,3-diethylpyrido[3,4-b]pyrazine (104 mg, 0.393 mmol, 1 equiv), Pd(PPh₃)₂ Cl₂ (10 mol%), CuI (5 mol%) and Triphenylphosphine (10 mg) in Triethylamine (1.5 mL) was de-oxygenated using argon gas for 10 minutes. A de-oxygenated solution of alkyne (190 mg, 0.476 mmol, 1.2 equiv) in DMF (4 mL) was added slowly over a period of 10 min to the TEA solution. The reaction temperature was increased to 55°C and allowed to stir overnight. The crude compound was concentrated under reduced pressure. The pure product obtained via flash column chromatography (10 % MeOH/CH₂Cl₂). Yield = 52 % TLC R_f = 0.3 (10 % MeOH /CH₂Cl₂). ¹H NMR (500 MHz, DMSO-*d*₆) δ 10.80 (s, 1H), 9.38 (s, 1H), 9.13 (d, *J* = 2.2 Hz, 1H), 9.00 (d, *J* = 2.0 Hz, 2H), 8.55 (t, *J* = 2.1 Hz, 1H), 8.20 (d, *J* = 2.2 Hz, 1H), 8.04 (dd, *J* = 8.5, 2.2 Hz, 1H), 7.72 (d, *J* = 8.5 Hz, 1H), 3.59 (s, 2H), 3.15 (q, *J* = 7.3 Hz, 2H), 3.10 (q, *J* = 7.3 Hz, 2H), 2.62 (s, 8H), 2.37 (s, 3H), 1.42 (t, *J* = 7.2 Hz, 3H), 1.36 (t, *J* = 7.3 Hz, 3H).



HSL476:5-((7-amino-2,3-dimethylpyrido[3,4-b]pyrazin-8-yl)ethynyl)-N-(4-((4-methylpiperazin-1-yl)methyl)-3-(trifluoromethyl)phenyl)nicotinamide

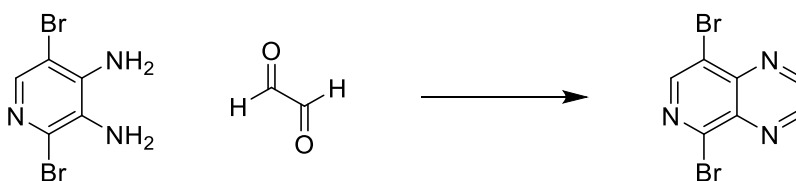
A solution of 8-iodo-2,3-dimethylpyrido[3,4-b]pyrazin-7-amine (78.1 mg, 0.261 mmol, 1 equiv), Pd(PPh₃)₂Cl₂ (10 mol%), CuI (5 mol%) and Triphenylphosphine (10 mg) in Triethylamine (1.5 mL) was de-oxygenated using argon gas for 10 minutes. A de-oxygenated solution of alkyne (126 mg, 0.313 mmol, 1.2 equiv) in DMF (4 mL) was added slowly over a period of 10 min to the TEA solution. The reaction temperature was increased to 55°C and allowed to stir overnight. The crude compound concentrated under reduced pressure. The pure product obtained via flash column chromatography (10 % MeOH/CH₂Cl₂). Yield = 40.7 % TLC R_f = 0.12 (10 % MeOH/CH₂Cl₂). ¹H NMR (500 MHz, DMSO-*d*₆) δ 10.84 (s, 1H), 9.06 (s, 2H), 8.86 (s, 1H), 8.62 (s, 1H), 8.22 (s, 1H), 8.05 (d, *J* = 8.6 Hz, 1H), 7.72 (d, *J* = 8.5 Hz, 1H), 7.04 (s, 2H), 3.57 (s, 2H), 2.67 (s, 3H), 2.58 (s, 3H), 2.42 (s, 8H), 2.21 (s, 3H). ¹³C NMR (126 MHz, DMSO) δ 164.2, 160.4, 159.9, 154.5, 153.3, 151.1, 147.9, 146.0, 138.4, 137.7, 132.8, 131.8, 130.3, 128.1, 125.8, 124.0, 120.6, 117.8, 117.7, 95.3, 90.4, 88.5, 57.8, 54.9, 52.7, 45.7, 40.5, 24.0, 22.7.



HSL507: 5-((7-amino-2,3-diethylpyrido[3,4-b]pyrazin-8-yl)ethynyl)-N-(4-((4-methylpiperazin-1-yl)methyl)-3-(trifluoromethyl)phenyl)nicotinamide

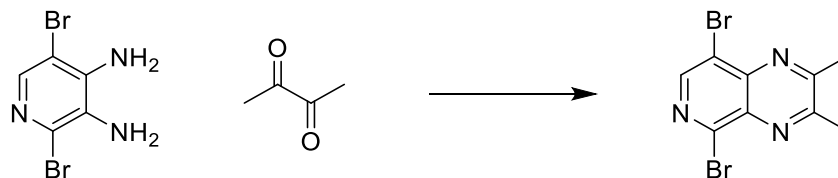
A solution of 8-iodo-2,3-diethylpyrido[3,4-b]pyrazin-7-amine (80 mg, 0.243 mmol, 1 equiv), Pd(PPh₃)₂ Cl₂ (10 mol%), CuI (5 mol%) and Triphenylphosphine (10 mg) in Triethylamine (1.5 mL) was de-oxygenated using argon gas for 10 minutes. A de-oxygenated solution of alkyne (117

mg, 0.292 mmol, 1.2 equiv) in DMF (4 mL) was added slowly over a period of 10 min to the TEA solution. The reaction temperature was increased to 55°C and allowed to stir overnight. The crude compound concentrated under reduced pressure. The pure product obtained via flash column chromatography (10 % MeOH/CH₂Cl₂). Yield = 63.1 % TLC R_f = 0.13 (10 % MeOH/CH₂Cl₂). ¹H NMR (500 MHz, DMSO-*d*₆) δ 10.84 (s, 1H), 9.05 (d, *J* = 2.2 Hz, 1H), 9.00 (d, *J* = 2.0 Hz, 1H), 8.88 (s, 1H), 8.58 (t, *J* = 2.1 Hz, 1H), 8.20 (d, *J* = 2.2 Hz, 1H), 8.04 (dd, *J* = 8.6, 2.2 Hz, 1H), 7.72 (d, *J* = 8.5 Hz, 1H), 7.04 (s, 2H), 3.58 (s, 2H), 3.02 (q, *J* = 7.3 Hz, 2H), 2.94 (q, *J* = 7.4 Hz, 2H), 2.54 (s, 8H), 2.31 (s, 3H), 1.38 (t, *J* = 7.3 Hz, 3H), 1.29 (t, *J* = 7.4 Hz, 3H). ¹³C NMR (126 MHz, DMSO) δ 164.3, 162.6, 160.3, 154.4, 154.2, 153.4, 147.7, 145.8, 138.4, 137.7, 132.7, 131.9, 130.4, 130.1, 127.9, 125.8, 124.0, 120.8, 117.7, 95.4, 90.6, 88.6, 57.7, 54.6, 52.2, 45.2, 28.2, 27.2, 11.9, 11.3.



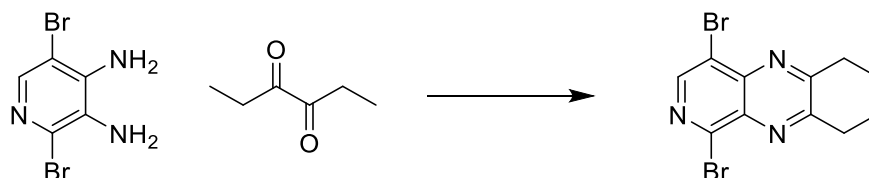
HSL521: 5,8-dibromopyrido[3,4-*b*]pyrazine

To a reaction vial, 2,5-dibromopyridine-3,4-diamine (300 mg, 0.123 mmol, 1 equiv.) and ethanol (10 mL) were added. Oxalaldehyde (130 mg, 2.25 mmol, 2 equiv.) was then added. The reaction was then allowed to stir at room temperature for 4 hours. After 4 hours 2 more equivalents of oxalaldehyde was added. The reaction was then allowed to stir for 3 days. Upon reaction completion, crude mixture was concentrated under reduced pressure. Pure compound was obtained via column chromatography (1:1 EA/Hex). Yield = 31 % TLC R_f = 0.2 (100 % Hexanes). ¹H NMR (500 MHz, DMSO-*d*₆) δ 9.32 (d, *J* = 1.8 Hz, 1H), 9.23 (d, *J* = 1.8 Hz, 1H), 8.93 (s, 1H). ¹³C NMR (126 MHz, DMSO) δ 152.1, 149.7, 147.7, 146.7, 144.5, 137.8, 120.8.



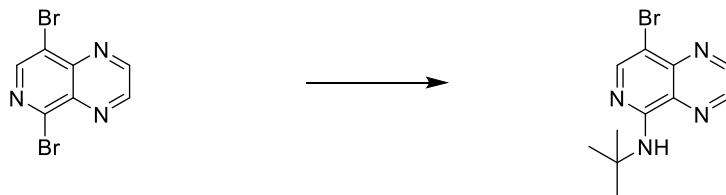
HSL522: 5,8-dibromo-2,3-dimethylpyrido[3,4-b]pyrazine

To a reaction vial, 2,5-dibromopyridine-3,4-diamine (300 mg, 0.123 mmol, 1 equiv.) and ethanol (10 mL) were added. Biacetyl (130 mg, 2.25 mmol, 2 equiv.) was then added. The reaction was then allowed to stir at room temperature for 4 hours. After 4 hours 2 more equivalents of biacetyl was added. The reaction was then allowed to stir for 3 days. Upon reaction completion, crude mixture was concentrated under reduced pressure. Pure compound was obtained via column chromatography (1:1 EA/Hex). Yield = 82 % TLC Rf = 0.7 (1:1 EA/Hex) ^1H NMR (500 MHz, DMSO- d_6) δ 8.78 (s, 1H), 2.79 (s, 3H), 2.77 (s, 3H). ^{13}C NMR (126 MHz, DMSO) δ 162.0, 159.3, 146.8, 145.1, 142.7, 135.9, 119.9, 23.7, 23.5.



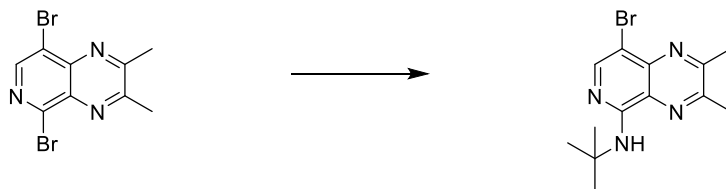
HSL523: 5,8-dibromo-2,3-diethylpyrido[3,4-b]pyrazine

To a reaction vial, 2,5-dibromopyridine-3,4-diamine (300 mg, 0.123 mmol, 1 equiv.) and ethanol (10 mL) were added. Hexane-3,4-dione (256 mg, 2.25 mmol, 2 equiv.) was then added. The reaction was then allowed to stir at room temperature for 4 hours. After 4 hours, 2 more equivalents of hexane-3,4-dione was added. The reaction was then allowed to stir for 3 days. Upon reaction completion, crude mixture was concentrated under reduced pressure. Pure compound was obtained via column chromatography (1:1 EA/Hex). Yield = 82 % TLC Rf = 0.85 (1:1 EA/Hex) ^1H NMR (500 MHz, DMSO- d_6) δ 8.79 (s, 1H), 3.13 (p, J = 7.4 Hz, 4H), 1.37 (td, J = 7.2, 2.7 Hz, 6H). ^{13}C NMR (126 MHz, DMSO) δ 164.7, 162.1, 146.8, 145.4, 142.4, 135.7, 120.3, 28.0, 27.7, 11.1, 11.0.



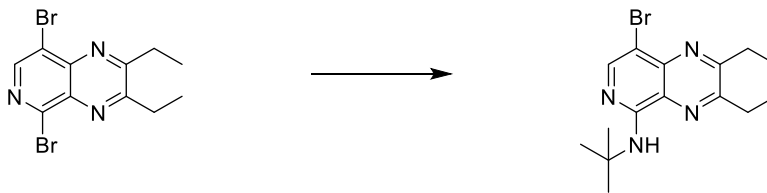
HSL524: 8-bromo-N-(tert-butyl)pyrido[3,4-b]pyrazin-5-amine

To a pressure tube fitted with a magnetic stir bar, 5,8-dibromopyrido[3,4-b]pyrazine (83 mg, 0.290 mmol, 1 eq) in ethanol (2 mL) were added. Tert-butylamine (63.5 mg, 0.870 mmol, 3 eq) was then added and reaction was capped and moved to 110 °C. The reaction was then allowed to run for 16 hours. Following 16 hours, 3 additional equivalents of tert-butylamine was then added. The reaction then 3 days. Crude product was then cooled to room temperature and concentrated under reduced pressure. Pure product was obtained via column chromatography (1:1 Hex/DCM). Yield = 57 % TLC Rf = 0.3 (1:1 Hex/DCM) ¹H NMR (500 MHz, DMSO-*d*₆) δ 9.12 (d, *J* = 2.0 Hz, 1H), 8.84 (d, *J* = 1.9 Hz, 1H), 8.35 (s, 1H), 7.08 (s, 1H), 1.50 (s, 9H). ¹³C NMR (126 MHz, DMSO) δ 155.7, 150.4, 147.6, 144.3, 143.8, 130.1, 103.7, 52.0, 28.7.



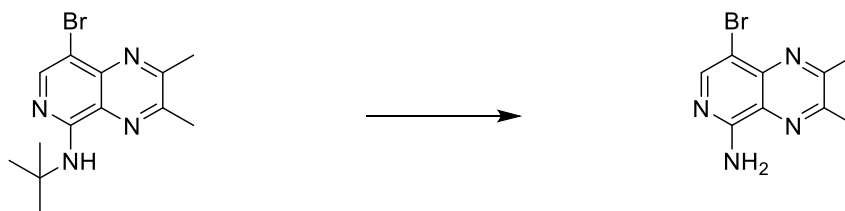
HSL525: 8-bromo-N-(tert-butyl)-2,3-dimethylpyrido[3,4-b]pyrazin-5-amine

To a pressure tube fitted with a magnetic stir bar, 5,8-dibromo-2,3-dimethylpyrido[3,4-b]pyrazine (147 mg, 0.468 mmol, 1 eq) in ethanol (3 mL) was added. Tert-butylamine (106 mg, 1.4 mmol, 3 eq) were then added and reaction was capped and moved to 110 °C. The reaction was then allowed to run for 16 hours. Following 16 hours, 3 additional equivalents of tert-butylamine was then added. The reaction then run for 3 days. Crude product was then cooled to room temperature and concentrated under reduced pressure. Pure product was obtained via column chromatography (1:1 Hex/DCM). Yield = 16.6 % TLC Rf = 0.5 (25% EA/Hex) ¹H NMR (500 MHz, DMSO-*d*₆) δ 8.23 (s, 1H), 6.83 (s, 1H), 2.68 (s, 3H), 2.66 (s, 3H), 1.50 (s, 9H). ¹³C NMR (126 MHz, DMSO) δ 159.4, 155.1, 153.3, 146.2, 141.6, 127.5, 103.6, 51.7, 28.8, 23.4, 22.8.



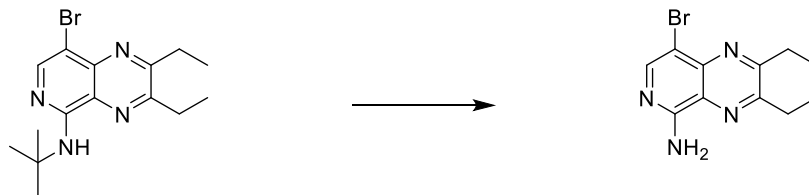
HSL526: 8-bromo-N-(tert-butyl)-2,3-diethylpyrido[3,4-b]pyrazin-5-amine

To a pressure tube fitted with a magnetic stir bar, 5,8-dibromo-2,3-diethylpyrido[3,4-b]pyrazine (153 mg, 0.443 mmol, 1 eq) in ethanol (3 mL) were added. Tert-butylamine (97.1 mg, 1.433 mmol, 3 eq) was then added and reaction was capped and moved to 110 °C. The reaction was then allowed to run for 16 hours. Following 16 hours, 3 additional equivalents of tert-butylamine was then added. The reaction then run for 3 days. Crude product was then cooled to room temperature and concentrated under reduced pressure. Pure product was obtained via column chromatography (1:1 Hex/DCM). Yield = 14 % TLC Rf = 0.7 (25% EA/Hex) ¹H NMR (500 MHz, DMSO-*d*₆) δ 8.25 (s, 1H), 6.82 (s, 1H), 3.02 (dq, *J* = 12.9, 7.3 Hz, 4H), 1.51 (s, 9H), 1.34 – 1.30 (m, 6H).



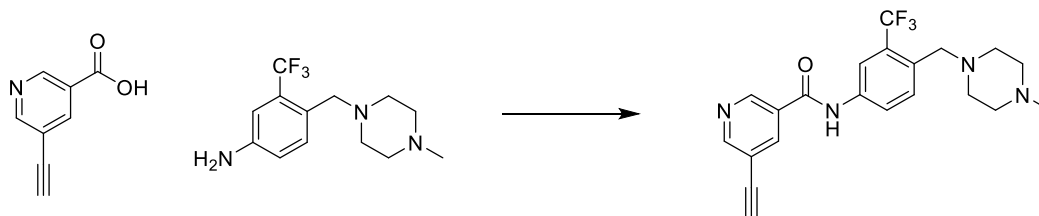
HSL544: 8-bromo-2,3-dimethylpyrido[3,4-b]pyrazin-5-amine

To a pressure tube fitted with a magnetic stir bar, 8-bromo-N-(tert-butyl)-2,3-dimethylpyrido[3,4-b]pyrazin-5-amine (88 mg, 0.285 mmol) in concentrated HCl (1.0 mL) were added. The reaction was capped and moved to 80°C and run for 2 hours. The reaction was then diluted with water (50 mL) and neutralized using saturated sodium bicarbonate solution. Product was then extracted with ethyl acetate (3x 100 mL). Organic layers were dried over anhydrous sodium sulfate, filtered, and concentrated under reduced pressure. Pure product was obtained via column chromatography (1:1 EA/Hex). Yield = 62.6%; TLC Rf = 0.5 (1:1 EA/Hex). ¹H NMR (500 MHz, DMSO-*d*₆) δ 8.14 (s, 1H), 7.16 (s, 2H), 2.68 (s, 3H), 2.67 (s, 3H). ¹³C NMR (126 MHz, DMSO) δ 164.6, 163.1, 158.4, 151.4, 147.1, 132.0, 108.4, 28.5, 27.8.



HSL545: 8-bromo-2,3-diethylpyrido[3,4-b]pyrazin-5-amine

To a pressure tube fitted with a magnetic stir bar, 8-bromo-2,3-diethylpyrido[3,4-b]pyrazin-5-amine (163 mg, 0.445 mmol) in concentrated HCl (1.5 mL) were added. The reaction was capped and moved to 80°C and run for 2 hours. The reaction was then diluted with water (50 mL) and neutralized using saturated sodium bicarbonate solution. Product was then extracted with ethyl acetate (3x 100 mL). Organic layers were dried over anhydrous sodium sulfate, filtered, and concentrated under reduced pressure. Pure product was obtained via column chromatography (1:1 EA/Hex). Yield = 68.2%; TLC Rf = 0.45 (1:1 EA/Hex). ¹H NMR (500 MHz, DMSO-*d*₆) δ 8.16 (s, 1H), 7.14 (s, 2H), 3.01 (dq, *J* = 16.0, 7.3 Hz, 4H), 1.33 (q, *J* = 7.3 Hz, 6H). ¹³C NMR (126 MHz, DMSO) δ 162.5, 158.2, 156.6, 146.7, 141.7, 126.7, 103.8, 27.9, 27.2, 11.8, 11.7.

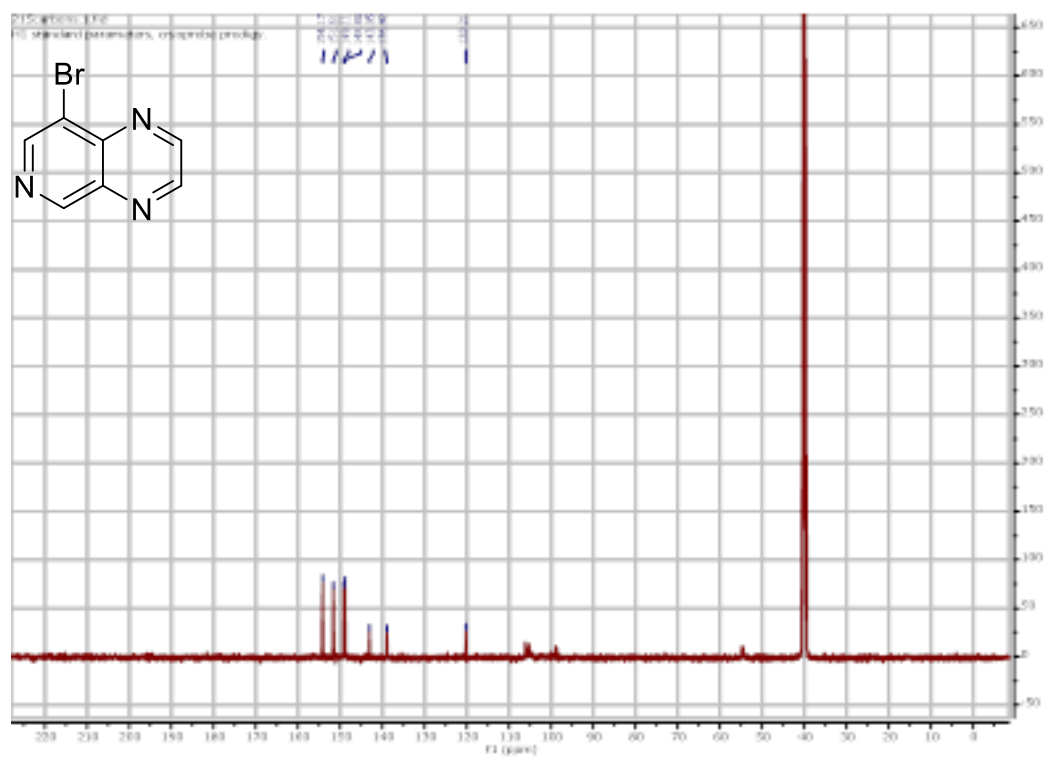
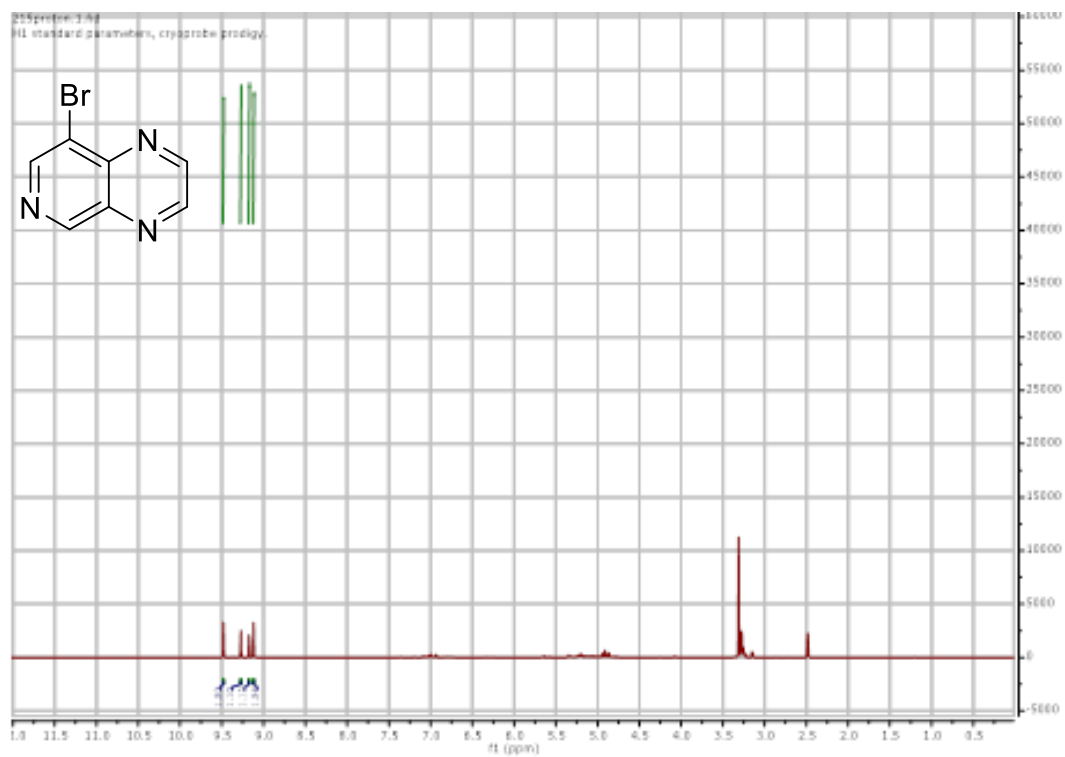


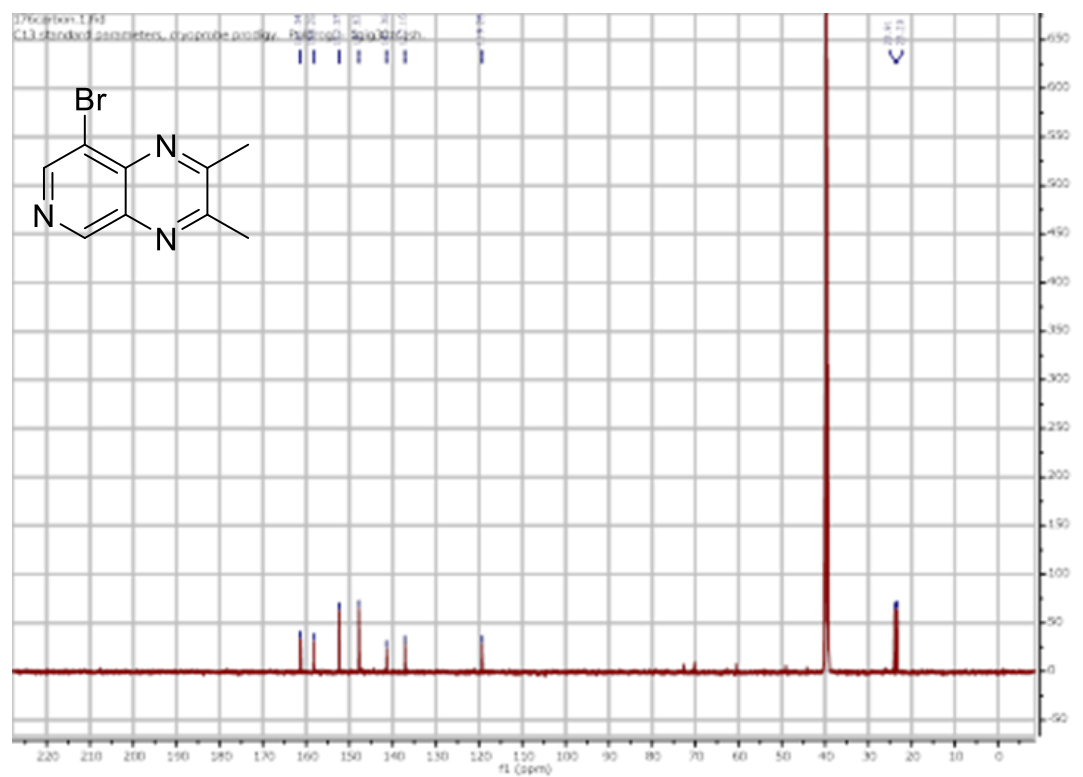
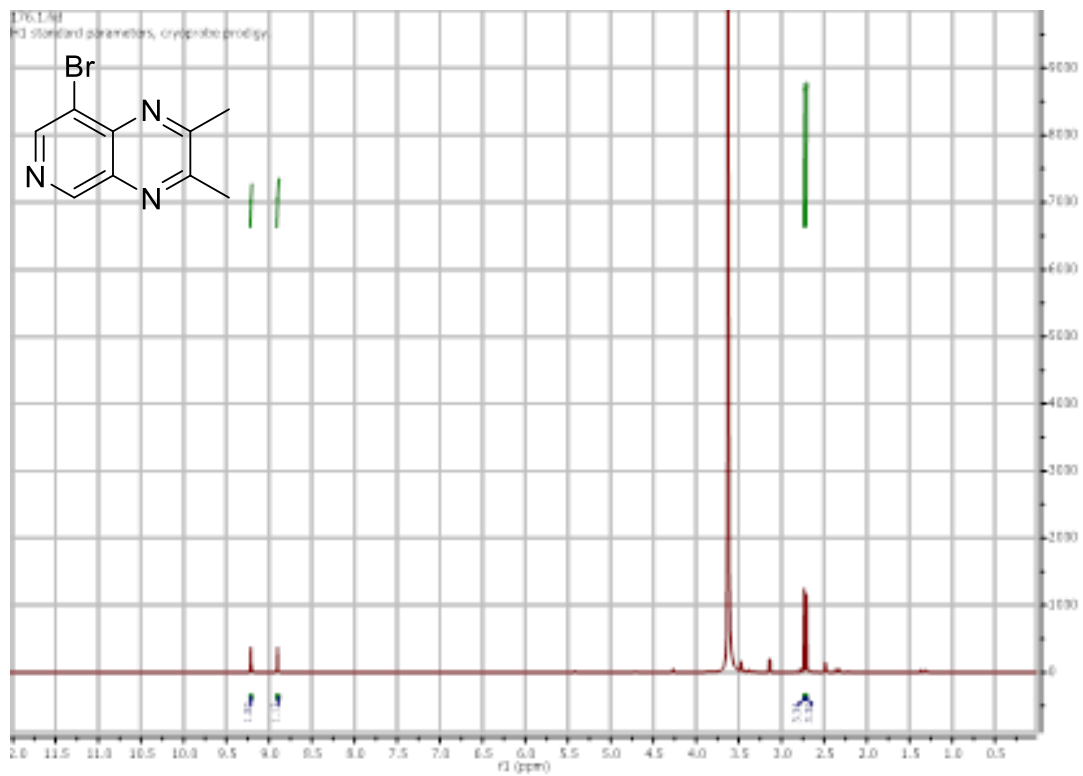
5-ethynyl-N-(4-((4-methylpiperazin-1-yl)methyl)-3-(trifluoromethyl)phenyl)nicotinamide

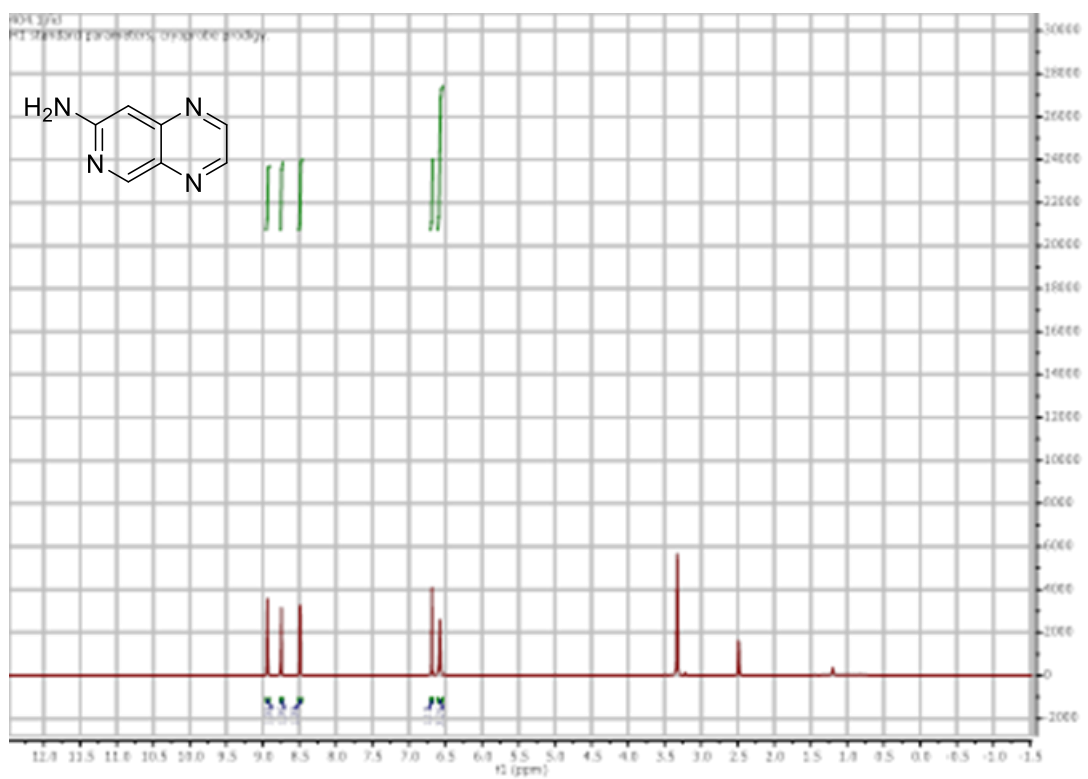
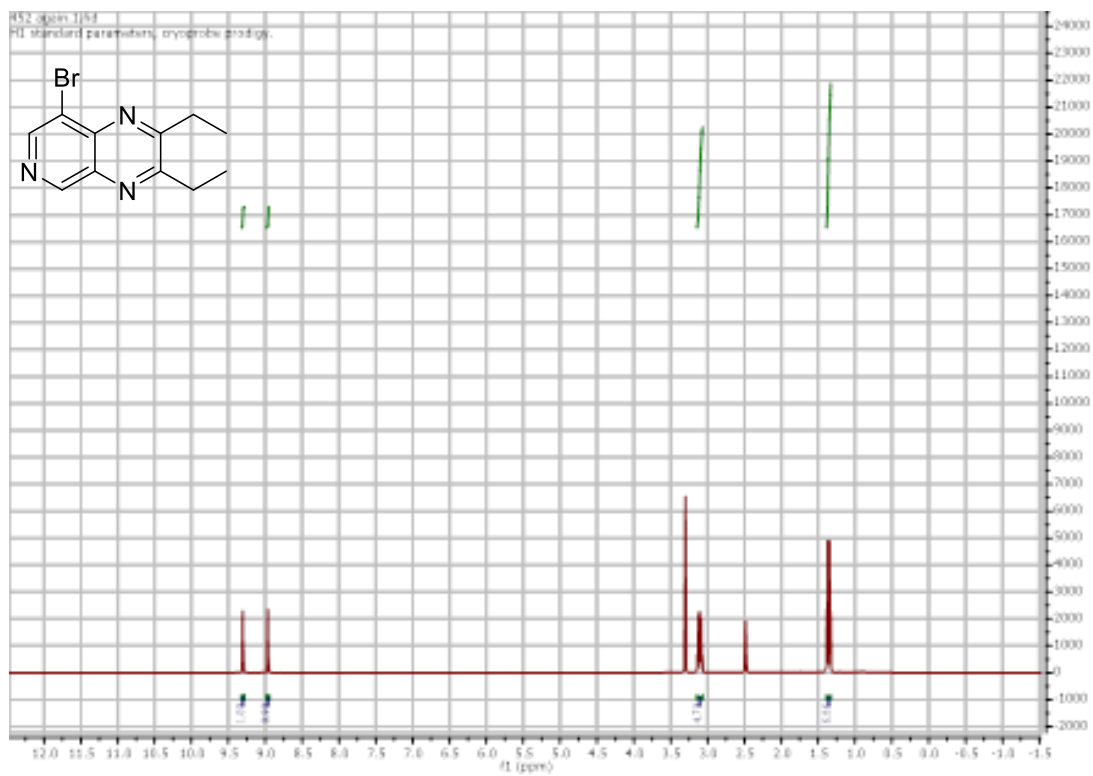
5-Ethynynicotinic acid (1 g, 6.8 mmol, 1 equiv) and HATU (1.8 g, 8.2 mmol, 1.2 equiv) were added to a round bottom. Air was vacuumed out and vessel was then protected with a balloon of argon gas. DMF (8 mL) was then added and the reaction was cooled to 0°C. DIPEA (2.6 g, 2.4 mmol, 3 equiv) was then added. Upon addition of 4-((4-methylpiperazin-1-yl)methyl)-3-(trifluoromethyl)aniline (1.8 g, 6.8 mmol, 1 equiv), the reaction was then moved to 55°C and allowed to run over night. Reaction was then concentrated under reduced pressure and purified via column chromatography (10 % MeOH/DCM). Yield: 94.5 %

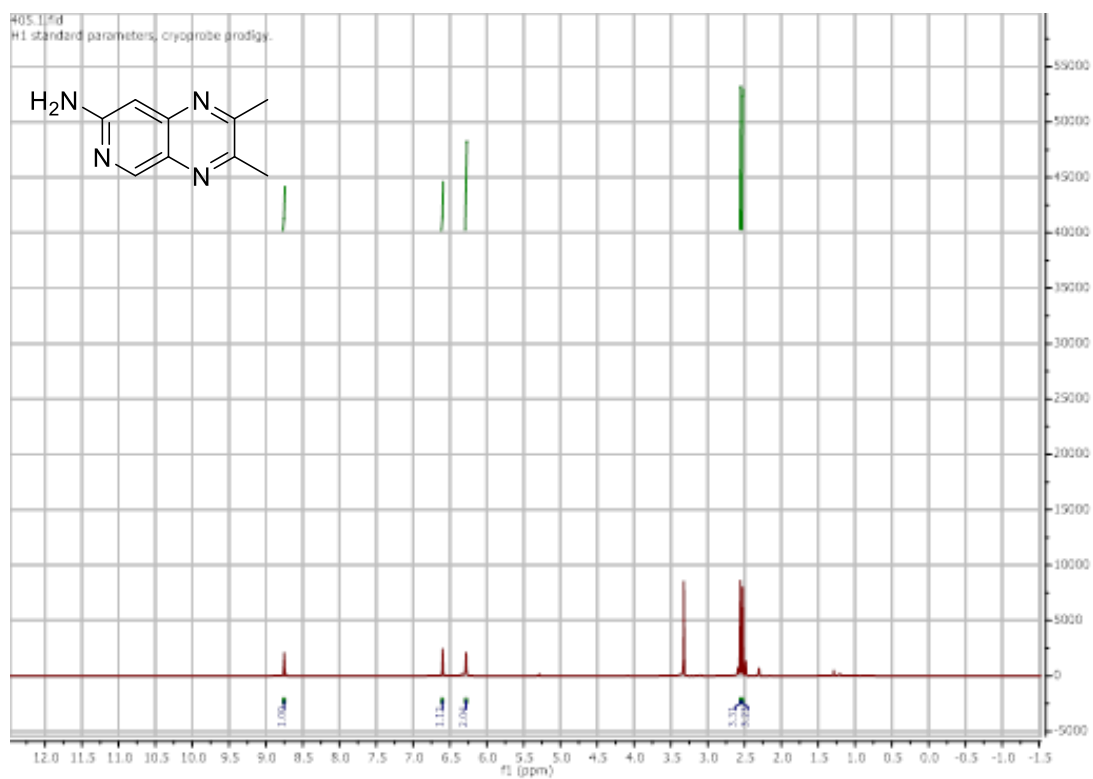
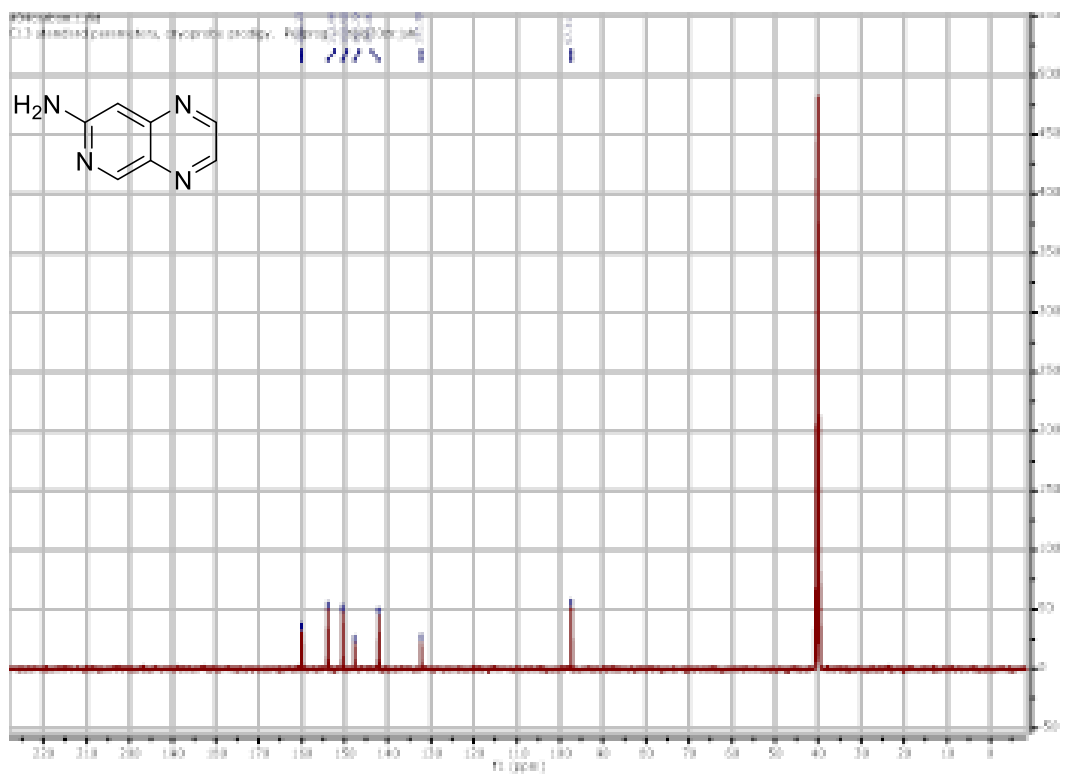
^1H NMR (500 MHz, $\text{DMSO-}d_6$) δ 10.70 (s, 1H), 9.07 (d, $J = 2.1$ Hz, 1H), 8.86 (d, $J = 2.0$ Hz, 1H), 8.41 (t, $J = 2.1$ Hz, 1H), 8.17 (d, $J = 2.3$ Hz, 1H), 8.00 (dd, $J = 8.5, 2.2$ Hz, 1H), 7.71 (d, $J = 8.5$ Hz, 1H), 4.58 (s, 1H), 3.56 (s, 2H), 2.41 (s, 8H), 2.22 (s, 3H). ^{13}C NMR (126 MHz, DMSO) δ 163.8, 154.8, 148.9, 138.4, 138.3, 132.9, 131.8, 130.2, 128.1, 127.8, 125.8, 124.0, 123.6, 118.9, 117.7, 85.6, 80.2, 57.8, 54.9, 52.7, 45.7.

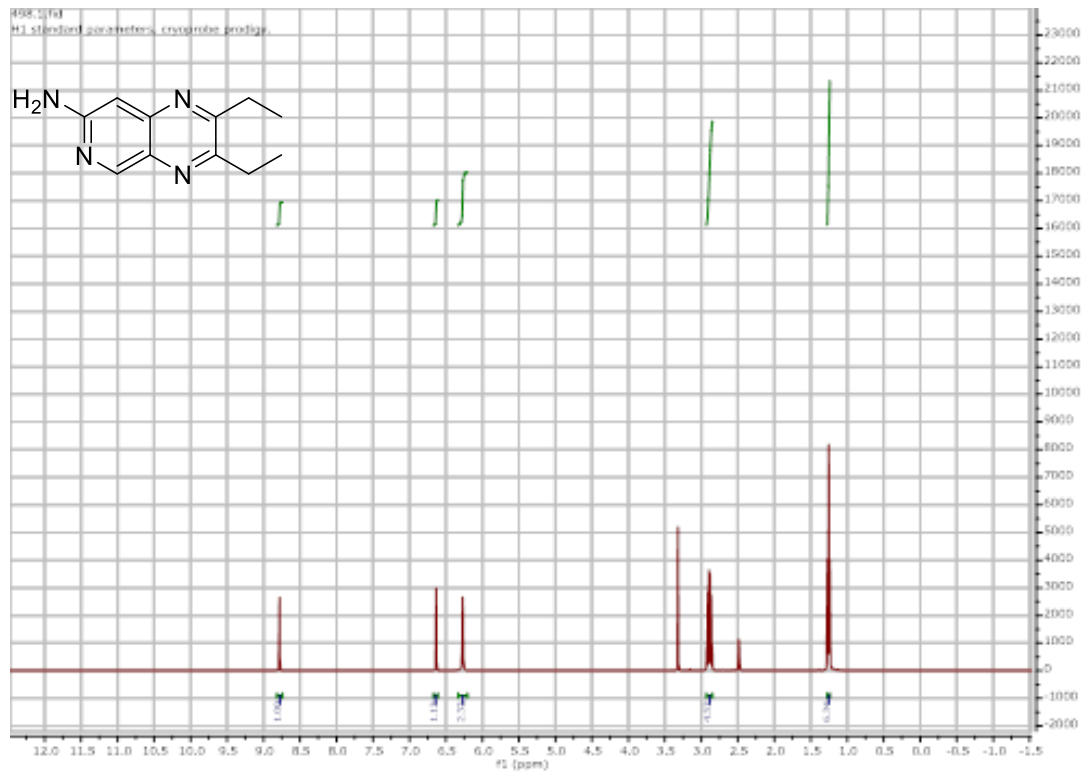
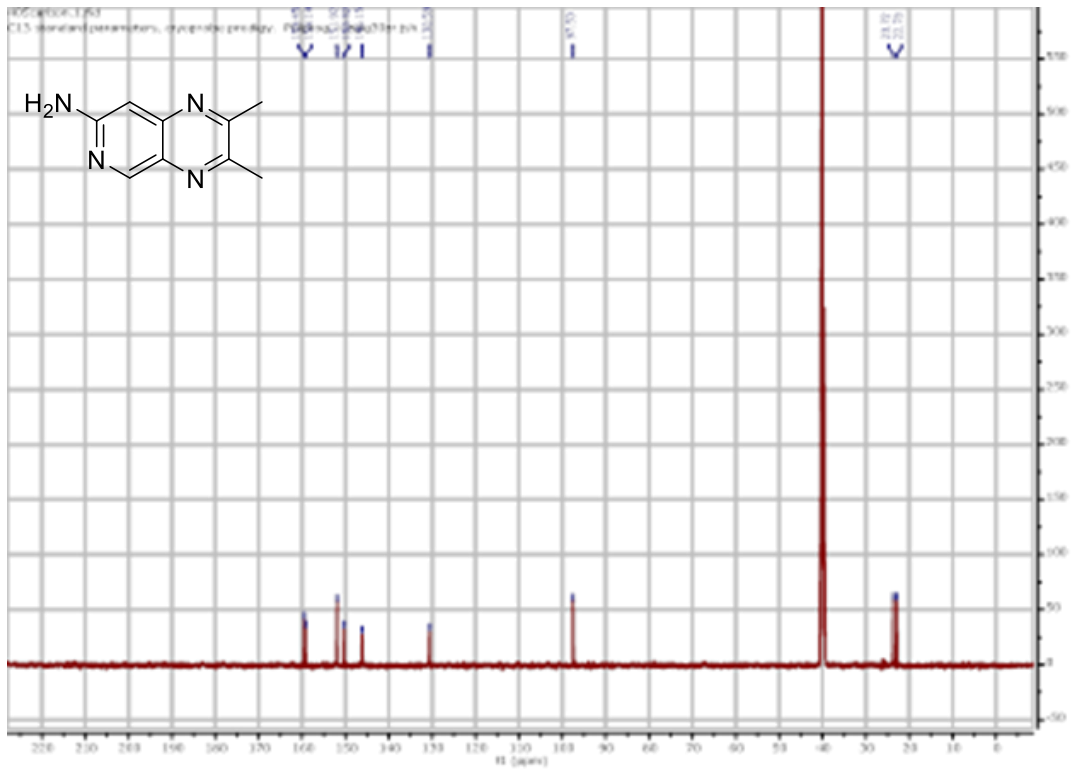
NMR Spectra

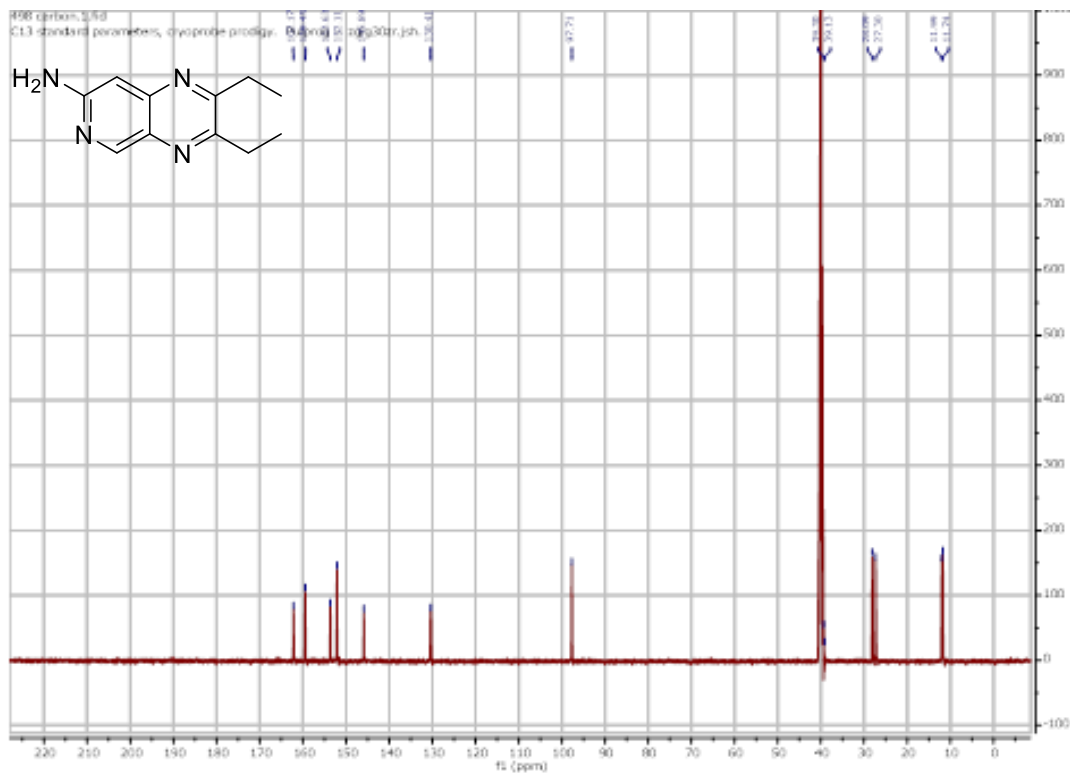


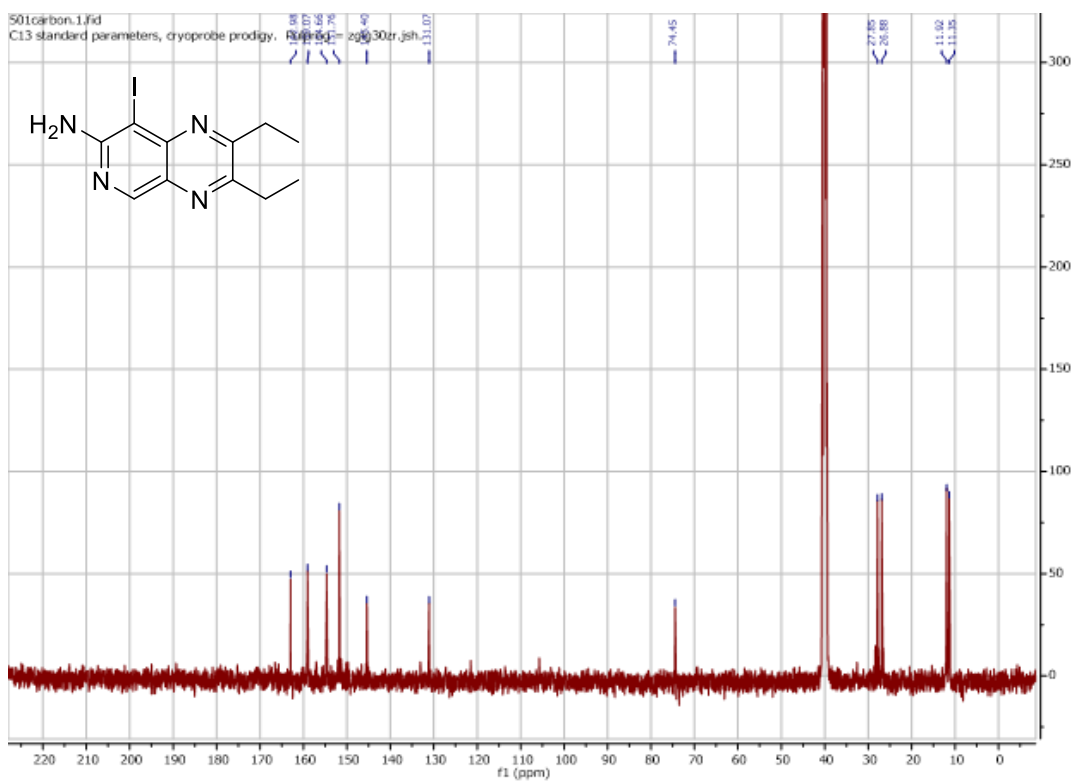
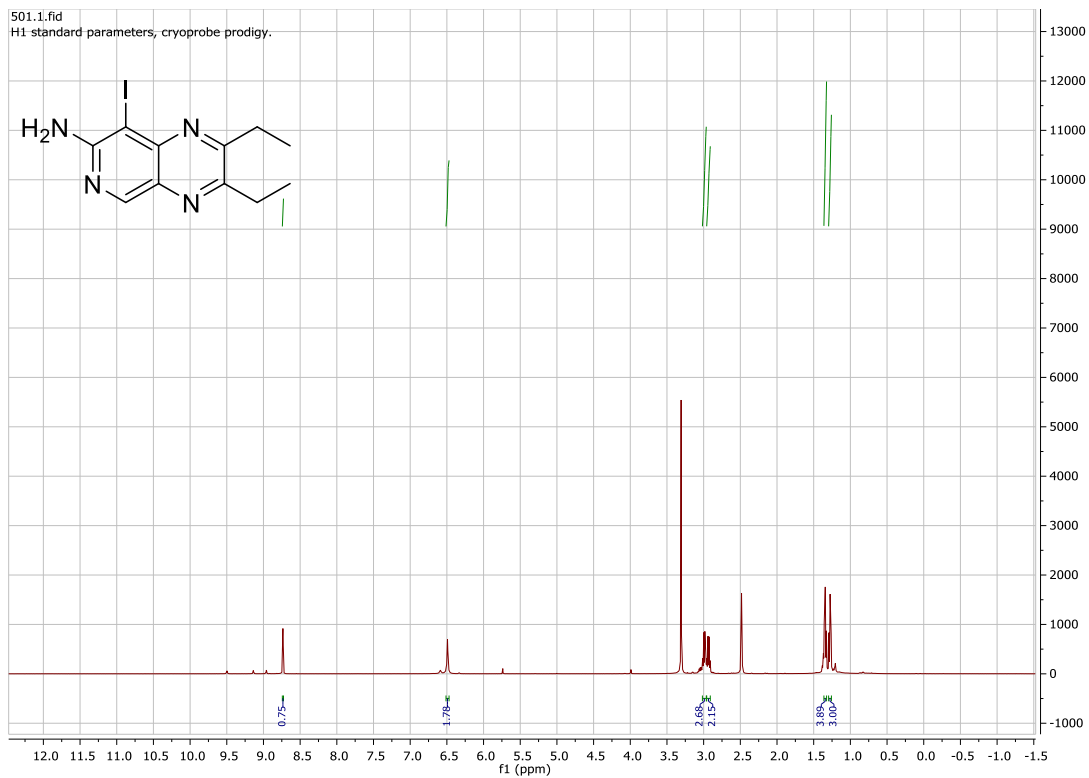


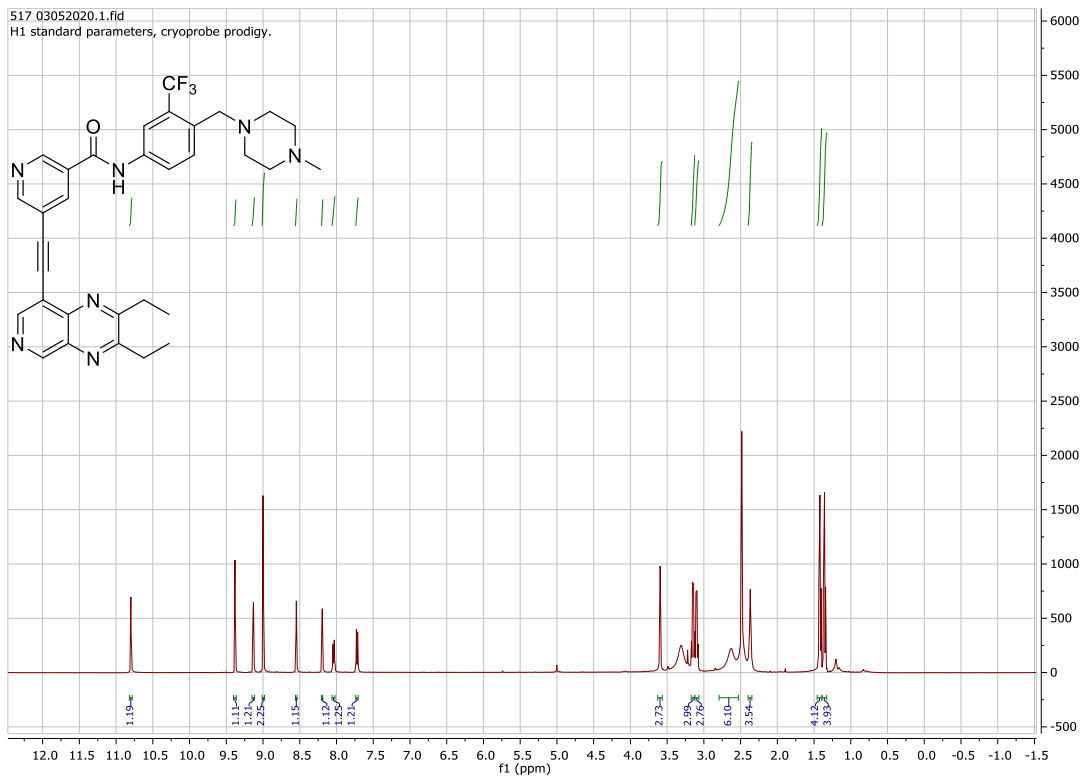
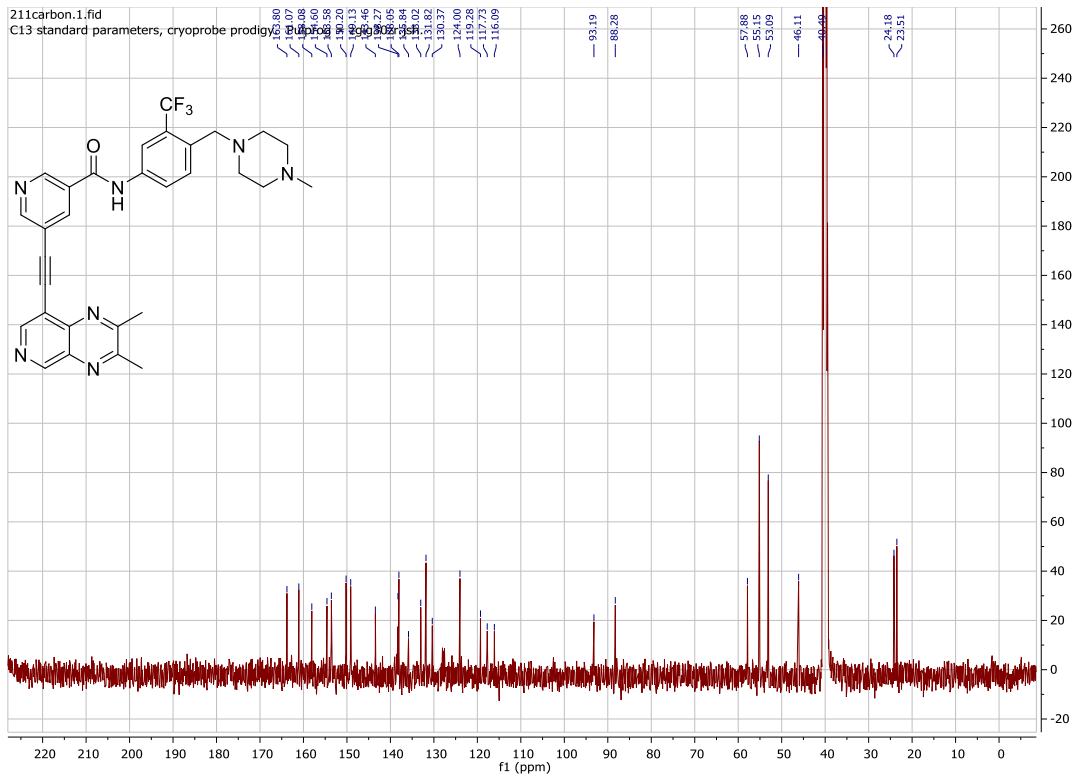


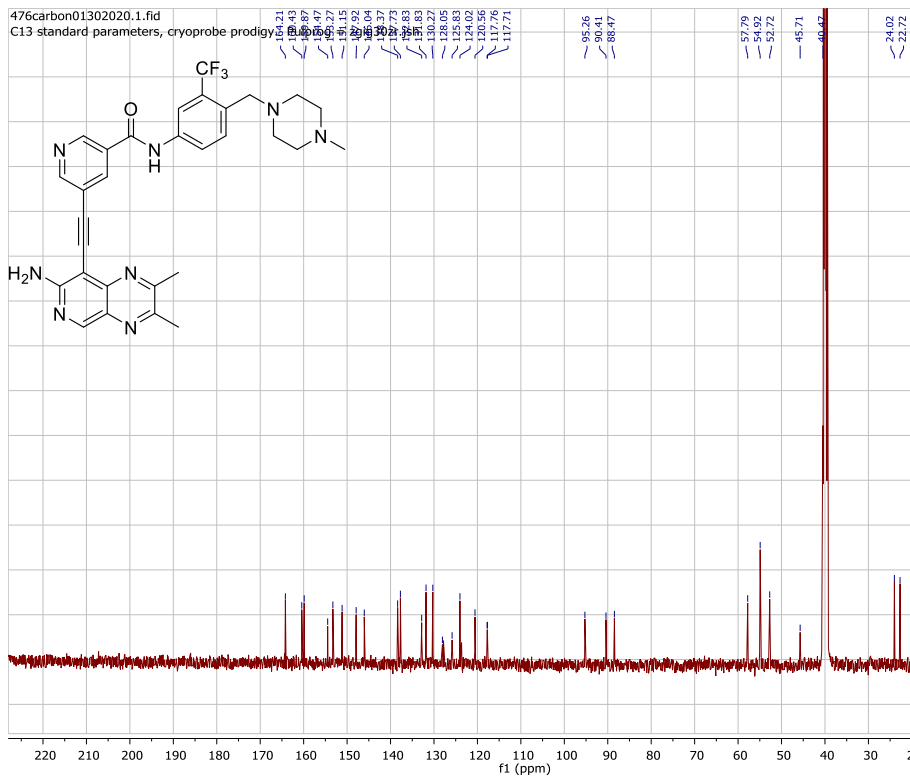
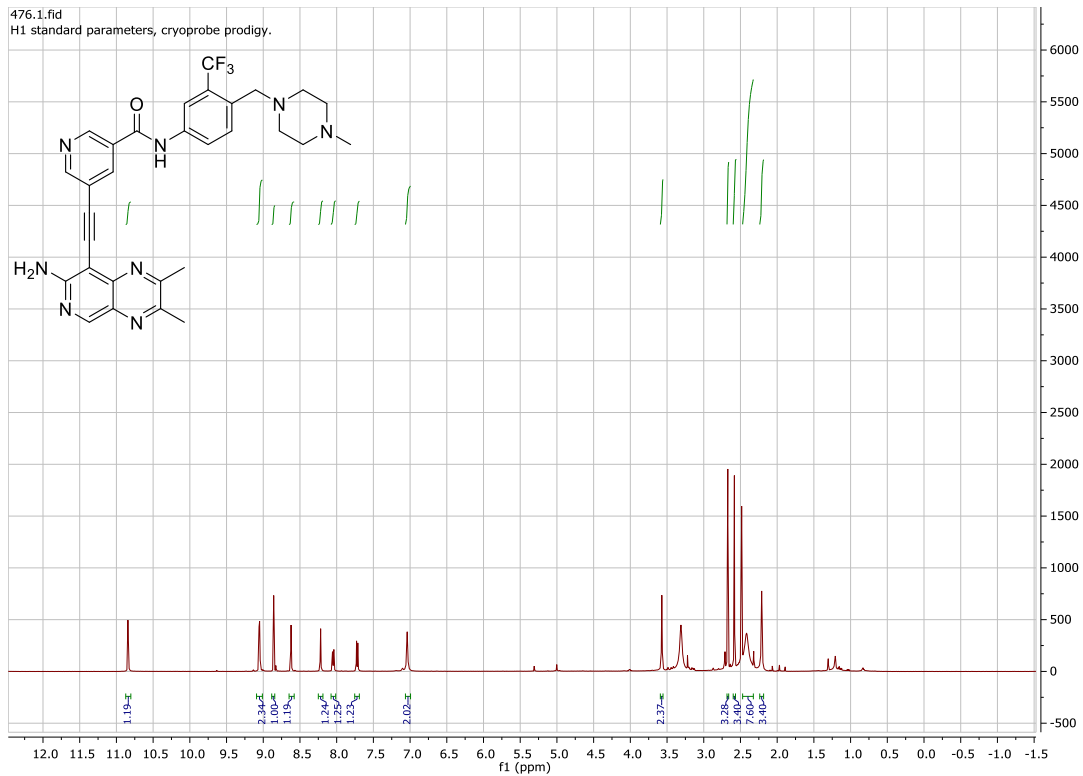


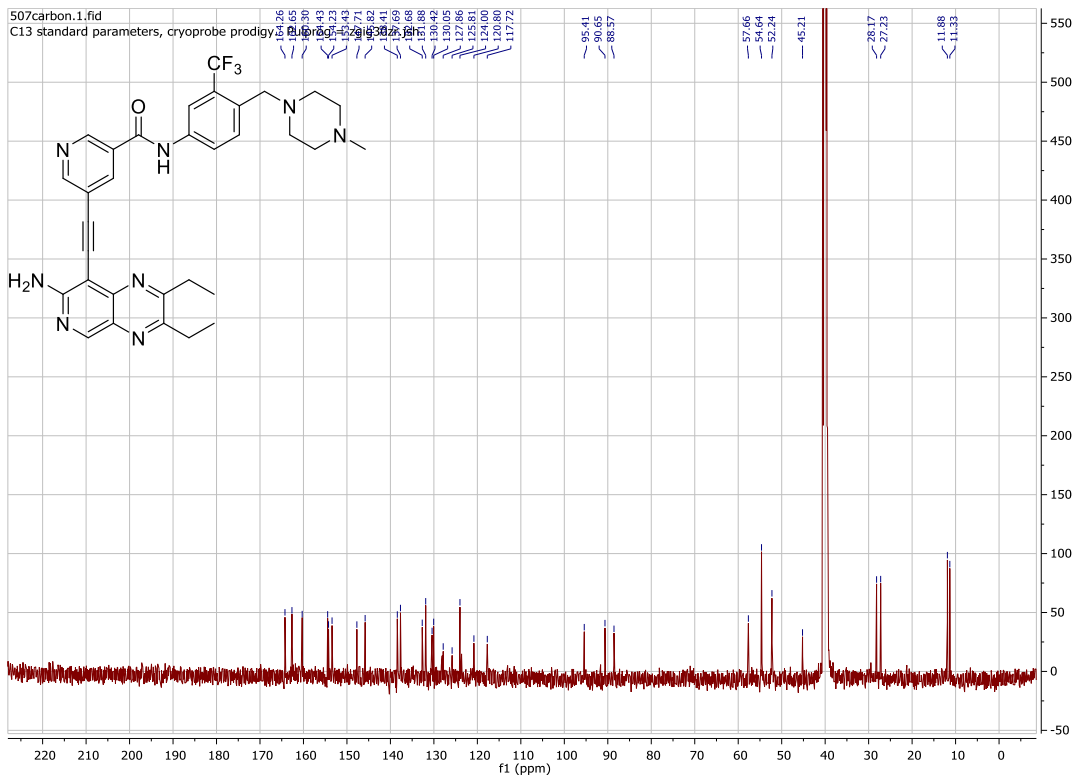
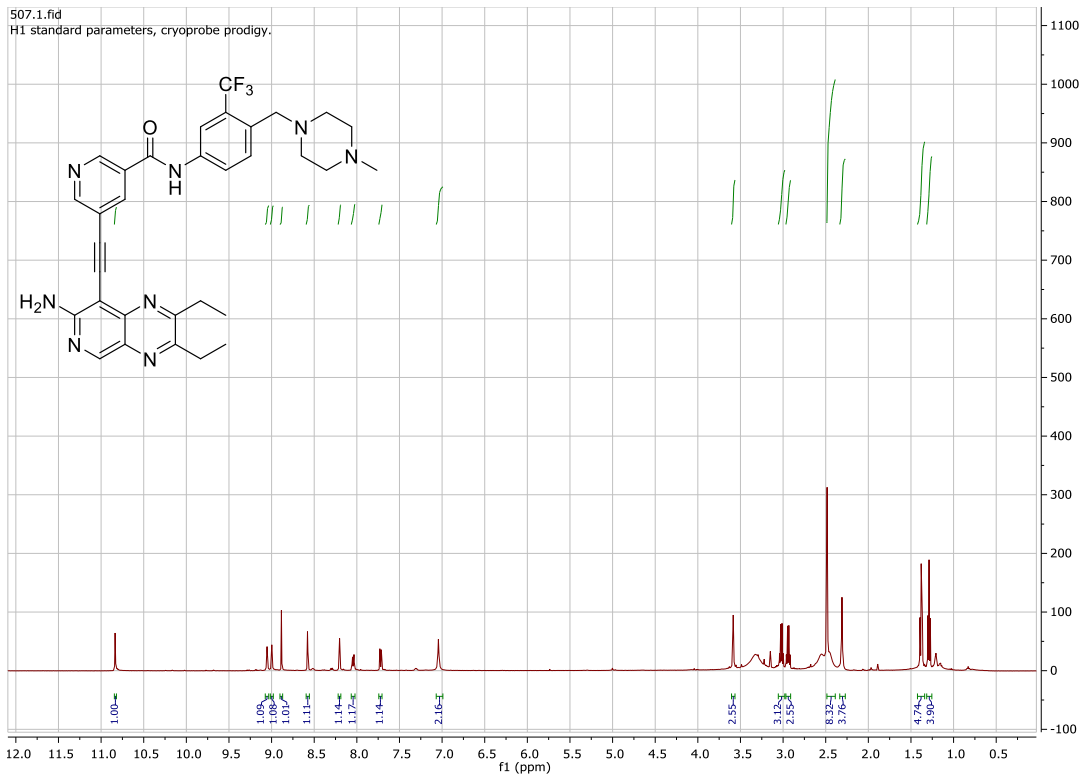


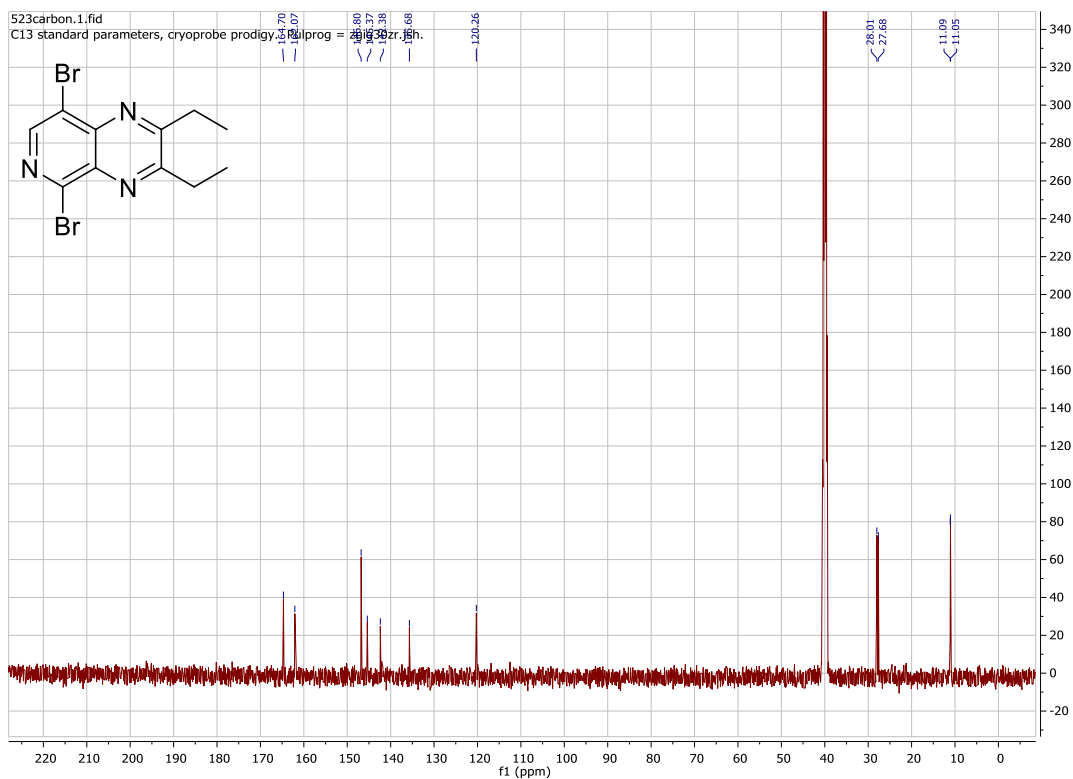


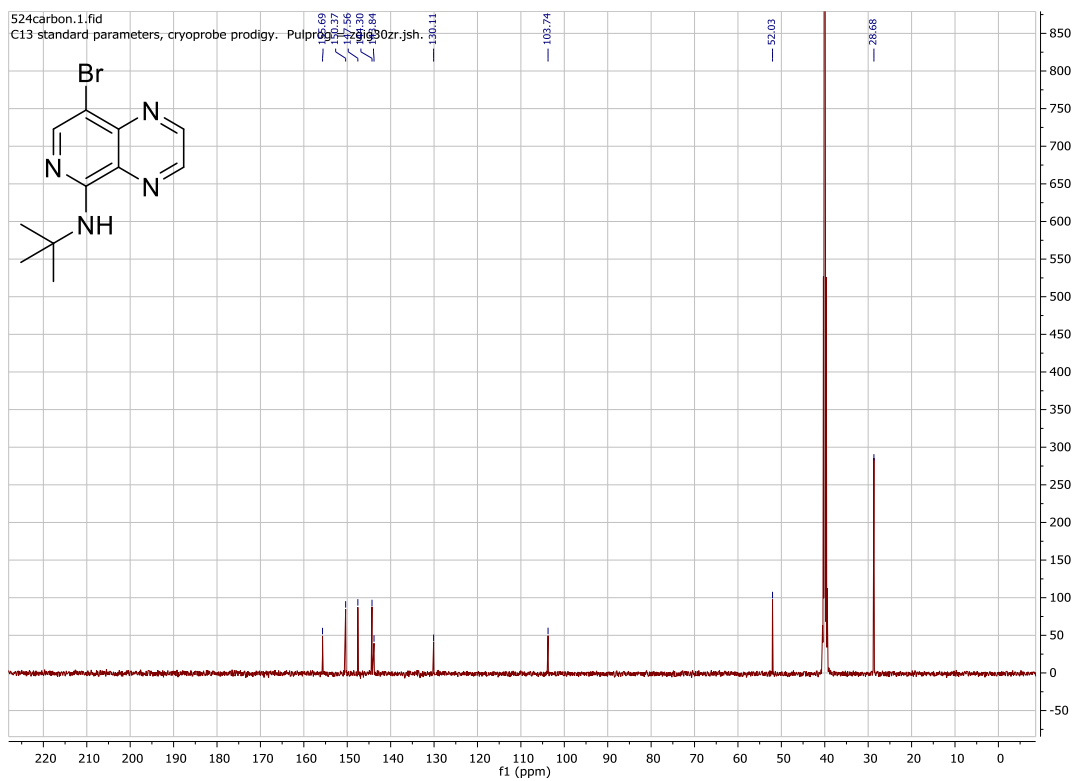
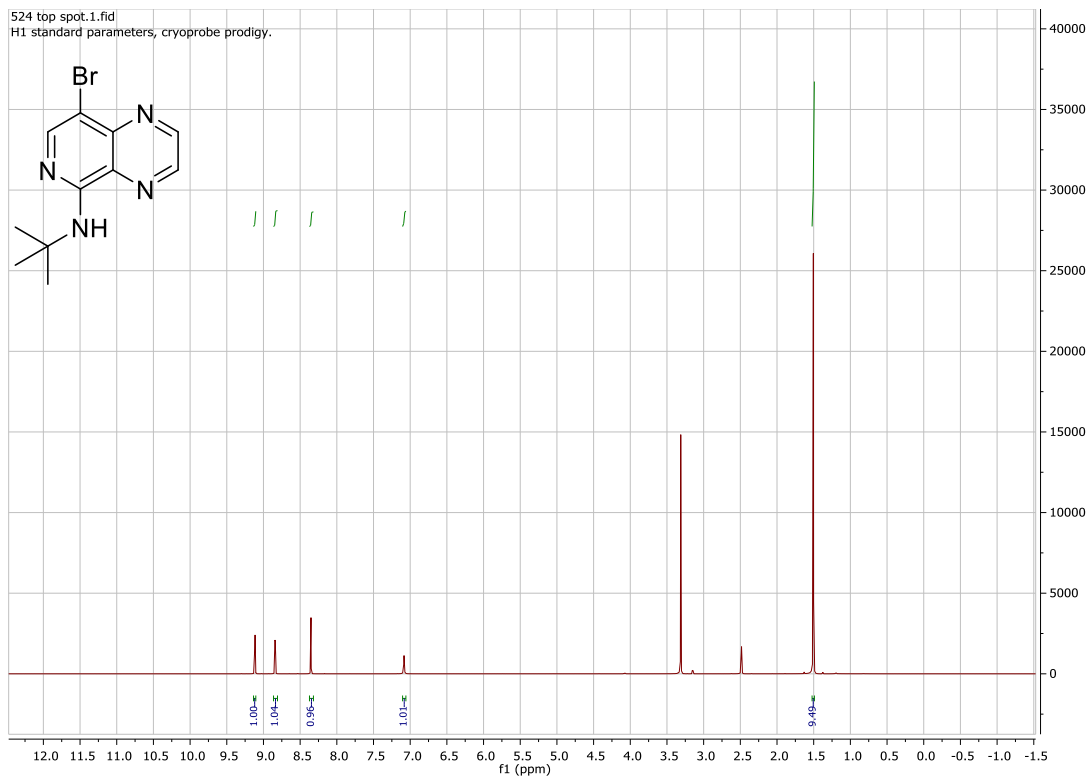


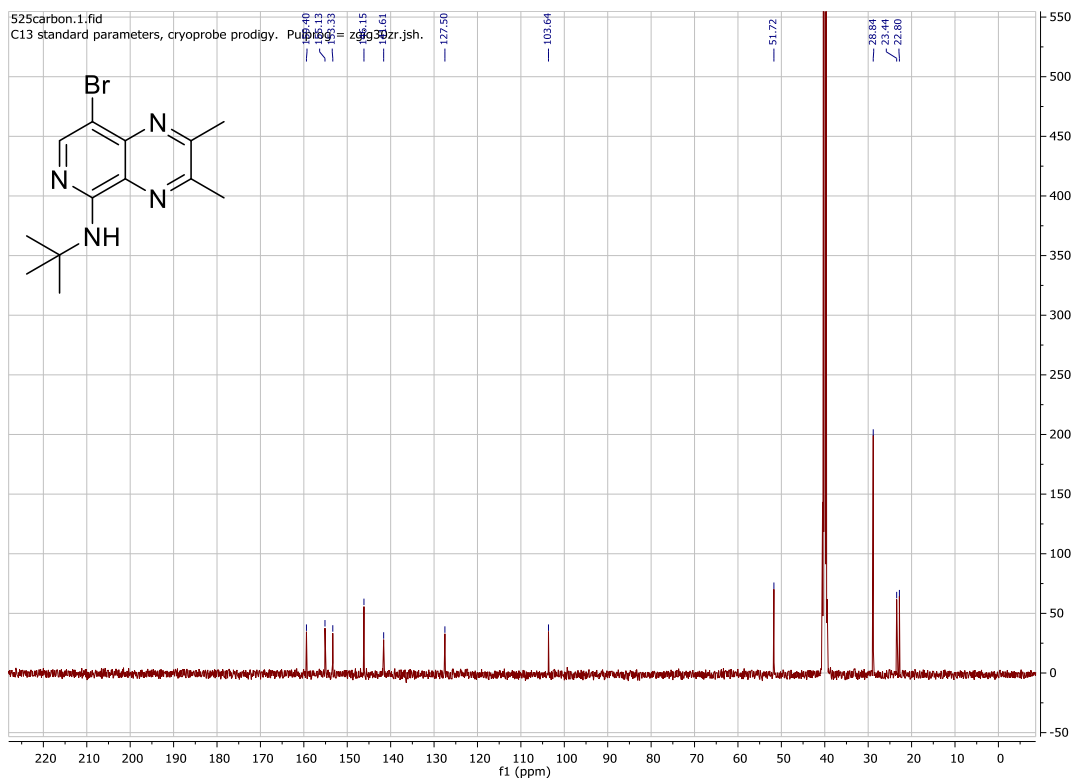
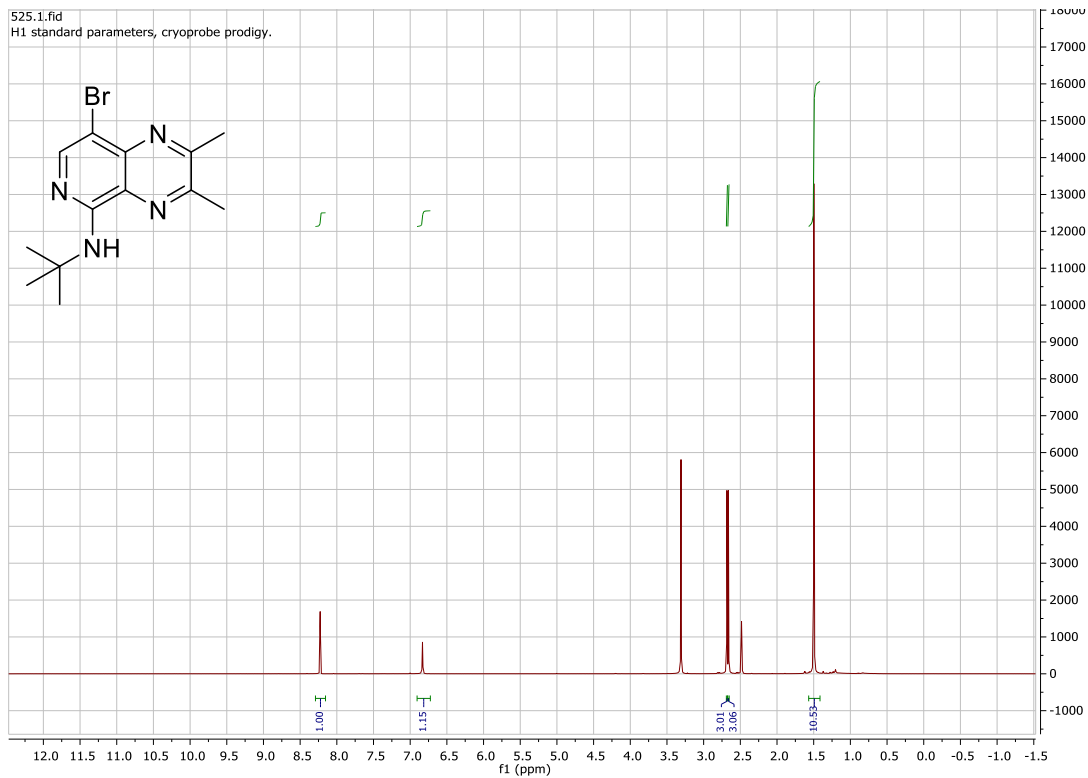


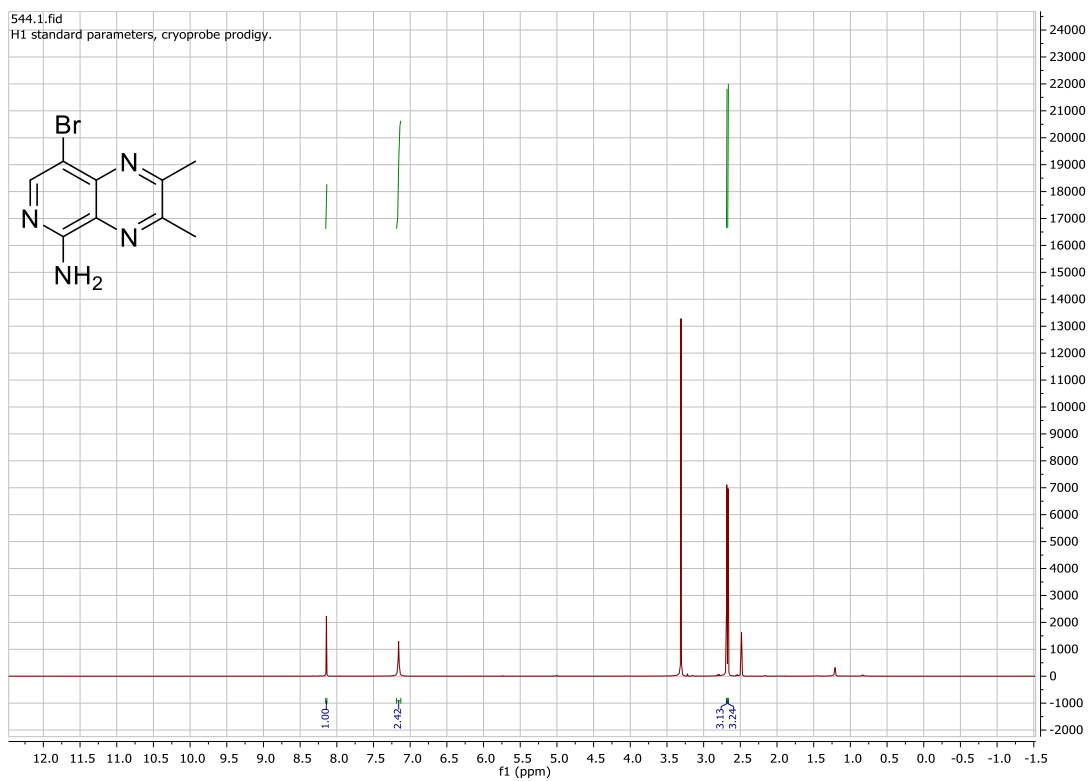


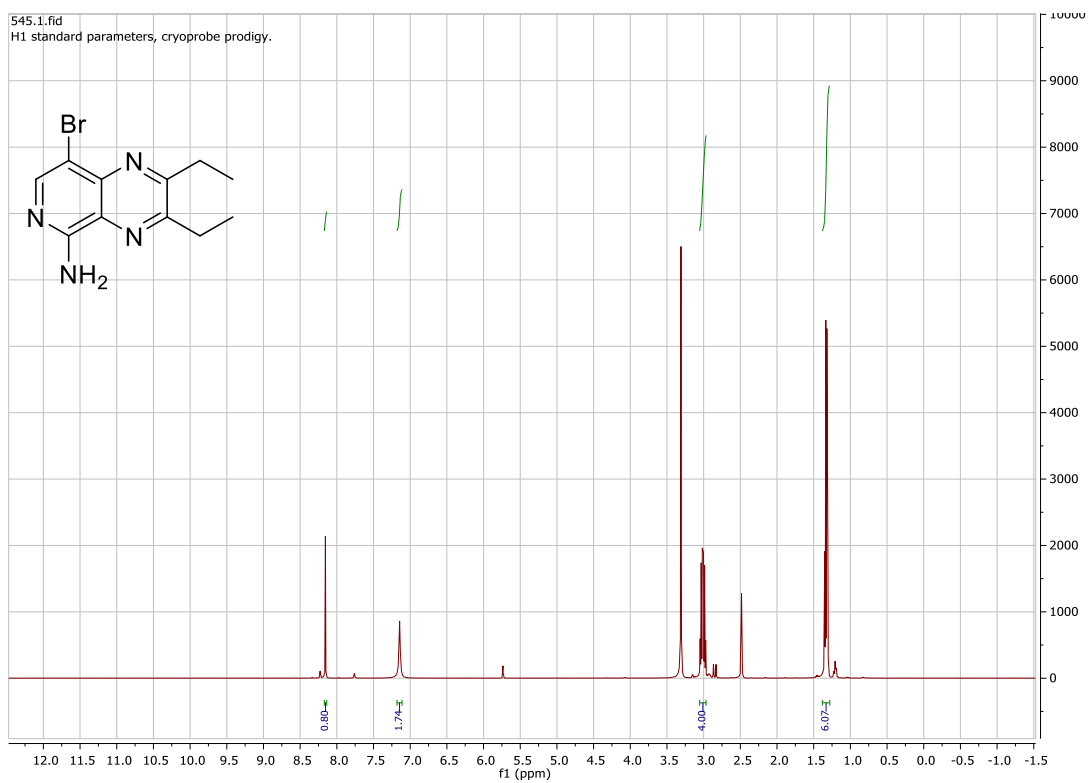
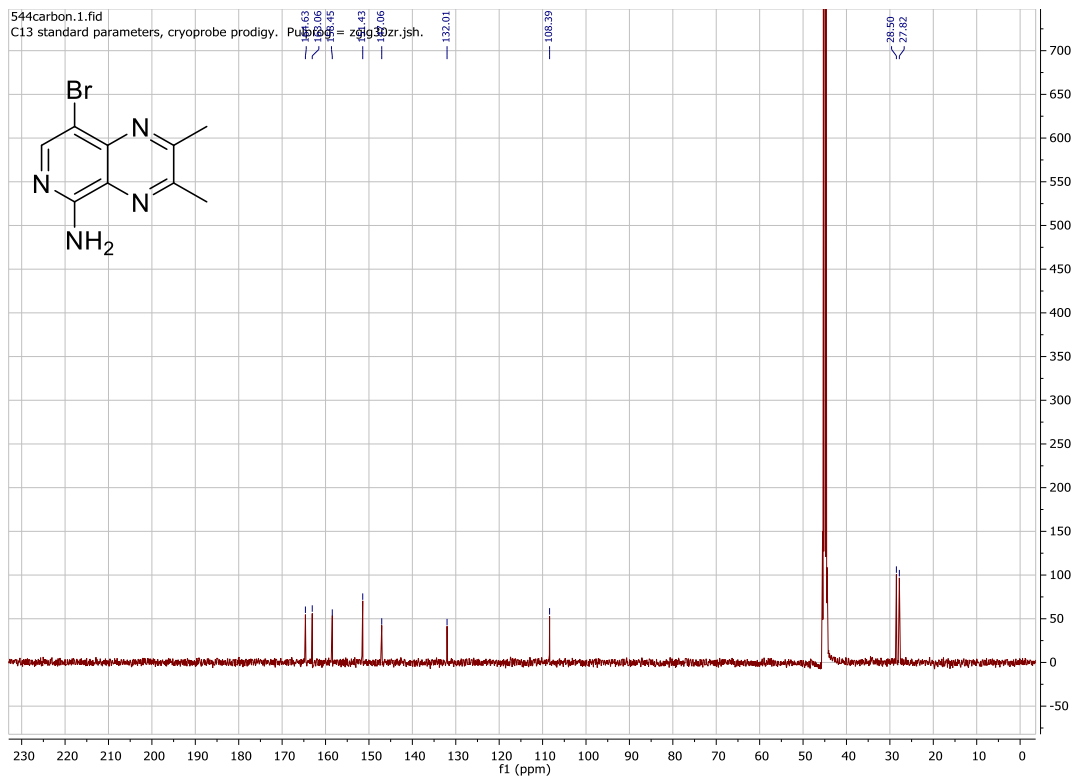


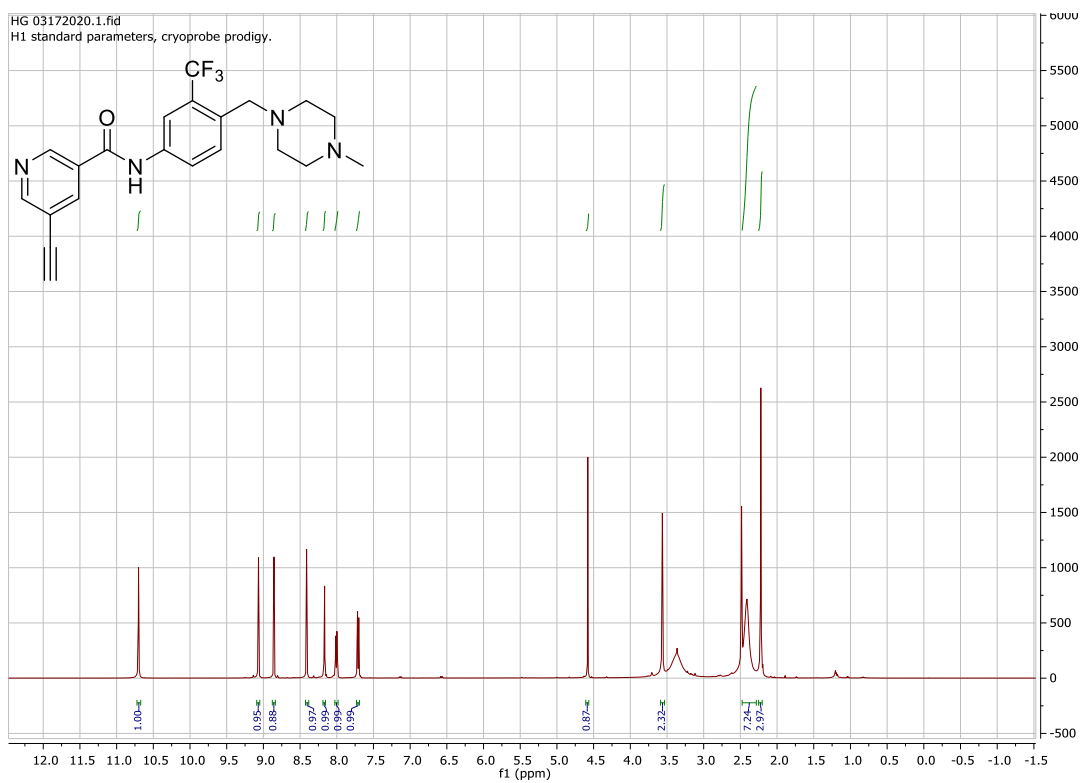
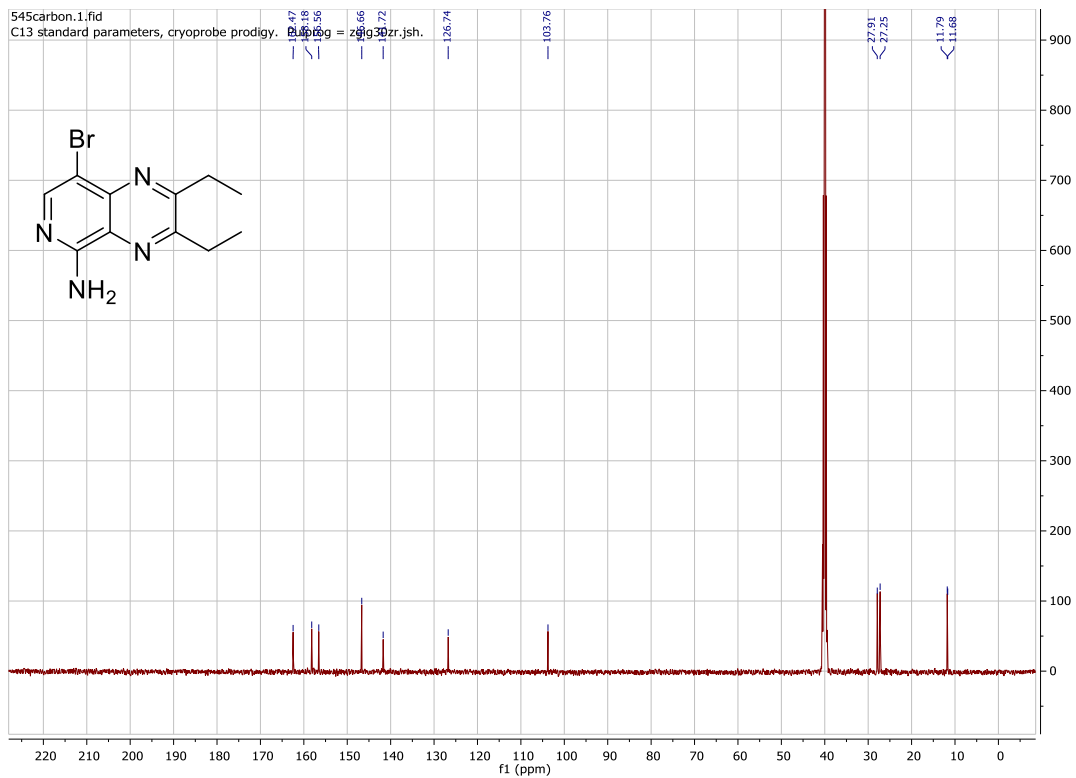


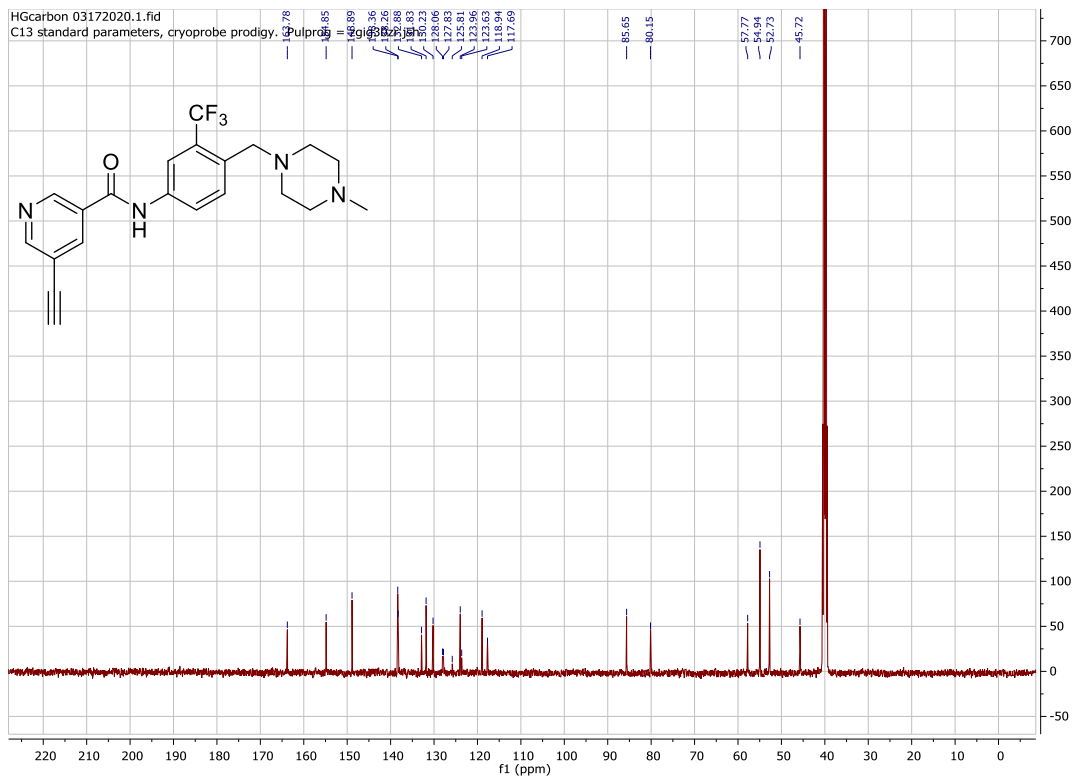












PUBLICATIONS

1. **Larocque, E.**, Chu, E. F. Y., Naganna, N. & Sintim, H. O. Nicotinamide–Ponatinib Analogues as Potent Anti-CML and Anti-AML Compounds. *ACS Omega* **5**, 2690–2698 (2020).
2. N. Naganna, Choi E.Y., Opoku-Temeng C, **Larocque E**, Chang E.T., Aklaki M., Carter- Cooper B., Torregrosa-Allen S.E., Elzey B.D., Lapidus R, Sintim H.O. Amino alkynylisoquinoline and alkynyl naphthyridine compounds potently inhibit acute myeloid leukemia proliferation in mice. *EBioMedicine* **40**, 231–239 (2019).
3. **Larocque, E. A.**, Naganna, N., Opoku-Temeng, C., Lambrecht, A. M. & Sintim, H. O. Alkynylnicotinamide-Based Compounds as ABL1 Inhibitors with Potent Activities against Drug-Resistant CML Harboring ABL1(T315I) Mutant Kinase. *ChemMedChem* **13**, 1172–1180 (2018).
4. **Larocque E**, Nimishetti N, Ma X, Opoku-Temeng C, Carter- Cooper B, Chopra G, Lapidus R, Sintim H.O. Aminoisoquinoline benzamides, FLT3 and Src-family kinase inhibitors, potently inhibit proliferation of acute myeloid leukemia cell lines. *Future Med. Chem.* **9**, 1213–1225 (2017).
5. Ma X, Zhou J, Wang C, Carter-Cooper B, Yang F, **Larocque E**, Fine J, Tsuji G, Chopra G, Lapidus R, Sintim H.O. Identification of New FLT3 Inhibitors That Potently Inhibit AML Cell Lines via an Azo Click-It/Staple-It Approach. *ACS Med. Chem. Lett.* **8**, 492–497 (2017).